TEAMER REPORT

VIVACE-W; AN INTEGRATED CURRENT-WAVE HYDROKINETIC ENERGY HARVESTER

Awardee: Vortex Hydro Power, LLC

Awardee point of contact:

Michael M. Bernitsas, Ph.D. bernitsasmm@vortexhydroenergy.com
Stergios Liapis, Ph.D. liapis101@gmail.com

Facility: Marine Hydrodynamics Laboratory, University of Michigan

Facility point of contact: Prof Kevin Maki, MHL Director. kjmaki@umich.edu

Date: August 31, 2024

Report Authors: Michael M. Bernitsas, Ph.D.
Salman Sadiq, Ph.D.
Stergios I Liapis, Ph.D.
Christopher C. Bernitsas, VHP Intern, BS in ECE
Onggo Nichita, VHP Intern, MS in NA&ME
Nipit Congpuong, Ph.D. Candidate in ME

TABLE OF CONTENTS:

1. LIST OF FIGURES

2. LIST OF TABLES

3. EXECUTIVE SUMMARY

PROJECT: A VIVACE Converter was tested in the Marine Hydrodynamics Laboratory (MHL) of the University of Michigan (UofM) under constant flow. Testing conditions simulate a river flow for converting Marine Hydrokinetic (MHL) energy to electricity. The Converter was designed and built with up to four oscillators consisting of circular cylinders with large turbulence stimulation. The underlying principle is that such cylinders get excited in fluid-structure interactions (FSI). FSI in this case are Vortex Induced Vibrations, galloping, and their coexistence. Such FSIs are typically catastrophic for engineered structures and are suppressed. VIVACE enhances them and controls them, thus, converting MHK energy to mechanical energy in the oscillators and subsequently to electricity. VIVACE is environmentally compatible, based on natural phenomena with cylinders moving only 20%-40% faster that the flow, presenting no danger to fish or humans, making no noise.

TESTING:
Results have been posted at the following google-drive link:

https://drive.google.com/drive/folders/1ZBaZk9jpTjzkukG1m5Gbr8II7OvANMph?usp=sharing

The Converter was tested in a variety of configurations, in several different ways, under different conditions, and for individual components. Specifically:

- Number of cylinders
- Cylinder spacing
- Dry testing
- Wet testing
- Magnetic ends vs. actual spring bumpers
- Transmission
- Simple and sophisticated Power Take Off (PTO) configurations and power electronics arrangements
- Computational Fluid Dynamics (CFD)
- Stress time-simulations using FEA (Finite Element Analysis)
- Fatigue analysis using FEA results
- Post-processing of experimental data
- Post-processing of CFD data
- Design for wave and FSI energy conversion
- The converter was shipped to PNNL (Dr. Ruth Branch) for further testing in collaboration with VHP

CONCLUSIONS:

- Number of cylinders: Best design would be with two cylinders.
- Cylinder spacing: For synergistic FSI of cylinders, latitude of center-to-center spacing of 2-4 diameters is efficient because of the turbulence stimulation design.
- Dry testing: All components were designed very well and are durable.

- Wet testing: Several successful tests were conducted. Minimum flow velocity for energy production was 0.7m/s with high output and motion at high speeds. Flow speeds up to 1.5m/s were tested. There is no upper limit on the flow speed to VIVACE's ability to convert MHK to electricity because of the back-to-back VIV and galloping making the RAO (Response Amplitude Operation) open-ended. Towing Carriage limitations made testing at higher speeds potentially unsafe. However, the device was designed for speeds up to 6 m/s.
- Magnetic ends vs. actual spring bumpers: High intensity magnets proved to be very fragile; hence, they are not practical for high speeds >1.2 m/s due to potential bumping with cylinders. Secondly, the design would require precision installation with shielding so that the magnetic field does not interfere with the generator magnets. (Distance between bumpers and generator is approximately 8 inches). In the future, for potential use of magnetic end bumpers a simple non-magnetic casing may be used to protect the magnets from cylinder bumping.
- Transmission: The pulley and belt system works very well and has been tested extensively. In future tests, we may adjust the pulley diameter. At even lower flow speeds, to achieve energy harnessing, the pulley diameter may be slightly decreased. At higher flow speeds, to increase the generator efficiency even more, the pulley diameter will be decreased to increase the generator RPM since the initial generator torque would not be a problem at higher flow speeds.
- Simple and sophisticated Power Take Off (PTO) configurations and power electronics arrangements: Four different configurations have been tested:

  Dumb system proved applicable to practical applications, where monitoring/control may not be required. Target flow velocities >1.0 m/s without physical springs; >0.3 m/s with springs.

  Kick-Start system: The system is required when the oscillators stall or stop moving. The kick-start algorithm initiates when the RPM ns generator stays below 150 RPM for 3 seconds. Once the kick is activated, hydrodynamics take over and the oscillators start moving (VIV/ Galloping). This proved practical for low speeds from 0.55m/s to 0.8 m/s, but it takes the energy from battery to operate. At kick-start, the generator acts in motor mode and hence takes energy from the battery to do so. Kick-start for long runs is expected to be least efficient.

  Virtual Spring Control system proved to be applicable for wider range of velocities, but more electronic equipment need to be attached that makes it less practical. Moreover, this requires energy consumption from generator acting as motor.

  Adaptive control system gives highest efficiency and produces higher power due fish undulation patterns. It does need all the electronics, but at speeds above 1.0 m/s this is the most efficient one.
- Computational Fluid Dynamics (CFD): An MRELab (Marine Renewable Energy Laboratory) dedicated tool, which was developed based on OpenFOAM, has been proven to be an excellent way of visualizing the FSI and explaining the response of VIVACE with 1-4 cylinders with the specially designed large turbulence stimulators. The caveat is that it takes about 10 hours of simulation time on a 24-core workstation to generate about 30 seconds of real time (See separate CFD Report in Appendix IV).

- Stress time-simulations using FEA (Finite Element Analysis): Using the output of our CFD code as input to ANSYS, simulations were performed showing the stress levels as a function of time. The maximum stress point always lies on the shaft connecting the oscillators with the wheel cart. The Converter can easily sustain the hydrodynamic loads. The caveat is that it takes about 12 hours of simulation time on a 24-core workstation to generate about 30 seconds of real time simulation (FEA & Fatigue Report, Appendix V).
- Fatigue analysis using FEA results: This is calculated from the results of FEA. It is revealed that at the highest flow speed for this project, the projected life of the Converter is 12.7 years (separate FEA & Fatigue Report, Appendix V).
- Post-processing of experimental data: MRELab software was to analyze data for displacement, velocity, acceleration of each cylinder; lift force in phase with velocity (added damping) and in phase with acceleration (added mass); current, voltage, and power.
- Post-processing of CFD data: MRELab OpenFOAM based software was used to postprocess the CFD results to analyze the wet tests from the UofM towing tank.
- Design for wave and FSI energy conversion: This is an easy task analytically to design the cylinders to match wave resonance with VIV initial branch with exactly the same hardware.
- The Converter was shipped to PNNL (Dr. Ruth Branch) for further testing in collaboration with VHP: These will be ocean testing conditions. We look forward to long term collaboration with the PNNL team. The team of UofM, PNNL, VHP works is the best possible team to push VIVACE to commercialization.

CHALLENGES:

- The biggest challenge is finding an off-the-shelve underwater generator. A custom-designed, one-of-a-kind would cost $89,000 for a single cylinder rendering the Converter non-viable for commercialization.
- We tried something that was never achieved before which was to use the generator both as a motor for control and as a generator. That would enable emulation of spring without wasting much of the harnessed energy - rather than using physical spring. In the past, in the MRELab, this was achieved using separate generator and motor servomotor [21].

FAILURE:

- Because of the prohibitive cost of a one-of-a-kind generator, we switched to a sealed, welded box to house a dry generator underwater. The box failed after several days of testing; it took water which damaged the generator.

DESIRED PLAN:

- To design a portable VIVACE with less weight, having IP-69 enclosure for generator and physical low stiffness springs.

A workable SolidWorks model has been finalized with all the possible improvements that were observed during the towing Tank experiments at UofM. Improvements are listed below:

IMPROVEMENTS: Based on challenges and failure we made the following decisions in the redesign for future testing:

- The volume of prototype model was 1 m^3, and weight was 161Kg. Whereas, volume of modified design is 3m x 1.357m x 2.33m (9.48 m^3) and weight is 180 Kg. Volume wise weight of a single module has been reduced by **12%**. This was achieved by selecting different design strategies.
- Underwater Box to host the generator is proposed by selecting off the shelf watertight enclosures from Blue Robotics. Only one cable comes out of the box, which makes the system very practical. This improvement has already been implemented in the Converter shipped to PNNL.
- To increase the RPM's of generator pulley size has been adequately reduced. This arrangement produces **30%** more speed; that helps the generator to be in the optimum power range/ efficiency most of the time.
- Cart has been fully redesigned to host skate wheels to ensure much less friction. It is now smoother and is more quiet.
- Diameter of oscillators has been increased from 3.5" to 8.62". This change would increase the potential harvesting power by about **45%** for each oscillator.
- 4 oscillators have been reduced to 2 oscillators with larger spacing (2x2.57xDia). It was observed that in 4x oscillator configuration, the last downstream oscillators did not produce much power than the first two. Whereas, once two oscillator configuration was tested in towing tank, it was revealed that there was a lock-in state at various low speed velocities. Hence according to our 15 years of research and experience, we have decided to go for 2 oscillator configuration with doubling the distance of 2.57 x Diameter between the oscillators. This will ensure us to avoid lock-in or shielding effect from first oscillator onto second oscillator.
- The overall travel length of converter has been increased from 0.56m to 1.75m, while the height has been increased from 1m to 2.4m. This will have hydrodynamic and electronics advantages. As the oscillator stops when it changes the direction, having a longer travel will ensure less interruption in electronic signal. Hence the power generated will be more refined and much controllable.
- Transmission belt width has been increased since the travel length has been increased. This will ensure safe operation and avoid lateral vibrations.
- Physical low stiffness springs have been introduced, which will ensure VIV and Galloping at very low speeds (0.4m/s). This will also eliminate the banging sound of cart hitting the end bumpers as was observed in prototype design. Using physical springs for low flow speeds omits the need of electronic Kick-Start, and hence saves the energy. At higher flow speeds (>1.0 m/sec), a motor can be used to emulate springs without expending significant amount of harnessed energy for long operations.
- The oscillators are designed in such a way that they will have a minor positive buoyancy, hence the upper channel will take the load, meaning thereby that the travel friction will be almost negligible.
- Additional slots for debris/ sand etc. have been made on the channel on which the wheel cart runs. This will ensure any blockage in channel arising from debris/ sand etc. Likewise the

support bearing housing the synchronous bar has been modified by introducing carvings to avoid debris.

- The stainless-steel parts have been fully isolated from Aluminum parts to avoid any oxidation resulting to rust. Nevertheless, to ensure further sacrificial Zinc anodes have also been fixed on various points.
- Belt adjustment mechanism has also been improved to ensure loosening of the transmission belts during long constant operations.
- Bosch structural profiles along with Bosch fasteners have been used for ease of assembling.

PART I: Preparation

4. INTRODUCTION TO THE PROJECT
5. ROLES AND RESPONSIBILITIES OF PROJECT PARTICIPANTS
6. PROJECT OBJECTIVES
7. TEST FACILITY, EQUIPMENT, SOFTWARE, AND TECHNICAL EXPERTISE
8. TEST OR ANALYSIS ARTICLE DESCRIPTION
9. WORK PLAN

4. Introduction to the Project

PROJECT: A novel marine hydrokinetic energy converter called VIVACE-W has been designed and needs to be tested thoroughly. VIVACE-W harnesses marine hydrokinetic (MHK) energy from currents [horizontal MHK] and waves [vertical MHK] and is, thus, a natural evolution of the VIVACE Converter which harnesses only horizontal MHK from rivers, currents, and tides.
The core of VIVACE consists of 1-4 cylinders (Fig. 1) with turbulence stimulation (Fig. 2), supported by springs and connected to dampers. Pictures from laboratory testing and field testing are shown in Figs. 7-9; other concepts are shown in Figs. 10-12.The horizontal flow excites cylinders to move transversely to the flow in flow induced oscillation (FIO). Vortex Induced Vibration (VIV) and galloping are the two FIO phenomena being implemented in VIVACE to convert horizontal MHK to kinetic in the oscillating cylinders. Through a transmission system (Fig. 4), the shaft of a generator (Fig. 6) is rotated to convert the kinetic energy of one cylinder to electricity. VIVACE has several advantages: (a) The underlying phenomena are based on alternating lift thus generating a wake beneficial to fish. (b) The two FIOs are nonlinear phenomena enabling high response with a RAO (Response Amplitude Operator) starting with linear resonance in quiescent water and never ending (Figs. 13, 17). (c) The underlying phenomena are highly scalable and VIVACE has a potential to harness energy from flows as slow as 0.2m/s. (d) Its parts being blunt and moving slowly (Fig. 14), thus, presenting no danger to fish or people (Fig. 9). (e) We have designed and built a worldwide unique controller (Vck [15,21]) which emulates the oscillator without biasing the measured phenomena. As a result, in the laboratory, we can adjust the spring stiffness *K* of an oscillator on the run to optimize its performance if needed.
A natural side benefit is that *K* can be adjusted to resonate the cylinder-oscillator with incident waves and move vertically harnessing vertical MHK energy from waves. That is, with the same motion and the same physical components VIVACE can harness energy from either waves and currents and potentially from combined action of waves and currents.

OBJECTIVES: The overall objective is to design and build a versatile portable converter that can harness hydrokinetic energy from currents, waves, and waves+currents where they coexist. The potential of harnessing both horizontal and vertical MHK energy simultaneously is high but the available data in over 100 years of studying VIV are practically nonexistent. This will be studied for the first time in our tests.
In this specific project the objectives are:
Objective 1: Model assembly

Objective 2: Measure power output of VIVACE-W under wave excitation for 0.5Hz < fwave <2Hz

Objective 3: Measure power output of VIVACE-W under the combined action of steady flow excitation for 0.2m/s<Vflow<3m/s and wave excitation for 0.5Hz < fwave <2Hz

Objective 4: Test mechanical components for durability during the six days of tow-tank testing

Objective 5: Test electrical components for effectiveness.

Subsystems and main dimensions of proposed VIVACE-W to be tested		
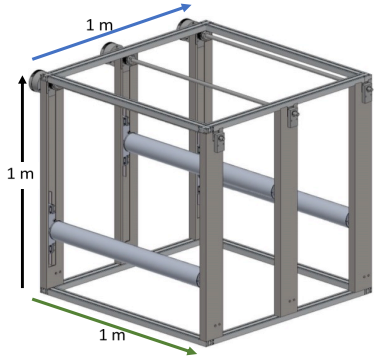	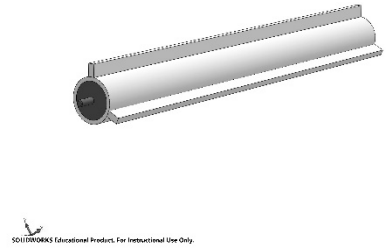	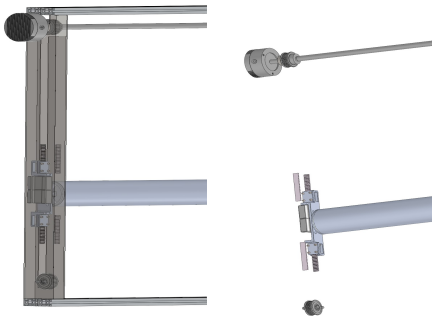
Figure 1. 3-cylinder VIVACE-W Converter with 7 subsystems	**Figure 2**. Subsystem #1: Cylinder and turbulence stimulation	**Figure 3.** Subsystem #2: Magnetic restraint and support
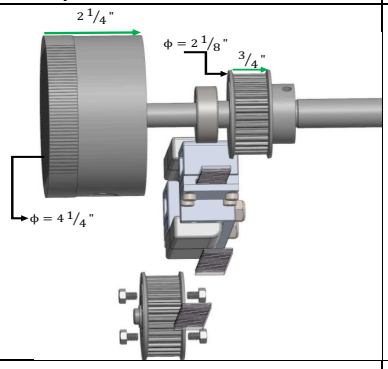	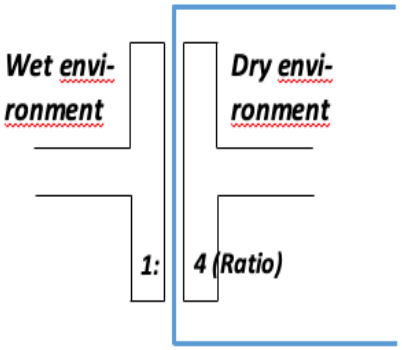	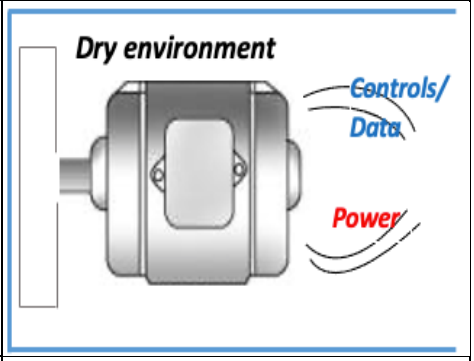
Figure 4. Subsystem #3: Trans-mission: belt-sprocket-synch.	**Figure 5.** Subsystem #4: Magnetic gear with wet/dry parts	**Figure 6.** Subsystem #5: VIVACE motor/generator

It should be noted though that the Testing Tasks are more detailed than the objectives and include

(1) Model Assembly
(2) Subsystem 7: Frame
(3) Subsystem 1: Cylinders with 28% turbulence stimulation (PTC)
(4) Subsystem 2: Magnetic Restraints and Support (EMARS)
(5) Subsystem 3: Linear to Rotational Transmission
(6) Subsystem 4: Magnetic Gear Transmission
(7) Subsystem 5: Motor/Generator
(8) Model Reassembly
(9) Instrumentation
(10) Two-Cylinder VIVACE-W testing
(11) Three-Cylinder VIVACE-W testing

WORK TO BE PERFORMED: The aim is to test the portable VIVACE-W converter thoroughly. That involves testing each of the seven subsystems shown in Figs. 1-6. Most importantly, after reassembling the portable converter, test the entire system in the wet environment of the Towing Tank of the Marine Hydrodynamics Laboratory of the University of Michigan.
The specific work to be performed is tabulated in Section 6.3 with the time schedule.

Lab-tests and field-tests

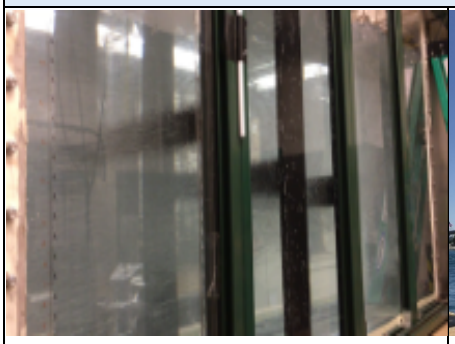

Figure 7. 3-cylinder VIVACE in the MRELab with fish-body undulation pattern to maximize energy

Figure 8. Four vertical cylinder VIVACE launching in the St. Clair River (2016)

Figure 9. Fish thrive in cylinder wakes [17]. 4-cylinder,field-tests in the St. Clair River (2016)

Sample applications of VIVACE-W in the Blue Economy

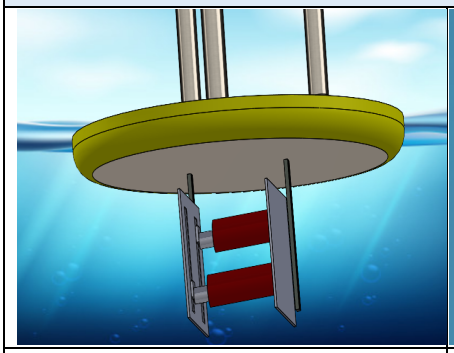

Figure 10. Powering buoys for navigation and observation

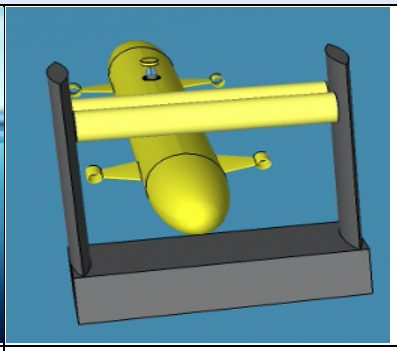

Figure 11. UUV Powering station even in slow flows

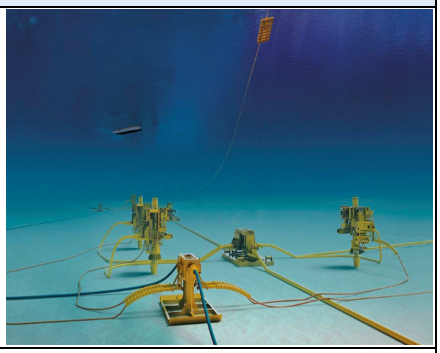

Figure 12. Subsea offshore installations

Previous, releavant, measured proof of performance

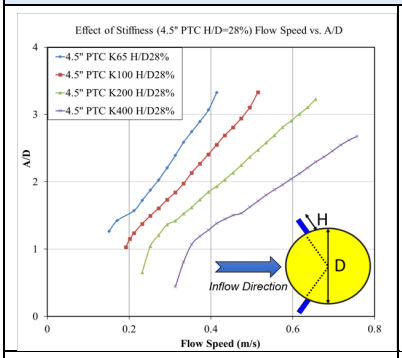

Figure 13. Turbulence stimulation initiates FIO at low flow speed and forms open-ended RAO

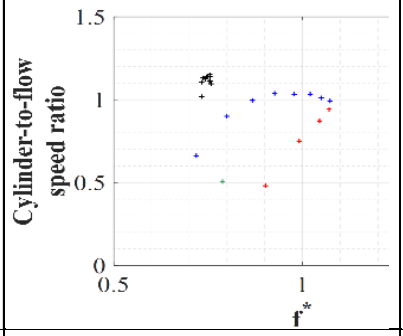

Figure 14. Cylinder speed $U_{cyl} < 1.2U_{flow}$; no noise and no danger to fish or humans

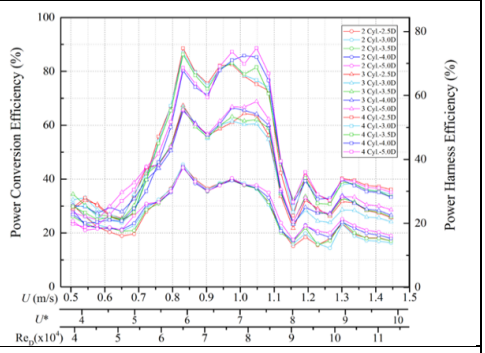

Figure 15. Four-cylinder synergistic FIO; η=88% of Betz Limit [12]. Broad range. Made broader in Fig. 9

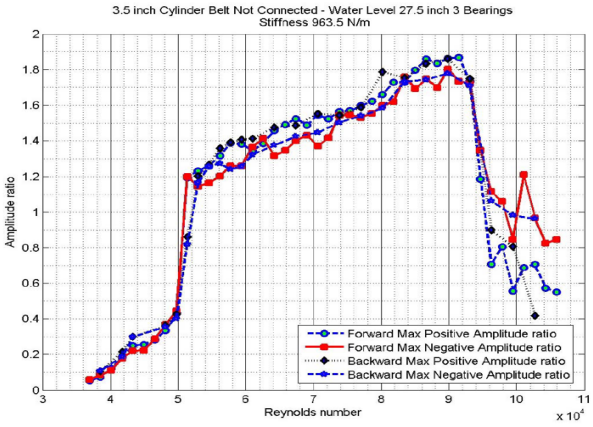

Figure 16. VIV response of smooth cylinder in the TrSL3 flow regime of fully turbulent shear layers

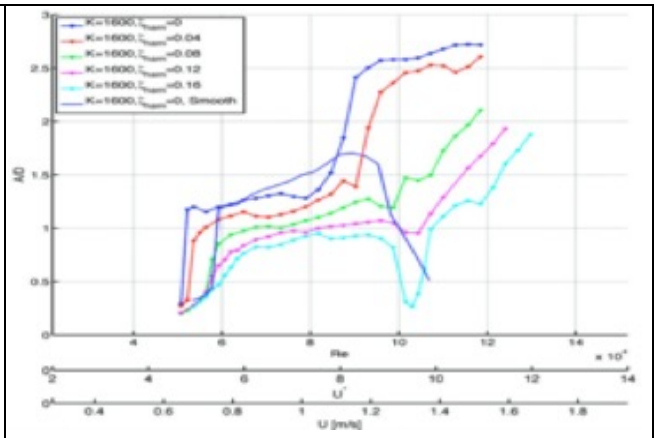

Figure 17. Cylinder with turbulence stimulation in back-to-back VIV and galloping; open ended RAO

5. Roles and Responsibilities of Project Participants

5.1. Applicant Responsibilities and Tasks Performed

Vortex Hydro Power, LLC will:

(1) Provide the portable VIVACE-W Converter with three oscillators.
(2) Identify the seven subsystems of the VIVACE-W.
(3) Be responsible for the assembly and disassembly of VIVACE-W into its seven subsystems.
(4) Supervise the testing of each subsystem as per Testing Tasks 1-11.
(5) Verify real time the soundness of the measurements.
(6) Analyze the data and report to the sponsor, DOE.

Personnel:

(1) Dr. Stergios Liapis with expertise in testing, offshore engineering analysis and design, wave mechanics for energy harnessing.
(2) Prof. Michael M. Bernitsas with expertise in flow induced oscillations, hydrodynamic testing, marine hydrokinetic energy harnessing.

5.2. Network Facility Responsibilities and Tasks Performed

The Marine Hydrodynamics Laboratory of the University of Michigan will:

(1) Mount the portable VIVACE-W under the towing tank carriage.
(2) Wet-test in the towing tank VIVACE-W per Test-Tasks 10 and 11.
(3) Make sure all equipment needed for the successful performance and completion of the tests function properly including but not limited to the carriage, the wave maker, the underwater camera, the data acquisition and storage systems.

Personnel:

(1) Dr. Salman Sadiq, with expertise in flow induced oscillations, hydrodynamic testing, marine hydrokinetic energy harnessing.
(2) Jason Bundoff, Engineering Technician with expertise in operating the towing tank and conducting testing.
(3) Alexander Flick, Senior Electrical Engineer with expertise in power electronics.
(4) James Smith, Engineering Technician

6. Project Objectives

• Overall Objectives: VIVACE-W is the only converter we know that can harness MHK energy both from currents and waves using the same physical components and motion (vertical) to harness both energy sources. We have a plethora of data for harnessing horizontal MHK in the MRELab at the University of Michigan where VIVACE was invented. It has been patented through the University of Michigan and VHP has been granted exclusive license to commercialize the technology based on all seven patents [1-7]. Also, there is a lot of data in the literature for harnessing vertical MHK energy [20]. The tests we propose will quantify the ability of VIVACE-W to harness energy from currents and waves using the same physical components and motion. The tests can be performed only in a towing tank where the current is emulated by mounting VIVACE-W under the moving carriage. Waves are generated by the wave generator.

Objective 1: Model assembly

Task 1.1: Per Fig.1 assemble frame

Task 1.2: Per Figs.2-4 assemble all mechanical components with three oscillators and assemble watertight box for generator.

Task 1.3: Per Figs.5-6 assemble all electrical components with three oscillators (PTO)

Objective 2: Measure power output of VIVACE-W under wave excitation for 0.5Hz < fwave <2Hz

Task 2.1: Measure power output of VIVACE-W with two cylinders in tandem

Task 2.2: Measure power output of VIVACE-W with three cylinders in tandem

Objective 3: Measure power output of VIVACE-W under the combined action of steady flow excitation for 0.2m/s<Vflow<3m/s and wave excitation for 0.5Hz < fwave <2Hz

Task 3.1: Measure power output of VIVACE-W with two cylinders in tandem

Task 3.2: Measure power output of VIVACE-W with three cylinders in tandem

Objective 4: Test mechanical components for durability during the five days of testing. That includes

Task 4.1: Durability of Subsystem #2: Restrain and Support

Task 4.2: Durability of Subsystem #3: Transmission

Objective 5: Test electrical components for effectiveness. That includes

Task 5.1: Durability of Subsystem #5: Motor/generator

Task 5.2: Durability of Subsystem #6: Control

Task 5.3: Durability of Subsystem #7: Power management

• Physical attributes that the project will investigate: The underlying objective is to be able to build a portable, durable, functional converter that can harness horizontal and vertical MHK energy with only vertical motions. Accordingly, we want to test:

(1) The ability of the Vck controller to emulate oscillator properties (damping c and stiffness k) not only for harnessing horizontal MHK energy from currents rivers and tides, but also from waves only, and from waves+currents.
(2) Effectiveness of the magnetic restraints to minimize frictional losses.
(3) Effectiveness of the magnetic gears to enable separation of dry and wet environments.
(4) Effectiveness of the electrical components to charge a battery or power a consumer.
(5) Overall efficiency of the PTO and power electronics.

• Performance metrics that the project is targeting:

We are targeting the metrics that affect the efficiency and portability of VIVACE-W. Specifically

(1) Compact and light-weight motor for the Vck system.
(2) Light but durable frame.
(3) Contactless support against drag to minimize frictional losses.
(4) Contactless transmission with magnetic gear to minimize friction and secure a dry environment for the power electronics.
(5) Hydrodynamic efficiency in wave and wave+current harnessing. Efficiency in current harnessing has been investigated extensively and is understood to a functional level.

Our target is to maximize the overall power output. For that we need to improve on the overall efficiency as defined next. For currents, it is defined as

$$P_{output} = \eta_{Betz}\eta_{hydro}\eta_{support}\eta_{Vck}\eta_{transmission}\eta_{gear}\eta_{generator}\frac{1}{2}\rho v^3 L(D+2A)$$

where

$$P_{fluid} = \frac{1}{2}\rho v^3 L(D+2A)$$

is the energy flowing through the area swept by the cylinder.

η_{Betz} =16/27 is the theoretical upper limit of the energy available in the fluid flow to be harnessed by a single device, not multiple rows of devices

η_{hydro} =is to be measured experimentally with wave excitation. Only with current excitation it has been measured over ten years for 1-4 cylinders as shown in Fig. 15.

$\eta_{support}$ =is about 0.8 for rollers and we aim to increase it to 1.0 with contactless magnetic support [5]

η_{Vck} =is the energy loss in emulating the oscillator by the Vck controller. Presently, power is taken from the wall but will be replaced with regenerative motor/generator in the near future. This will be about 0.97-0.99

η_{gear} =will become 1.0 for magnetic gear

$\eta_{generator}$ =includes all power electronics and will be tested in this project for various frequencies and amplitudes of oscillations. Dry as well as wet tests will be used.

That is our targets for this project are as set above for η_{hydro} , $\eta_{support}$, η_{gear} , $\eta_{generator}$

7. Test Facility, Equipment, Software, and Technical Expertise

- Physical equipment, hardware, instrumentation, and other capabilities essential to achieving project objectives
    - MHL Self-powered Towing Carriage
    - MHL cRIO data collection hardware
- Simulation or data analysis software utilized
    - National Instruments LabView
- Critical personnel expertise utilized to achieve the project objectives
    - MHL Director, Kevin Maki
        - Project management
        - Hydrodynamic expertise
    - MHL Research Project Engineer, Jim Smith
        - Fabrication support
        - Physical setup expertise
    - MHL Senior Electrical Engineer, Alexander Flick
        - Electronic sensor setup
        - Data acquisition
    - MHL Lead Engineer in Research, Jason Bundoff
        - Physical test campaign expertise
        - Naval Architecture support
- Ocean test site conditions and equipment need to accomplish the testing

  N/A

8. Test or Analysis Article Description

• Purpose for the device: Test the performance of VIVACE-W to harness energy from waves only, and from currents+waves. Its ability to harness energy from currents only has been tested and recorded for longer than a decade. All seven subsystems of VIVACE-W (Figs. 1-6) will be tested as well.

• Advancement of MHL energy technologies:

(1) Advancement of current energy converters by improving on restraint for friction, transmission gear, and power electronics.
(2) Advancement in portability by making it a compact converter with high power density.
(3) Advancement in versatility by harnessing energy from waves and currents with the same vertical motion and the same physical components due to our unique Vck controller.

VIVACE-W is depicted in Figs. 1-6 in the portable scale. In Figs. 8-9, it is depicted in field tests in 2016.

9. Work Plan

9.1. Experimental Setup, Data Acquisition System, and Instrumentation

Data System Capabilities

The Marine Hydrodynamics Laboratory's Physical Model Basin data collection system is comprised of two National Instruments cRIO's in FPGA mode and a Kistler amplifier. One cRIO 9045 and the Kistler LabAmp 5167A is on the carriage and one cRIO 9057 in the alcove. The systems are time synchronized over ethernet using NTP (Network Time Protocol) the concept is that the Host computer sends a time stamp (future time) 2 seconds rounded down, then when the systems reach that time, they start collection. The cRIOs are modern versions with excellent stability, dual core, 2 GB of memory, 512MB of Micro SD storage, running NI's 64-bit Linux OS. The Kistler charge amplifier with a 3-component piezoelectric load cell are high quality and basically indestructible.

This data collection system is flexible, time synced, well tested with high channel count and we believe it is well suited for this project.

Details

The carriage cRIO 9045: Running in FPGA mode and is collecting at 2K Samples per Second. has several channels available. All analog channels are scalable to fit a calibration from many sensor types.

1) 4 strain (load cells) 5VDC excitation - full bridge, 24-bit, Sample rate: 2K
2) 16 Voltage +- 10Volt type sensors, 24-bit, Sample rate: 2K
3) 8 current 4-20mA, 16-bit, Sample rate: 2K
4) 4 Current 5Amp, 16-bit, Sample rate: 2K
5) 32 digital outputs, Sample rate: 2K
6) 8 Digital inputs, Sample rate: 2K
7) 2 Counters, 1 for the Carriage position, Sample rate: 2K

The Alcove cRIO 9057: Running in FPGA mode and is collecting at 50K Samples per Second has several channels available. All analog channels are scalable to fit a calibration from many sensor types.

1) 4 Voltage +- 10Volt, 16-bit, Sample rate: 50K – Used for Hydrophones
2) 16 Voltage +- 10Volt, 16-bit, Sample rate: 2K – Used for Capacitance Probes
3) 8 Current, 4-20mA, 16-bit, Sample rate: 2K
4) 16 Digital Output, Sample rate: 2K
5) 8 Digital input, Sample rate: 2K

Sensor	Range	Accuracy	Calibration	Calibration Method
Encoder	Inf	0.27 mm	05/26/2022	Direct Measure
Capacitance Probe	1m	0.15% FSO	07/07/2021	Incremental
Kistler Load Cell	Fx 500N Fy 500N Fz 3000N	$\leq \pm$ 0.5 % FSO	09/30/2020	Loaded/Unloaded To Standard

9.2. Numerical Model Description

LEFT BLANK INTENTIONALLY (PER INSTRUCTIONS)

9.3. Test and Analysis Matrix and Schedule

The test matrix is provided in an excel spread sheet in "7 APPENDIX" under "7.3. TEST MATRIX". It has been uploaded as a separate document.

9.4. Safety

- All safety procedures are outlined in the safety presentation PPT and will be followed at all times. See "7 APPENDIX" under "7.2. FACLITY SAFETY".

9.5. Contingency Plans

- Testing will be conducted according to the safety procedures listed in the safety presentation. Any testing that is deemed unsafe for personnel or equipment will be stopped/postponed until a safe means of proceeding has been determined and agreed upon by the MHL staff.

9.6. Data Management, Processing, and Analysis

i. Data Management

- Description on the location of the data storage, for the raw and processed data, data structure and metadata.
    - Data will be stored as CSV files on the onboard PCs on the powered towing carriage.
    - Data files will be backed up to a secure cloud server upon the end of every test day
- The data measured in each run will be the time history of the displacement of each cylinder in the Converter. Three columns are recorded: (i) Time, (ii) Displacement of each cylinder, and (c) Motor torque. The latter is not needed as we reconstruct the transverse force based on displacement and velocity as recorded by the motor encoder.

ii. Data Processing

Sample post processing of data are presented in "7 APPENDIX" under "7.5. FIGURES FOR SAMPLE POST-PROCESSING OF COLLECTED DATA". We conduct extensive analysis of the cylinder response as shown in Figs. 18-28.

- Discuss any data processing that will be performed during testing to help identify any errors that can be corrected during testing
    - No data processing will be performed by the MHL during testing
    - Offsets before and after running (i.e., carriage and converter are stationary) will be recorded to verify sensor functionality and repeatability

- Describe data quality assurance and quality control procedures
    - Data will be monitored on-the-fly via a live read-out display
- Uncertainty in measurements will be quantified as shown in Figs. 19-20 in the measured cylinder displacement. Specifically, the mean value of 60 seconds of recorded data will be lotted with error bars showing the extent of +/- one standard deviation.

iii. Data Analysis

- Description, diagrams, and other information on data scaling
    - The MHL will not be conducting any data scaling
- Description of statistical processing of results, including any sensitivity analysis performed
    - The displacement and acceleration history of all cylinders will be measured. Statistical properties of the displacements and accelerations will be computed.

The data collected are analyzed as shown in Figures 18-28. Specifically, the following information is extracted.

1. The time history of displacement showing the exact position of all cylinders (Fig. 18a).
2. The Phase Angle Difference (PAD) between cylinders (Fig. 18b).
3. The amplitude spectrum vs. frequency revealing the frequency content of each cylinder oscillation as well as the existence of other major oscillation components (Fig. 18c).
4. The instantaneous power generated by each cylinder as function of time (Fig. 18d).
5. The phase plots of all oscillating cylinders (Fig. 18e).
6. The amplitude of each cylinder as function of flow velocity *U*, Reynolds number *Re*, and reduced velocity *U** (Fig. 19). The error bars are shown as well.
7. Comparison of amplitude of 2^{nd} and 3^{rd} cylinders compared to the 1^{st} cylinder as function of flow velocity *U*, Reynolds number *Re*, and reduced velocity *U** (Fig. 20).
8. Frequency spectra plotted with *Re* and *U** as parameters (Fig.21).
9. Power generation for the complete converter (Figs. 22, 24, 26).
10. Efficiency on power generation for the complete converter (Figs. 23, 25, 27).
11. Possibly animation with our OpenFOAM based CFD codes we have developed in the MRELab (Figs. 28).

PART II: Execution

10. VIVACE CONVERTER TESTED
11. DRY TESTING
12. CFD SIMULATIONS
13. FEA AND FATIGUE ANALYSIS
14. WET-TEST DATA DOCUMENTATION

10. VIVACE Converter Tested

Wet tests in the Towing Tank of the Marine Hydrodynamics Laboratory (MHL) of the University of Michigan (UofM) were conducted with two and four oscillators. The corresponding drawings and dimensions are provided below.

10.1. Four-Oscillator VIVACE Converter

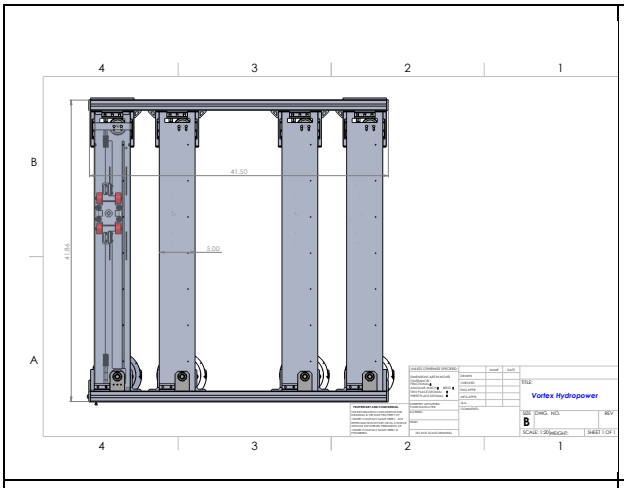

Figure 18. Overall dimensions

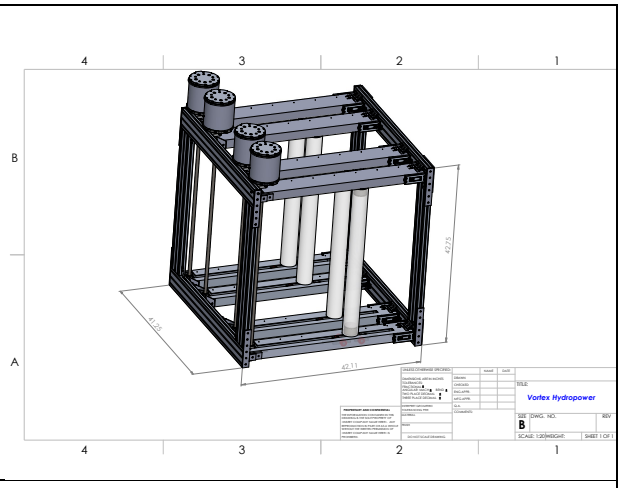

Figure 19. Complete converter with underwater boxes

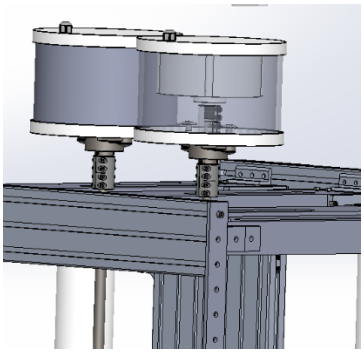

Figure 20. Underwater boxes installed on converter

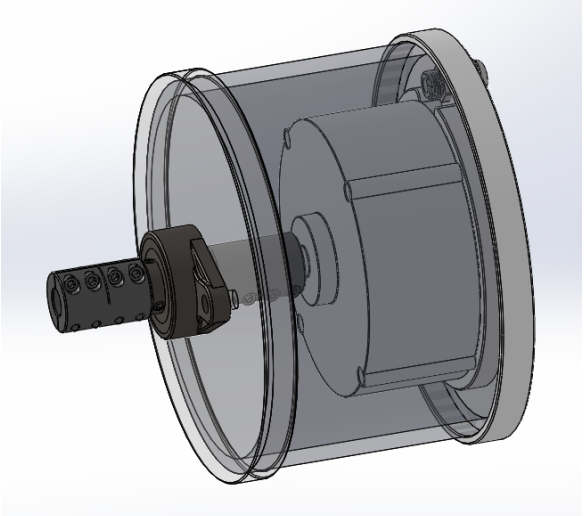

Figure 21. Underwater/watertight box hosting the generator

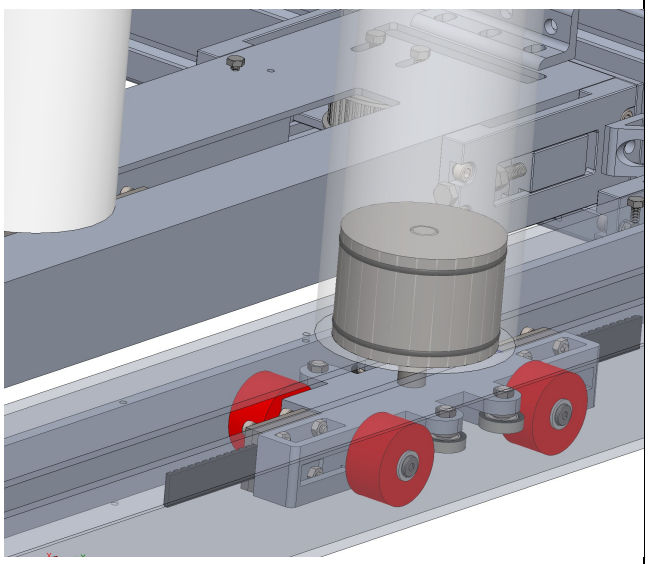

Figure 22. Wheel cart

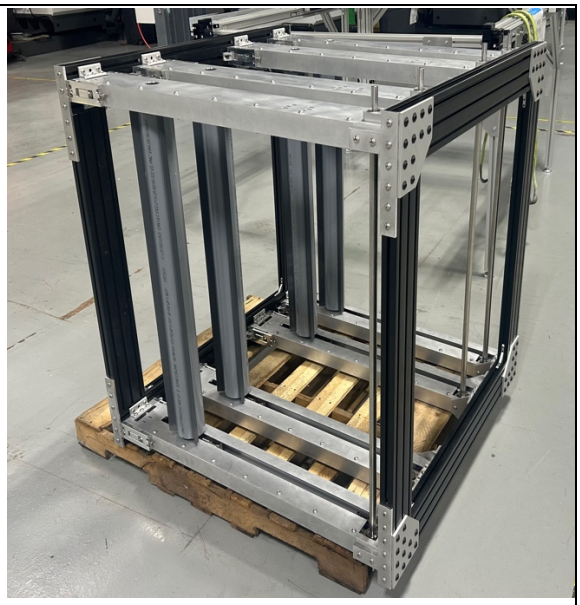

Figure 23. Assembled Converter at workshop

Figure 24. Engineering diagram of oscillating cylinder with dimensions in inches.

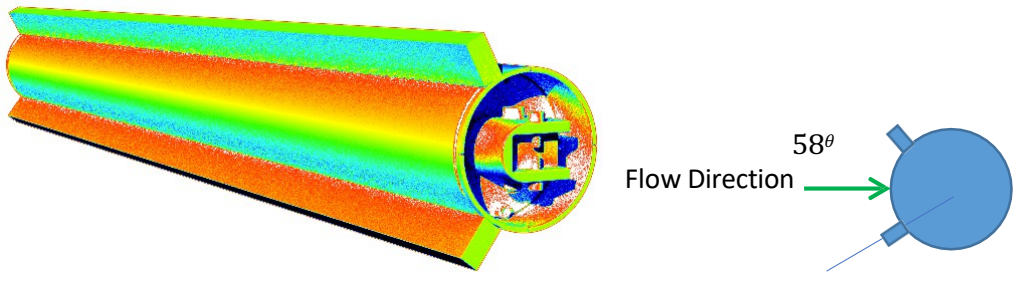

10.2. Four-Oscillator VIVACE Converter Horizontally for VIVACE-W

Figures below are CAD drawings of the VIVACE-W cylinders, the frame, the sliding block and the transmission belts. The total weight of the system without electronics is calculated to be 62 kg. This enables VIVACE-W to be transported by 2 people.

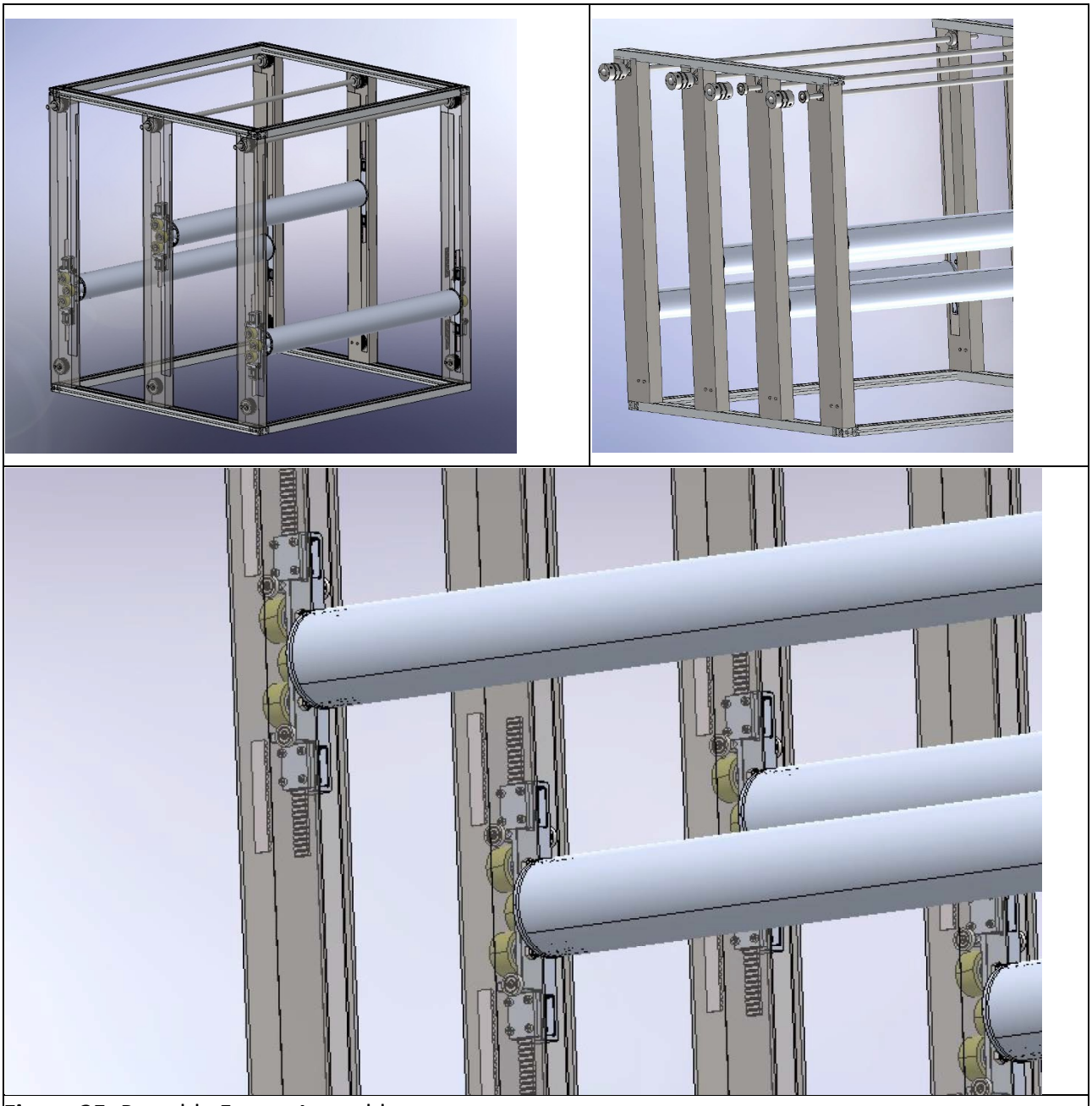

Figure 25. Portable Frame Assembly

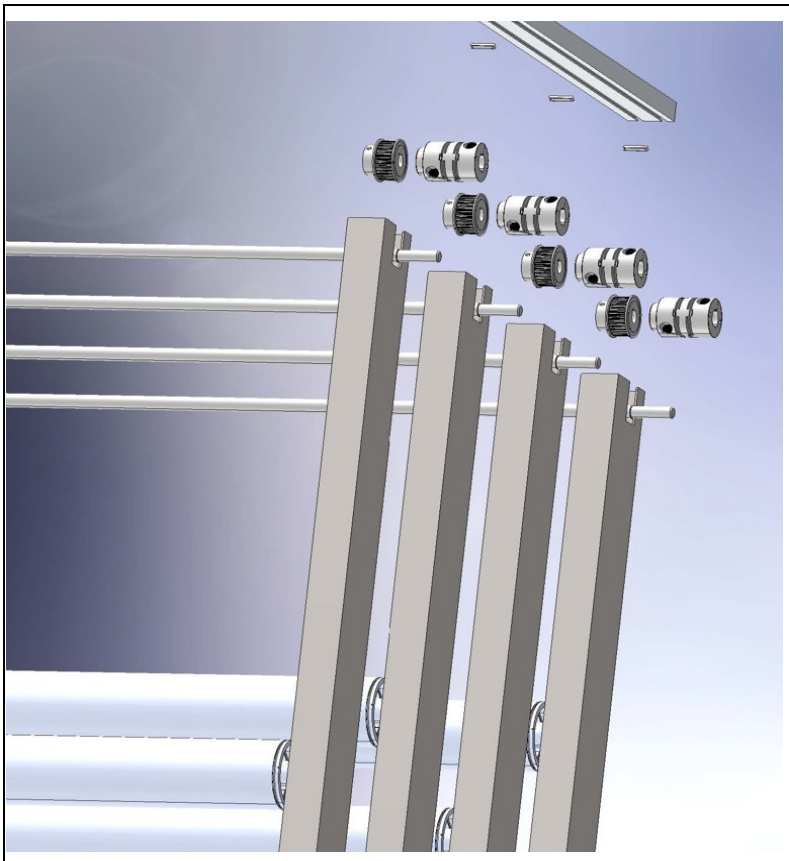

Figure 26. Transmission Assembly

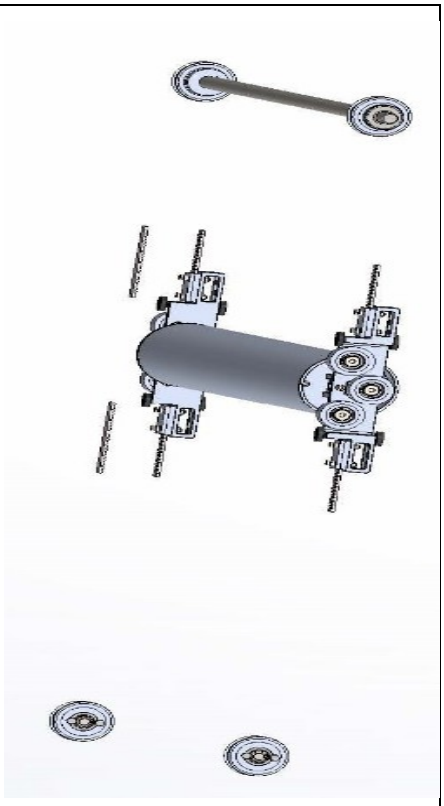

Figure 27. Synchronization Bar

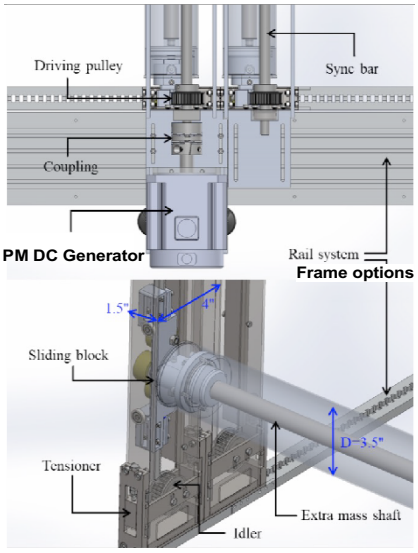

Figure 28. Transmission to PMDC Generator

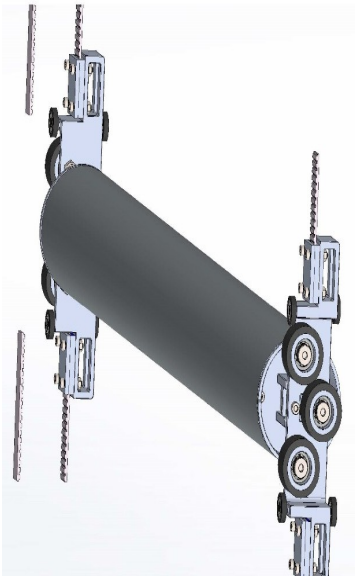

Figure 29. Oscillator

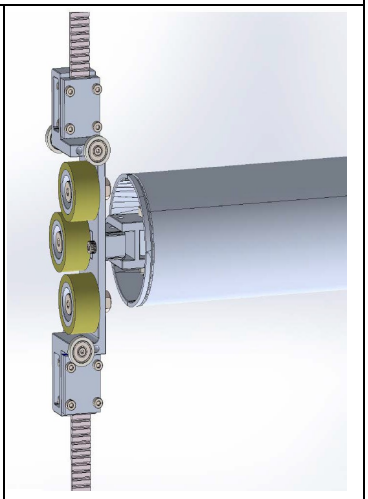

Figure 30. Transmission Belt

10.3. Two-Oscillator VIVACE Converter

SOLIDWORKS EDUCATIONAL PRODUCT

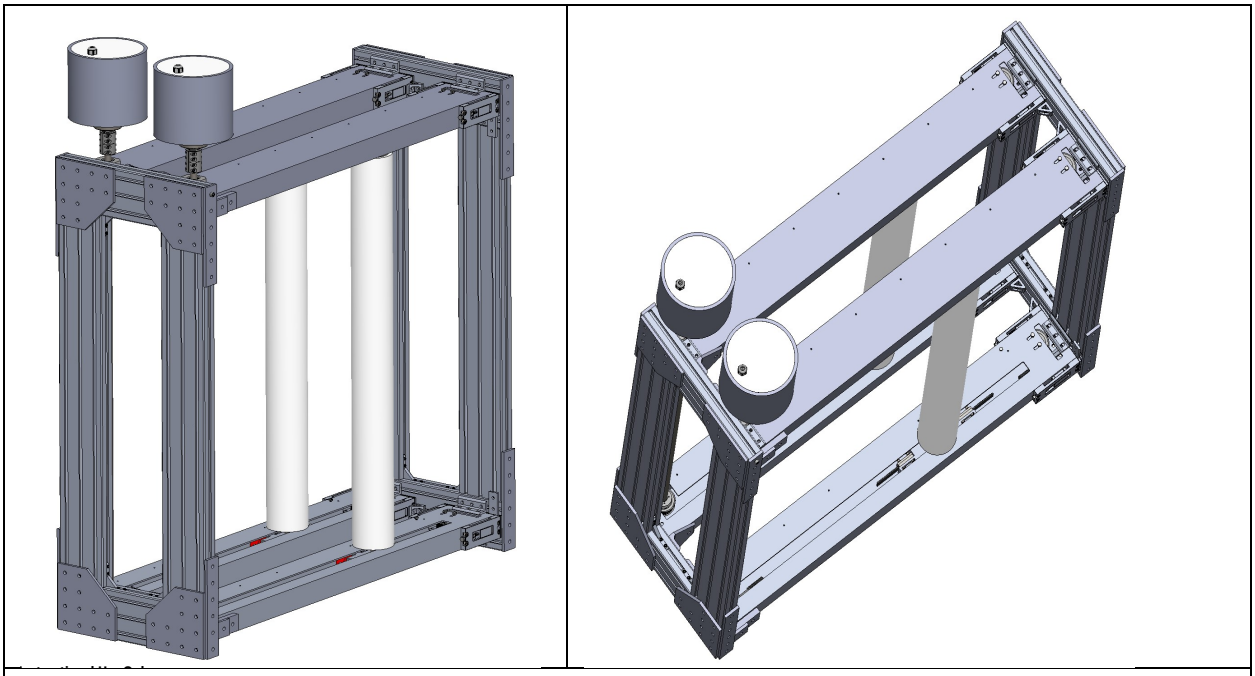

Figure 31. Two cylinder Converter shipped to PNNL for field testing

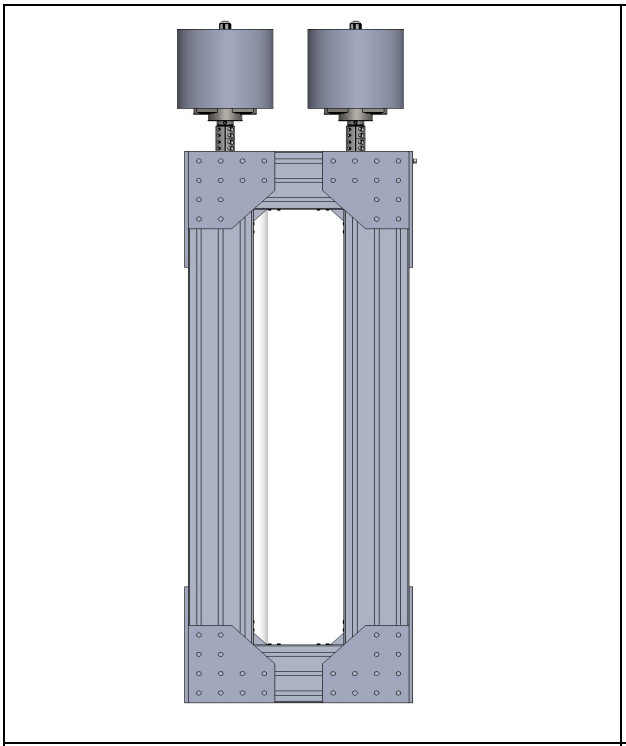

Figure 32. Two cylinder Converter; side view

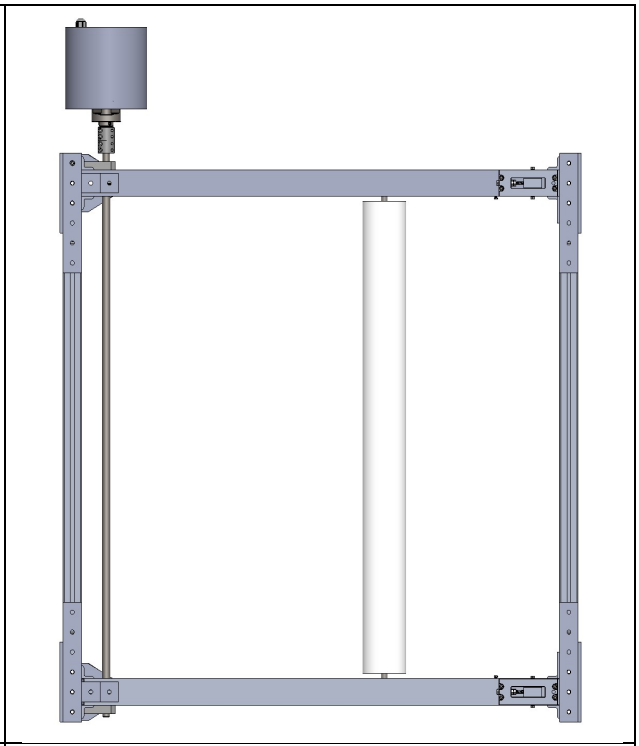

Figure 33. Synchronization shaft

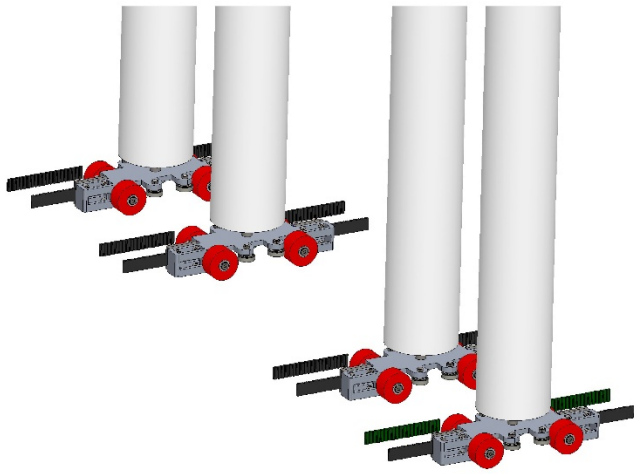

Figure 34. 4-cylinder Converter; wheel-carts and connection to transmission belt

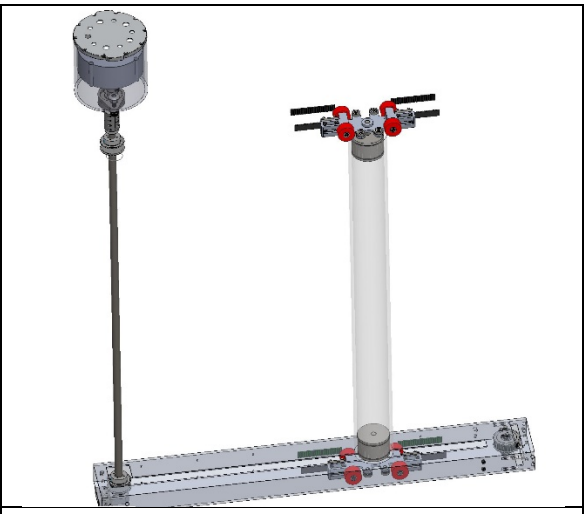

Figure 35. Cylinder, wheel cart, transmission belt, synchronization shaft and generator

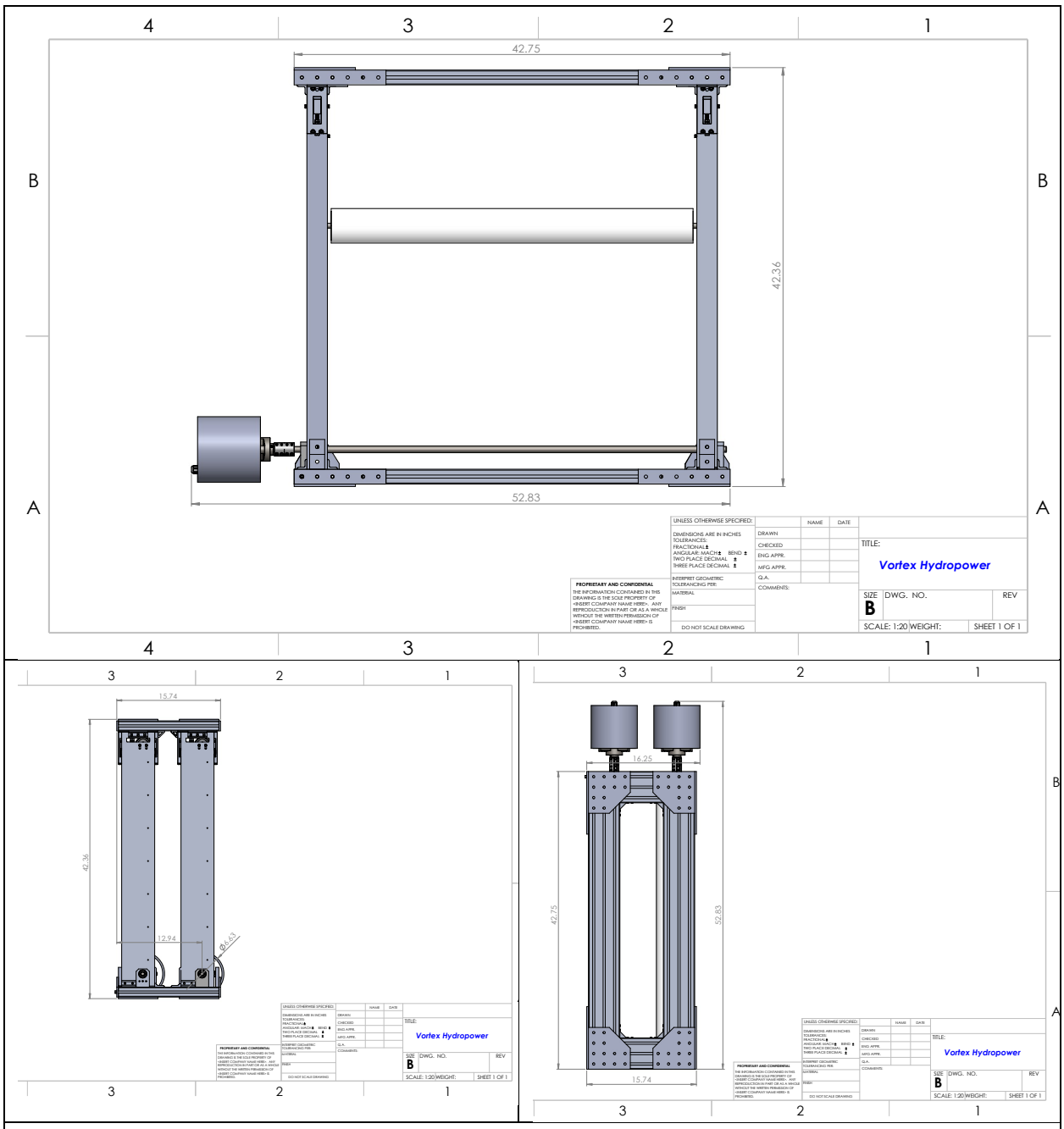

Figure 36. Dimensions of two-cylinder Converter shipped to PNNL for field testing

11. Dry Testing

Dry testing of a two-oscillator and a three-oscillator VIVACE Converter was performed at VHP. There were several goals:

(a) Test the adaptive damping through the unique VCK system developed by the MRELab and used for years in the MRELab. VCK uses a servomotor (upper right corner in the pictures) to emulate spring and damper with any mathematical model linear or nonlinear.

The software worked perfectly, and adaptive damping was verified.

(b) Test the power electronics and software to verify energy generation. It worked perfectly using a DC power supply and battery.

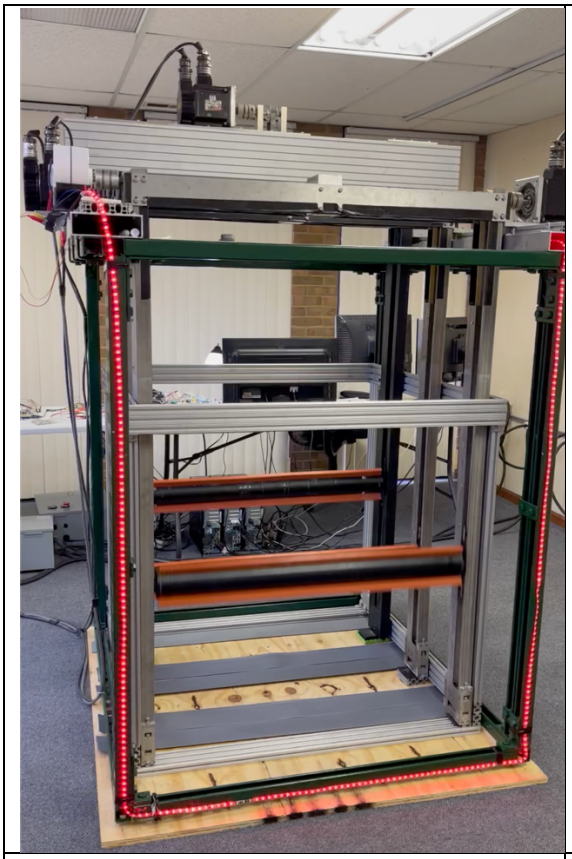

Figure 37. Three-cylinder Converter dry tested in the shop of VHP

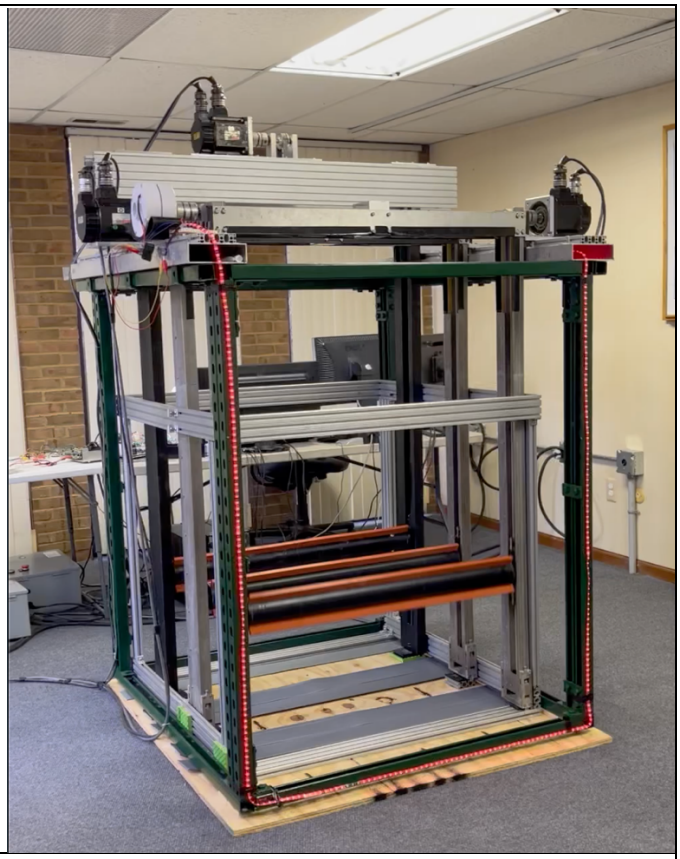

Figure 38. Dry testing in the shop of VHP using the Vck system with servomotor to emulate spring and damping (upper right corner). Generator in upper left corner

11.1. First Working Set-up:

The following flowchart shows a system with 3 PTO generators (We can have multiple PTO's also). Each PTO generator has

(1) A PMDC Generator
(2) Full Wave Rectifier
(3) Incremental Encoder on shaft

(4) Programmable DC Load

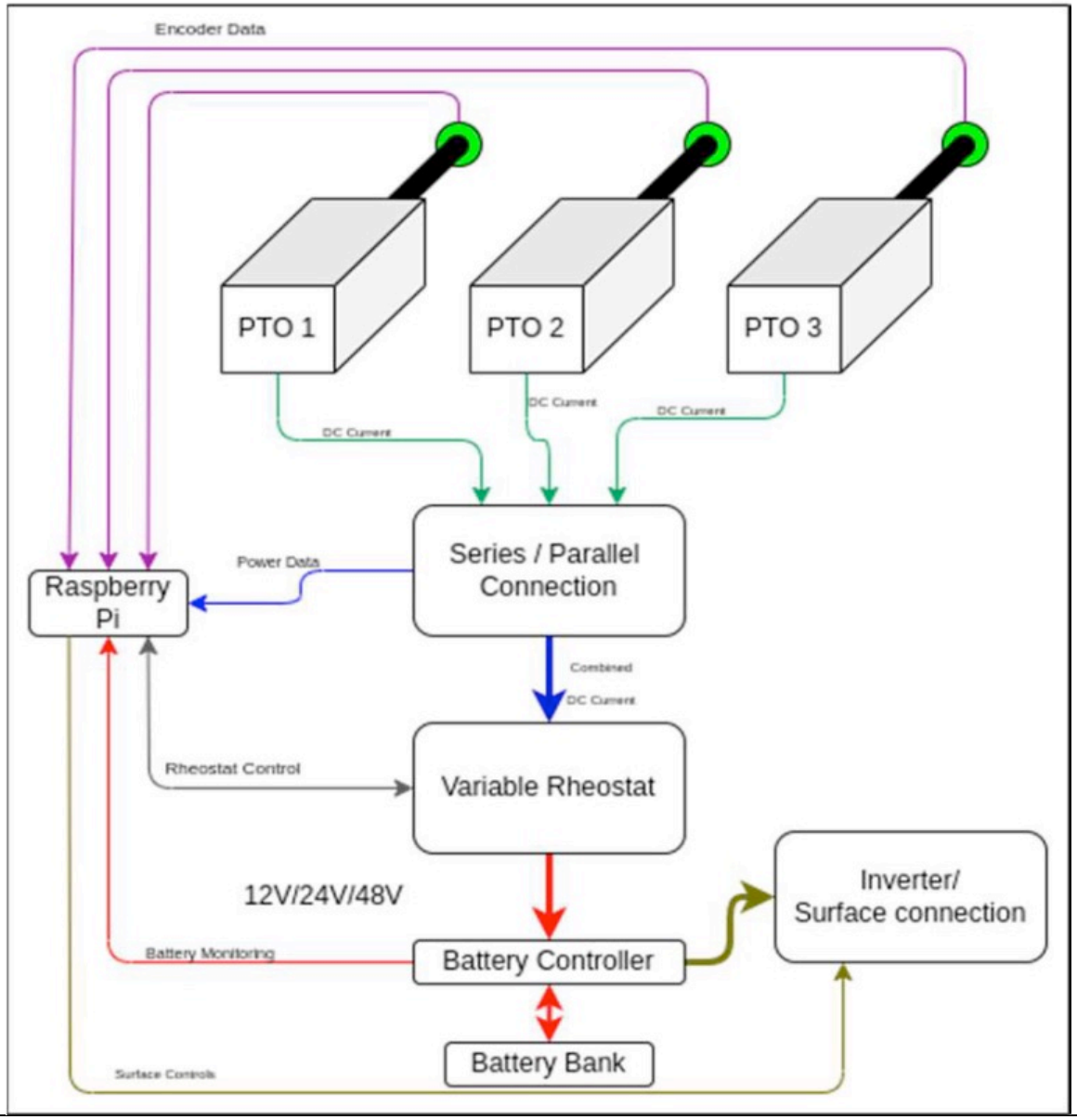

Figure 39. Three-PTO generator system (We can have multiple PTO's)

The PMDC generate AC current, which is converted to DC using the rectifier. This DC current is given to a "Series/Parallel Controller". This controller connects these lines in either series/parallel for optimum power generation. This DC current is then fed to a variable rheostat, which helps the raspberry pi control the dampening of the generator. The generated DC current is stored in an on-board Power bank. The energy stored in the power bank can be used in multiple ways. It can either be connected to an inverter to generate AC voltage, or the DC current can be used directly.

We have an on-board raspberry pi, which handles the power generation, logs all the data and provides a GUI for the user.

Conclusion:

DC load was used as a source to control the resistance to implement the Adaptive Damping through coding. However, it is to note that DC Load burns the power and energy cannot be extracted from it; hence DC load could not be used for practically capturing the energy out of a VVACE ocean Converter.

11.2. Second Working Set-up: Addition of VESC 'Variable Electric Speed Controller'

To harness, control and measure the output harnessed energy we need a device that would be robust and allows multiple communication ports along with flexible coding options. VESC 6 MkVI by TRAMPA (UK) was selected to do the job.

Reason for choosing VESC 6 MkVI:

- VESC is an open-source speed controller for Brushless Motors.
- It is capable of regenerating energy that is, converting the mechanical energy of the BLDC motor to electrical energy and ultimately charging the battery.
- A VESC can drive the motor, which is required when the system has stalled and needs a jump start.
- VESC has multiple communication protocols, unlike the DC load, which only communicated via NI-VISA protocol. VESC is capable of communication over Serial, PPM signal, CAN bus communication, which is compatible with almost every microcontroller/microcomputer.
- Heat dissipation is minimum hence it is highly efficient.
- Being palm side, it is easier to waterproof a VESC controller (if need be)

Circuit:

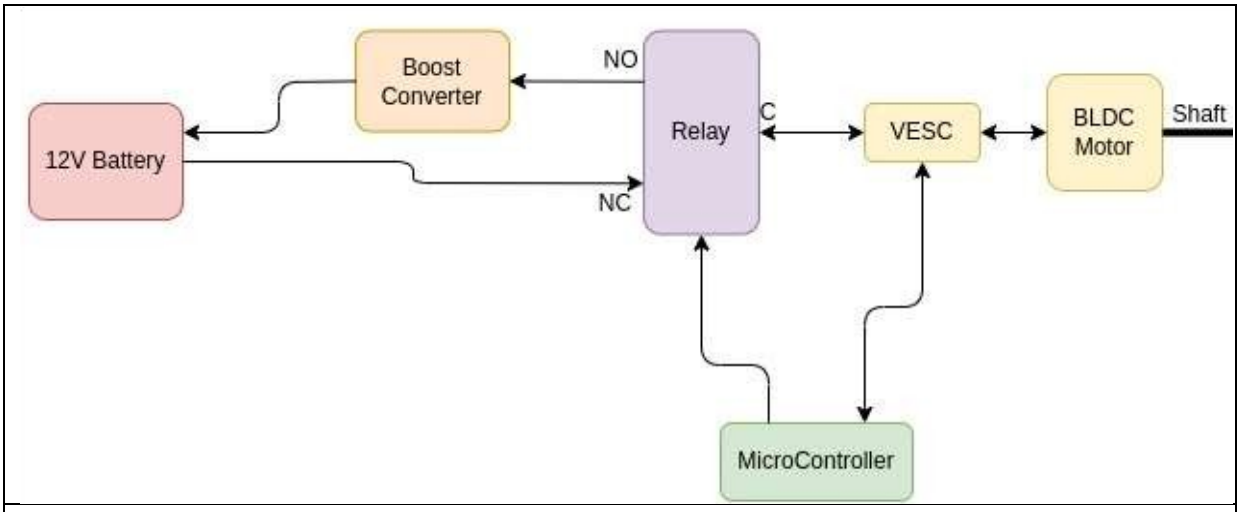

Figure 40. Power electronics for one oscillator. We have tested up to four used to charge the battery.

- **BLDC Motor:** M200 from blue Robotics has been ordered. It will be used as a generator. It is IP69 rated and hence can work subsea. It is designed to run in harsh ocean conditions. The operating voltages and current ranges are well within our prototype qualification before going into a medium sized VIVACE like the Detroit project.
- **Microcontroller:** Arduino Due has been selected.
- **Relay:** This is being selected and will be used to provide a kick-off if the oscillators stop due to either loss in flow velocity or any other unknown reasons.
- **Boost converters:** This is also being selected and will be used to provide the required amount of charging current to the batteries in order to ensure health of the battery.

Detailed connections of components.

M200 Motor: Input: Mechanical Shaft, Output: 3-phase AC power.

VESC: Input: Will be connected to the output 3 phase wires of the M200 Motor. Output: Battery to charge/discharge, Serial Communication with microcontroller.

Relay: 6 Pin Relay Module: 3 for low-level signals (Vcc to power the relay, ground and input), 3 for high-voltage signals (Com input, Open and close operation)

Boost Converter: Boosts the generated voltage from 5~13V to a steady 13V to charge the battery.

12V Battery: To store the energy and jump-start the system from a stand still.

Working:

The VESC is responsible for controlling the BLDC motor. It sends/ reads data to/ from the microcontroller. The microcontroller continuously monitors the system and takes appropriate decisions. During energy generation, the microcontroller triggers the relay, which connects the "COM" terminal to "NO".

Power flows from VESC->Relay->Boost Converter->Battery

When the Sync-Bar is not moving, the VESC is powered by the 12V battery. This energy is used to move the Sync-Bar to jump-start the system. Once we reach the desired velocity, the relay triggers and restores the energy harnessing.

M-200 Motor qualification process:

- Communication was accomplished between VESC and Microcontroller.
- Setup was qualified with a non-branded BLDC.
- M-200 motor from blue Robotics was used as a generator.
- A New design of VIVACE with 1x1 m dimensions was designed on Solidworks; with external pulley in order to increase the RPM's of the sync bar. M200 max efficiency spot lies between 1400 to 1600 RPM's.

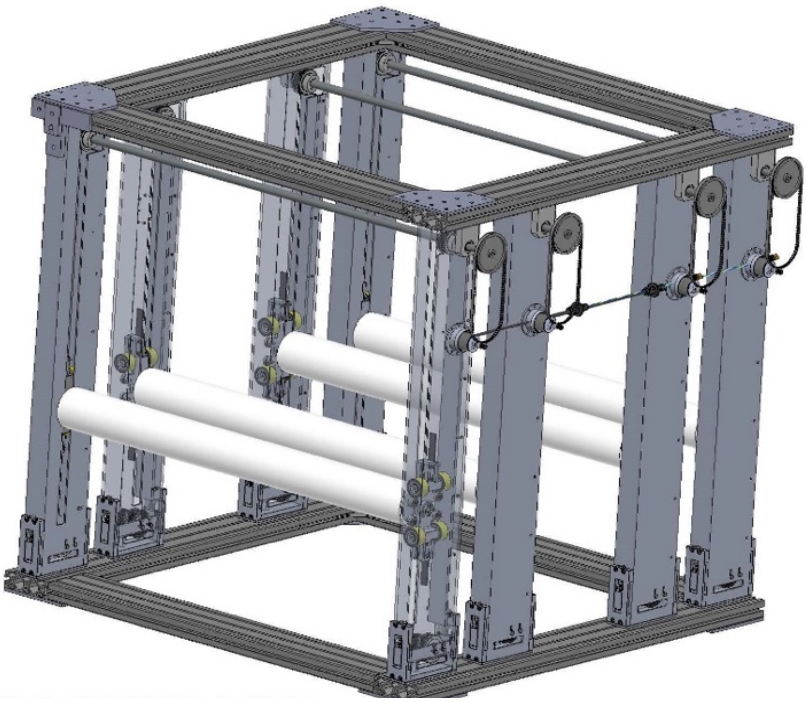

Figure 41. Four-cylinder Converter assembled with frequency increasing pulley-belt system. Not used in tests.

12. CFD Simulations

A full report on CFD with simulations of several cases is presented in Appendix IV.

13. FEA and Fatigue Analysis

A full report on FEA and Fatigue Analysis with simulations of several cases is presented in Appendix V.

14. Wet-Test Data Documentation

14.1. Two Days of Plain Hydrodynamic Observations; no data collection

Table 1: Day 0.a (June 5, 2024) tests for hydrodynamic interactions only. Tests were analyzed visually only. No measurements were made.
https://drive.google.com/drive/folders/1ZBaZk9jpTjzkukG1m5Gbr8II7OvANMph?usp=sharing

Run #	Flow Speed [m/s]	Push	OBSERVATIONS Cylinder			
			A	B	C	D
1	0.8	-	No motion	Small mot	No motion	Gallop
2	-0.8	-	VIV	VIV	No motion	Wake VIV
3	0.8	A	Galop	Galop	Stuck left	Stuck left
4	-0.8	A	Wake VIV	Wake VIV	Stuck left	Stuck left
5	0.8	B	Galop	Galop	Wake VIV	Wake VIV
6	-0.8	C	Wake VIV	Wake mot	Wake mot	No motion
7	0.8	B	Galop	Galop	Wake VIV	Wake VIV
8	-0.8	D	Stop	Line up	Line up	Line up
9	0.8	D	Galop	Galop	Small mot	Small mot
10	-0.8	D	Small mot	Line up	Line up	Line up
11	0.7	-	No motion	No motion	No motion	No motion
12	-0.7	-	Wake VIV	Wake VIV	Small mot	No motion
13	0.7	A	Galop	Galop/Trap	Galop/Trap	Galop/Trap
14	-0.7	A	VIV	VIV	VIV	Stuck left
15	0.7	B	Galop	Galop/Wake	Galop/Wake	Galop/Wake
16	-0.7	B	VIV	VIV	VIV	Stuck left
17	0.7	C	Galop	Galop/Wake	Galop/Wake	Galop/Wake
18	-0.7	C	Wake mot	Wake mot	Wake mot	Stuck left
19	0.7	D	Stuck center	Stuck center	Stuck center	Small galop
20	-0.7	D	Wake mot	Wake mot	Wake mot	Stuck left
21	0.9	-	No motion	No motion	No motion	Stuck left
22	-0.9	-	Wake	Wake	Wake mot	Stuck left
23	0.9	A	Galop	Wake galop	Wake galop	No motion
24	-0.9	A	No motion	No motion	Wake mot	No motion
25	0.9	B	Galop	Galop	Wake galop	Small motion
26	-0.9	B	No motion	No motion	No motion	No motion
27	0.9	C	Galop	Galop	Galop/Wake	Galop/Wake
28	-0.9	C	Galop	Galop	Small mot	Small mot
29	0.9	D	Galop	Galop	Small mot	Small mot
30	-0.9	D	No motion	No motion	No motion	No motion

Table 1: Day 0.a (CONTINUED) (June 5, 2024) tests for hydrodynamic interactions only. Tests were analyzed visually only. No measurements were made.
https://drive.google.com/drive/folders/1ZBaZk9jpTjzkukG1m5Gbr8II7OvANMph?usp=sharing

Run #	Flow Speed [m/s]	Push	OBSERVATIONS Cylinder			
			A	B	C	D
31	1.0	-	Galop	Galop	Small mot	Small mot
32	-1.0	-	VIV	VIV	VIV 0.5D	Small mot
33	1.0	-	Galop	Galop	Small mot	Small mot
34	-1.0	-	VIV	VIV	Small mot	Small mot
35	1.0	B				
36	-1.0	B				
37	1.0	C				
38	-1.0	C				
39	1.0	D				
40	-1.0	D				
41	1.1	-	Galop	Galop	Small mot	Small mot
42	-1.1	-	VIV	VIV	VIV 0.5D	Small mot
43	1.1	-	Galop	Galop	Small mot	Small mot
44	-1.1	-	VIV	VIV	Small mot	Small mot
45	1.1	B				
46	-1.1	B				
47	1.1	C				
48	-1.1	C				
49	1.1	D				
50	-1.1	D				
51	1.2	-	High turbulence; no change			
52	-1.2	-	High turbulence; no change			
53	1.2	-	High turbulence; no change			
54	-1.2	-	High turbulence; no change			
55	1.3	B				
56	-1.3	B				
57	1.3	C				
58	-1.3	C				
59	1.3	D				
60	-1.3	D				
61	1.0					
62	-1.0					
63	1.0					
64	-1.0					

Table 2: Day 0.b (June 6&7, 2024) tests for hydrodynamic interactions only. Videos are available in the Google.Drive. Tests were analyzed visually only. No measurements were made.
https://drive.google.com/drive/folders/1ZBaZk9jpTjzkukG1m5Gbr8II7OvANMph?usp=sharing

Table 1: Day 0.a (June 5, 2024) tests for hydrodynamic interactions only. Tests were analyzed visually only. No measurements were made.
https://drive.google.com/drive/folders/1ZBaZk9jpTjzkukG1m5Gbr8II7OvANMph?usp=sharing

Run #	Flow V [m/s] & U-Water Cam		Push	OBSERVATIONS Cylinder			
				A	B	C	D
61	1.0	#22	-	Galop	Galop	Less galop	Less galop
62	-1.0		-				
63	1.0		-	Galop	Galop	Less galop	Less galop
64	-1.0		-				
65	1.1	#23	-	Galop	Galop	Less galop	Less galop
66	-1.1		-				
67	1.1		-	Galop	Galop	Less galop	Less galop
68	-1.1		-				
69	1.2	#24	-	Galop	Galop	Less galop	Less galop
70	-1.2		-				
71	1.2		-	Galop	Galop	Less galop	Less galop
72	-1.2		-				
73	1.3	#25	-	Galop	Galop	Less galop	Less galop
74	-1.3		-				
75	1.3		-	Galop	Galop	Less galop	Less galop
76	-1.3		-				
77	1.4	#26	-	Galop	Galop	Less galop	Less galop
78	-1.4		-				
79	1.4		-	Galop	Galop	Less galop	Less galop
80	-1.4		-				
81	1.5	#27	-	Galop	Galop	Less galop	Less galop
82	-1.5		-				
83	1.5		-	Galop	Galop	Less galop	Less galop
84	-1.5		-				
85	1.6	#28	-	Galop	Galop	Less galop	Less galop
86	-1.6		-				
87	1.6		-	Galop	Galop	Less galop	Less galop
88	-1.6		-				
89	1.55	#29	-	Galop	Galop	Less galop	Less galop
90	-1.55		-				

Table 2: Day 0.b (CONTINUED) (June 6&7, 2024) tests for hydrodynamic interactions only. Tests were analyzed visually only. No measurements were made.
https://drive.google.com/drive/folders/1ZBaZk9jpTjzkukG1m5Gbr8II7OvANMph?usp=sharing

Run #	Flow Speed [m/s]		Push	OBSERVATIONS Cylinder			
				A	B	C	D
91	1.55		-	Galop	Galop	Less galop	Less galop
92	-1.55		-				
93	1.45	#30	-	Galop	Galop	Less galop	Less galop
94	-1.45		-				
95	1.45		-	Galop	Galop	Less galop	Less galop
96	-1.45		-				
97	1.35	#31	A	Galop	Galop	Less galop	Less galop
98	-1.35		-				
99	1.35		Staggered	Galop	Galop	Less galop	Less galop
100	-1.35		-				
101	1.25	#32	Staggered	Galop	Galop	Less galop	Less galop
102	-1.25		Staggered				
103	1.25		Staggered	Galop	Galop	Less galop	Less galop
104	-1.25		Staggered				
105	1.15	#33	A	Galop	Galop	Less galop	Less galop
106	-1.15		Staggered				
107	1.15		Staggered	Galop	Galop	Less galop	Less galop
108	-1.15		Staggered				
109	1.05	#34	Staggered	Galop	Galop	Less galop	Less galop
110	-1.05		Staggered				
111	1.05		Staggered	Galop	Galop	Less galop	Less galop
112	-1.05		Staggered				
113	0.95	#35	Staggered	Galop	Galop	Less galop	Less galop
114	-0.95		Staggered				
115	0.95		Staggered	Galop	Galop	Less galop	Less galop
116	-0.95		Staggered				
117	0.90	#36	Staggered	Galop	Galop	Less galop	Less galop
118	-0.90		Staggered				
119	0.90		Staggered	Galop	Galop	Less galop	Less galop
120	-0.90		Staggered				

Table 2: Day 0.b (CONTINUED) (June 6&7, 2024) tests for hydrodynamic interactions only. Tests were analyzed visually only. No measurements were made.
https://drive.google.com/drive/folders/1ZBaZk9jpTjzkukG1m5Gbr8II7OvANMph?usp=sharing

Run #	Flow Speed [m/s]		Push	OBSERVATIONS Cylinder			
				A	B	C	D
121	0.85	#37	Staggered	Gallop	Gallop	Weak mot	Weak mot
122	-0.85		Staggered				
123	0.85		Staggered	Gallop	Gallop	Weak mot	Weak mot
124	-0.85		Staggered				
125	0.80	#38	Staggered	Gallop	Gallop	Weak mot	Weak mot
126	-0.80		Staggered				
127	0.80		Staggered	Gallop	Gallop	Weak mot	Weak mot
128	-0.80		Staggered				
129	0.75	#39	A, B	Gallop	Gallop	Rear interference	
130	-0.75						
131	0.75		No need for staggering if we push C, D out of the wake				
132	-0.75						
133	0.70	#40	A, B	Gallop	Gallop	Rear interference	
134	-0.70			Weak mot	Weak mot	Weak mot	No motion
135	0.70			Gallop	Gallop	Rear interference	
136	-0.70			Weak mot	Weak mot	Weak mot	No motion
137	0.65	#41	Stagger A,B				
138	-0.65						
139	0.65		NEED SPRINGS BELOW FOR FLOW SPEED LESS THAN 0.70m/s				
140	-0.65						
141	0.60	#42					
142	-0.60						
143	0.60		NEED SPRINGS BELOW FOR FLOW SPEED LESS THAN 0.70m/s				
144	-0.60						

14.2. Five Days of Wet-Tests with Power Electronics: Sorted by Day

Postprocessing of several wet-test cases are provided in Chapter 15. Sample graphs from Google Drive follow as summarized in Table 3. Graphs and videos are available at:

https://drive.google.com/drive/folders/1ZBaZk9jpTjzkukG1m5Gbr8II7OvANMph?usp=sharing

Table 3: Day 1 tests. Postprocessing of several cases in Chapter 13. Sample graphs from Google-Drive follow. Graphs and Videos in Google-Drive

DAY 1: DUMB SYSTEM

Trial #	Flow Speed (m/s)	Electronics Configuration Figure #	Date	Cylinder(s)	Observations	Video: Surface	Video: Under-water
1	1	1	June 11th, 11:06 A.M.	A		Yes	
2	1	1	June 11th, 11:09 A.M.	A		Yes	
3	1.5	1	June 11th, 11:26 A.M.	A	**See Figure 42**	Yes	
4	1.5	1	June 11th, 11:29 A.M.	A		Yes	
5	1.5	1	June 11th, 11:33 A.M.		NO DATA	Yes	
6	1.5	1	June 11th, 11:37 A.M.	A		Yes	
7	1.5	1	June 11th, 1:29 P.M.	A		No	
8	1.5	2	June 11th, 1:44 P.M.	B		No	
9	1.5	2	June 11th, 1:56 P.M.	A		No	
10	1.5	3	June 11th, 2:11 P.M.	A+B		No	
11	1.5	4	June 11th, 2:38 P.M.	A+B	**See Figure 43**	Yes	
12	1.5	4	June 11th, 2:45 P.M.	A+B		Yes	
13	1.5	4	June 11th, 2:50 P.M.	A+B		Yes	
14	1.5	5	June 11th, 2:59 P.M.		NO DATA (Charge Controller couldn't charge)	Yes	
15	1.5	5	June 11th, 3:10 P.M.		NO DATA	Yes	
16	1.5	5	June 11th, 3:21 P.M.		NO DATA	Yes	
17	1.5	5	June 11th, 3:34 P.M.		NO DATA	Yes	

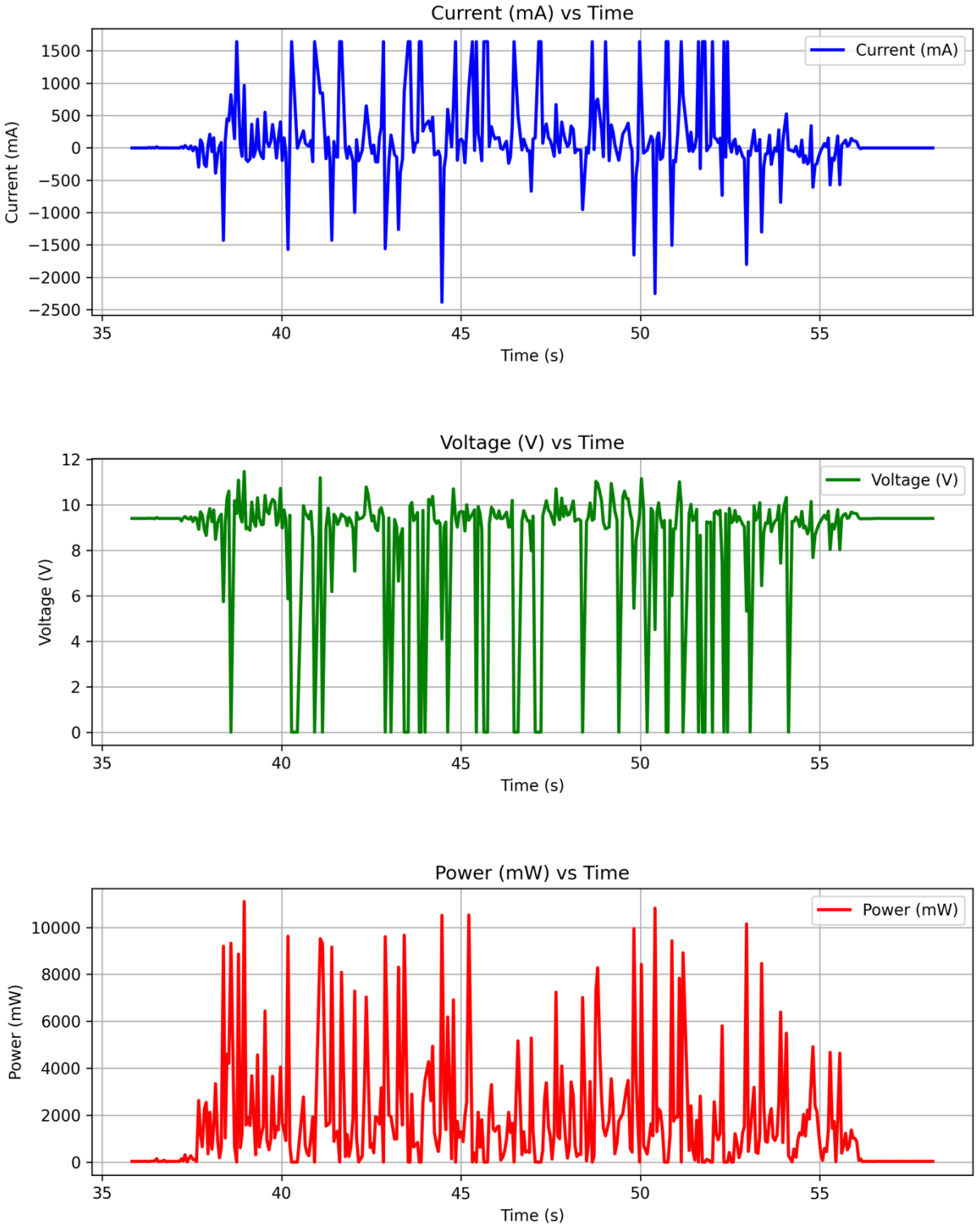

Figure 42. Day 1, Trial #3. See Google Drive

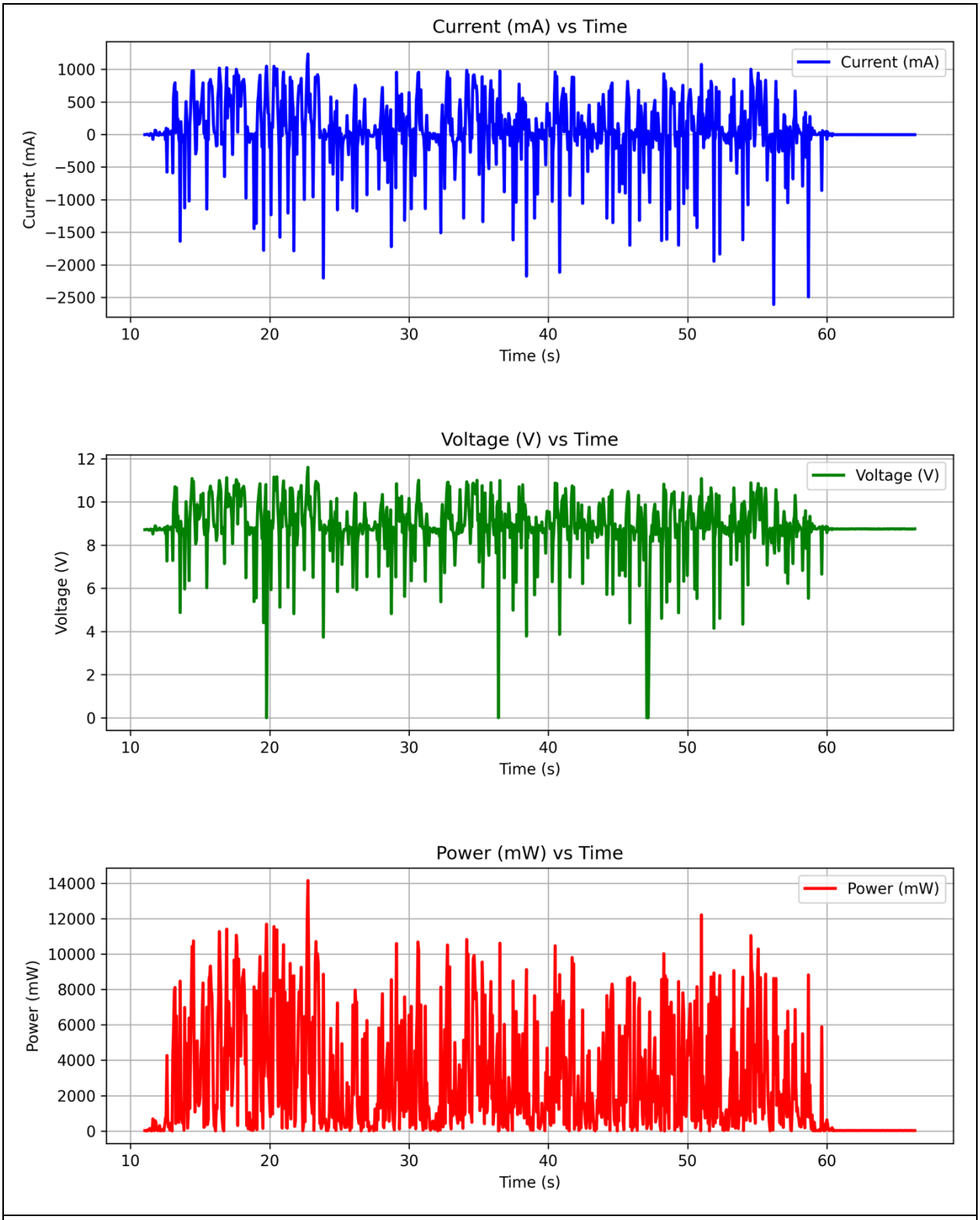

Figure 43. Day 1, Trial #11. See Google Drive

https://drive.google.com/drive/folders/1ZBaZk9jpTjzkukG1m5Gbr8II7OvANMph?usp=sharing

Table 4: Day 2 tests. Postprocessing of several cases in Chapter 15

DAY 2: DUMB SYSTEM

Trial #	Flow Speed (m/s)	Electronics Configuration Figure #	Date	Cylinder(s)	Observations	Video: Surface	Video: Under-water
1	1.5	1	June 13th, 1:22 P.M.	A		No	
2	1.5	2	June 13th, 1:30 P.M.	A		No	
3	1.5	1	June 13th, 1:38 P.M.	A		Yes	
4	1.5	2	June 13th, 2:01 P.M.	A		No	
5	1.5	2	June 13th, 2:13 P.M.	A		Yes	
6	1.4	2	June 13th, 2:17 P.M.	A		Yes	
7	1.4	2	June 13th, 2:24 P.M.	A		Yes	
8	1.3	2	June 13th, 2:30 P.M.	A		Yes	
9	1.2	2	June 13th, 2:37 P.M.	A		Yes	
10	1.1	2	June 13th, 2:42 P.M.	A		Yes	
11	1	2	June 13th, 2:48 P.M.	A	**See Figure 44**	Yes	
12	0.9	2	June 13th, 2:54 P.M.	A		Yes	
13	0.9	2	June 13th, 3:00 P.M.	A		Yes	
14	0.8	2	June 13th, 3:09 P.M.	A		Yes	
15	1.5	6	June 13th, 3:16 P.M.	A		Yes	
16	1	6	June 13th, 3:20 P.M.	A	**See Figure 45**	Yes	
17	1	6	June 13th, 3:25 P.M.		NO DATA	Yes	

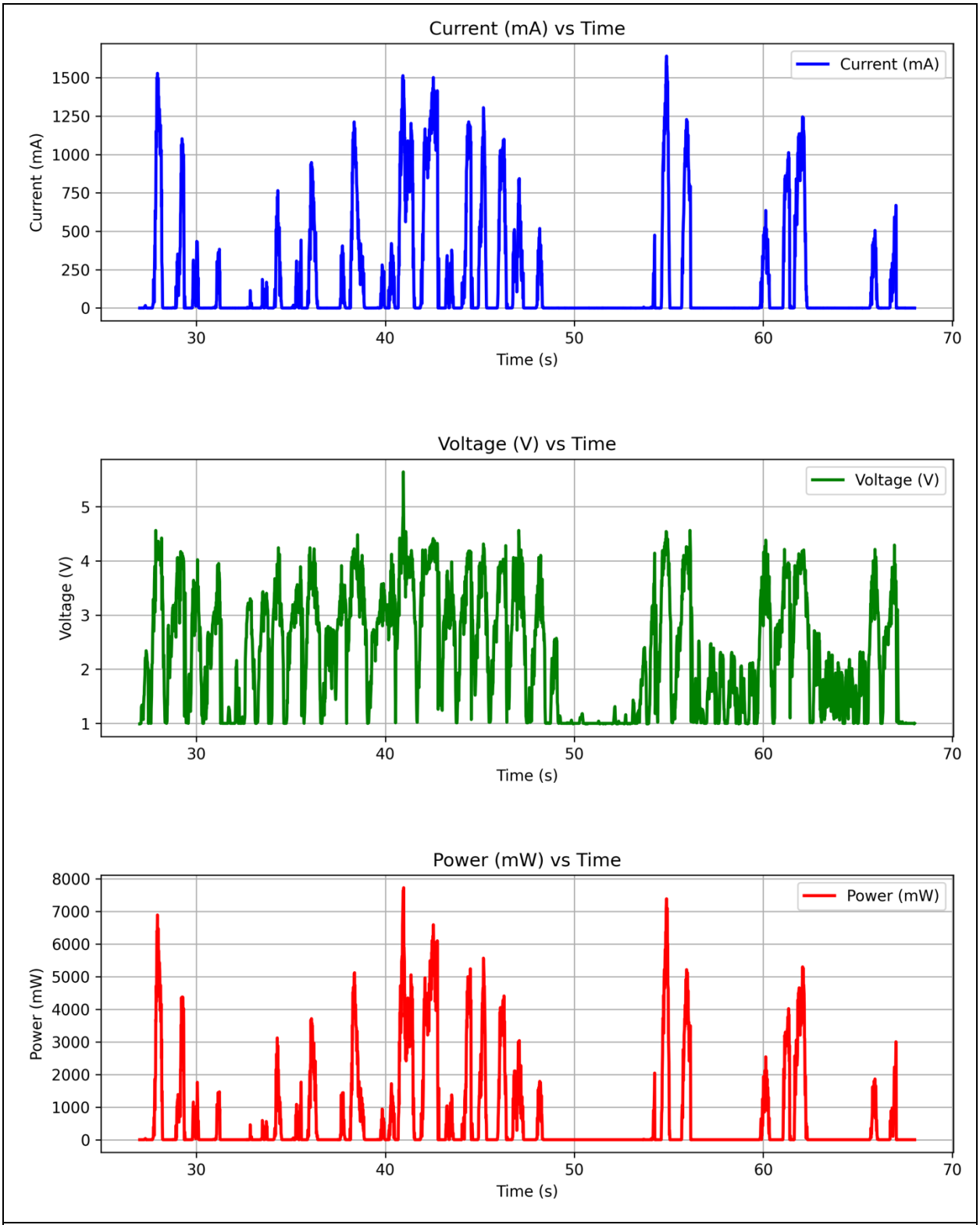

Figure 44. Day 2, Trial #11. See Google Drive

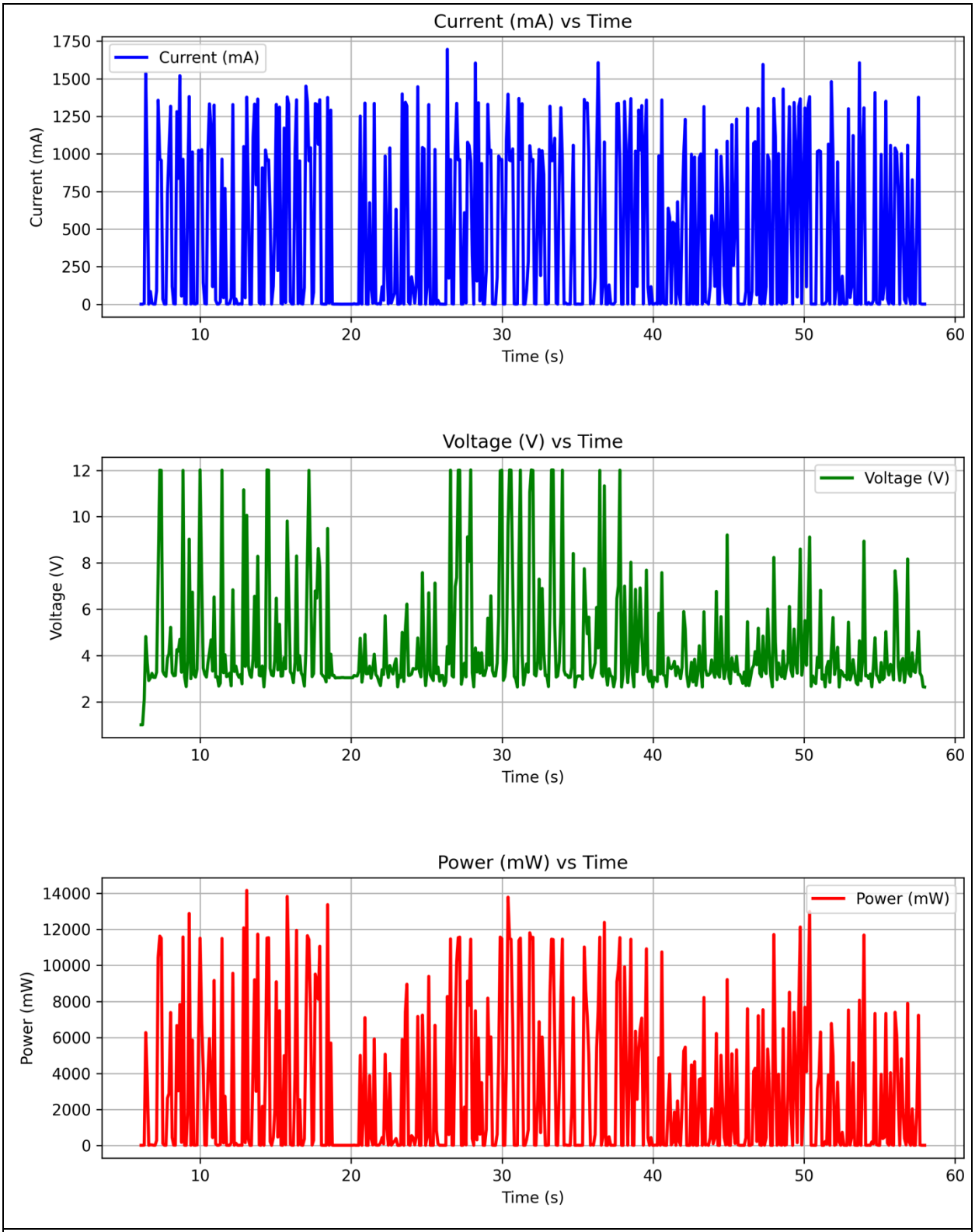

Figure 45. Day 2, Trial #16. See Google Drive

https://drive.google.com/drive/folders/1ZBaZk9jpTjzkukG1m5Gbr8II7OvANMph?usp=sharing

Table 5: Day 3 tests. Postprocessing of several cases in Chapter 15

DAY 3: SMART SYSTEM								
Trial #	Flow Speed (m/s)	Electronics Configuration Figure #	Date	Cylinder(s)	Features	Observations	Video: Surface	Video: Under-water
1	0.7	7	June 14th, 1:41 P.M.	A	Kickstart		Yes	
2	0.7	7	June 14th, 1:50 P.M.	A	Kickstart		Yes	
3	0.65	7	June 14th, 1:59 P.M.	A	Kickstart		Yes	
4	0.6	7	June 14th, 2:05 P.M.	A	Kickstart		Yes	
5	0.55	7	June 14th, 2:13 P.M.	A	Kickstart		Yes	
6	0.5	7	June 14th, 2:30 P.M.	A	Kickstart		Yes	
7	1	7	June 14th, 2:39 P.M.	A	Kickstart	**See Figure 46**	Yes	
8	1	7	June 14th, 2:43 P.M.	A		**See Figure 47**	Yes	
9	1	7	June 14th, 2:47 P.M.		Kickstart	NO DATA	Yes	
10	1.5	7	June 14th, 2:54 P.M.		Kickstart	NO DATA	Yes	
11	1.5	7	June 14th, 2:58 P.M.	A	Kickstart		Yes	
12	1.5	7	June 14th, 3:13 P.M.	A	Kickstart, beta = 301		Yes	
13	1.5	7	June 14th, 3:18 P.M.	A	Kickstart, beta = 50		Yes	
14	1.5	7	June 14th, 3:25 P.M.	A	Kickstart, Braking Current = 0.5A	BEST RUN **See Figure 48**	Yes	
15	1.5	7	June 14th, 3:28 P.M.	A	Kickstart, Braking Current = 1A		Yes	

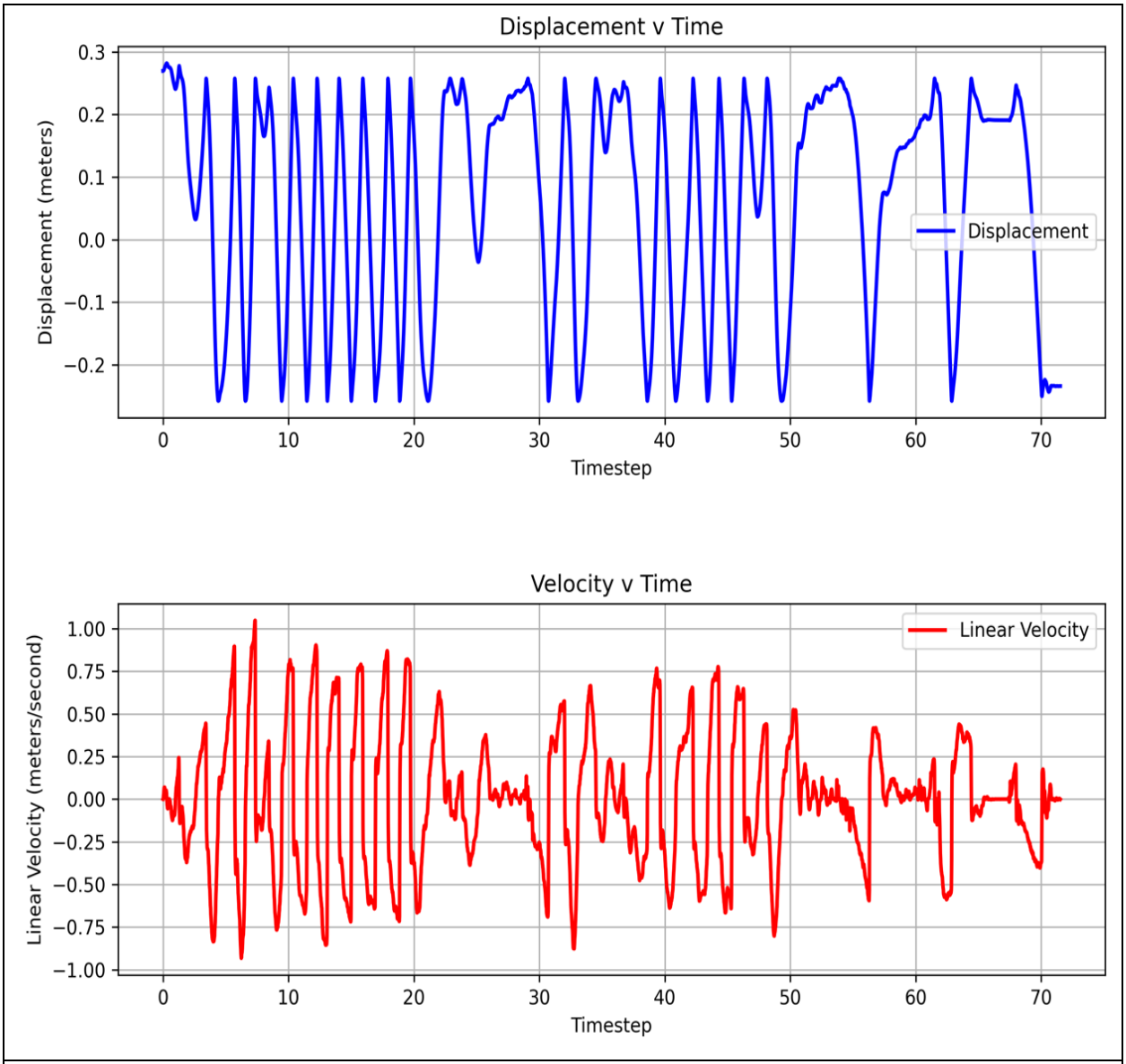

Figure 46. Day 3, Trial #7. See Google Drive

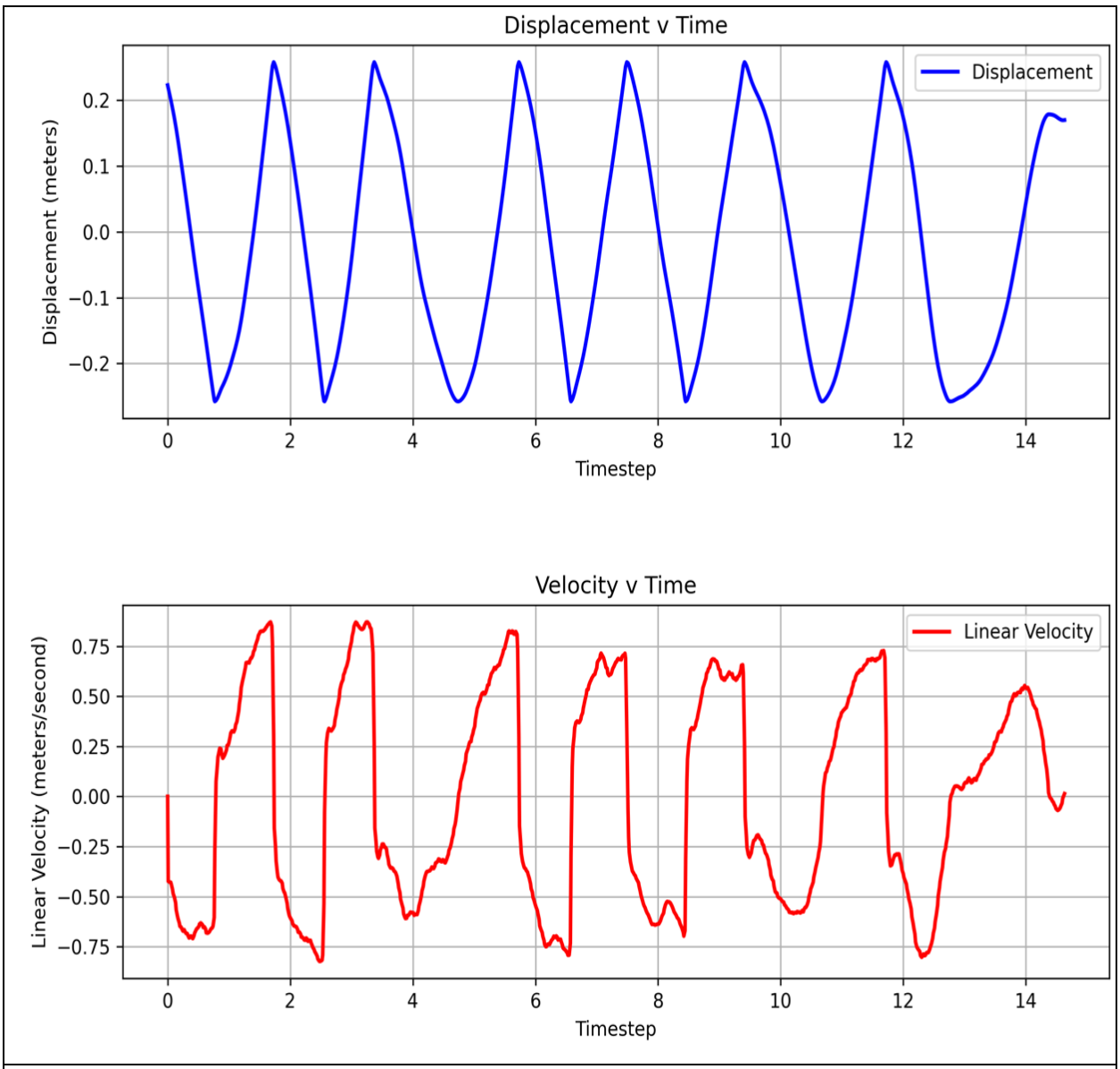

Figure 47. Day 3, Trial #8. See Google Drive

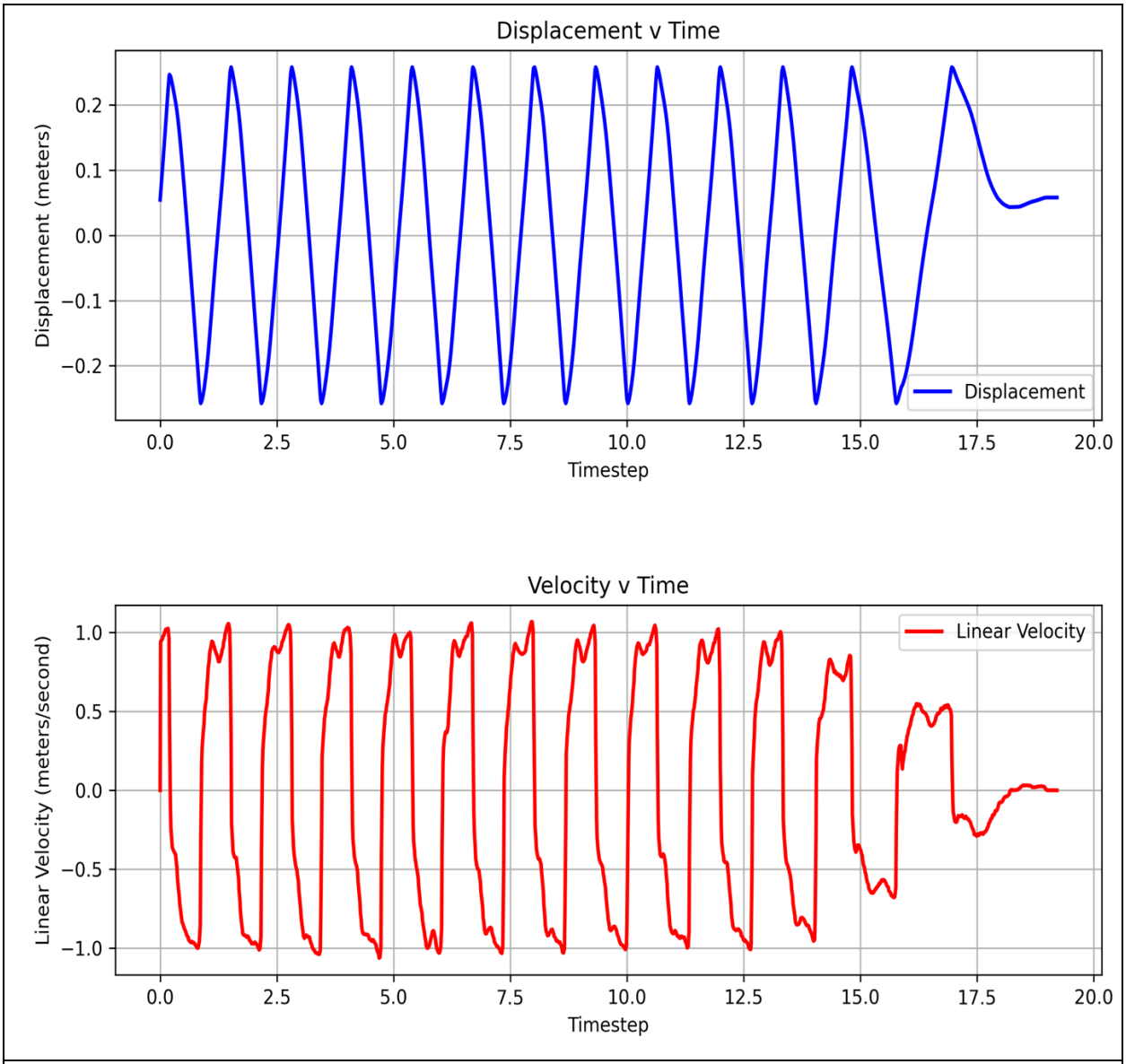

Figure 48. Day 3, Trial #14 (BEST RUN). See Google Drive

https://drive.google.com/drive/folders/1ZBaZk9jpTjzkukG1m5Gbr8II7OvANMph?usp=sharing

Table 6: Day 4 tests. Postprocessing of several cases in Chapter 15

DAY 4: SMART SYSTEM								
Trial #	Flow Speed (m/s)	Electronics Configuration Figure #	Date	Cylinder(s)	Features	Observations	Video: Surface	Video: Under-water
1	1.5	7	June 17th, 2:14 P.M.		k = 10	NO DATA	Yes	
2	1.5	7	June 17th, 2:23 P.M.	A	k = 10		Yes	
3	1.5	7	June 17th, 2:37 P.M.	A	k = 50		Yes	
4	1.5	7	June 17th, 2:49 P.M.	A	k = 100		Yes	
5	1	7	June 17th, 2:56 P.M.	A	k = 10	NO DATA	Yes	
6	1	7	June 17th, 3:02 P.M.	A	k = 10	NO DATA	Yes	
7	1.5	7	June 17th, 3:27 P.M.	A	b = 50	**See Figure 49**	Yes	
8	1.5	7	June 17th, 3:30 P.M.	A	k = 40	**See Figure 50**	Yes	

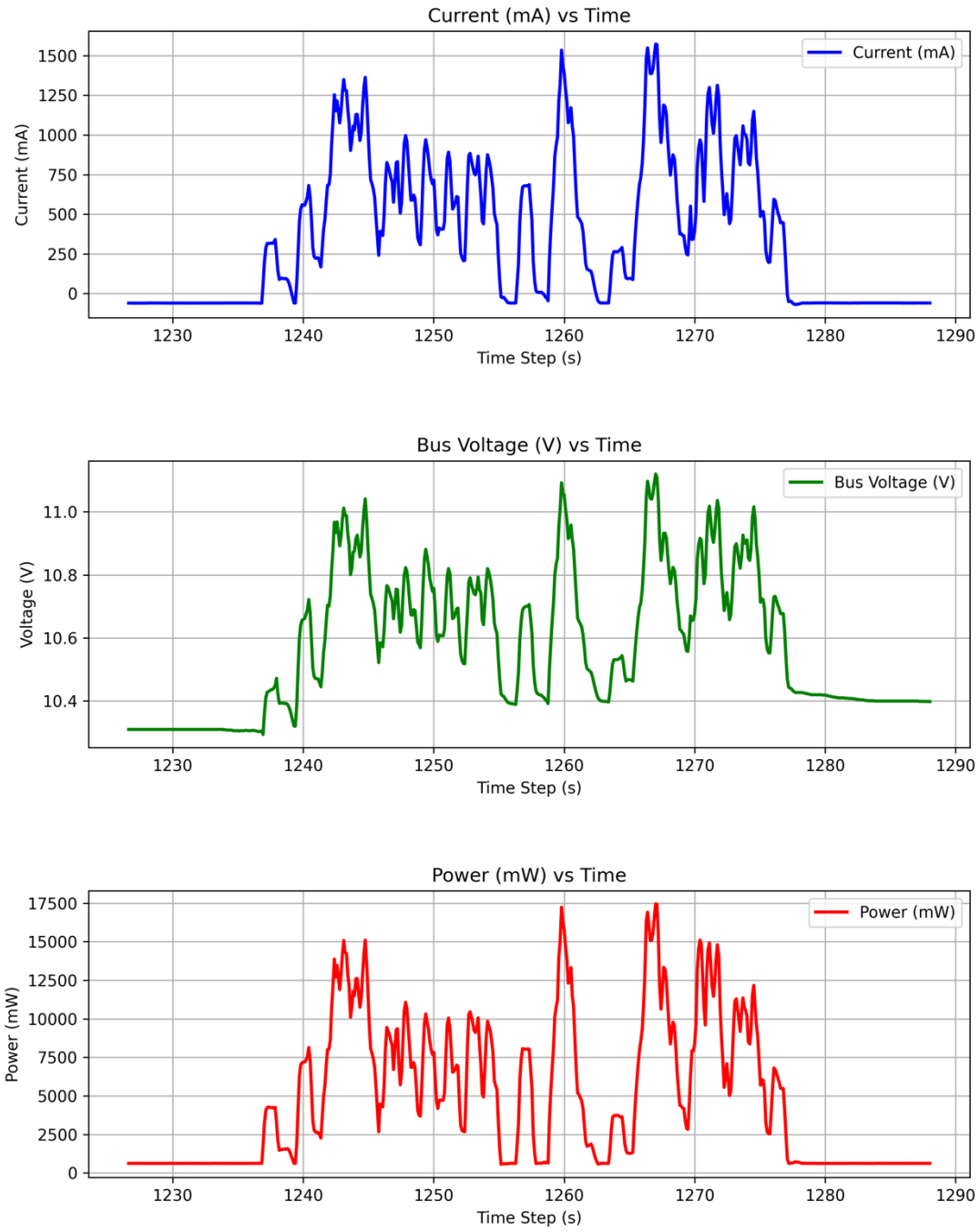

Figure 49. Day 4, Trial #7. See Google Drive

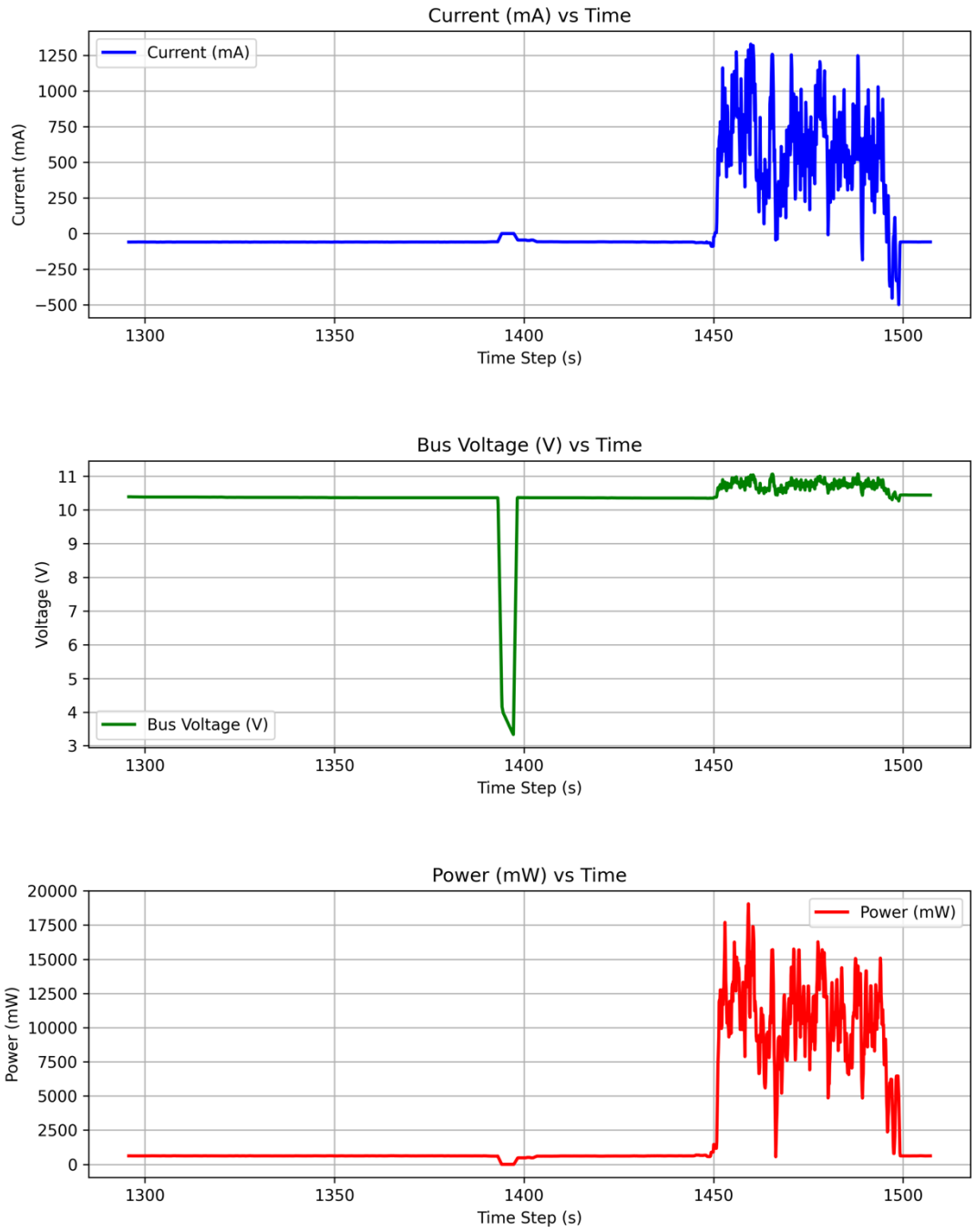

Figure 50. Day 4, Trial #8. See Google Drive

https://drive.google.com/drive/folders/1ZBaZk9jpTjzkukG1m5Gbr8II7OvANMph?usp=sharing

Table 7: Day 3 tests. Postprocessing of several cases in Chapter 15

DAY 5: SMART SYSTEM								
Trial #	Flow Speed (m/s)	Electronics Configuration Figure #	Date	Cylinder(s)	Features	Observations	Video: Surface	Video: Under-water
1	1.5	7	June 18th, 11:59 P.M.		Kickstart, k = 40	NO DATA	Yes	
2	1.5	7	June 18th, 2:00 P.M.	A	Kickstart		No	
3	1.5	7	June 18th, 2:04 P.M.	A	Kickstart		No	
4	1.4	7	June 18th, 2:31 P.M.	A	Kickstart		Yes	
5	1.3	7	June 18th, 2:35 P.M.	A	Kickstart		Yes	
6	1.2	7	June 18th, 2:39 P.M.	A	Kickstart		Yes	
7	1.1	7	June 18th, 2:43 P.M.	A	Kickstart		Yes	
8	0.9	7	June 18th, 2:51 P.M.	A	Kickstart	**See Figure 51**	Yes	
9	0.8	7	June 18th, 2:55 P.M.	A	Kickstart	**See Figure 52**	Yes	
10	1	7	June 18th, 3:01 P.M.	A	Kickstart, b = 1		Yes	
11	0.9	7	June 18th, 3:05 P.M.		Kickstart, b = 1	NO DATA	Yes	
12	1.3	7	June 18th, 3:13 P.M.	A	Kickstart, b = 20		Yes	
13	1.5	7	June 18th, 3:24 P.M.	A	Kickstart, b = 50		Yes	
14	1.3	1	June 18th, 3:27 P.M.			NO DATA	Yes	

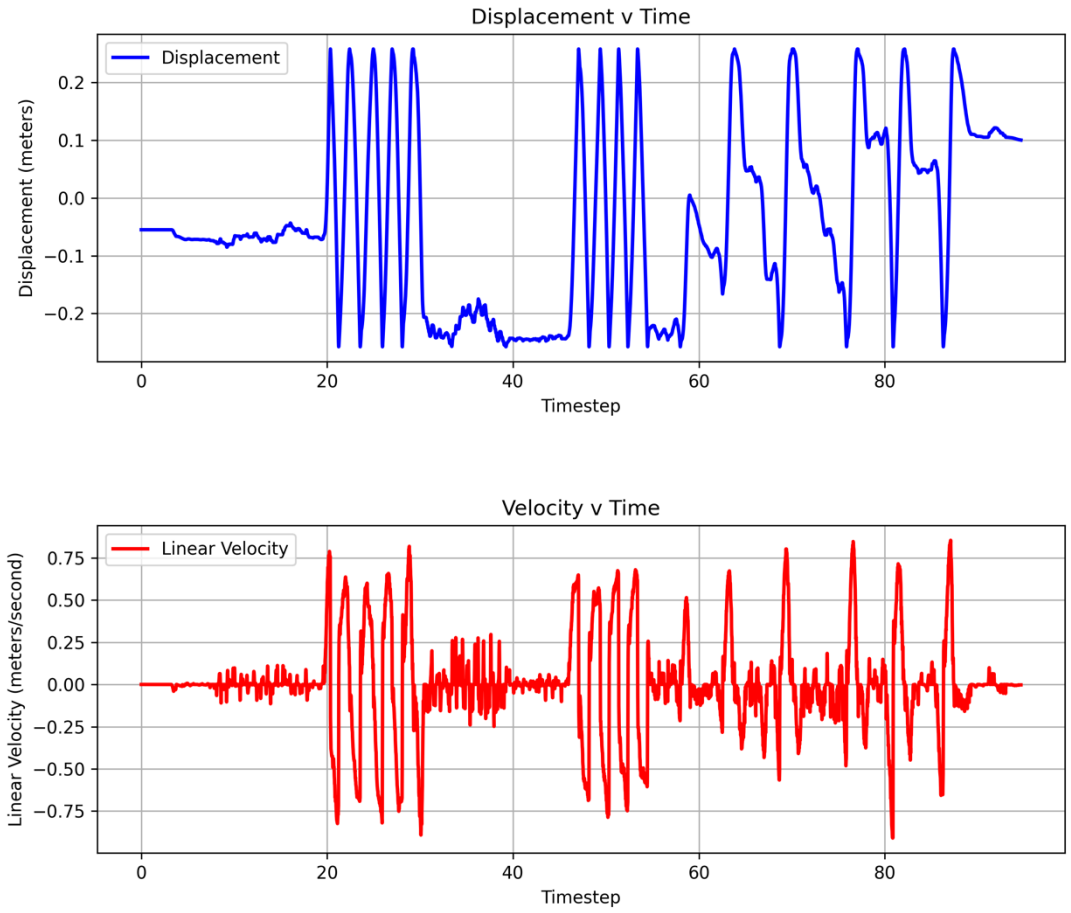

Figure 51. Day 5, Trial #8. See Google Drive

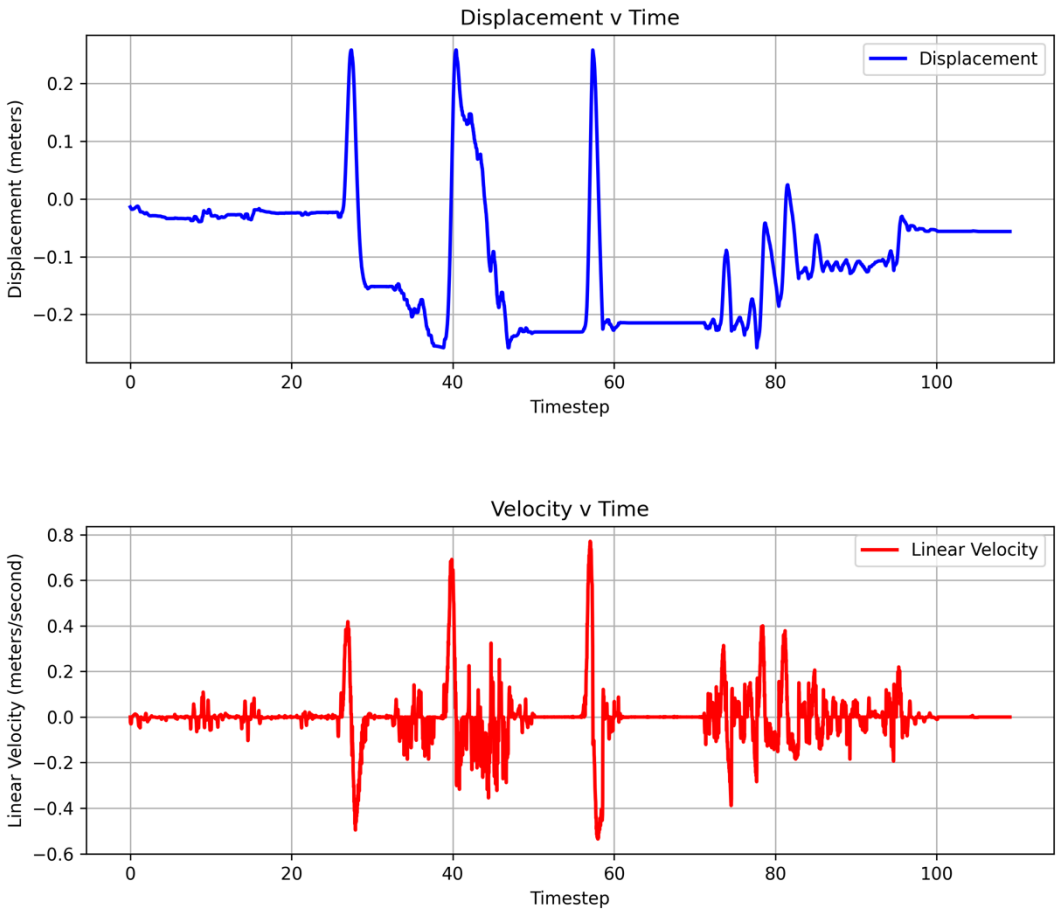

Figure 52. Day 5, Trial #9. See Google Drive

14.3. Five Days of Wet-Tests with Power Electronics: Sorted by Configuration

NOTE #1: For all configurations, we were generating power through a 100W 3-phase alternator which will be referred to as "the generator".

NOTE #2: For all configurations, the "battery" can be thought of as a 12V lead acid battery with the following parameters: 33Ah (Ampere-Hour) and 6 cells.

Configuration #1:
Rectifier: In this set up, we used the rectifiers as a way of converting the alternating current to direct current. This was needed in order to charge the battery as well as record how much current is passing through the battery.
DC-DC Booster: Because our battery voltage was typically 10V or higher, we needed more than the battery voltage to be able to charge the battery. At low speeds, this voltage level was not reached; hence, the use of a DC-DC booster with the following parameters was used: Input (7-12V), Output (12V).
Current Sensor + Arduino: A current sensor, the INA219 which contains a 0.1 Ohm resistor, was connected in series between the output of the DC-DC booster and the battery which recorded both current flowing into the battery as well as voltage levels.

Configuration #2:
Bulb: A 13W, 12V DC bulb was used in replacement of the DC-DC Booster and battery. The bulb acted as a method of closing the circuit and allowed for a direct connected from the output of the rectifier. This proved to be quite beneficial for simplifying the circuit/electronics since a booster was no longer needed to reach the minimum voltage that the battery required.

Configuration #3:
Rectifiers in parallel: As an attempt to measure the combined power output, we had connected the rectifiers in parallel in hopes that the currents from both generators would sum up and we would get the total output from both generators. However, since the generators cannot produce the exact same power at the exact same time, this created a voltage imbalance. The voltage imbalance caused a much larger current imbalance between the diodes inside one of the rectifiers and the diodes inside the other rectifier. This led to a noticeable interference with the motion of the cylinders.

Configuration #4:
Rectifiers in Series: Connecting the rectifiers in series was used as a method to sum the voltages produced by each generator and receive the total power output at the output of the rectifiers.

Configuration #5:
Charge Controller: An AC-DC Charge Controller was used in replacement of the rectifier allowing the Charge Controller to be directly connected between the generator and the battery. This was used as experimentation to see if there would be any difference with previous configurations

(Configuration #1 and Configuration #2). However, due to the charge controller requiring too high of an input voltage, we were not able to measure any output from the charge controller.

Configuration #6:
A bulb was used in this configuration in replacement of the battery from configuration #1. This was done in order to send and record a smoother output and proved to be quite an effective setup.

Configuration #7:
VESC: The VESC (Vedder Electronic Speed Controller) had multipurpose use. First, the VESC took in AC input and DC output which meant we no longer needed devices such as an AC-DC rectifier. Second, the VESC enabled collection of data such as RPM of the generator, current going into the battery, watt-hours charged, etc. Third, the VESC allowed current to be sent to the motor allowing for the implementation of the kickstart system and the virtual spring system. Fourth and most importantly, with the VESC we were able to implement adaptive damping through the use of regenerative braking. In our case, regenerative braking took the form of the slowing of the generator's speed (braking) and converting this kinetic energy into electrical power by outputting current directly from the VESC to the battery. This proved beneficial for the motion of the cylinders, the overall power generated, and the battery health.

https://drive.google.com/drive/folders/1ZBaZk9jpTjzkukG1m5Gbr8II7OvANMph?usp=sharing

Table 8: Cross-listing of tests classified by parameters

POWER ELECTRONICS CONFIGURATION #1 (see Figure 53)

Trial #	Flow Speed (m/s)	Date	Cylinder(s)	Observations	Video: Surface	Video: Under-water
Day 1, Trial #1	1	June 11th, 11:06 A.M.	A		Yes	
Day 1, Trial #2	1	June 11th, 11:09 A.M.	A		Yes	
Day 1, Trial #3	1.5	June 11th, 11:26 A.M.	A		Yes	
Day 1, Trial #4	1.5	June 11th, 11:29 A.M.	A		Yes	
Day 1, Trial #5	1.5	June 11th, 11:33 A.M.		NO DATA	Yes	
Day 1, Trial #6	1.5	June 11th, 11:37 A.M.	A		Yes	
Day 1, Trial #7	1.5	June 11th, 1:29 P.M.	A		No	
Day 2, Trial #1	1.5	June 13th, 1:22 P.M.	A		No	
Day 2, Trial #3	1.5	June 13th, 1:38 P.M.	A		Yes	
Day 5, Trial #14	1.3	June 18th, 3:27 P.M.		NO DATA	Yes	

https://drive.google.com/drive/folders/1ZBaZk9jpTjzkukG1m5Gbr8II7OvANMph?usp=sharing

Table 9: Cross-listing of tests classified by parameters

POWER ELECTRONICS CONFIGURATION #2 (see Figure 54)

Trial #	Flow Speed (m/s)	Date	Cylinder(s)	Observations	Video: Surface	Video: Under-water
Day 1, Trial #8	1.5	June 11th, 1:44 P.M.	B		No	
Day 1, Trial #9	1.5	June 11th, 1:56 P.M.	A		No	
Day 2, Trial #2	1.5	June 13th, 1:30 P.M.	A		No	
Day 2, Trial#4	1.5	June 13th, 2:01 P.M.	A		No	
Day 2, Trial #5	1.5	June 13th, 2:13 P.M.	A		Yes	
Day 2, Trial #6	1.4	June 13th, 2:17 P.M.	A		Yes	
Day 2, Trial #7	1.4	June 13th, 2:24 P.M.	A		Yes	
Day 2, Trial #8	1.3	June 13th, 2:30 P.M.	A		Yes	
Day 2, Trial #9	1.2	June 13th, 2:37 P.M.	A		Yes	
Day 2, Trial #10	1.1	June 13th, 2:42 P.M.	A		Yes	
Day 2, Trial #11	1	June 13th, 2:48 P.M.	A		Yes	
Day 2, Trial #12	0.9	June 13th, 2:54 P.M.	A		Yes	
Day 2, Trial #13	0.9	June 13th, 3:00 P.M.	A		Yes	
Day 2, Trial #14	0.8	June 13th, 3:09 P.M.	A		Yes	

https://drive.google.com/drive/folders/1ZBaZk9jpTjzkukG1m5Gbr8II7OvANMph?usp=sharing

Table 10: Cross-listing of tests classified by parameters

POWER ELECTRONICS CONFIGURATION #3 (see Figure 55)

Trial #	Flow Speed (m/s)	Date	Cylinder(s)	Observations	Video: Surface	Video: Under-water
Day 1, Trial #9	1.5	June 11th, 2:11 P.M.	A+B		No	

https://drive.google.com/drive/folders/1ZBaZk9jpTjzkukG1m5Gbr8II7OvANMph?usp=sharing

Table 11: Cross-listing of tests classified by parameters

POWER ELECTRONICS CONFIGURATION #4 (see Figure 56)

Trial #	Flow Speed (m/s)	Date	Cylinder(s)	Observations	Video: Surface	Video: Under-water
Day 2, Trial #11	1.5	June 11th, 2:38 P.M.	A+B		Yes	
Day 2, Trial #12	1.5	June 11th, 2:45 P.M.	A+B		Yes	
Day 2, Trial #13	1.5	June 11th, 2:50 P.M.	A+B		Yes	

https://drive.google.com/drive/folders/1ZBaZk9jpTjzkukG1m5Gbr8II7OvANMph?usp=sharing

Table 12: Cross-listing of tests classified by parameters

POWER ELECTRONICS CONFIGURATION #5 (see Figure 57)						
Trial #	Flow Speed (m/s)	Date	Cylinder(s)	Observations	Video: Surface	Video: Under-water
Day 1, Trial #14	1.5	June 11th, 2:59 P.M.		NO DATA (Charge Controller couldn't charge)	Yes	
Day 1, Trial #15	1.5	June 11th, 3:10 P.M.		NO DATA	Yes	
Day 1, Trial #16	1.5	June 11th, 3:21 P.M.		NO DATA	Yes	
Day 1, Trial #17	1.5	June 11th, 3:34 P.M.		NO DATA	Yes	

https://drive.google.com/drive/folders/1ZBaZk9jpTjzkukG1m5Gbr8II7OvANMph?usp=sharing

Table 13: Cross-listing of tests classified by parameters

POWER ELECTRONICS CONFIGURATION #6 (see Figure 58)

Trial #	Flow Speed (m/s)	Date	Cylinder(s)	Observations	Video: Surface	Video: Under-water
Day 2, Trial #15	1.5	June 13th, 3:16 P.M.	A		Yes	
Day 2, Trial #16	1	June 13th, 3:20 P.M.	A		Yes	
Day 2, Trial #17	1	June 13th, 3:25 P.M.		NO DATA	Yes	

https://drive.google.com/drive/folders/1ZBaZk9jpTjzkukG1m5Gbr8II7OvANMph?usp=sharing

Table 14: Cross-listing of tests classified by parameters

POWER ELECTRONICS CONFIGURATION #7 (see Figure 59)

Trial #	Flow Speed (m/s)	Date	Cylinder(s)	Features	Observations	Video: Surface	Video: Under-water
Day 3, Trial #1	0.7	June 14th, 1:41 P.M.	A	Kickstart		Yes	
Day 3, Trial #2	0.7	June 14th, 1:50 P.M.	A	Kickstart		Yes	
Day 3, Trial #3	0.65	June 14th, 1:59 P.M.	A	Kickstart		Yes	
Day 3, Trial #4	0.6	June 14th, 2:05 P.M.	A	Kickstart		Yes	
Day 3, Trial #5	0.55	June 14th, 2:13 P.M.	A	Kickstart		Yes	
Day 3, Trial #6	0.5	June 14th, 2:30 P.M.	A	Kickstart		Yes	
Day 3, Trial #7	1	June 14th, 2:39 P.M.	A	Kickstart		Yes	
Day 3, Trial #8	1	June 14th, 2:43 P.M.	A			Yes	
Day 3, Trial #9	1	June 14th, 2:47 P.M.		Kickstart	NO DATA	Yes	
Day 3, Trial #10	1.5	June 14th, 2:54 P.M.		Kickstart	NO DATA	Yes	
Day 3, Trial #11	1.5	June 14th, 2:58 P.M.	A	Kickstart		Yes	
Day 3, Trial #12	1.5	June 14th, 3:13 P.M.	A	Kickstart, beta = 301		Yes	
Day 3, Trial #13	1.5	June 14th, 3:18 P.M.	A	Kickstart, beta = 50		Yes	
Day 3, Trial #14	1.5	June 14th, 3:25 P.M.	A	Kickstart, Braking Current = 0.5A	BEST RUN	Yes	
Day 3, Trial #15	1.5	June 14th, 3:28 P.M.	A	Kickstart, Braking Current = 1A		Yes	
Day 4, Trial #1	1.5	June 17th, 2:14 P.M.		k = 10	NO DATA	Yes	
Day 4, Trial #2	1.5	June 17th, 2:23 P.M.	A	k = 10		Yes	

Day 4, Trial #3	1.5	June 17th, 2:37 P.M.	A	k = 50		Yes	
Day 4, Trial #4	1.5	June 17th, 2:49 P.M.	A	k = 100		Yes	
Day 4, Trial #5	1	June 17th, 2:56 P.M.	A	k = 10	NO DATA	Yes	
Day 4, Trial #6	1	June 17th, 3:02 P.M.	A	k = 10	NO DATA	Yes	
Day 4, Trial #7	1.5	June 17th, 3:27 P.M.	A	b = 50		Yes	
Day 4, Trial #8	1.5	June 17th, 3:30 P.M.	A	k = 40		Yes	
Day 5, Trial #1	1.5	June 18th, 11:59 P.M.		Kickstart, k = 40	NO DATA	Yes	
Day 5, Trial #2	1.5	June 18th, 2:00 P.M.	A	Kickstart		No	
Day 5, Trial #3	1.5	June 18th, 2:04 P.M.	A	Kickstart		No	
Day 5, Trial #4	1.4	June 18th, 2:31 P.M.	A	Kickstart		Yes	
Day 5, Trial #5	1.3	June 18th, 2:35 P.M.	A	Kickstart		Yes	
Day 5, Trial #6	1.2	June 18th, 2:39 P.M.	A	Kickstart		Yes	
Day 5, Trial #7	1.1	June 18th, 2:43 P.M.	A	Kickstart		Yes	
Day 5, Trial #8	0.9	June 18th, 2:51 P.M.	A	Kickstart		Yes	
Day 5, Trial #9	0.8	June 18th, 2:55 P.M.	A	Kickstart		Yes	
Day 5, Trial #10	1	June 18th, 3:01 P.M.	A	Kickstart, b = 1		Yes	
Day 5, Trial #11	0.9	June 18th, 3:05 P.M.		Kickstart, b = 1	NO DATA	Yes	
Day 5, Trial #12	1.3	June 18th, 3:13 P.M.	A	Kickstart, b = 20		Yes	
Day 5, Trial #13	1.5	June 18th, 3:24 P.M.	A	Kickstart, b = 50		Yes	

PART III: Analysis and Data Processing

15. WET-TEST DATA POST-PROCESSING

16. CFD RESULTS AND POST PROCESSING

15. Post-Processing of Wet-Test Data

15.1. Day #3 of Wet-Tests: Post-Processing of Experimental Data

The cases listed in the table below are analyzed further in this section. Specifically, the time histories of the cylinder(s) displacement is post-processed using software developed in the MRELab.

Table 15: Wet-test data from Day #3 postprocessed

Trial #	Flow Speed	Date	Figure #
DAY #3: TRIAL #1	0.7M/S	June 14th, 1:41 P.M.	60
DAY #3: TRIAL #2	0.7M/S	June 14th, 1:50 P.M	61
DAY #3: TRIAL #3	0.65	June 14th, 1:59 P.M.	62
DAY #3: TRIAL #4	0.6	June 14th, 2:05 P.M.	63
DAY #3: TRIAL #5	0.55	June 14th, 2:13 P.M.	64
DAY #3: TRIAL #6	0.5	June 14th, 2:30 P.M.	65
DAY #3: TRIAL #7	1	June 14th, 2:39 P.M.	66
DAY #3: TRIAL #8	1	June 14th, 2:43 P.M.	67
DAY #3: TRIAL #11	1.5	June 14th, 2:58 P.M.	68
DAY #3: TRIAL #12	1.5	June 14th, 3:13 P.M.	69
DAY #3: TRIAL #13	1.5	June 14th, 3:18 P.M.	70
DAY #3: TRIAL #14	1.5	June 14th, 3:25 P.M.	71
DAY #3: TRIAL #15	1.5	June 14th, 3:28 P.M.	72

DAY #3: TRIAL #1, 0.7M/S

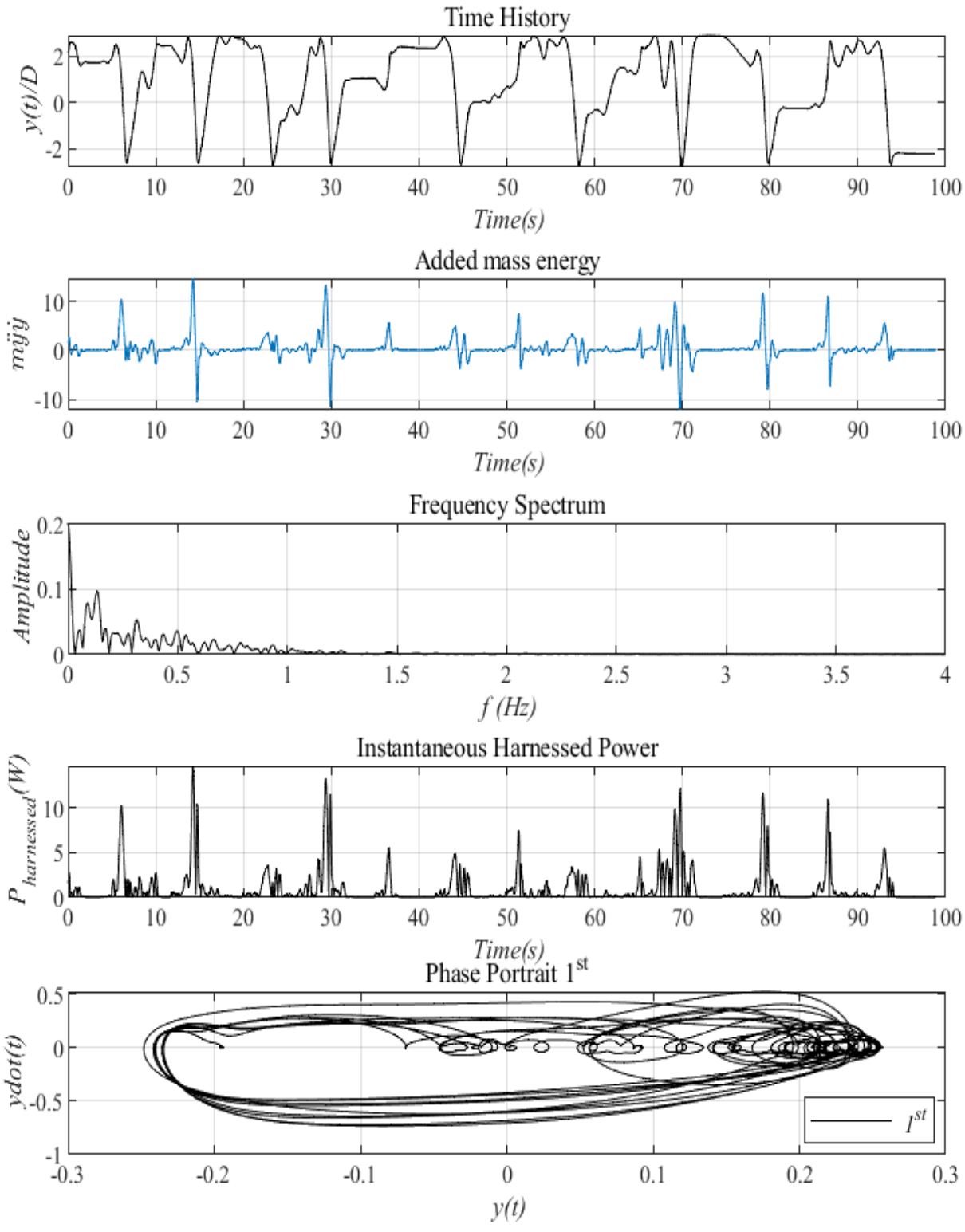

Figure 60. Postprocessing of wet-test cylinder motion

DAY #3: TRIAL #2, 0.7M/S

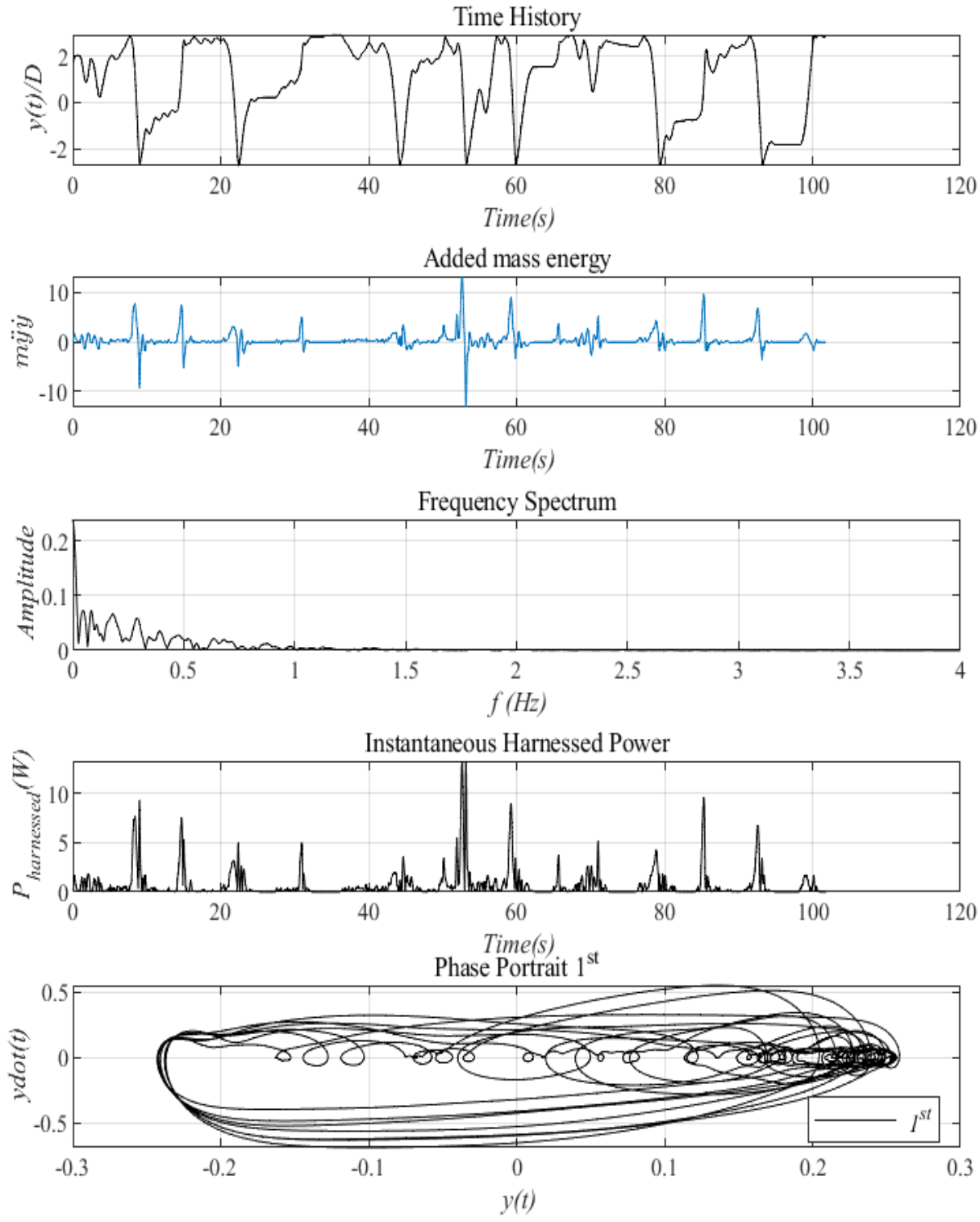

Figure 61. Postprocessing of wet-test cylinder motion

DAY #3: TRIAL #3, 0.65M/S

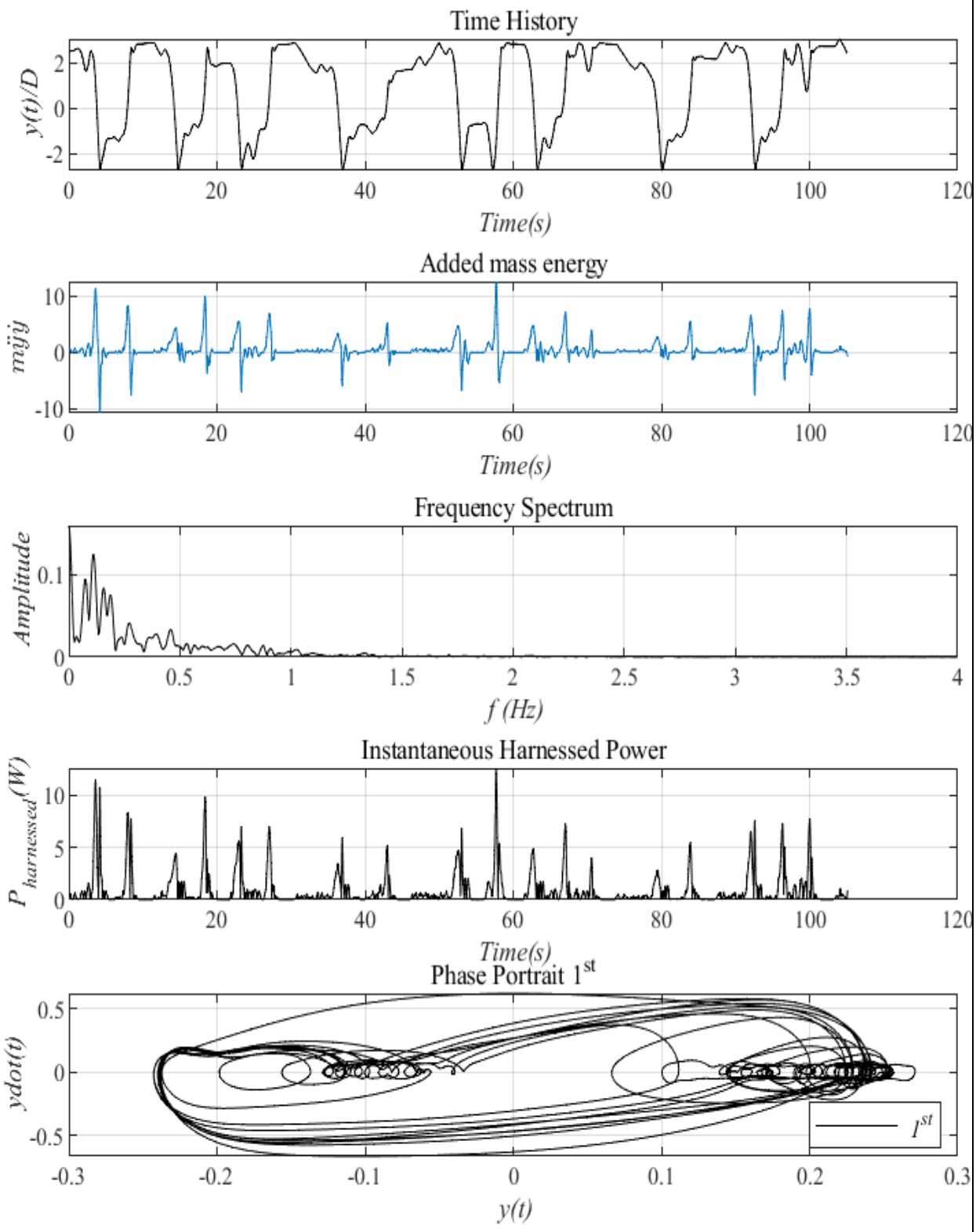

Figure 62. Postprocessing of wet-test cylinder motion

DAY #3: TRIAL #4, 0.6M/S

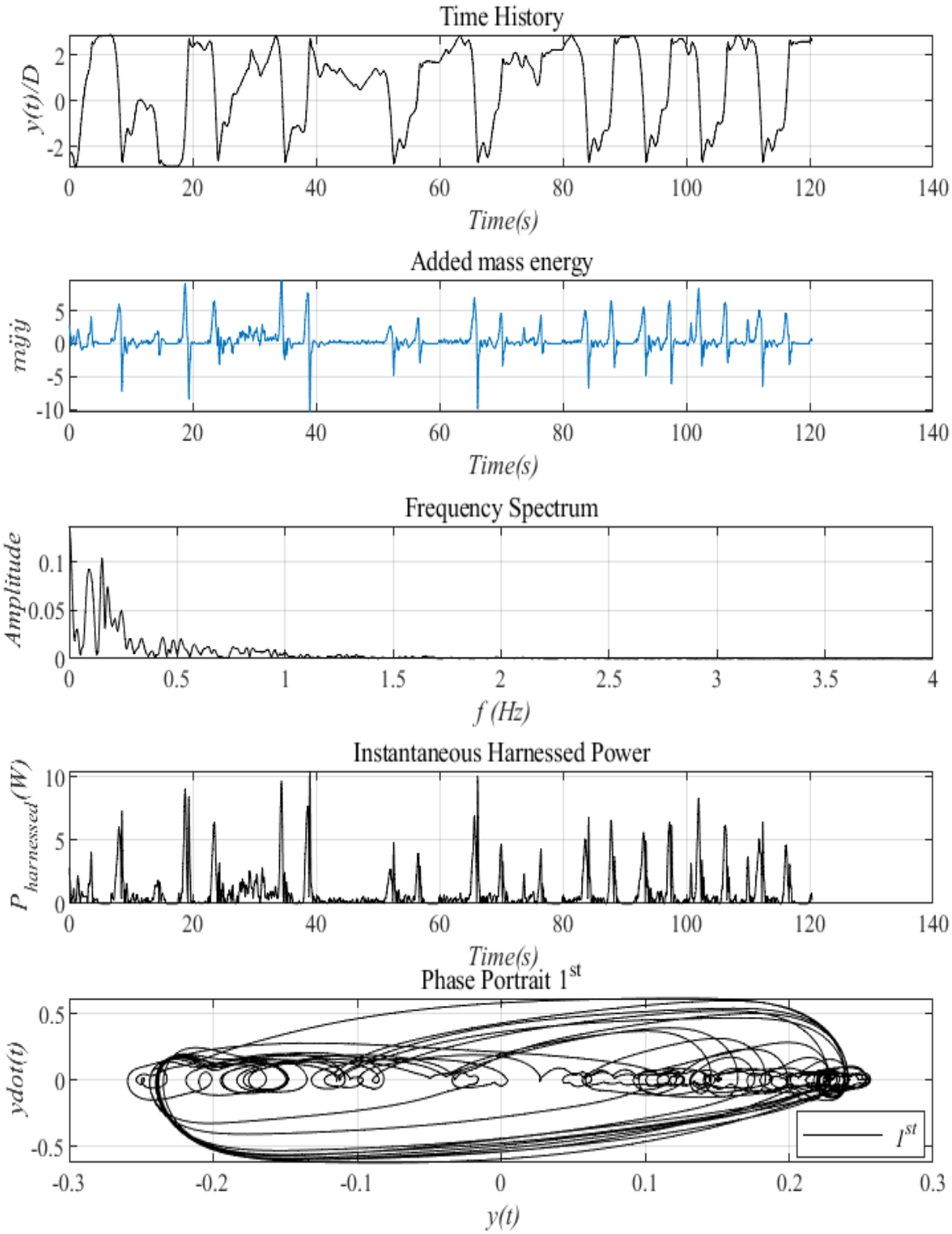

Figure 63. Postprocessing of wet-test cylinder motion

DAY #3: TRIAL #5, 055M/S

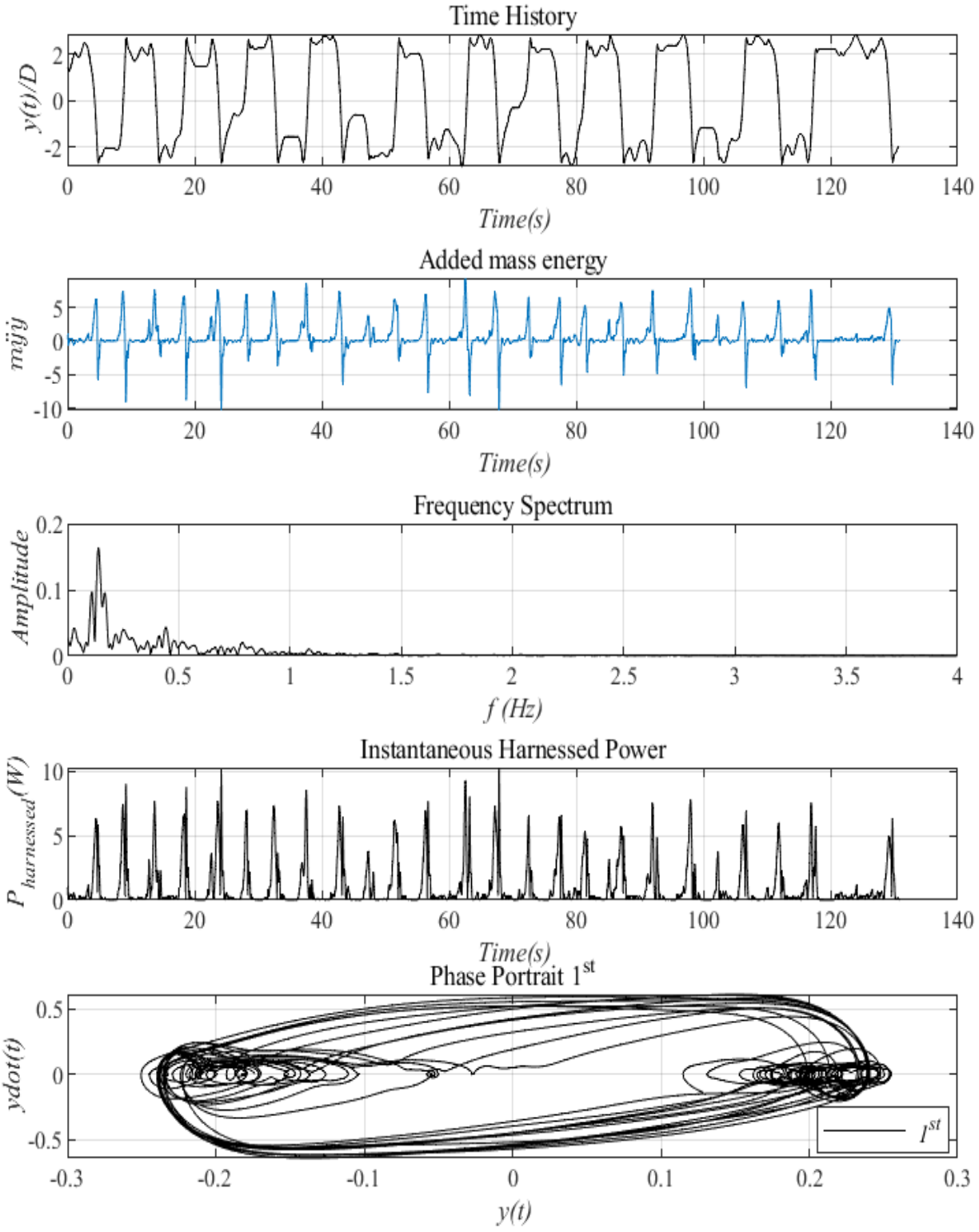

Figure 64. Postprocessing of wet-test cylinder motion

DAY #3: TRIAL #6, 0.5M/S

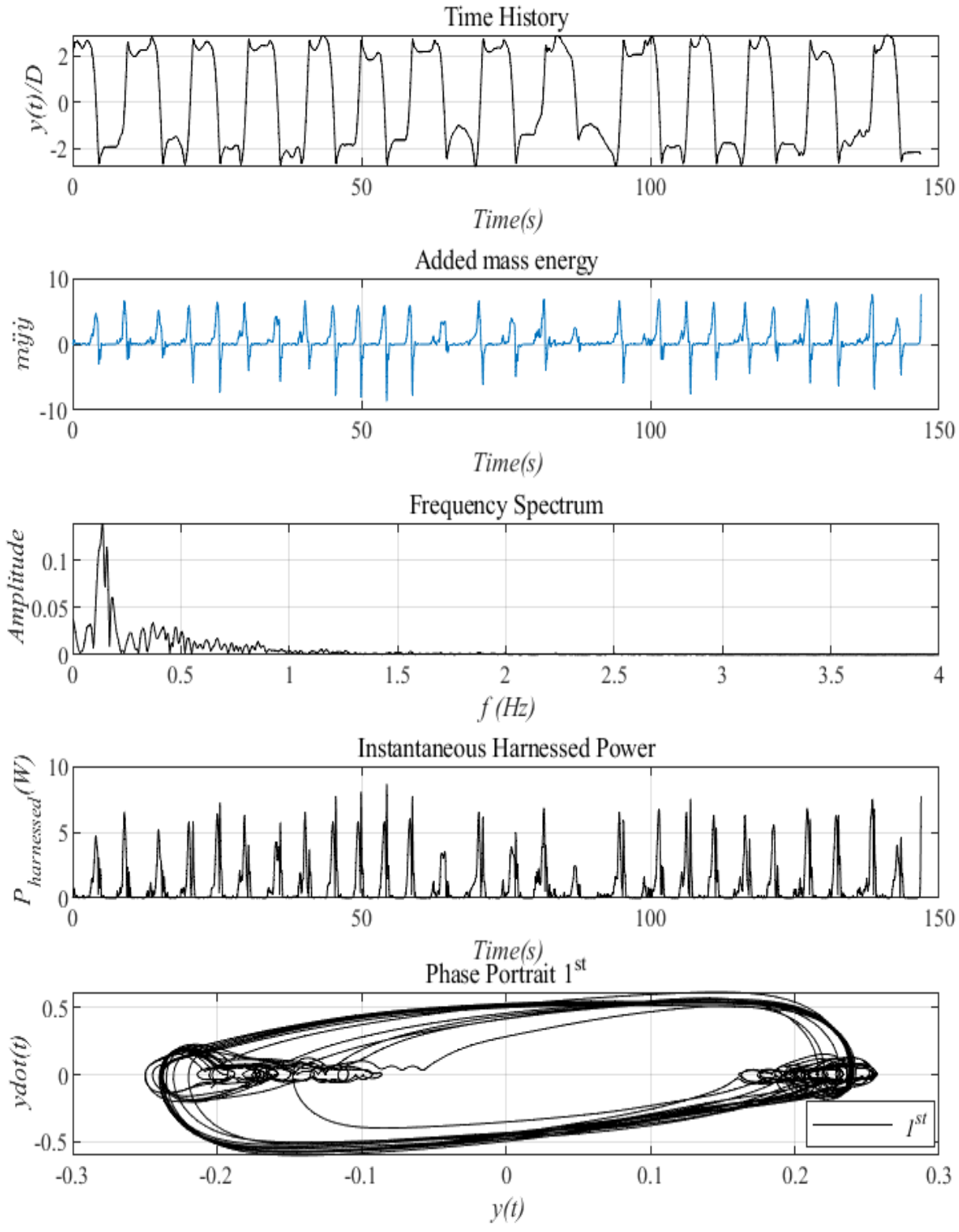

Figure 65. Postprocessing of wet-test cylinder motion

DAY #3: TRIAL #7, 1.0M/S

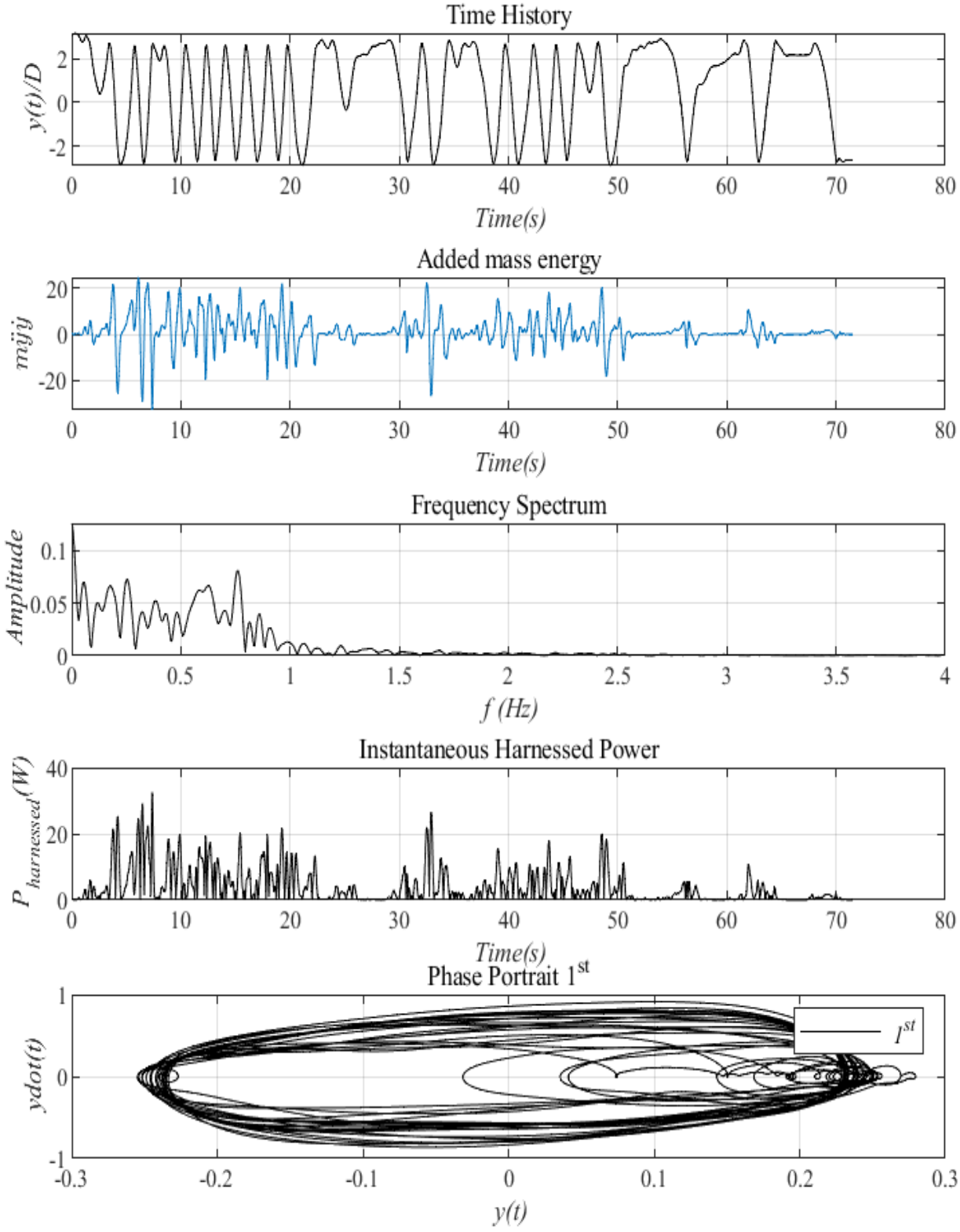

Figure 66. Postprocessing of wet-test cylinder motion

DAY #3: TRIAL #8, 1.0M/S – no kick-start

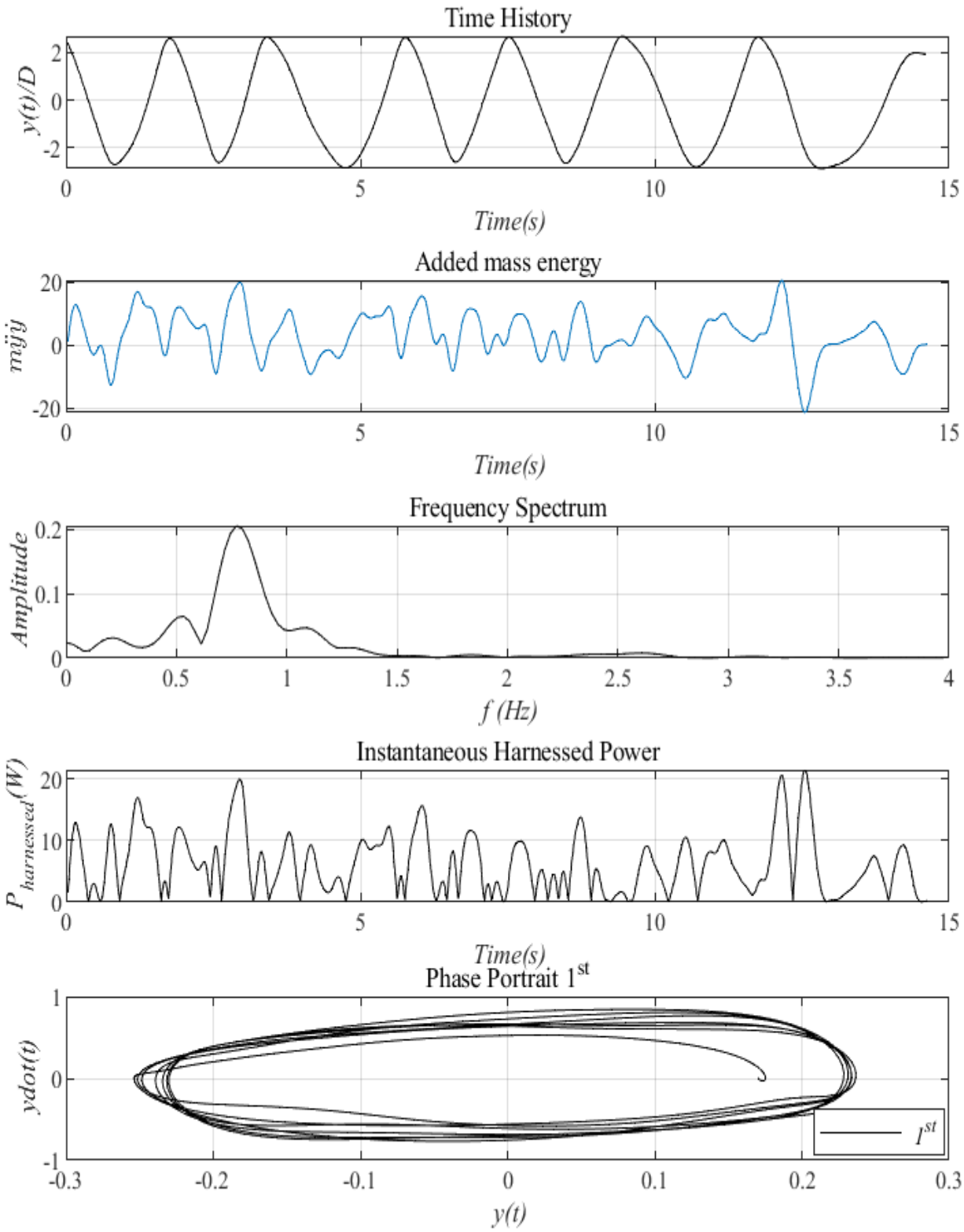

Figure 67. Postprocessing of wet-test cylinder motion

DAY #3: TRIAL #11, 1.5M/S

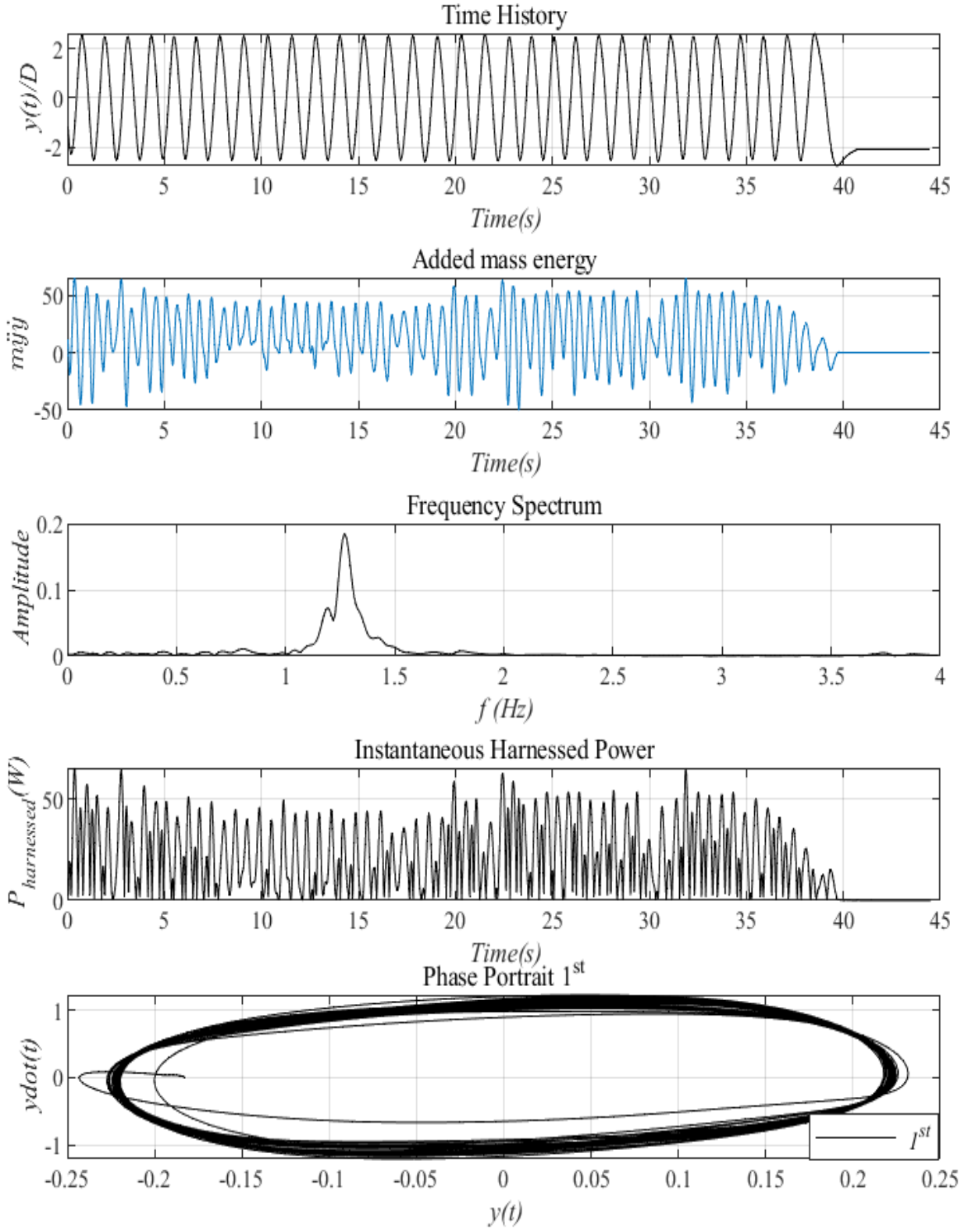

Figure 68. Postprocessing of wet-test cylinder motion

DAY #3: TRIAL #12, 1.5M/S - beta=301

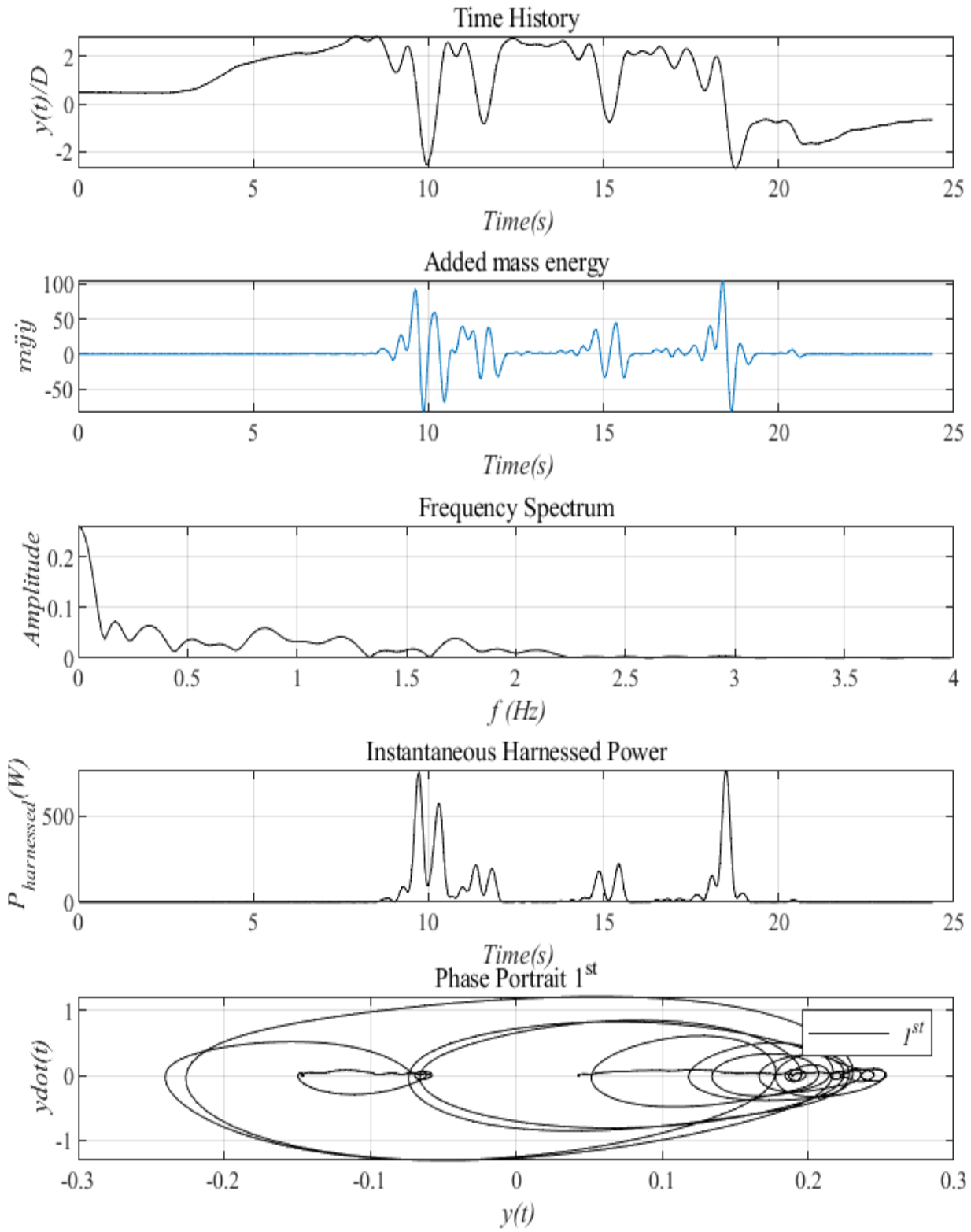

Figure 69. Postprocessing of wet-test cylinder motion

DAY #3: TRIAL #13, 1.5M/S - beta=50

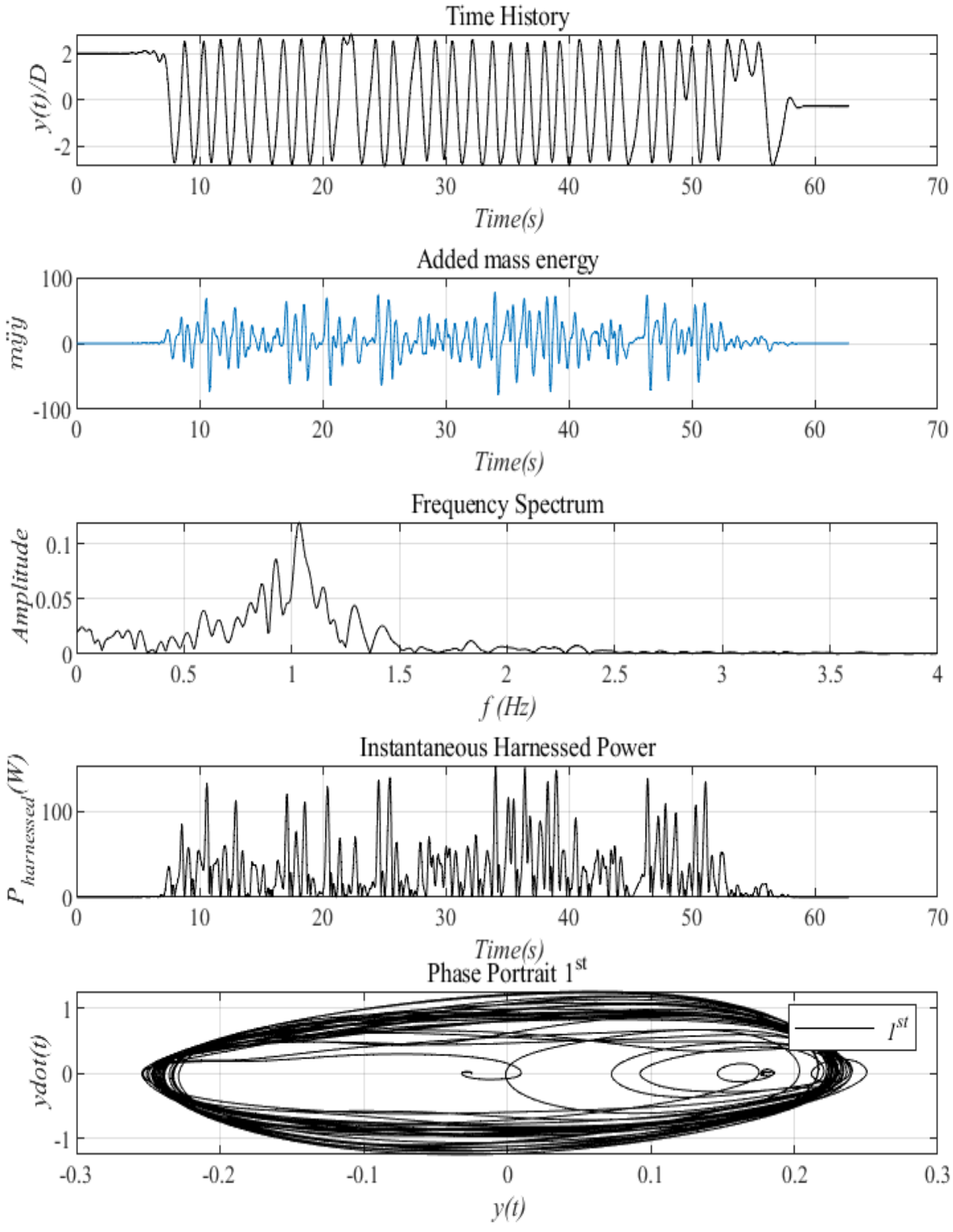

Figure 70. Postprocessing of wet-test cylinder motion

DAY #3: TRIAL #14, 1.5M/S, breaking current=0.5 Amp (constant)

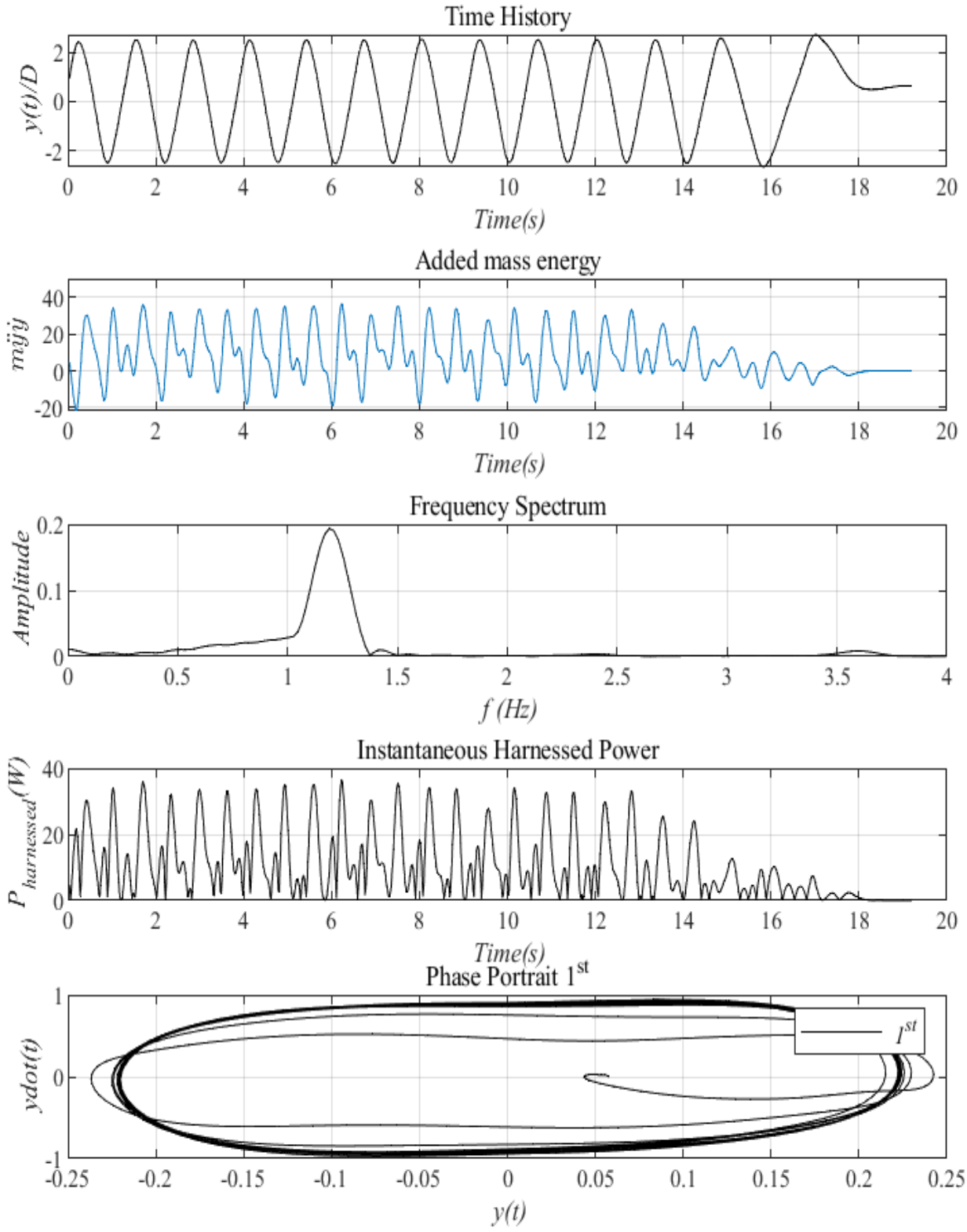

Figure 71. Postprocessing of wet-test cylinder motion

DAY #3: TRIAL #15, 1.5M/S, breaking current=1.0 Amp (constant)

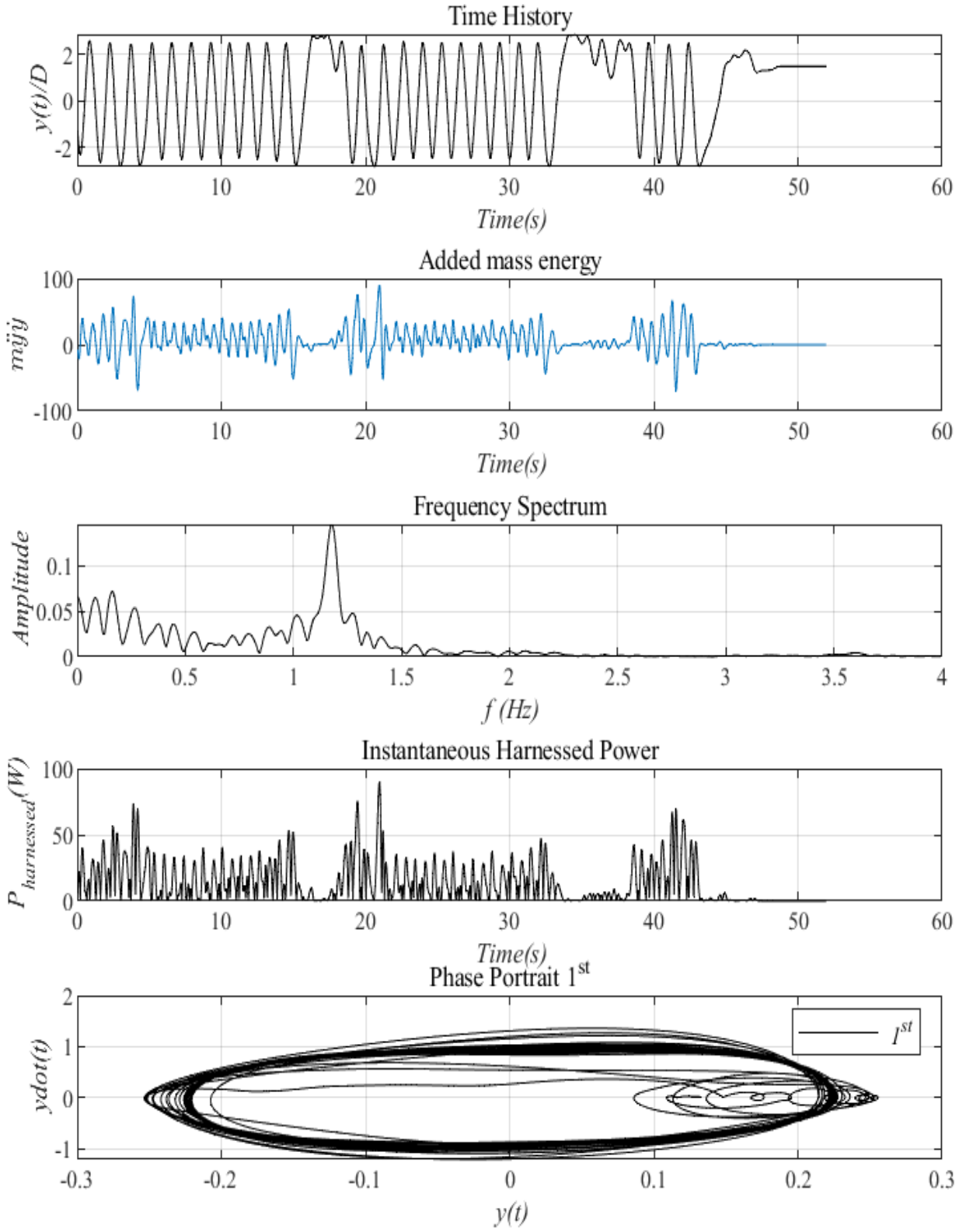

Figure 72. Postprocessing of wet-test cylinder motion

15.2. Day #5 of Wet-Tests: Post-Processing of Experimental Data

The cases listed in the table below are analyzed further in this section. Specifically, the time histories of the cylinder(s) displacement is post-processed using software developed in the MRELab.

Table 16: Wet-test data from Day #5 postprocessed

Trial #	Flow Speed [m/s]	Date	Figure #
DAY #5: TRIAL #2	1.5	June 18th, 2:00 P.M.	73
DAY #5: TRIAL #3	1.5	June 18th, 2:04 P.M.	74
DAY #5: TRIAL #4	1.4	June 18th, 2:31 P.M.	75
DAY #5: TRIAL #5	1.3	June 18th, 2:35 P.M.	76
DAY #5: TRIAL #6	1.2	June 18th, 2:39 P.M.	77
DAY #5: TRIAL #7	1.1	June 18th, 2:43 P.M.	78
DAY #5: TRIAL #8	0.9	June 18th, 2:51 P.M.	79
DAY #5: TRIAL #9	0.8	June 18th, 2:55 P.M.	80
DAY #5: TRIAL #10	1	June 18th, 3:01 P.M.	81
DAY #5: TRIAL #12	1.3	June 18th, 3:13 P.M.	82
DAY #5: TRIAL #13	1.5	June 18th, 3:24 P.M.	83

DAY #5: TRIAL #2, 1.5M/S

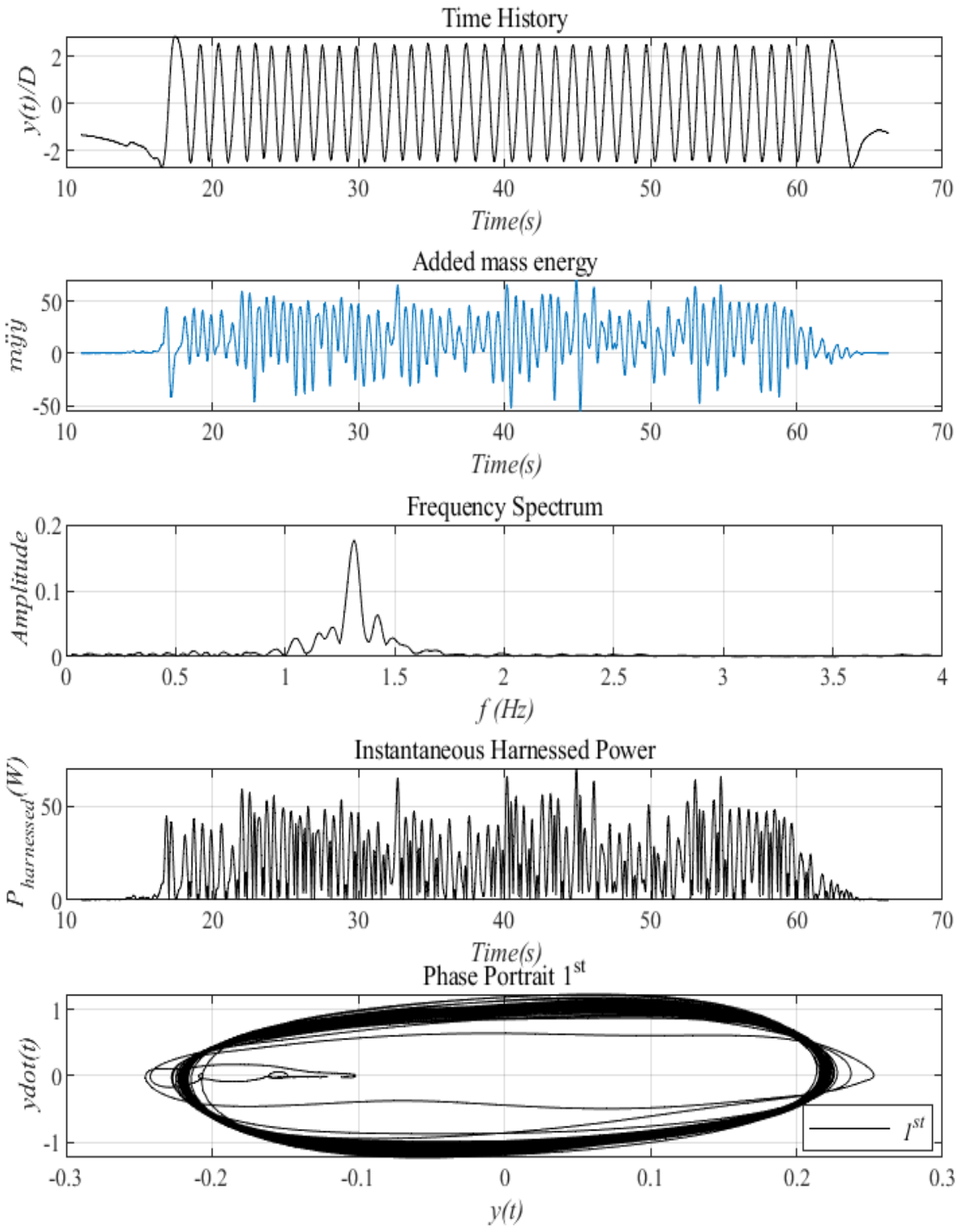

Figure 73. Postprocessing of wet-test cylinder motion

DAY #5: TRIAL #3, 1.5M/S

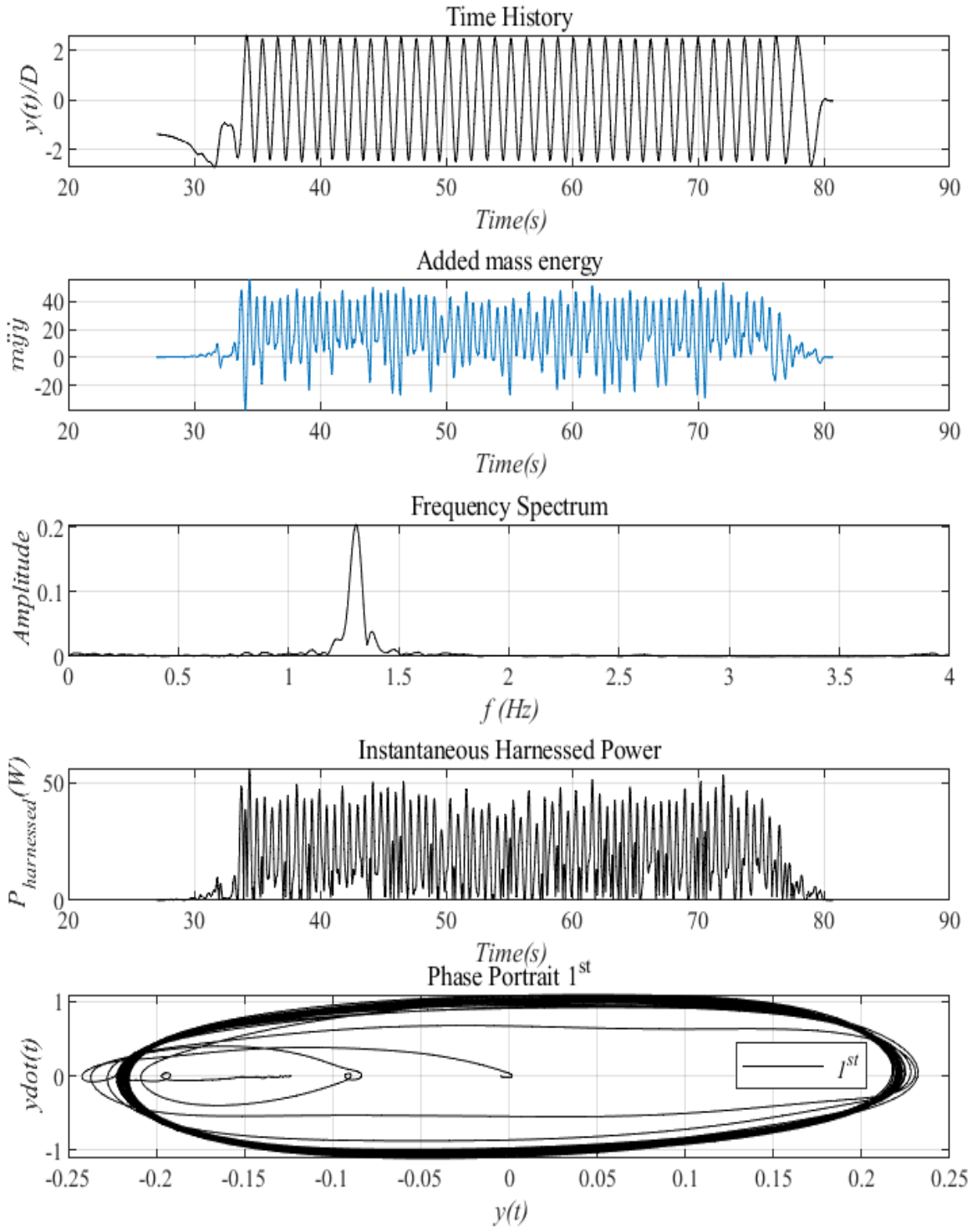

Figure 74. Postprocessing of wet-test cylinder motion

DAY #5: TRIAL #4, 1.4M/S

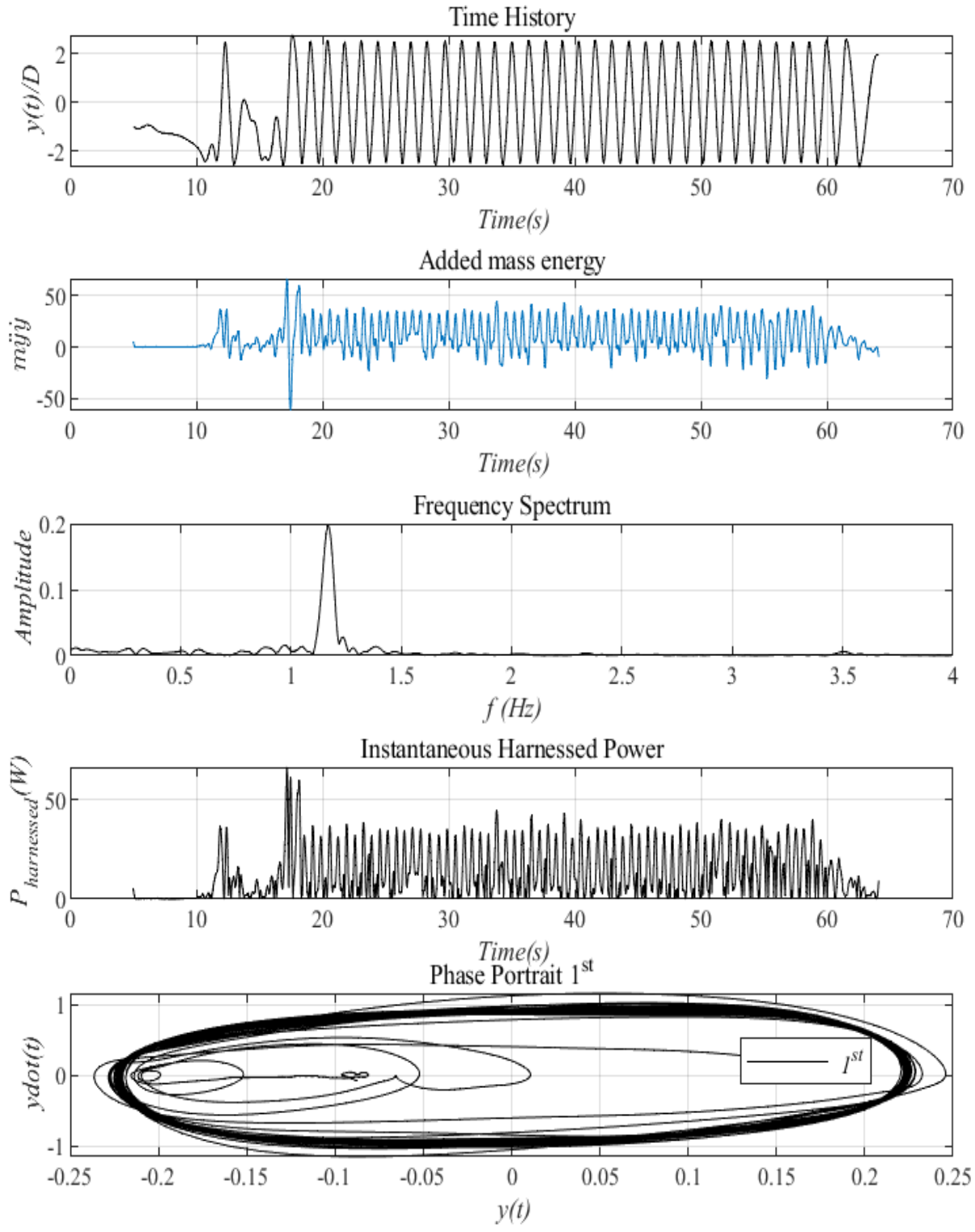

Figure 75. Postprocessing of wet-test cylinder motion

DAY #5: TRIAL #5, 1.3M/S

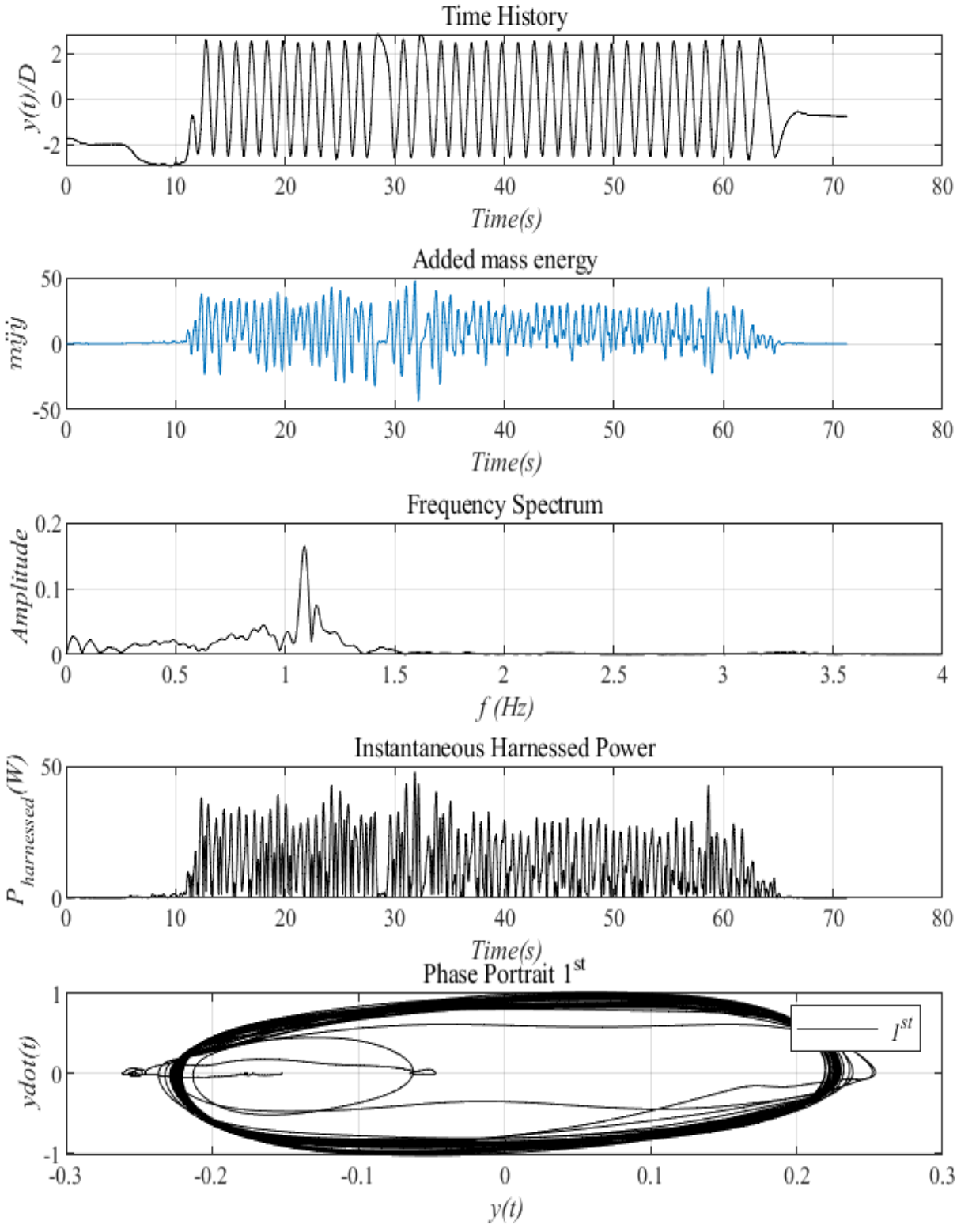

Figure 76. Postprocessing of wet-test cylinder motion

DAY #5: TRIAL #6, 1.2M/S

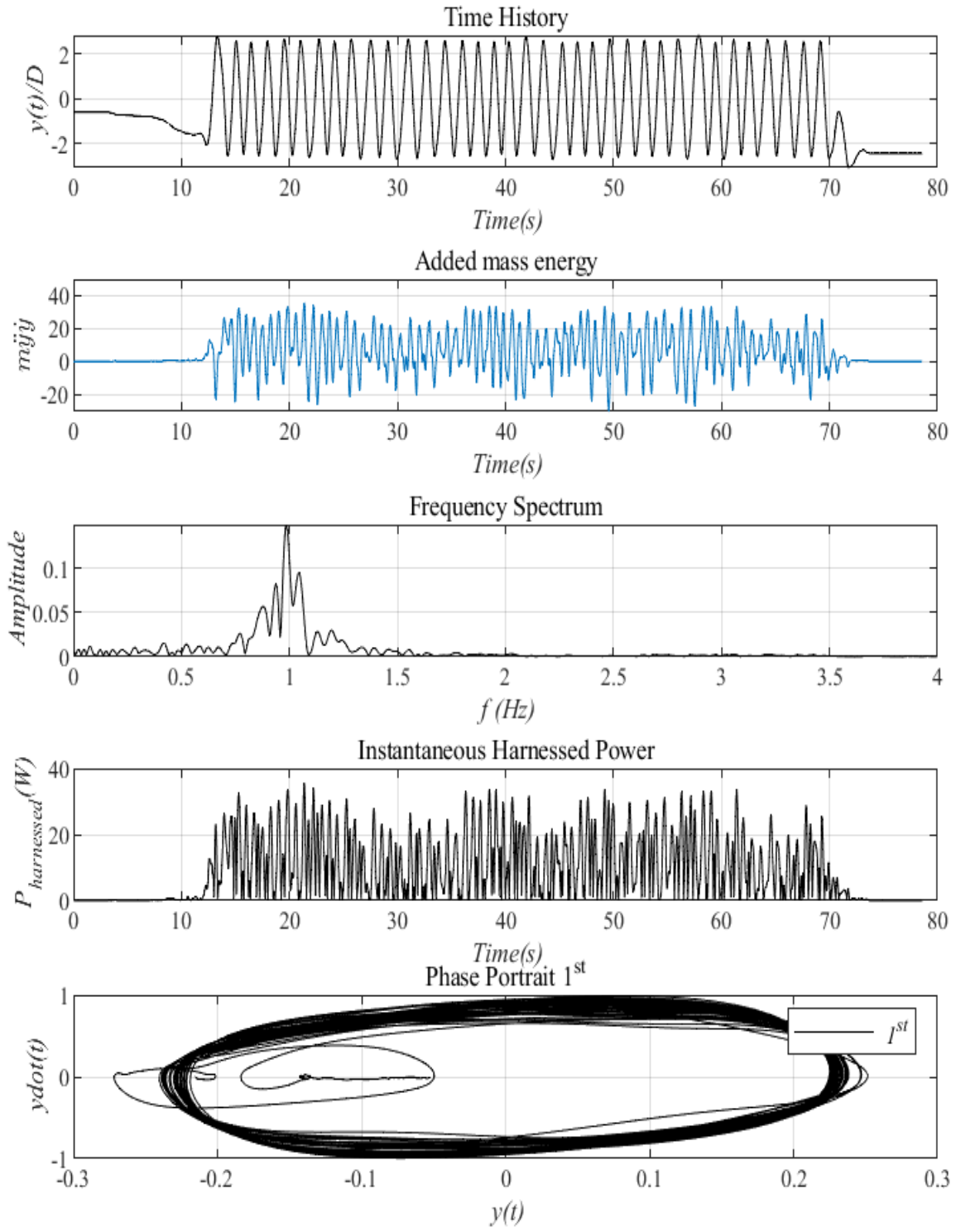

Figure 77. Postprocessing of wet-test cylinder motion

DAY #5: TRIAL #7, 1.1M/S

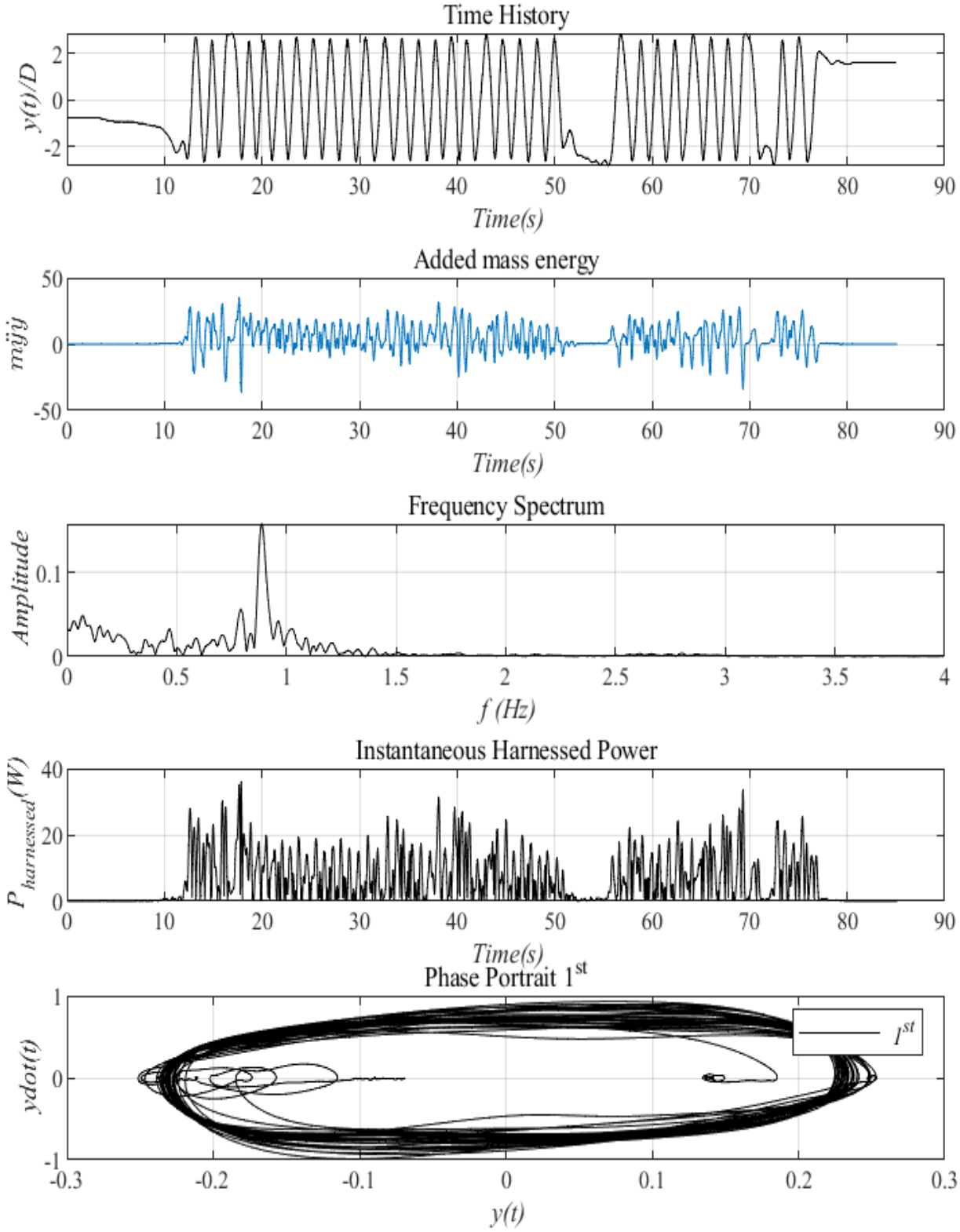

Figure 78. Postprocessing of wet-test cylinder motion

DAY #5: TRIAL #8, 0.9M/S

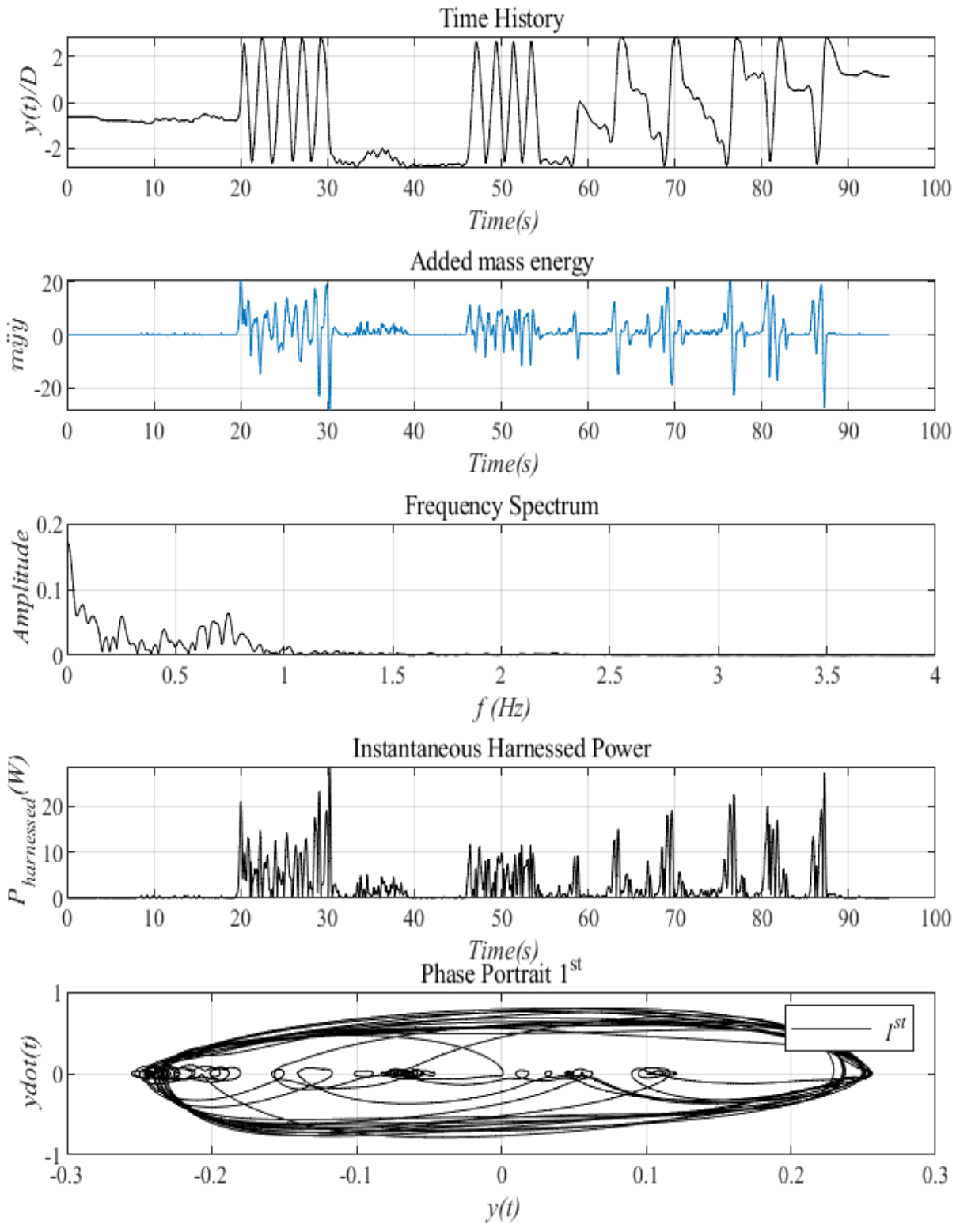

Figure 79. Postprocessing of wet-test cylinder motion

DAY #5: TRIAL #9, 0.8M/S

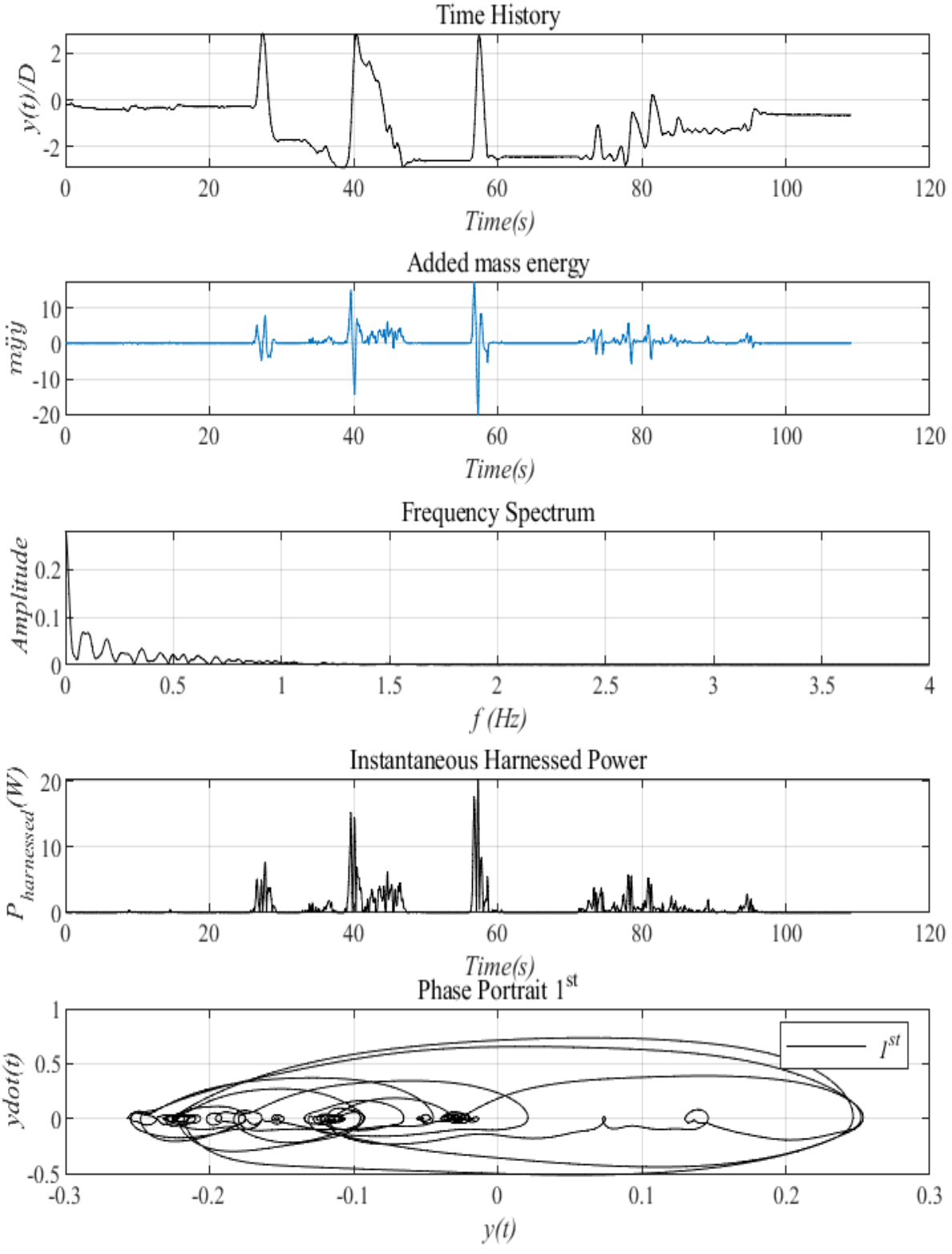

Figure 80. Postprocessing of wet-test cylinder motion

DAY #5: TRIAL #10, 1.0M/S - beta=1.0

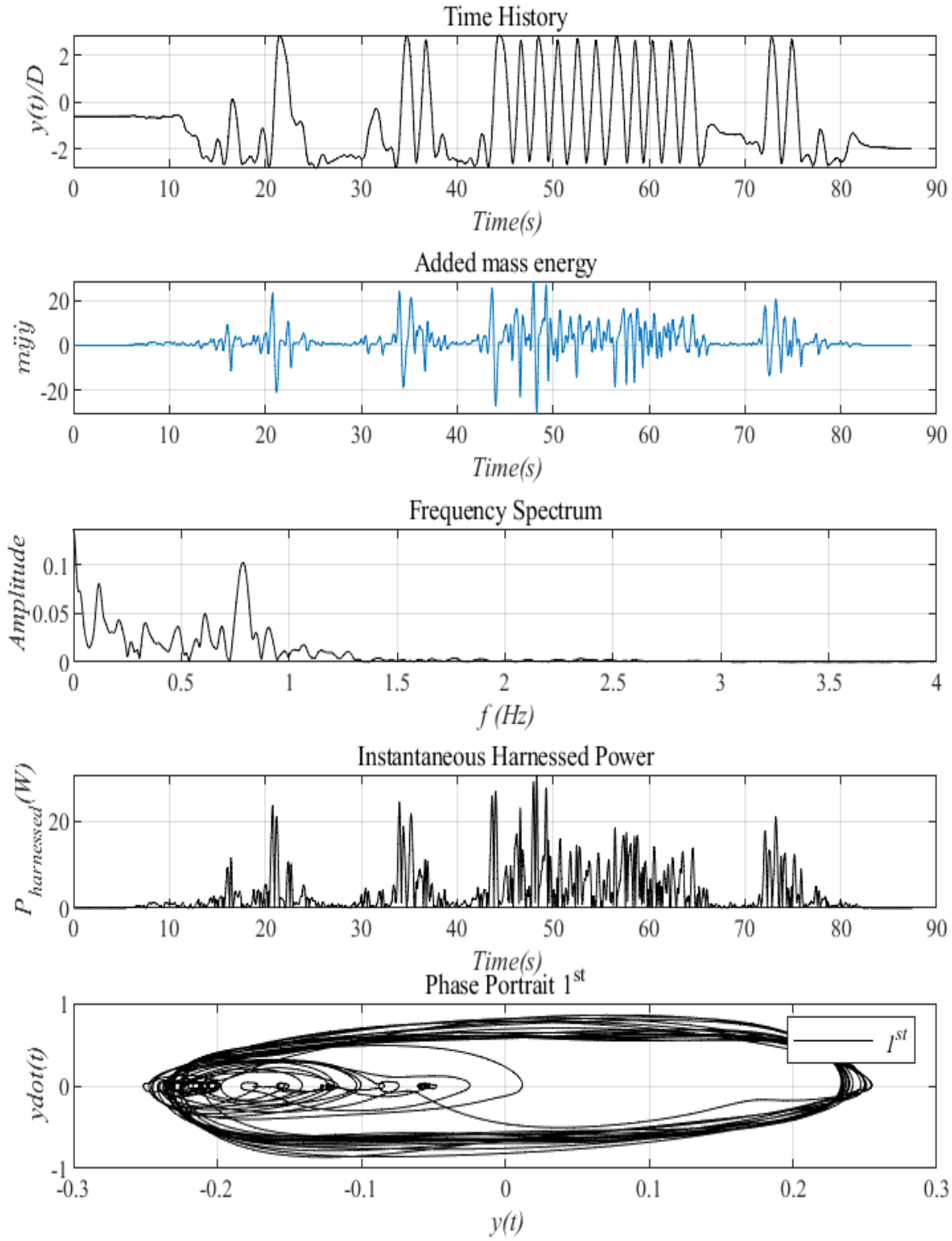

Figure 81. Postprocessing of wet-test cylinder motion

DAY #5: TRIAL #12, 1.3M/S - beta=20

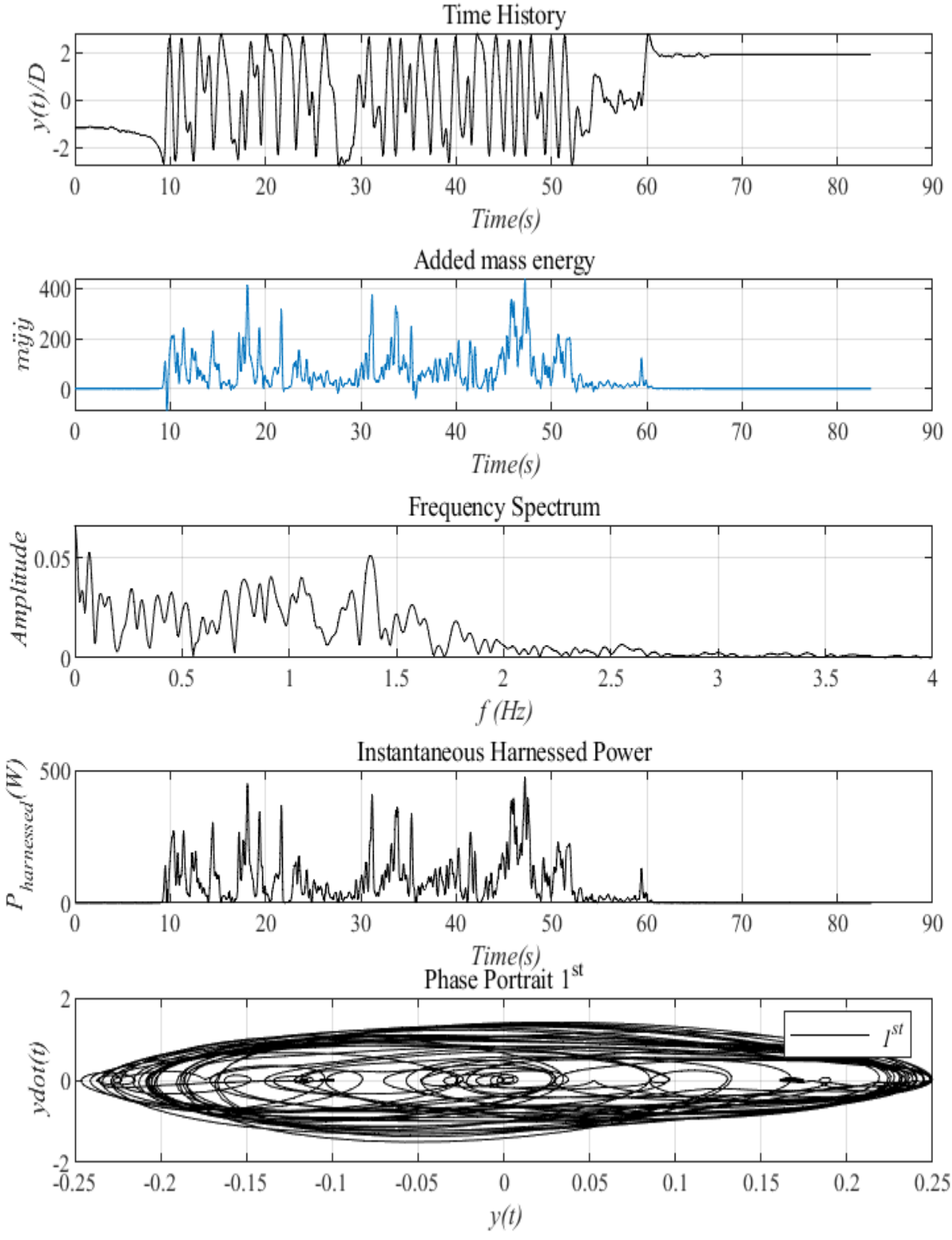

Figure 82. Postprocessing of wet-test cylinder motion

DAY #5: TRIAL #13, 1.5M/S - beta=50

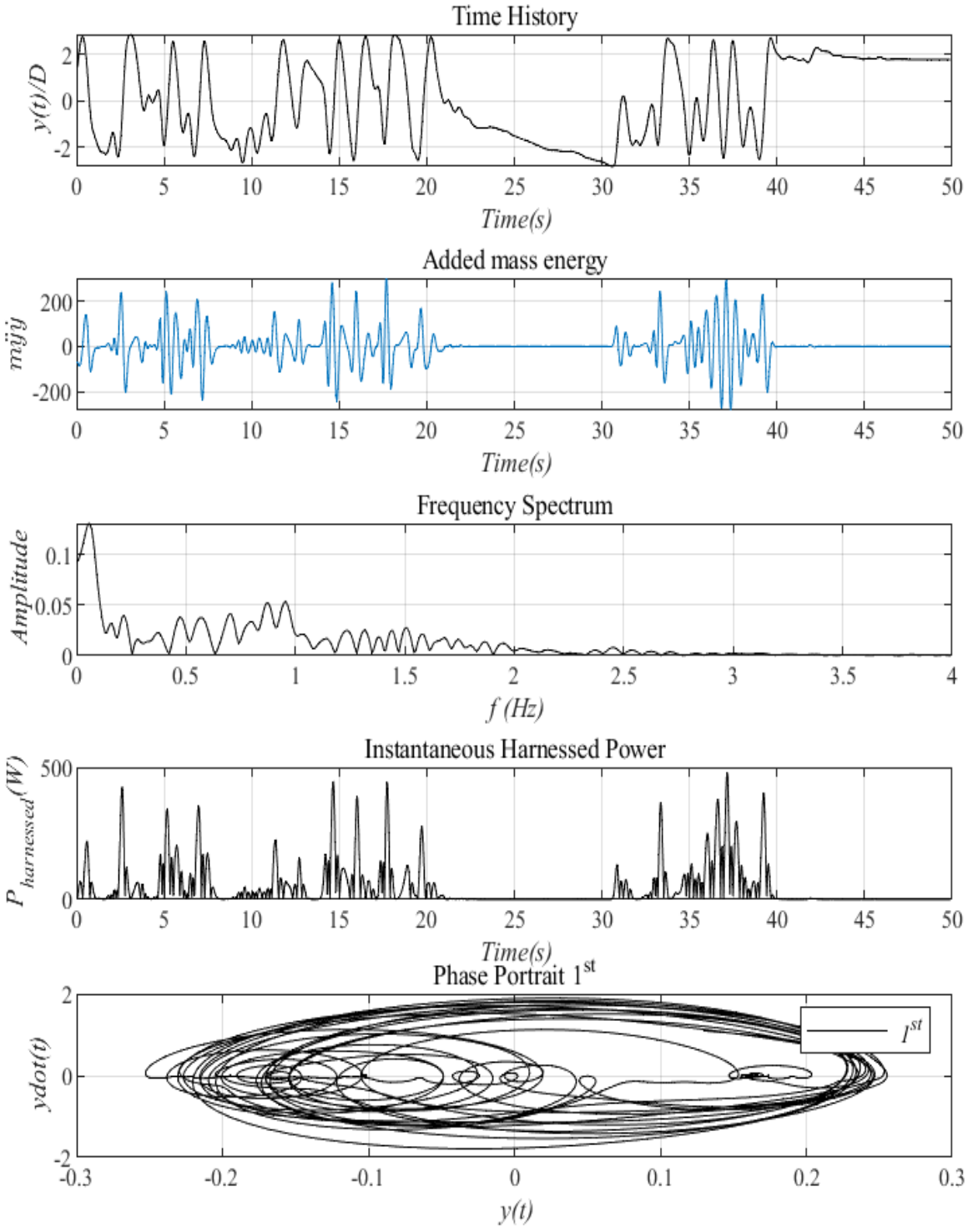

Figure 83. Postprocessing of wet-test cylinder motion

16. Post Processing of CFD Results

Appendix II includes the CFD report which explains and documents the procedure used in the CFD simulations. Appendix II also shows a few pictures from CFD animations to understand the interactions between bodies, boundary layers, shear layers, and vortical wakes. The time histories generated by CFD are post-processed further with the same software used in Chapter 15 to post process experimental data.

16.1. CFD Results for the 4-Cylinder VIVACE Converter

The cases listed in the table below are analyzed by the dedicated CFD software developed in the MRELab based on OpenFOAM.

The time history of the cylinder displacement is post-processed using the software developed in the MRELab. The next nine pages show the postprocessing of the CFD time histories analyzed in the same way the experimental data were analyzed in the Chapter 15.

Table 17: CFD Simulation Cases for the 4-Cylinder VIVACE Converter				
Case #	**Table #**	**Flow Speed U [m/s]**	**Adaptive Damping Coefficient β**	**Figure #**
1		0.50	2.00	84
2		0.50	4.00	85
3		0.50	6.00	86
4		0.50	20.00	87
5		0.50	40.00	88
6		0.50	60.00	89
7		1.00	2.00	90
8		1.00	4.00	91
9		1.00	6.00	92
10		1.00	40.00	93
11		1.50	2.00	94
12		1.50	4.00	95
13		1.50	6.00	96
14		1.50	20.00	97
15		1.50	40.00	98
16		1.50	60.00	99

CFD Case #1, 0.50m/s, beta=2.00 CFD Case #1, 0.50m/s, beta=2.00

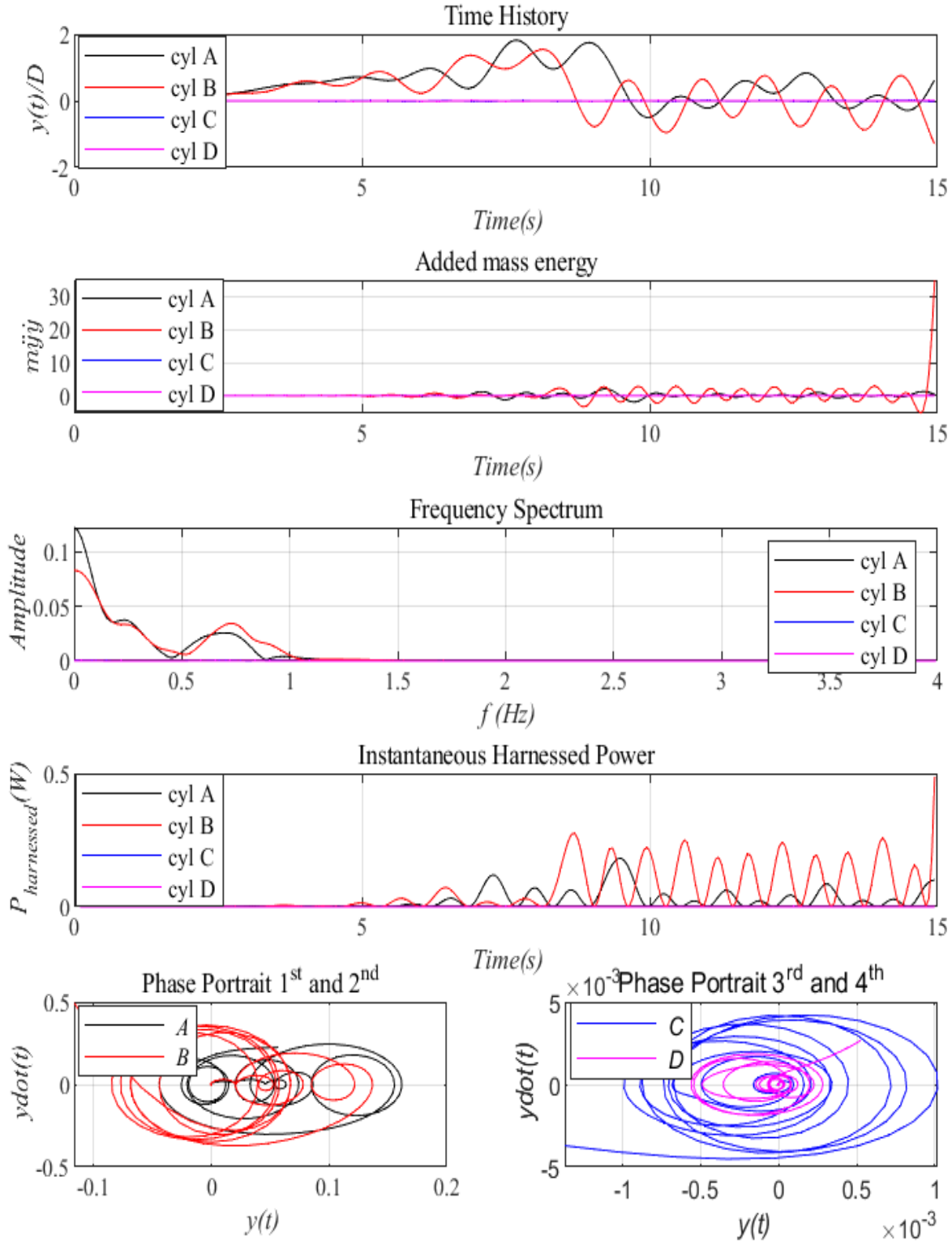

Figure 84. Postprocessing of CFD simulated cylinder motion

CFD Case #1, 0.50m/s, beta=2.00 CFD Case #2, 0.50m/s, beta=4.00

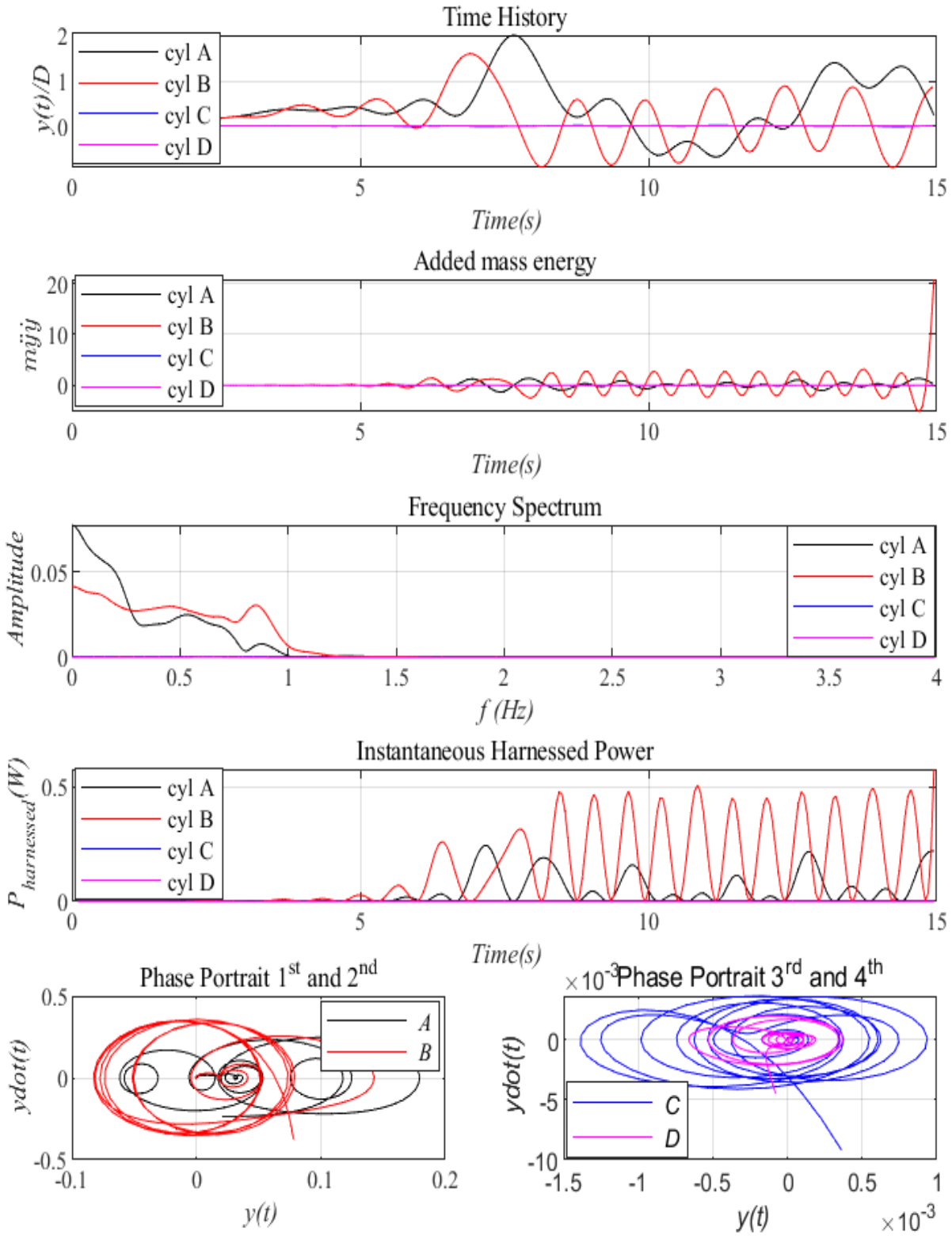

Figure 85. Postprocessing of CFD simulated cylinder motion

CFD Case #1, 0.50m/s, beta=2.00 CFD Case #3, 0.50m/s, beta=6.00

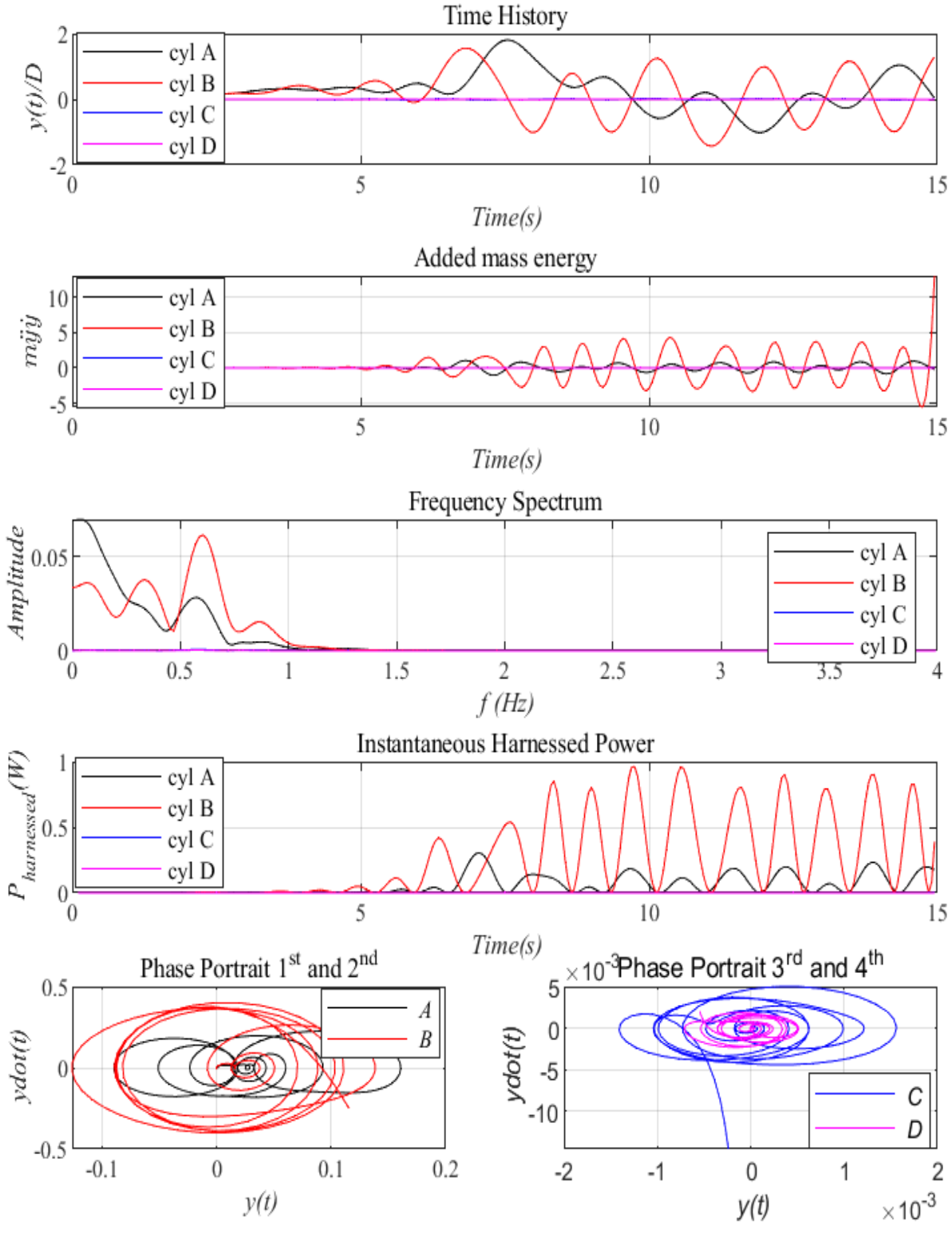

Figure 86. Postprocessing of CFD simulated cylinder motion

CFD Case #1, 0.50m/s, beta=2.00 CFD Case #4, 0.50m/s, beta=20.00

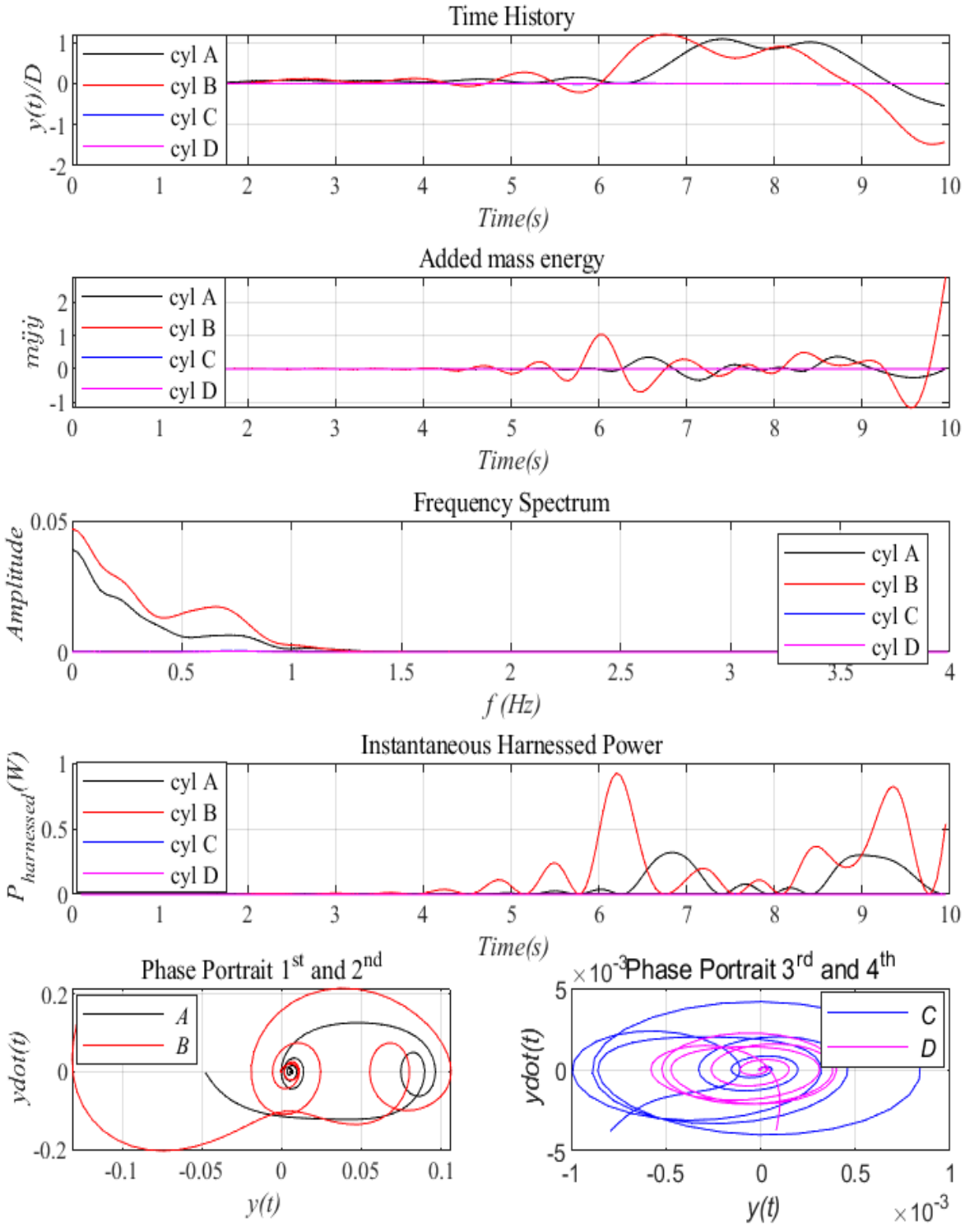

Figure 87. Postprocessing of CFD simulated cylinder motion

CFD Case #1, 0.50m/s, beta=2.00 CFD Case #5, 0.50m/s, beta=40.00

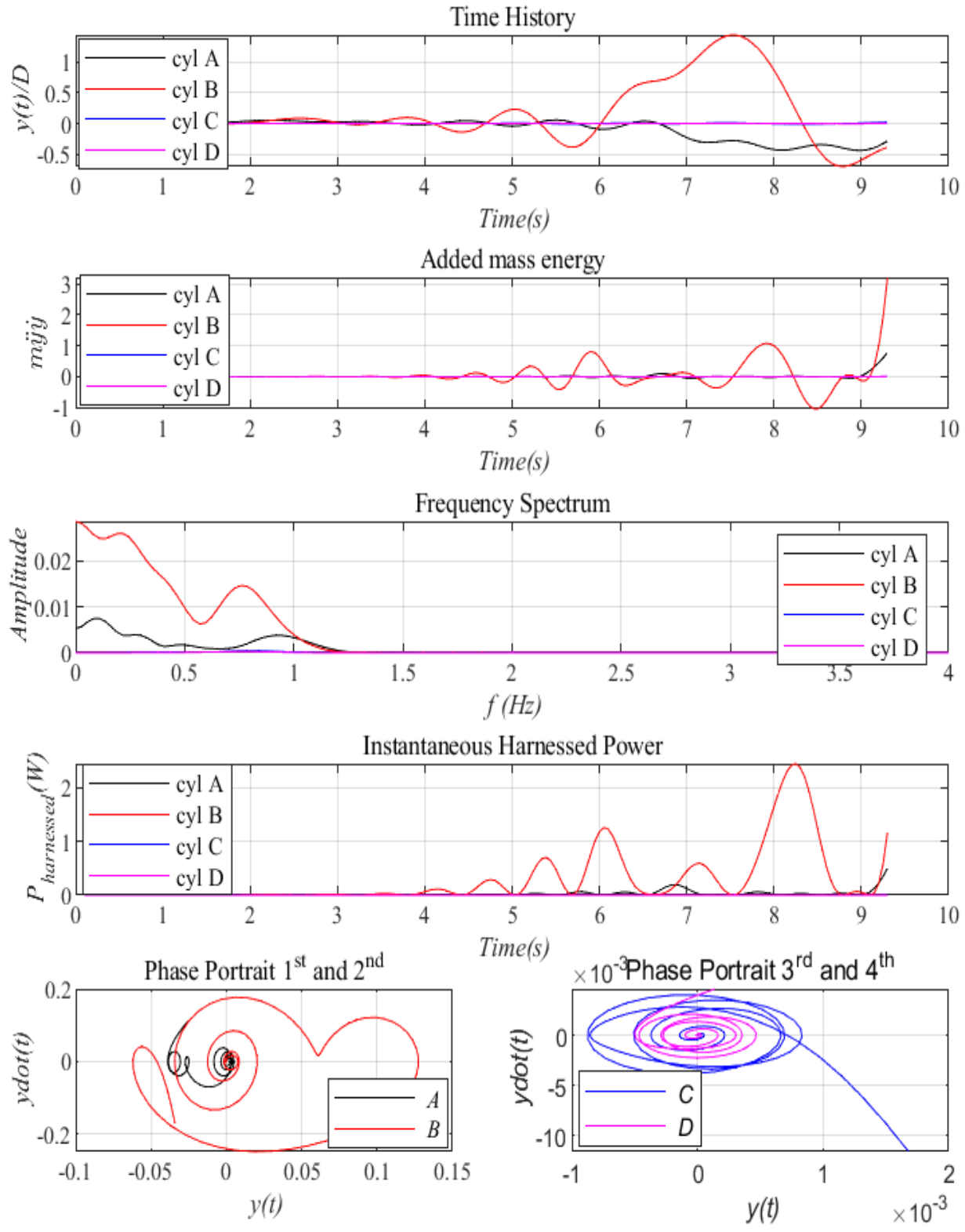

Figure 88. Postprocessing of CFD simulated cylinder motion

CFD Case #1, 0.50m/s, beta=2.00 CFD Case #6, 0.50m/s, beta=60.00

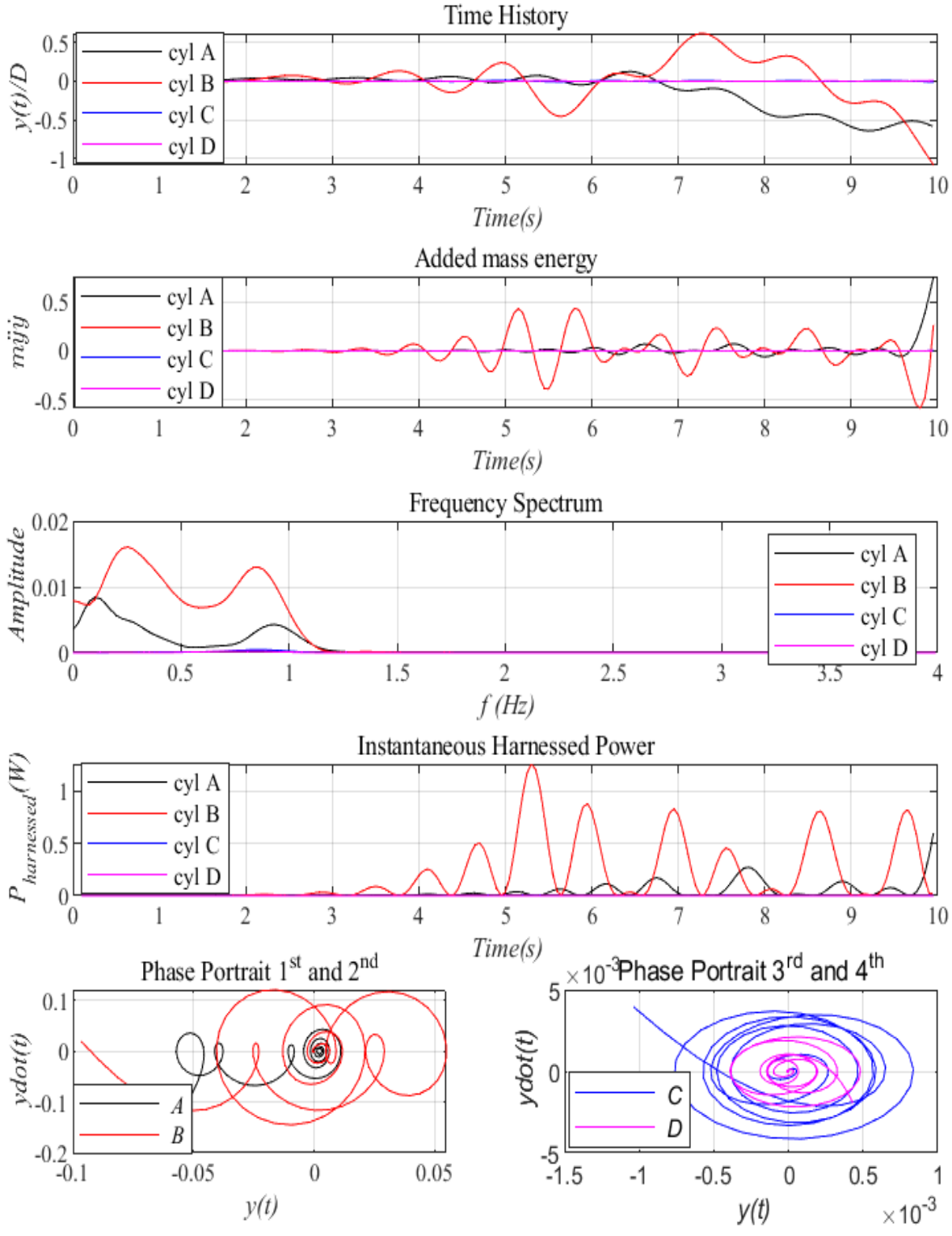

Figure 89. Postprocessing of CFD simulated cylinder motion

CFD Case #1, 0.50m/s, beta=2.00 CFD Case #7, 1.00m/s, beta=2.00

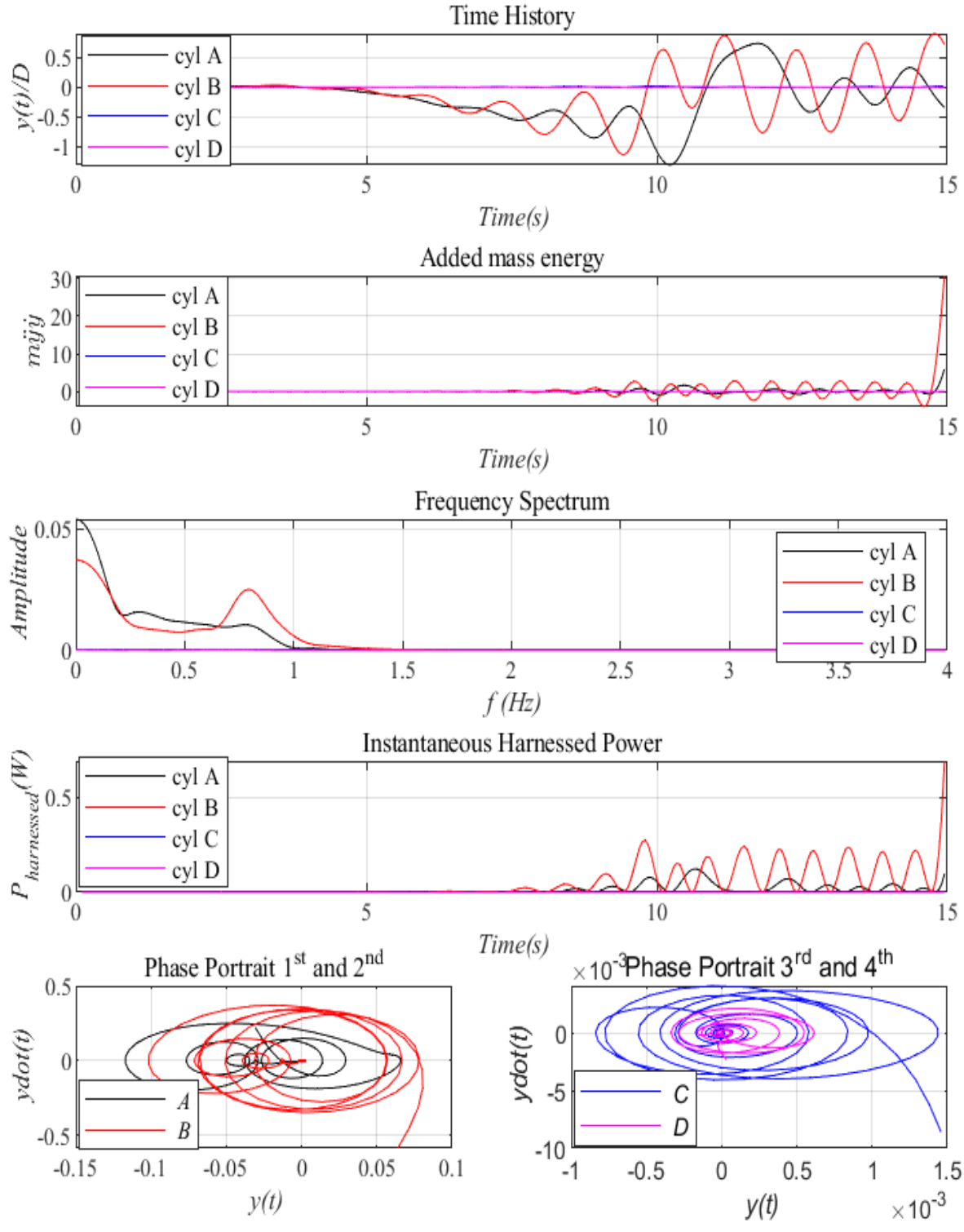

Figure 90. Postprocessing of CFD simulated cylinder motion

CFD Case #1, 0.50m/s, beta=2.00 CFD Case #8, 1.00m/s, beta=4.00

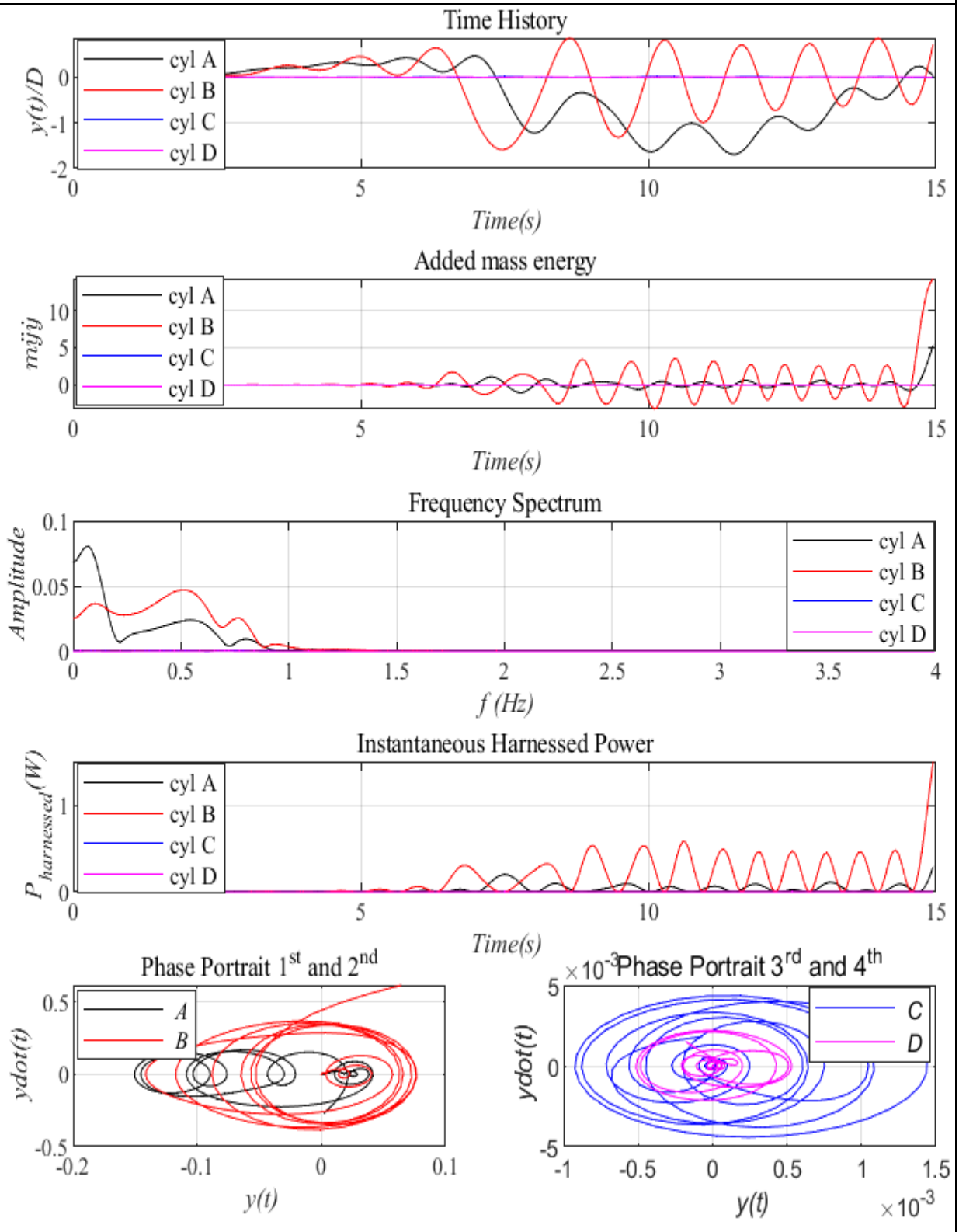

Figure 91. Postprocessing of CFD simulated cylinder motion

CFD Case #1, 0.50m/s, beta=2.00 CFD Case #9, 1.00m/s, beta=6.00

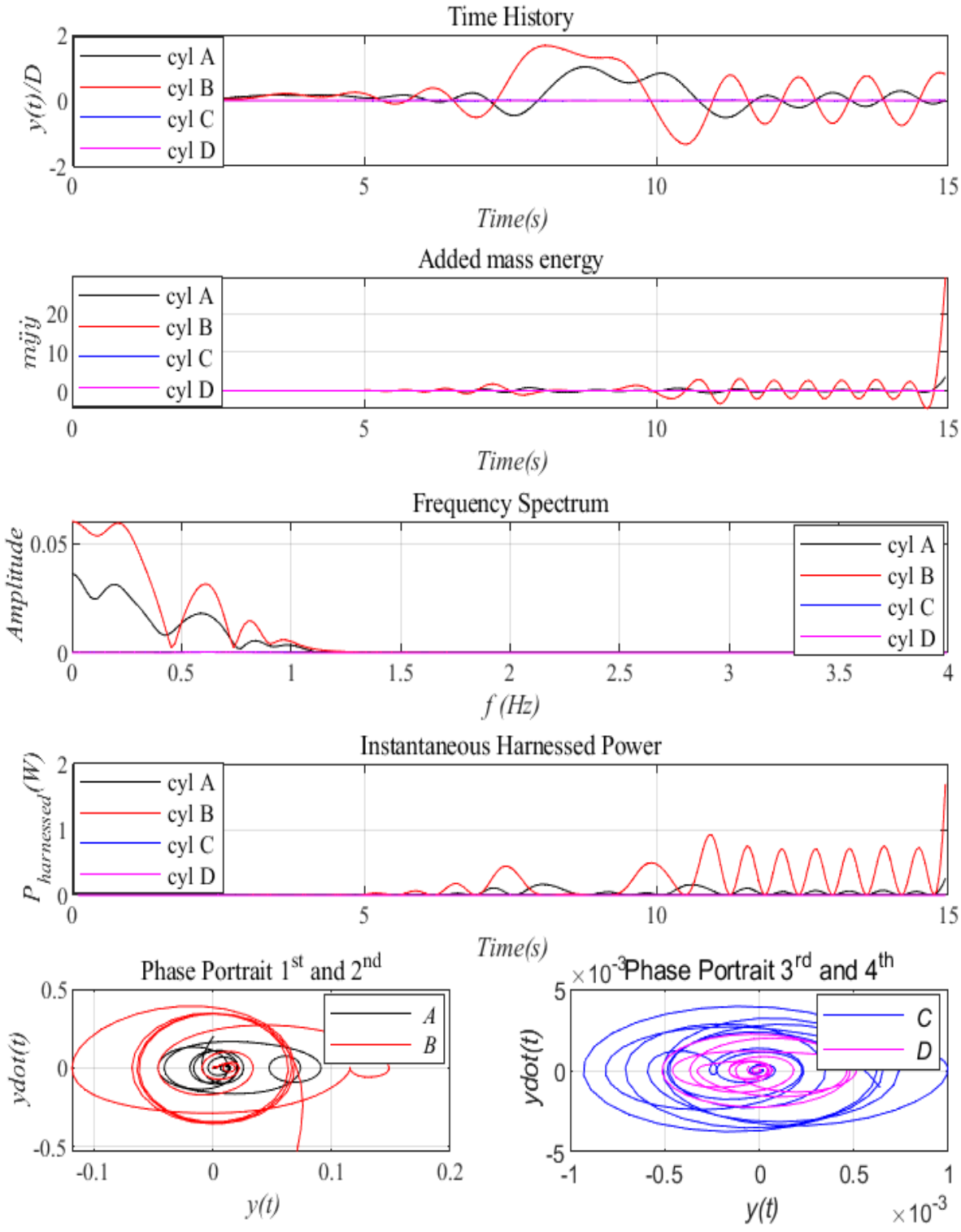

Figure 92. Postprocessing of CFD simulated cylinder motion

CFD Case #1, 0.50m/s, beta=2.00 CFD Case #10, 1.00m/s, beta=40.00

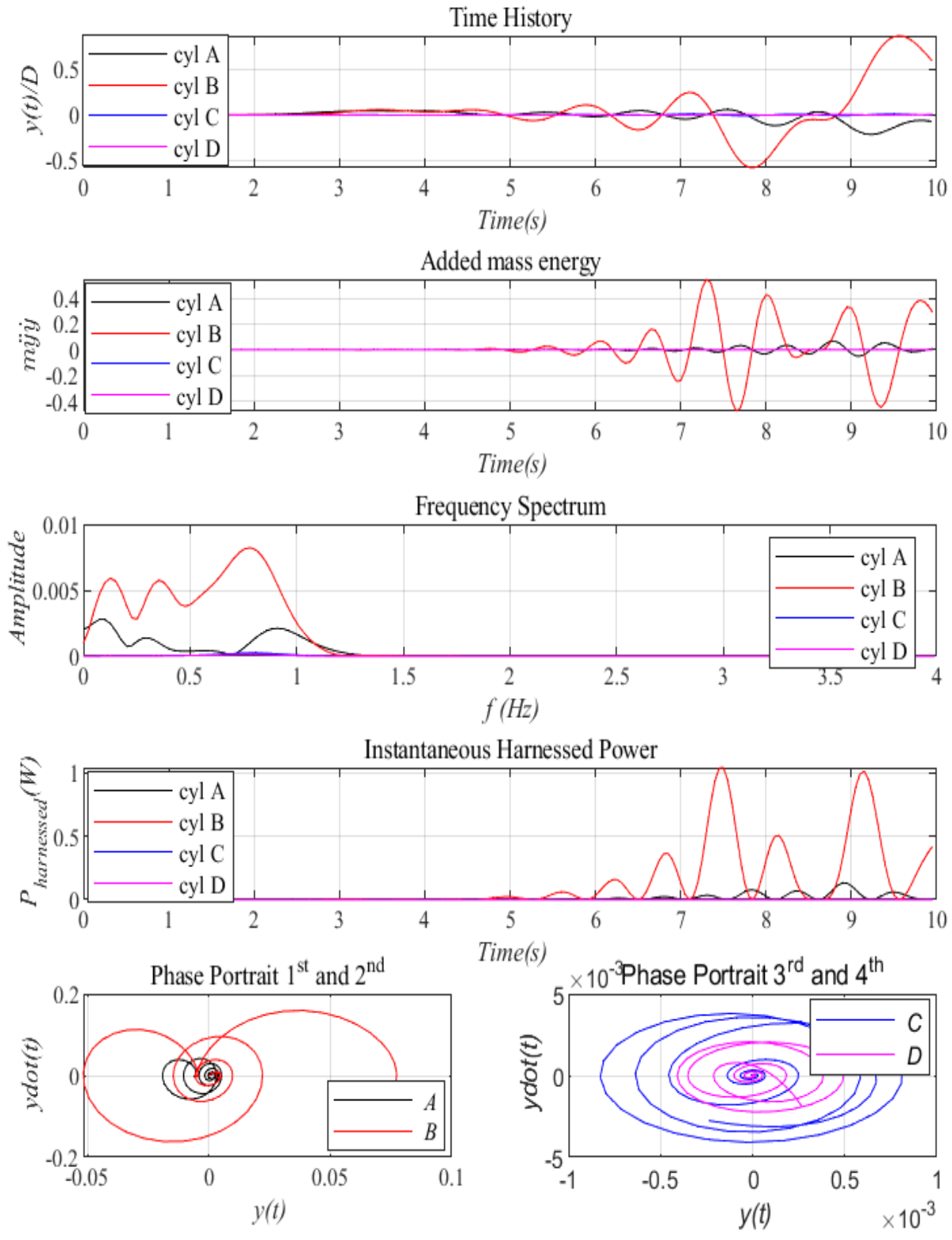

Figure 93. Postprocessing of CFD simulated cylinder motion

CFD Case #1, 0.50m/s, beta=2.00 CFD Case #11, 1.50m/s, beta=2.00

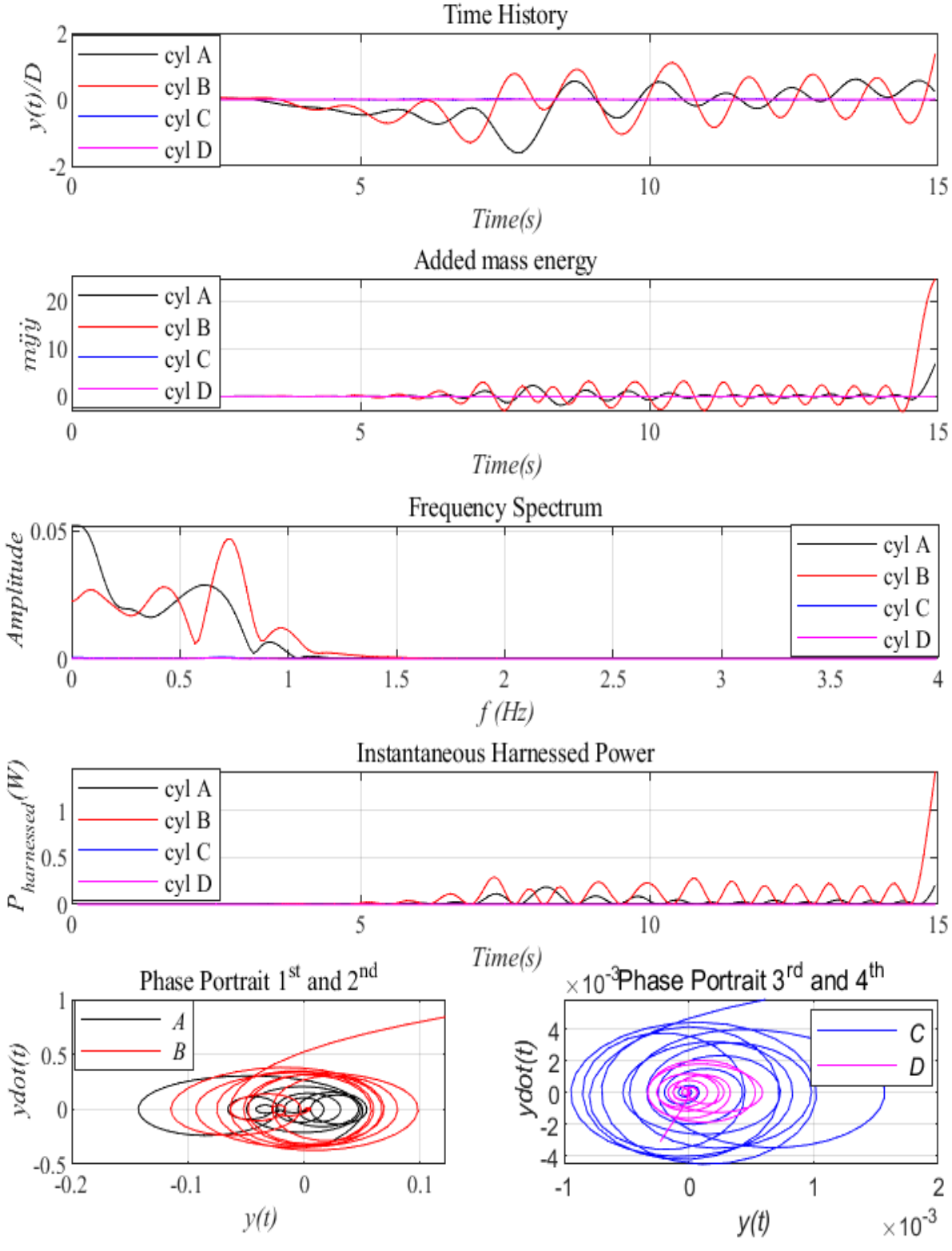

Figure 94. Postprocessing of CFD simulated cylinder motion

CFD Case #1, 0.50m/s, beta=2.00 CFD Case #12, 1.50m/s, beta=4.00

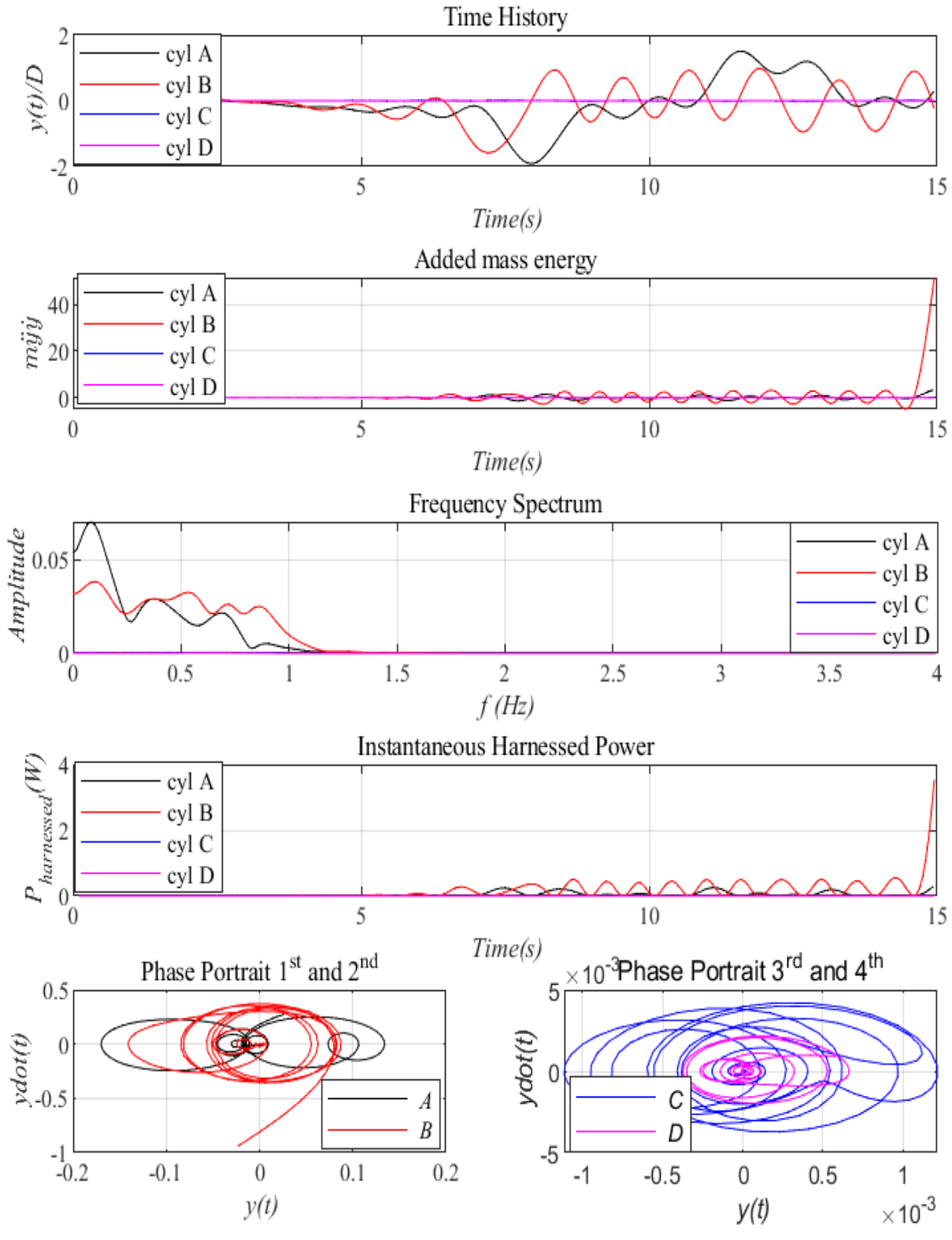

Figure 95. Postprocessing of CFD simulated cylinder motion

CFD Case #1, 0.50m/s, beta=2.00 CFD Case #13, 1.50m/s, beta=6.00

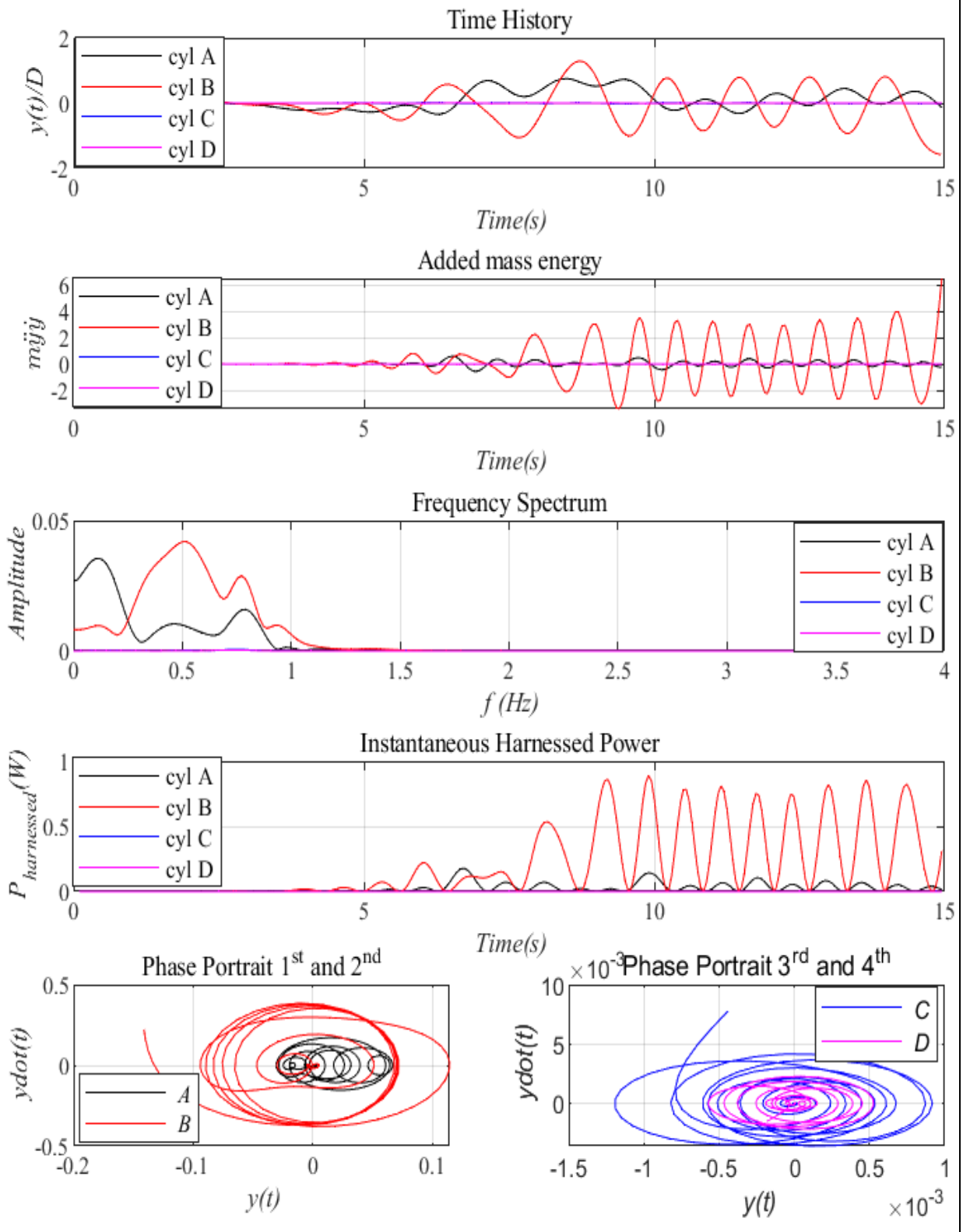

Figure 96. Postprocessing of CFD simulated cylinder motion

CFD Case #1, 0.50m/s, beta=2.00 CFD Case #14, 1.50m/s, beta=20.00

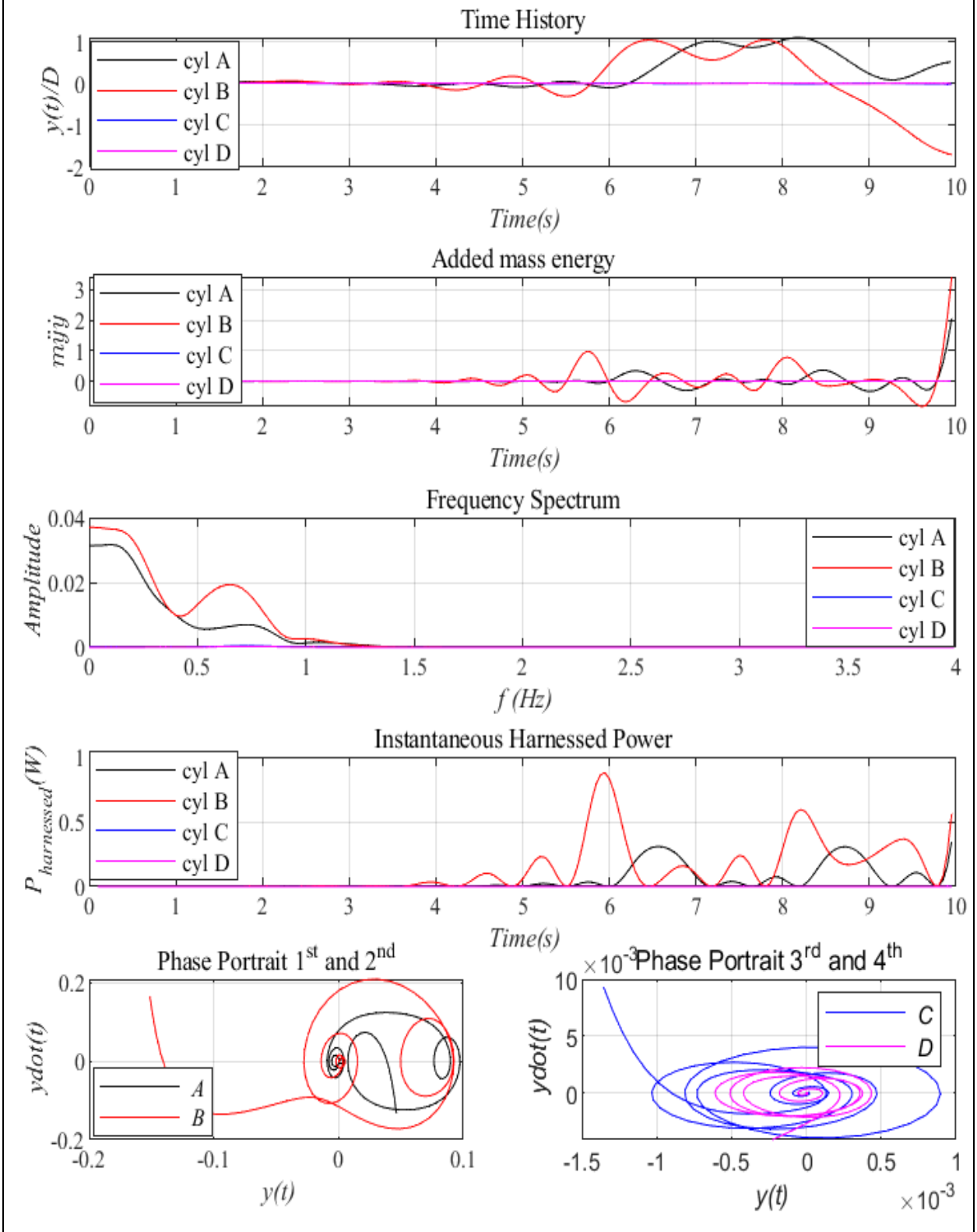

Figure 97. Postprocessing of CFD simulated cylinder motion

CFD Case #1, 0.50m/s, beta=2.00 CFD Case #15, 1.50m/s, beta=40.00

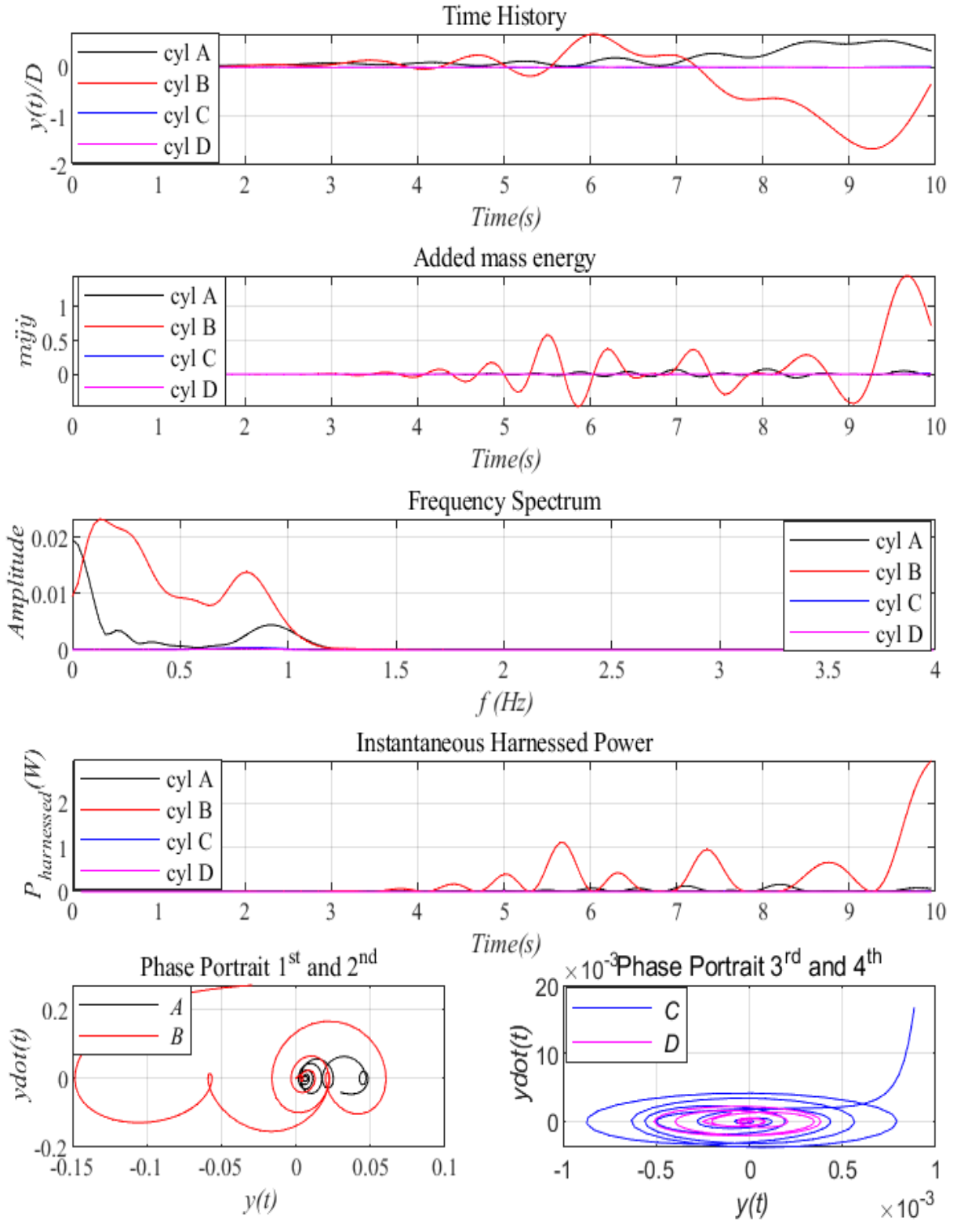

Figure 98. Postprocessing of CFD simulated cylinder motion

CFD Case #1, 0.50m/s, beta=2.00 CFD Case #16, 1.50m/s, beta=60.00

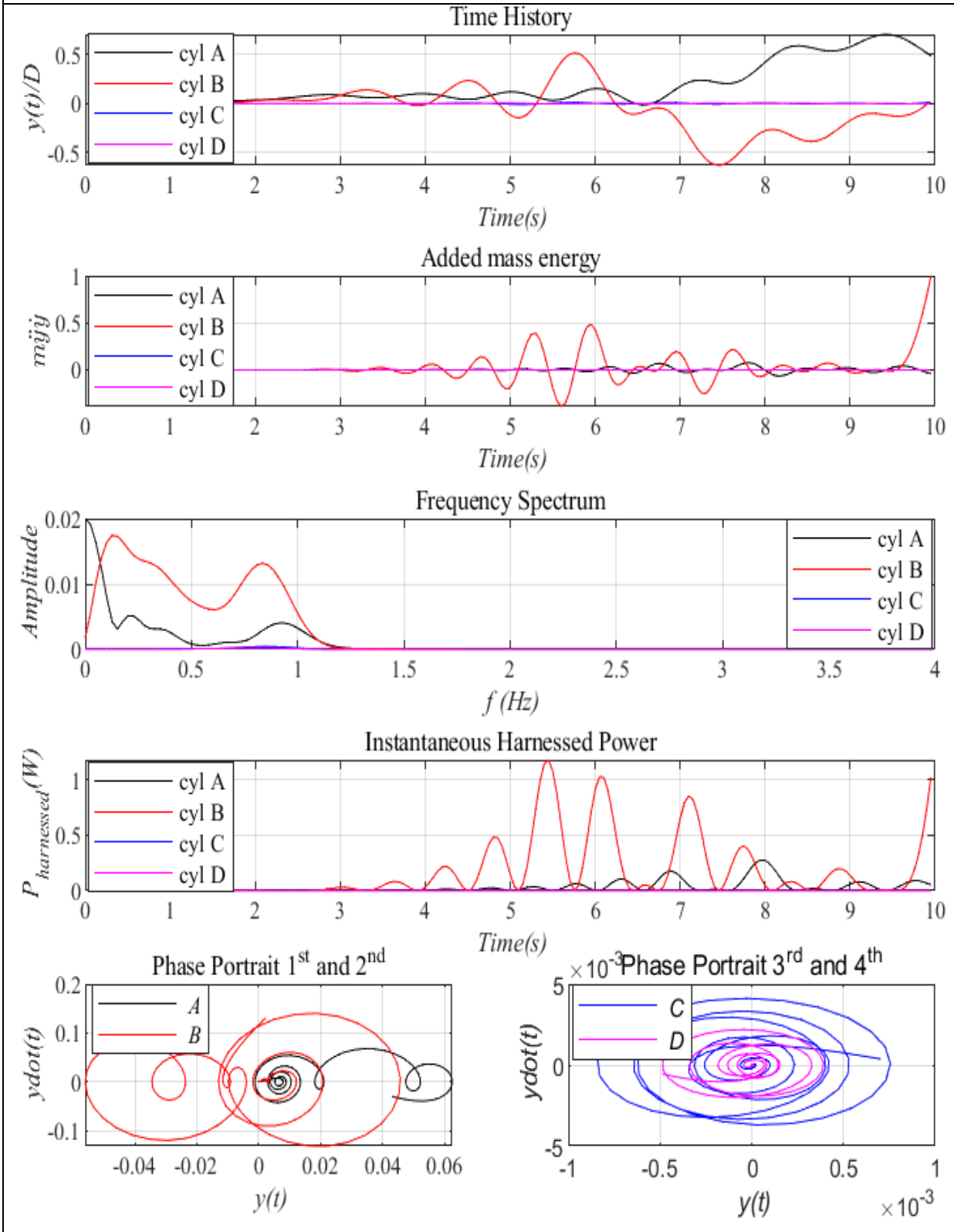

Figure 99. Postprocessing of CFD simulated cylinder motion

16.2. CFD Results for The 2-Cylinder VIVACE Converter

Table 18: CFD Simulation Cases for the 2-Cylinder VIVACE Converter

Case #	Table #	Flow Speed U [m/s]	Adaptive Damping Coefficient β	Figure #
1		1.00	2.00	100
2		1.30	20.00	101
3		1.50	50.00	102

CFD Case #1, 0.50m/s, beta=2.00 CFD Case #1, 1.00m/s, beta=2.00

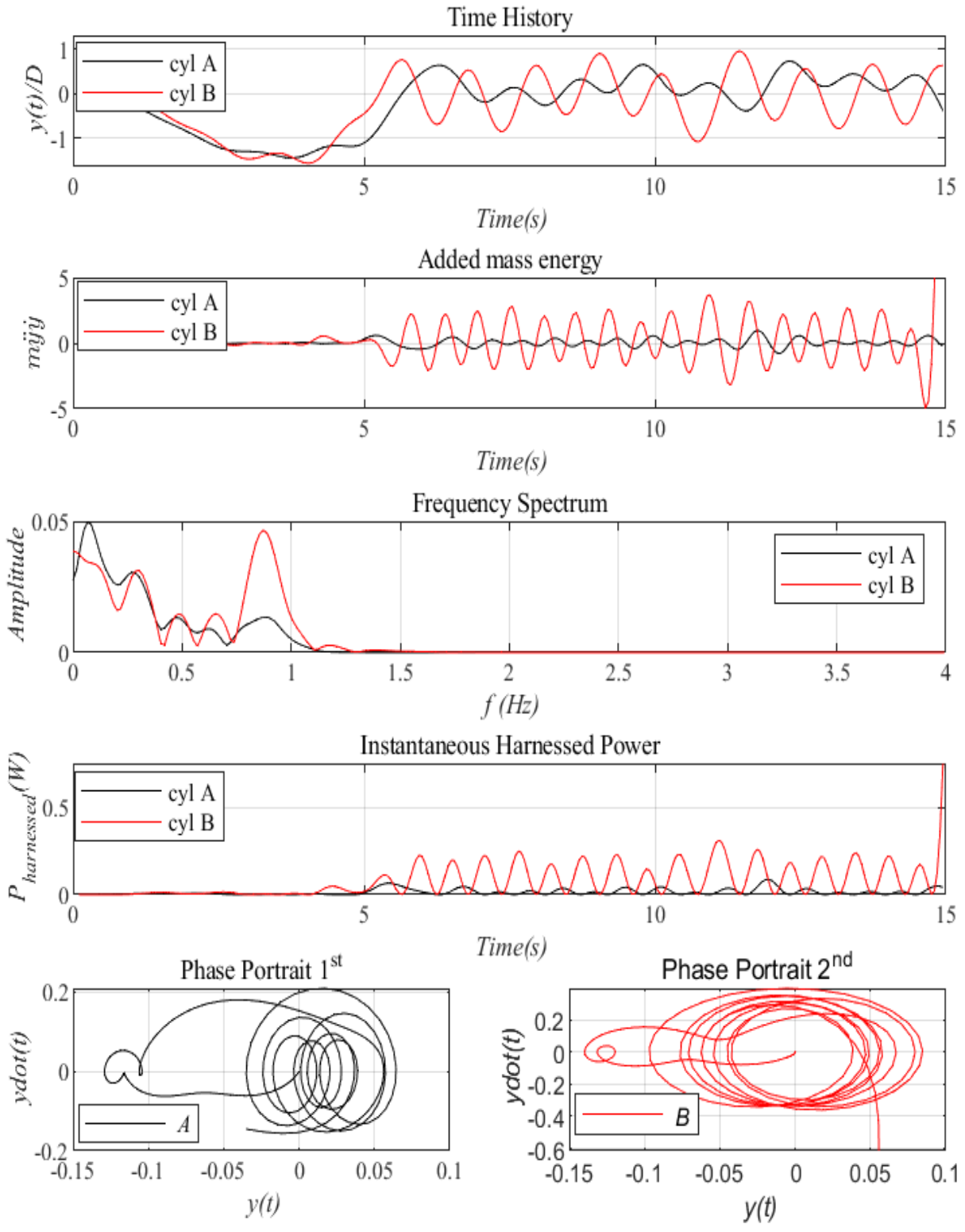

Figure 100. Postprocessing of CFD simulated cylinder motion

CFD Case #1, 0.50m/s, beta=2.00 CFD Case #2, 1.30m/s, beta=20.00

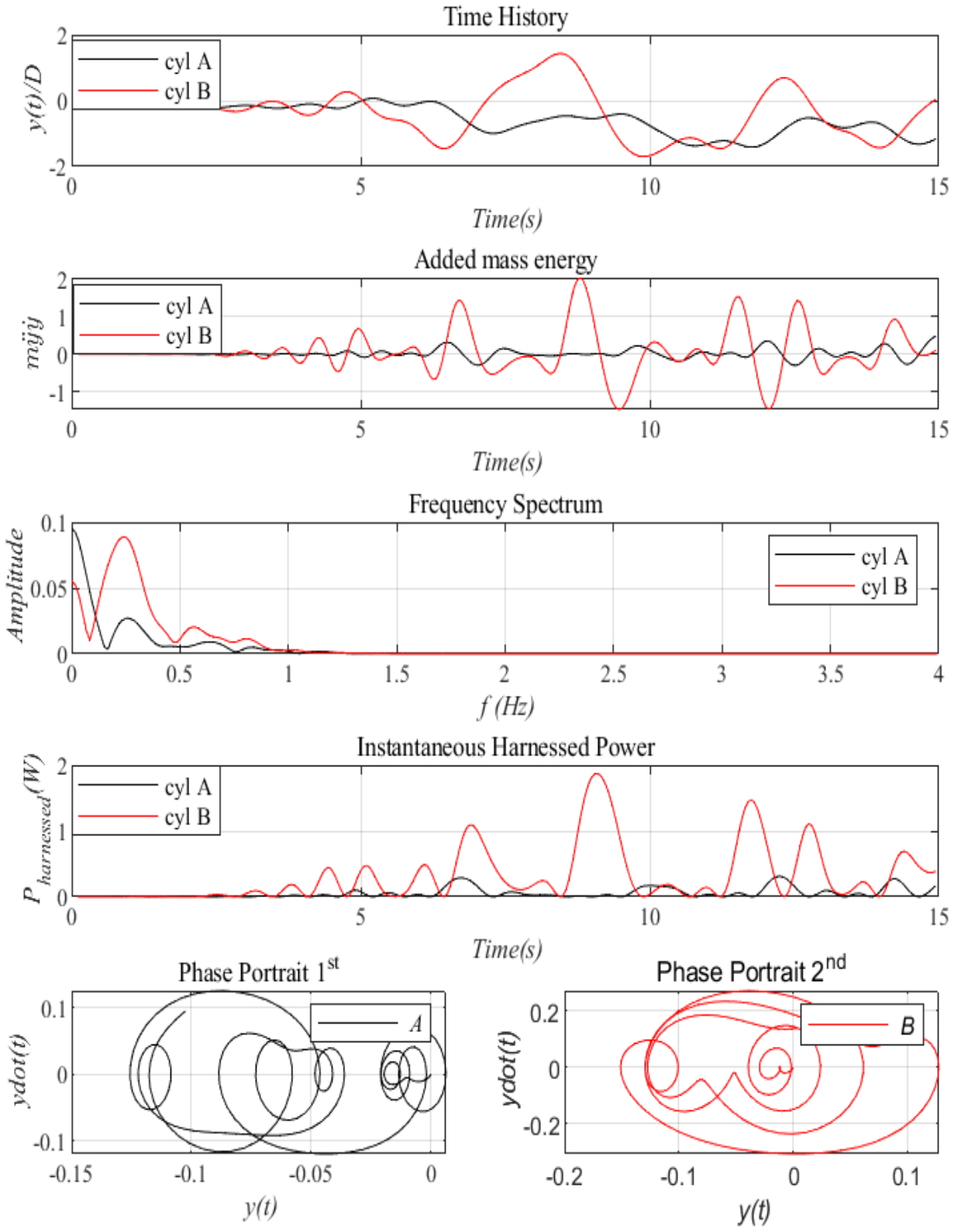

Figure 101. Postprocessing of CFD simulated cylinder motion

CFD Case #1, 0.50m/s, beta=2.00 CFD Case #3, 1.50m/s, beta=50.00

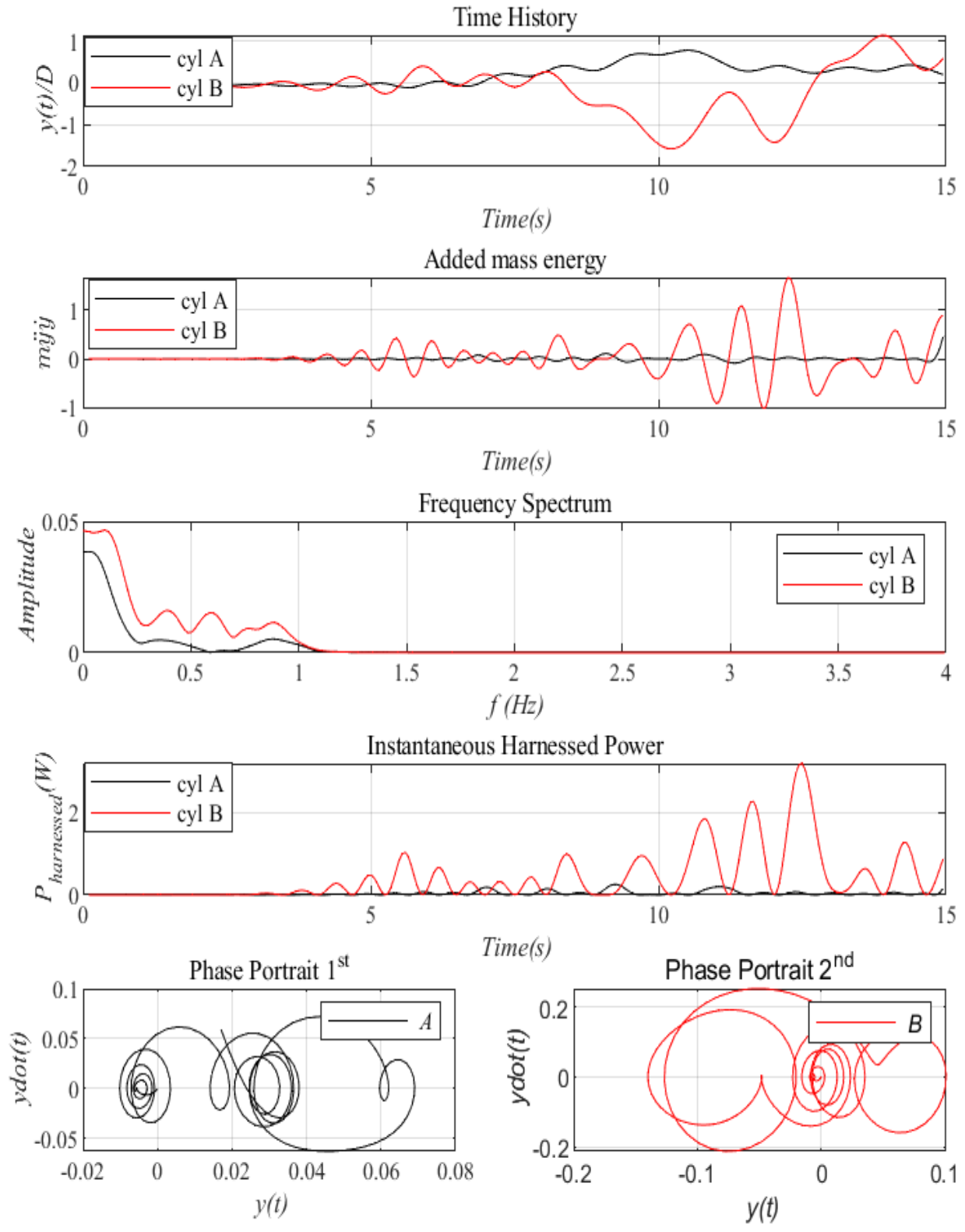

Figure 102. Postprocessing of CFD simulated cylinder motion

APPENDICES

APPENDIX I: REFERENCES

APPENDIX II: FACILITY SAFETY

APPENDIX III: VIVACE PMSG Quadrature Current

APPENDIX IV: CFD REPORT

APPENDIX V: FEA AND FATIGUE ANALYSIS REPORT

Appendix I: References

Patents

[1] Bernitsas M.M., Raghavan K., "Fluid Motion Energy Converter", US Patent and Trademark Office, Patent# 7,493,759 B2, February 24, 2009.

[2] Bernitsas, M. M, Raghavan, K., "Enhancement of Vortex Induced Forces & Motion through Surface Roughness Control" US Patent &Trademark Office, #8,047,232 B2, Nov. 1, 2011.

[3] Bernitsas M.M., Raghavan K., "Converter of Current, Tide, or Wave Energy", European Patent Office, Patent# EP 1 812 709 B1 issued on April 17, 2013.

[4] Bernitsas, M. M. and Raghavan, K., "Reduction of Vortex Induced Forces & Motion through Surface Roughness Control", United States Patent and Trademark Office, Patent# 8,684,040 B2, issued on April 1, 2014.

[5] Bernitsas, M. M. and Xiros, N., "Contact-Less Magnetic Supports for Marine Hydrokinetic Energy Harvesting Using Flow Induced Oscillation", US Patent & TM Office # 11,143,158

[6] Bernitsas M. M., C. C. Bernitsas, H. Sun, "Marine Hydrokinetic Energy Harvester with Multiple VIVACE Oscillators in Synergy", Patent Disclosure #2022-268, University of Michigan, February 1, 2022.

[7] Bernitsas, M. M. and Liapis, S., "Marine Hydrokinetic Energy Harvesting Using Flow Induced Oscillations and Waves", Patent Disclosure #2022-054, University of Michigan, August 16, 2021.

References

[8] Bernitsas, M. M., "Harvesting Energy by Flow Included Motions", Chapter 47, Springer Handbook of Ocean Engineering, Editors: Dhanak, M. R., Xiros, N. I., 2016, Springer-Verlag Berlin Heidelberg; ISBN 978-3-319-16648-3; pp. 1163-1244.

[9] Aktosun, E., Xiros, N.I., Dahl, J.M. "A Data Model for In-stream Forces on a Cylinder Using Neural Networks and Linear Prediction Filters", Acta Scient. Comp. Scien.3.8 (2021): 50-64.

[10] Bailey K., "National Strategy for a Sustained Network of Coastal Moorings", IOOS (Eyes on the Ocean), Oct. 25, 2017.

[11] Bhatnagar D., et al., "Grid Value Proposition of Marine Energy: A Preliminary Analysis", US Department of Energy, Report # PNNL-31123, Nov. 2021.

[12] Kim E. S., Bernitsas M. M., "Performance prediction of horizontal hydrokinetic energy converter using synergy of multiple cylinders in flow induced motion", Applied Energy 170 (2016) 92–100.

[13] Kim E. S., Park H, Sun H, Shin S C, Cho D S, Bernitsas M M (2021), "Development of an Alternating Lift Converter utilizing Flow Induced Oscillations to Harness Horizontal Hydrokinetic Energy", Renewable and Sustainable Energy Reviews 145, 111094

[14] R.W.J. Lacey, V.S. Neary, J.C. Liao, E.C. Enders, H.M. Tritico: The IPOS framework: Linking fish swimming performance in altered flows from laboratory experiments to rivers, River Res. 28, 429–443 (2011).

[15] Lee, J.H., Xiros, N.I., Bernitsas, M.M. (2011), "Virtual damper–spring-system for VIV experiments and hydrokinetic energy conversion", Ocean Engineering 38 (2011) 732–747.

[16] H. Li, C. C. Bernitsas, N. Congpuong, M. M. Bernitsas, H. Sun, "Patterns of flow induced oscillations of cylinder arrays match fish-shape undulation for optimal hydrokinetic energy harnessing", Applied Energy, Submitted Jan 2022.

[17] Liao, J. C., Beal, D. N., Lauder, G. V. & Triantafyllou, M. S., (2003a), "Fish exploiting vortices decrease muscle activity". Science 302, 1566–1569.

[18] LiVecchi, A., et al. "Powering the Blue Economy; Exploring Opportunities for Marine Renewable Energy in Maritime Markets." U.S. Department of Energy, Office of Energy Efficiency and Renewable Energy. Washington, D.C., 2019.

[19] Lv Y, Sun L, Bernitsas M M, Sun H, "A Comprehensive Review of Nonlinear Oscillators in Hydrokinetic Energy Harnessing using Flow-Induced Vibrations". Renewable & Sustainable Energy Reviews. 150 (2021) 111388.

[20] Mays T.W., Plaut R.H., Liapis S. "Three-Dimensional Analysis of Submerged, Moored, Horizontal, Rigid Cylinders Used as Breakwaters", Ocean Engin., V.26, pp.1311-1333, 1999.

[21] Sun, H., Bernitsas, M. P., Kim, E. S., Bernitsas, M. M., "Virtual Spring-Damping System for Fluid Induced Motion Experiments", Journal of Offshore Mechanics and Arctic Engineering, ASME Trans, Dec. 2015, Vol. 137, No. 1, 061801.

[22] Sun, H., M. M. Bernitsas, M.Turkol, "Adaptive Harnessing Damping in Hydrokinetic Energy Conversion by two Rough Tandem-Cylinders using Flow-Induced Vibrations", Renewable Energy, Vol. 149, April 2020, pp. 828-860.

[23] Sun, H., & Bernitsas, M. M. (2019). Bio-Inspired adaptive damping in hydrokinetic energy harnessing using flow-induced oscillations. Energy, 176, 940-960.

[24] Tsakyridis G., Xiros N.I. (2021) Dynamics and Control of a Magnetic Transducer Array Using Multi-Physics Models and Artificial Neural Networks, Sensors (Basel). 2021 Oct 13;21(20):6788. doi: 10.3390/s21206788. PMID: 34696001; PMCID: PMC8537558.

[25] Z. S. Willis and J. Pica, "National Strategy for a Sustained Network of Coastal Moorings", NOAA, National Data Buoy Center, January 2017.

[26] Xiros, N.I., Aktosun, E. (2022) Stabilization of Neural Network Models for VIV Force Data Using Decoupled, Linear Feedback. J. Mar. Sci. Eng. 2022, 10, 272.

Appendix II: Facility Safety

The PDF of a PPT on MHL safety procedures is appended.

Appendix III: VIVACE PMSG Quadrature Current

The equations for the Permanent Magnet Synchronous Generator (PMSG) used in the tests are appended.

Appendix IV: CFD Report

The CFD report describing in detail the process and the code developed in the MRELab based on OpenFOAM is appended.

Appendix V: FEA and Fatigue Analysis Report

The FEA and Fatigue report describing in detail the process and the ANSYS based process is appended.

Marine Hydrodynamics Laboratory

Safety Presentation

COLLEGE OF ENGINEERING
NAVAL ARCHITECTURE & MARINE ENGINEERING
UNIVERSITY OF MICHIGAN

MHL Staff

- Kevin Maki, Director
  - Room 126
  - kjmaki@umich.edu
  - 734-647-0249

- Nicole Cheesman, HR Associate
  - Room 126
  - ncheesma@umich.edu
  - 734-764-9432

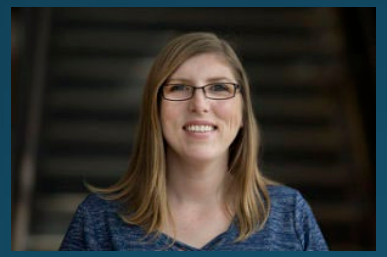

- Jason Bundoff, Lead Engineer in Research
  - Room 150
  - jasonjb@umich.edu
  - 734-764-4967

- Alex Flick, Senior Electrical Engineer
  - Room 149
  - aflick@umich.edu
  - 734-764-4654

- James Smith, Research Project Engineer
  - Room 164
  - jcsmi@umich.edu
  - 734-764-4970

MHL Front Office Phone #: 734-764-9432

Welcome to the MHL

- Built 1904
- Last vestige of College of Engineering on Central Campus
- Houses multiple different testing facilities
- On site mechanical, machine and wood shop

Site and Equipment Training

- Training by itself does not qualify you to use any machines in the MHL that have the potential to cause great bodily harm. Each zone has specific training to use tools such as power saws, drill presses, and lathes.
- If you do not have the appropriate training, you cannot use the machine, even if you think you are competent and have years of experience in another shop.

Safety is Key

- SAFETY! It is everyone's responsibility.
- Everyone starts from a different skill level. Some individuals have never even picked up a hammer and others have worked in machine shops and cabinet shops.
- Training is required to make sure everyone using the space has the skill level required for safe use of the tools and equipment.
- If you are wondering if a specific process or operation is safe, the answer is "no" until you get further training. It's ok to ask for help! This is a learning environment!

Think Before you Act

Awareness of your situation and surroundings is more effective at preventing accidents and injuries than anything else. We count on **YOU** to look out for yourself and your peers.

Check yourself:

- Does what I'm doing seem safe?
- What could go wrong?
- Is there a safer way to do this?
- Could this injure me or someone else?
- If I were injured, is anyone around to help me?

Help look out for:

- Improper use of tools
- Broken or compromised equipment
- Damaged electrical cords
- Open bottles, leaks, or spills of caustic or flammable chemicals
- Trip hazards on the floor
- Unprotected sharp objects
- Heavy objects that may fall
- Unsecured compressed gas containers
- Springs under tension
- Inappropriate or unsafe behavior
- Burn and fire hazards

The Buddy System

Be sure to have another person with you at all times in the workspace. If you were to get hurt, having someone nearby to assist you or quickly summon help could be the difference between life and death.

What are buddies good for?

- Helping to check your surroundings and tools for unsafe situations while you're working.
- Double checking your safe behavior and use of equipment.
- Offering extra hands, bodies, and minds for lifting, maneuvering, troubleshooting, etc.
- Dealing with emergencies together.
- Co-designing and making the workshop fun!

Dress Code

Everyone in workshop must wear:

- safety glasses (provided near entrance)
- long pants and durable closed-toed shoes (provided by you)

To prevent other attire from becoming a safety hazard, the following measures are required of anyone using equipment with moving parts:

- Any loose or flowing hair must be tied back in such a way as it will not come loose easily
- Long sleeve shirts must have the sleeves rolled up and out of the way
- Baggy clothing and drawstrings on hoodies must be tucked in or removed
- Remove all jewelry (i.e. necklaces, watches) that could catch in a machine
- Gloves are not allowed on saws, drill presses, sanding or grinding equipment

Emergency Preparedness

FIRE

- Become familiar with the fire exits, locations of fire extinguishers, and designated meeting areas
- You should only attempt to fight a fire if:
  - The fire is small and contained
  - You are safe from toxic smoke
  - You have a means of escape
  - Your instincts tell you it is ok
- Sound the alarm and exit the building in an orderly manner using the stairs (not elevators) and go to the designated meeting area
- Try to be aware of who was with you and make sure they have also exited the building. If you think someone is still inside, notify first responders
- Do NOT re-enter the building until directed by authorities
- When you reach safety, call Campus Police to confirm the fire

Emergency Preparedness (Continued)

SEVERE WEATHER

- Become familiar with the designated meeting area in your building
- In case of a tornado or severe weather alarm, close all doors and move quickly and calmly to the designated cover area
- Try to be aware of who was with you and make sure they have also exited the building. If you think someone is still inside, notify first responders
- Do NOT leave the severe weather area until directed by authorities
- Sign up for UM Emergency Alerts via Wolverine Access

Personal Emergency & Accident Response

In case of an accident:

1. Remove the person from immediate danger
2. Notify the staff member on duty and/or call 911. You must tell the dispatcher where you are (the building and room number)
3. After calling for help, assist the injured person
    a. For minor injuries, the first aid kit is located in Room 156 on the left when you walk in from the hallway.
    b. An AED is located outside of the North End PMB Tank doors on the wall.
4. Once all users are safe:
    a. Call the emergency workshop contact listed on the entry door
    b. Assist staff in submitting an incident report for any accident or injury

Emergency Contact Numbers

- MHL Main Line
  - 734-764-9432
- U of M DPSS
  - 734-763-1131
- Emergencies
  - 911

Best Locations to Direct Emergency Personnel

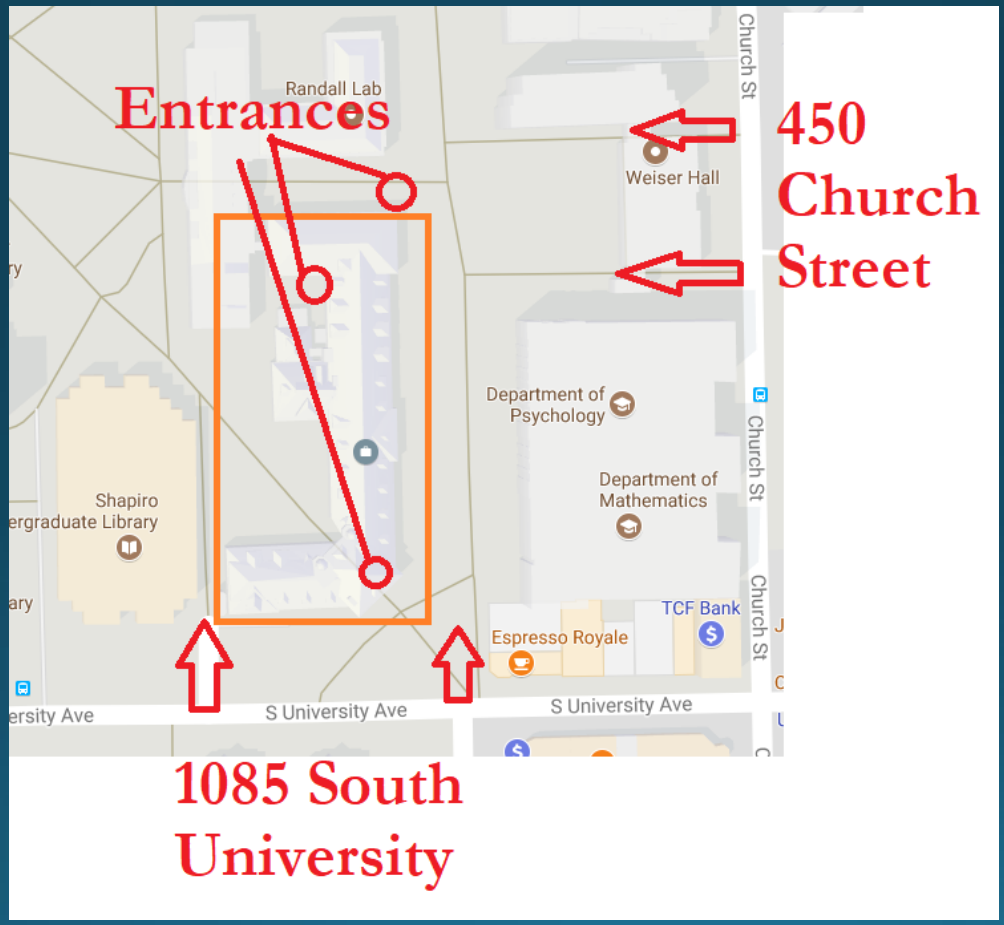

General Layout

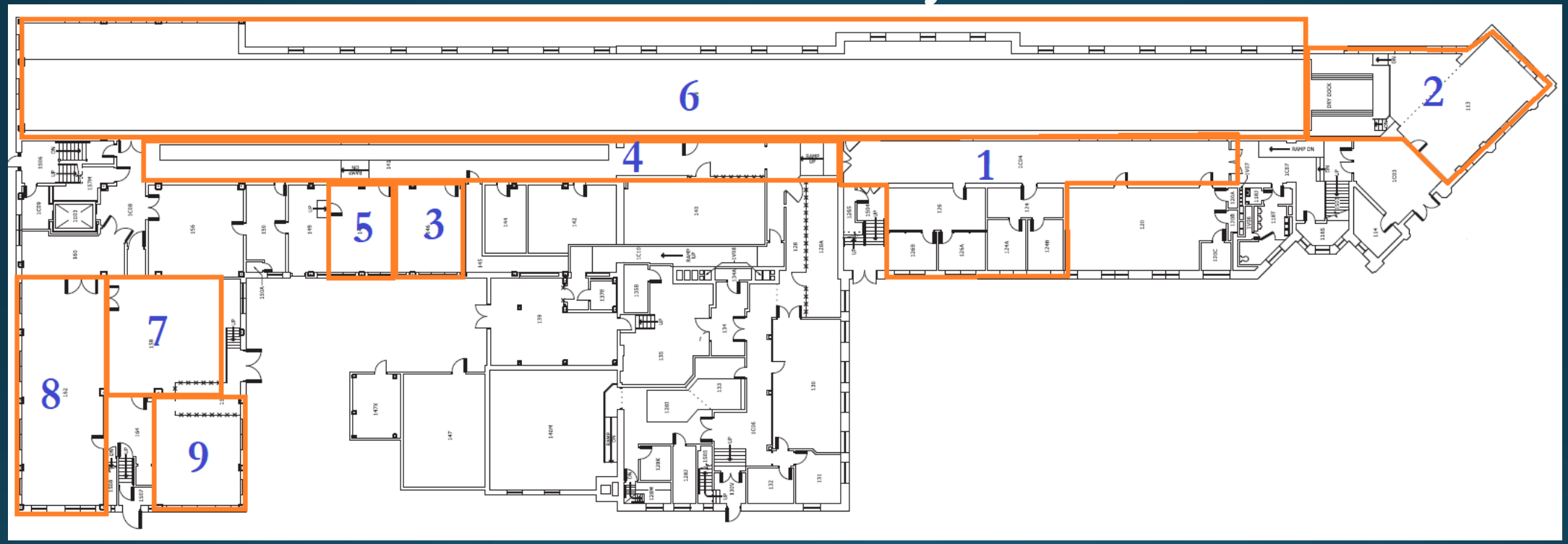

1). Front Office
2). Room 113
3). Conference Room
4). Hallway
5). Workshop
6). Physical Modeling Basin
7). Mechanical Shop
8). Wood Shop
9). Machine Shop

Hallway Exits

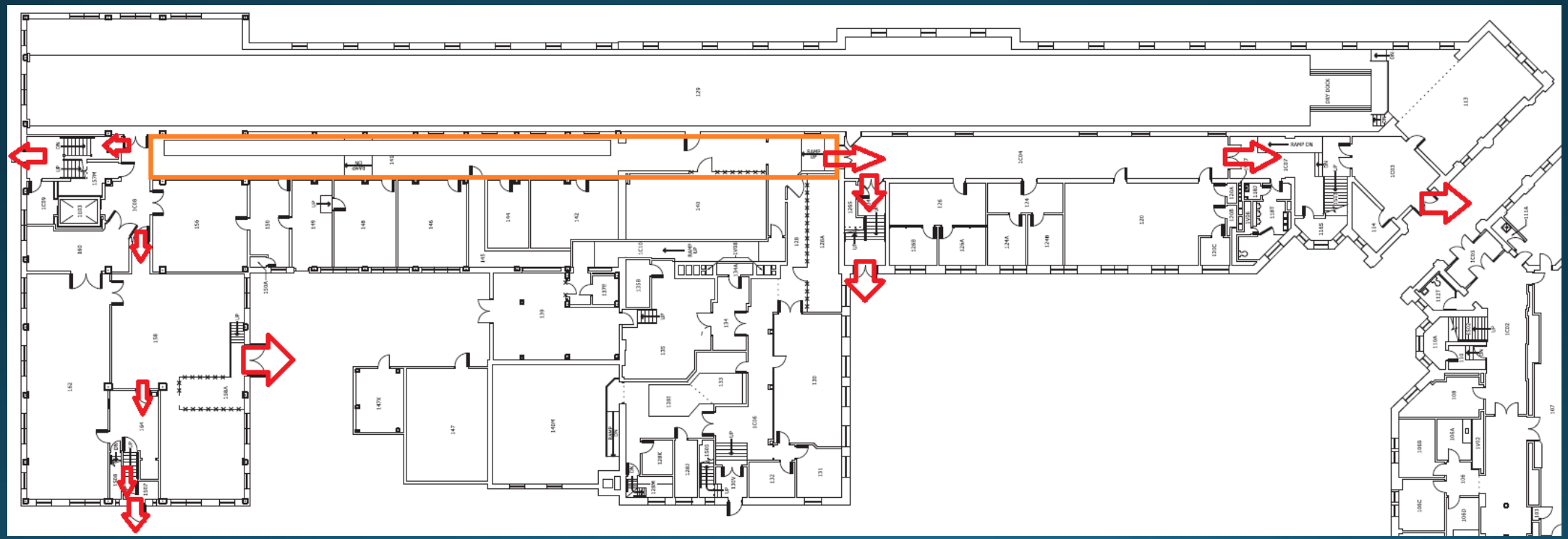

Physical Modeling Basin Safety

- Minimum of 3 personnel must be present
- All personnel must be able to swim without PFD
- PPE
  - Coast Guard certified PFDs on at all times
    - Must be passively buoyant or automatic inflating
  - Hard hats required if using hoists
  - Safety glasses are available
  - Throw-able floatation devices located throughout tank
    - 2 on powered carriage
    - 1 on unpowered sub-carriage
    - 1 North End on inside of door
    - 1 Mid Tank on inside of door

PMB Safety Continued

- Trip Hazards
  - Watch your feet at all times
  - Rails, landing platform, carriage decks, equipment, etc.
- Fall Hazards
  - Use hand holds whenever possible
- Water Hazards
  - Remove jackets/sweaters
  - Leave bags out of the tank

PMB Safety Continued

- Do not walk along rails
- High Voltage Overhead
  - Assume cable-ways are always powered on
  - Do not use conductive material near them
- Ventilation fan may be turned off for better communication
- Unpowered Sub-Carriage
  - Can be moved by hand by one person
  - To be used as safety platform
  - Do not climb ladder to top platform

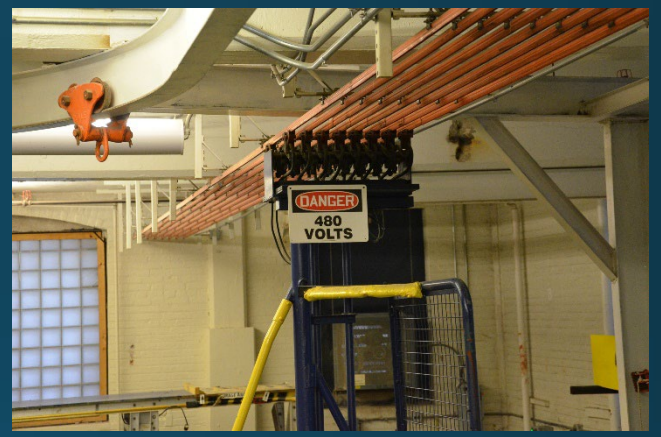

Powered Carriage Safety

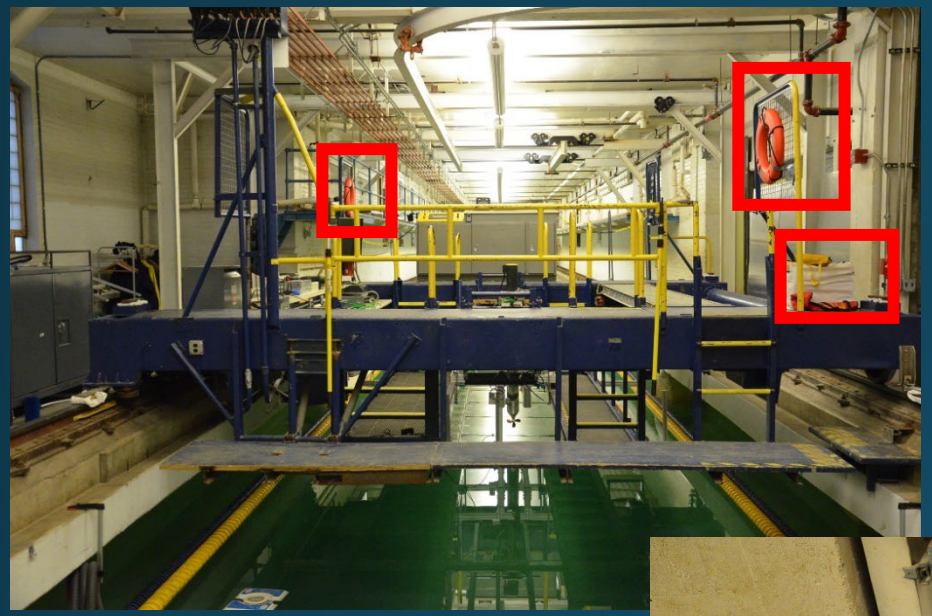

Un-powered Sub-Carriage Safety

VIVACE PMSG Quadrature Current

Proposed by Mohammad Bahru Sholahuddin

1 Base Equations

1.1 Mass-Spring-Damper System [1]

The general form of the mass-spring-damper system is:

$$m_{osc}\ddot{y} + c_{total}\dot{y} + Ky(t) = F_{fluid} \tag{1}$$

$$c_{total} = \zeta_{total}\ 2\sqrt{m_{osc}K} \tag{2}$$

Where:
- m_{osc} is the oscillating system mass.
- c_{total} is the total damping coefficient for a linear viscous damping model.
- K is the spring constant.
- $\ddot{y}$ is the linear acceleration.
- $\dot{y}$ is the linear velocity.
- y is the linear displacement.
- F_{fluid} is the force exerted by the fluid on the body.
- ζ_{total} is the total (structure + harness) damping ratio.

For a non-linear system:

$$c_{total} = \beta|\dot{y}| \tag{3}$$

Where β is the non-linear (adaptive) damping constant.

1.2 Electrical Torque as a Function of Flux Linkage and Quadrature Current [2]

$$\begin{aligned} T_e &= \frac{3P}{4}\lambda_q i_q \\ &= \frac{3(2n_{pole\_pairs})}{4}\lambda_q i_q \\ &= 1.5\lambda_q n_{pole\_pairs} i_q \end{aligned} \tag{4}$$

Where:
- T_e is the electromagnetic torque.
- P is the number of poles.
- n_{pole_pairs} is the number of pole pairs.

- i_q is the quadrature-axis current (q-axis current).
- λ_q is the flux linkage.

1.3 Mechanical Torque Equation

$$T_m = Fr \tag{5}$$

Where:
- T_m is the mechanical torque.
- F is the amount of force directed perpendicularly to the position of the object or force at the generator pulley/pinion perpendicular to the shaft center.
- r is the distance between the force and the object or the radius of the pulley/pinion.

2 Quadrature Braking/Generating Current

To emulate the damping action, we only observe the damping term from Eq.(1):

$$F_{damping} = c_{total}\dot{y} \tag{6}$$

As the motion converts from the VIVACE cylinder's translational motion to the rotational generator shaft via belt and pulley, the translational Eq.(6) can be converted to the rotational form as:

$$\dot{y} = r\omega \tag{7}$$

$$F_{damping} = c_{total} r\omega \tag{8}$$

Where:
- r is the pulley/pinion radius.
- ω is the angular velocity.

Thus, the mechanical torque for the damping action in Eq.(5) becomes:

$$\begin{aligned} T_m &= F_{damping} r \\ &= c_{total} r^2 \omega \end{aligned} \tag{9}$$

2.1 Linear Damping

Equate the electrical torque in Eq.(4) to the mechanical torque in Eq.(9), and introduce a negative (-) sign as the machine is used to convert mechanical to electrical force to get the quadrature current as:

$$\begin{aligned} T_e &= -T_m \\ 1.5\lambda_q n_{pole\_pairs} i_q &= -c_{total} r^2 \omega \\ i_q &= -\frac{c_{total} r^2 \omega}{1.5\lambda_q n_{pole\_pairs}} \end{aligned} \tag{10}$$

As a function of damping ratio ζ, using Eq.(2), the equation can be shown as:

$$\begin{aligned} i_q &= -\frac{c_{total} r^2 \omega}{1.5 \lambda_q n_{pole\_pairs}} \\ i_q(linear) &= -\zeta_{total}\ 2\sqrt{m_{osc} K} \frac{r^2 \omega}{1.5 \lambda_q n_{pole\_pairs}} \end{aligned} \tag{11}$$

2.2 Non-Linear Damping

For non-linear damping, using Eq.(3) and the translational-rotational conversion in Eq.(7), the mechanical torque due to the damping in Eq.(9) becomes:

$$\begin{aligned} T_m &= c_{total} r^2 \omega \\ &= \beta |\dot{y}| r^2 \omega \\ &= \beta |r\omega| r^2 \omega \\ &= \beta r^3 \omega |\omega| \end{aligned} \tag{12}$$

Using the electrical torque Eq.(4) and non-linear mechanical torque Eq.(12), to get the non-linear damping generative quadrature current we equate as:

$$\begin{aligned} T_e &= -T_m \\ 1.5 \lambda_q n_{pole\_pairs} i_q &= -\beta r^3 \omega |\omega| \\ i_q(non-linear) &= -\frac{\beta r^3 \omega |\omega|}{1.5 \lambda_q n_{pole\_pairs}} \end{aligned} \tag{13}$$

References

[1] W. Wu, H. Sun, B. Lyu, and M. Bernitsas, "Modelling of a hydrokinetic energy converter for flow-induced vibration based on experimental data," *Ocean Engineering*, vol. 155, pp. 392–410, 05 2018.

[2] D. Ocen, "Direct torque control of a permanent magnet synchronous motor", 2005, Online Available https://api.semanticscholar.org/CorpusID:106536949

TEAMER Report on Numerical Investigation of Flow Induced Oscillations of a 4-Cylinder VIVACE Converter and a 2-Cylinder VIVACE Converter

Vortex Hydro Power

2350 Washtenaw Avenue, Suite #26

Ann Arbor, MI 48104

August 30, 2024

Authors: Onggo Nichita, Intern

Michael M Bernitsas, Ph.D., CEO of VHP

Stergios I Liapis, CTO of VHP

Salman Sadiq, Ph.D., Senior Engineer of VHP

TABLE OF CONTENTS

1. ABSTRACT

Flow induced oscillations (FIOs) of 4 rigid, smooth cylinders, with large turbulence stimulators, placed in tandem are investigated for hydrokinetic energy conversion at flow speed from 0.1m/s to 3.0 m/s. This range is selected to cover the wide range of flow speed in rivers, and ocean currents and tides. Most flows are slower than 2m/s and rivers are typically slower than 1m/s. Numerical solutions are performed by two-dimensional analysis using Unsteady Reynolds-Averaged Navier-Stokes (URANS) equations with the Spalart-Allmaras turbulence model.

Input parameters, which are important in this numerical solution, are cylinder spacing, damping, flow speed, and spring stiffness. The center-to-center spacing between cylinders d/D is set at 2.57D.

The parametric values in the simulations presented in this report are:

(a) The adaptive damping coefficient β takes the values of 2, 4, and 6. In adaptive damping, the damping coefficient *C* is modeled as $C = \beta y(\dot{t})$ where β is a constant and $y(\dot{t})$ is the oscillatory velocity of the cylinder. Thus, high motion results in increased harnessed energy and low motion in less harnessed energy.

(b) Flow speed tested is 0.5, 1.0 and 1.5 m/s. The results of CFD provide excellent visualization, which is a powerful tool in identifying bi-stabilities, bifurcations, wake flows, and vortex structures as observed in experiments.

It takes about 10 hours of computations on a 24-core Mac Studio workstation to generate about 30 seconds of real time simulation. In this report, the following cases are presented:

(i) Nine simulations for the combinations of the three flow-speed values and the three β values mentioned above.

(ii)

2. LIST OF FIGURES

3. INTRODUCTION

Flow induced oscillations (FIOs) considered in this study consist of Vortex Induced Vibrations (VIV), galloping, and their coexistence. These are natural fluid-structure interaction instabilities which are very destructive and have applications in several engineering disciplines and particularly offshore engineering. In this study, the Marine Hydrokinetic (MHK) energy from a steady uniform flow is converted to mechanical energy in the oscillators. The latter can be converted to electricity. The converter, called VIVACE, has a set of rigid cylinders in tandem with spacing between the cylinders.

In previous research, VIVACE converters have been designed with single cylinder, two cylinders, three cylinders, and four cylinders. The highest efficiency (88% of Betz limit) was reached by a four-cylinder VIVACE Converter. In this study, we use four cylinders with spacing selected based on previous research. The reason for implementing adaptive damping is to enhance FIO in the third and fourth cylinders, which are shielded in a four-cylinder VIVACE converter with same spacing between cylinders. As cylinders are added in tandem, returns diminish. The question arises as to the optimal number of cylinders; would it be 2, 3, or 4.

In this study, the parameters are flow speed and adaptive damping coefficient β. The other parameters which are kept constant are spring rate and cylinder spacing. The flow speed varies from 0.5, 1.0 and 1.5 m/s. These are representative of flow speeds on the low to medium ranges. For higher speeds, a stronger heavier Converter will be designed. The main reason is to make the VIVACE reliable and durable in most current flow speeds. Damping defines the performance of VIVACE because the energy extracted depends mainly on the value of damping. The damping coefficient β values that we choose to test are 2, 4, and 6. Spring rate doesn't determine the maximum power extracted, but it defines the VIV synchronization range. As the spring rate increases, the natural frequency of the oscillator and, thus, the onset of VIV also increases. Spring rate value of 27 N/mm has been selected for all simulations only as a bumper spring at the end of the travel. The cylinder surface also determines how the cylinder in FIO behaves. In this research we use a smooth cylinder with turbulence stimulation of height 28% of the diameter and covering 16 degrees on each side of the cylinder [1].

The simulations conducted use Unsteady Reynold-Averaged Navier Stokes (URANS) with Spalart-Allmaras turbulence model. They are solved and numerically in 2D to increase the efficiency of computational time. The model uses spring-mounted rigid circular cylinder with single degree of freedom in the direction perpendicular to the flow and the cylinder axis.

4. NOMENCLATURE

A	Mean amplitude of peaks [m]
$A^* = A/D$	Amplitude ratio
c_{total}	Linear viscous damping [Ns/m]
D	Cylinder diameter [m]
f_{osc}	Oscillating frequency [Hz]
$f_{n,vac}$	Natural frequency in vacuum
f^*	Frequency ratio
FIOs	Flow-Induced Oscillations
K	Spring stiffness [N/m]
L	Cylinder length [m]
LTFSW	Low Turbulence Free Surface Water [Channel]
m_d	Displaced fluid mass [kg]
m_{osc}	Oscillating mass [kg]
m^*	Mass ratio
MRELab	Marine Renewable Energy Laboratory
PTC	Passive Turbulence Control
Re	Reynolds number
$U^*=U/(f_{n,vac}D)$]	Reduced velocity
VCK	Virtual damper-spring controller
VIV	Vortex-Induced Vibrations
VIVACEVIV	for Aquatic Clean Energy

Greek Symbols

β	Adaptive damping coefficient [Ns^2/m^2]
ζ	Damping ratio

5. COMPUTATIONAL METHOD

5.1. Governing Equations

In this study, the code developed to perform the CFD simulations and animations uses open source CFD tool OpenFOAM which consists of C++ libraries to solve continuum mechanics problems by using a finite-volume discretization method. The time-dependent viscous flow solutions are generated by numerical approximation of the incompressible URANS equation in conjunction with the one-equation Spalart-Allmaras (S-A) turbulence model. The basic equations are

$$\frac{\partial U_i}{\partial x_i} = 0 \quad (1)$$

$$\frac{\partial U_i}{\partial t} + U_j \frac{\partial U_i}{\partial x_i} = -\frac{1}{\rho}\frac{\partial p}{\partial x_i} + \frac{\partial}{\partial x_j}(2\nu S_{ji} - \underline{u_j' u_i'}) \quad (2)$$

where ν is the molecular kinematic viscosity and S_{ji} is the strain rate tensor

$$S_{ji} = \frac{1}{2}\left(\frac{\partial U_i}{\partial x_j} + \frac{\partial U_j}{\partial x_i}\right) \quad (3)$$

Further, U_i is the mean flow velocity vector. The quantity $\rho\underline{u_j' u_i'}$ is known as the Reynold-stress tensor and is further modeled through the Boussinesq approximation as $\nu\left(\frac{\partial U_i}{\partial x_j} + \frac{\partial U_j}{\partial x_i}\right)$. In the Spalart-Allmaras model, the turbulent eddy viscosity is defined as $\nu_t = \tilde{\nu} f_{v1}, f_{v1} = \frac{\chi^3}{\chi^3 + c_{v1}^3}, \chi = \frac{\tilde{\nu}}{\nu}$, where $\tilde{\nu}$ represents an intermediate working variable of the turbulence model and obeys the following transport equation

$$\frac{\partial \tilde{\nu}}{\partial t} + U_j \frac{\partial \tilde{\nu}}{\partial x_j} = c_{b1}(1 - f_{t2})\tilde{S}\tilde{\nu} - \left(c_{w1} f_w - \frac{c_{b1}}{\kappa^2} f_{t2}\right)\left(\frac{\tilde{\nu}}{d}\right)^2 + \frac{1}{\sigma}\left\{\frac{\partial}{\partial x_j}\left[(\nu + \tilde{\nu})\frac{\partial \tilde{\nu}}{\partial x_j}\right] + c_{b2}\frac{\partial \tilde{\nu}}{\partial x_i}\frac{\partial \tilde{\nu}}{\partial x_i}\right\} + f_{t1}\Delta U^2 \quad (4)$$

The original Spalarat-Allmaras model is employed to solve a transport equation for kinematic eddy viscosity. This model is different from other one-equation models and algebraic models in the sense that it is a local model, which means the equation in one location does not depend on the solutions at other points. Therefore, it is compatible with grids of any structure. This model has been shown to give acceptable results for a wide variety of situations and is known for its stability.

In order to introduce the cylinder dynamics in FIO, the mass-damper-spring oscillator is modelled by a second order linear differential equation. The one-degree of freedom equation of motion can be expressed as

$$m\ddot{y} + C\dot{y} + Ky = F_{fluid,y} \tag{5}$$

where $F_{fluid,y}$ is an input representing the total fluid force acting on the cylinder in the y-direction; m is the total inertial mass including the Vck system; C is the total damping, which includes the structural damping $C_{structure}$ and the harnessing damping $C_{harness}$. Equation (5) can be recast in the form of the following system of two first-order differential equations:

$$m\dot{u} = F_{fluid,y} - C\dot{y} - Ky \tag{6}$$

and

$$\dot{y} = u$$

where u is the velocity of the cylinder in the y-direction. A compounded implicit-explicit method is employed to solve the equation of motion together with the Reynolds-Averaged Navier-Stokes equations for velocity u and displacement y of the cylinder. Superscript n represents values at the current time step and $(n+1)$ for the new time step. Then,

$$\dot{u^n} = \frac{u^{n+1} - u^n}{\Delta t} \tag{7}$$

$$u^{n+1} = u^n + \Delta t \dot{\left(\frac{F_{fluid,y} - C\dot{y} - Ky}{m}\right)} \tag{8}$$

$$y^{n+1} = y^n + \Delta t \cdot u^{n+1} \tag{9}$$

The divergence, gradient, and Laplacian terms in the governing equations are solved through a second-order Gauss integration scheme with a linear interpolation for the face-centered value of the unknown. The time integration is performed by the second-order backward Euler method. Therefore, second order accuracy is ensured by the numerical discretization scheme in space and time. Momentum and continuity equations are solved together in a segregated way through a pressure implicit with a splitting of operators (PISO) algorithm.

5.2. Computational Domain and Grid Generation

For the grid in the near-wall region, different strategies are adopted for smooth and rough cylinder to achieve sufficient accuracy and capture flow properties with reasonable computational time. For the smooth cylinder with large turbulence stimulation, a boundary layer resolving grid is used. The computational domain size is 23*D*x17*D* and the boundaries are inflow, outflow, top, bottom, and the cylinder walls. The distance between the inlet boundary and the center of the 1st cylinder, lup, is set at 6*D*. The downstream length of the domain, ldown, is set at 8.2*D*. Initially, the cylinder is positioned vertically, evenly with respect to upper and lower

boundaries. The horizontal spacing between the four cylinders is set at 2.75*D* center-to-center. The inflow velocity is considered as uniform and constant. At the outflow boundary, a zero gradient condition is specified for the flow velocity as well as v_t and $\tilde{v}$. The bottom condition is defined as a wall-boundary to match the experimental conditions. In the present numerical study, the free-surface is simplified by modeling it as a wall.

Enhanced grid resolution in the vicinity of the boundary layer is important to resolve flow properties. The grid is designed to place the first grid point away from the wall to ensure y+ on the order of 1. This is in agreement with the principles under which the Spalart–Allmaras turbulence model was developed and implemented. As Reynolds number *Re* increases, the boundary layer thickness decreases dictating a reduction of the grid dimension normal to the wall to ensure proper y+ value. The near-wall grid spacing is designed to ensure y+ is on the order of 1 for the highest *Re*. For the off-wall region, grids have a higher resolution in a circular region of radius 2*D*. Grid spacing increases away from the body (see Figs. 2-3).

To determine the overall grid resolution required to have a grid independent solution, a grid sensitivity study was conducted on three different grid resolutions for the smooth stationary cylinder. The basic parameters describing the grids used in the resolution study are summarized in Table 1.

Mesh Quality	Number of Cells
Coarse	89,651
Medium	136,651
Fine	325,800
Table 1. Mesh Grid Number of Cells	

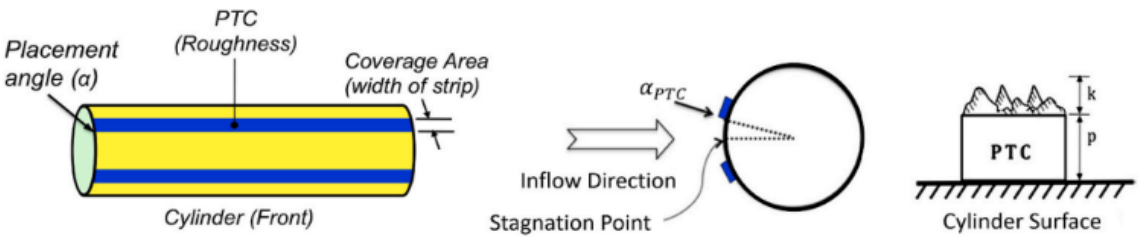

Figure 1. Cylinder with large turbulence stimulation

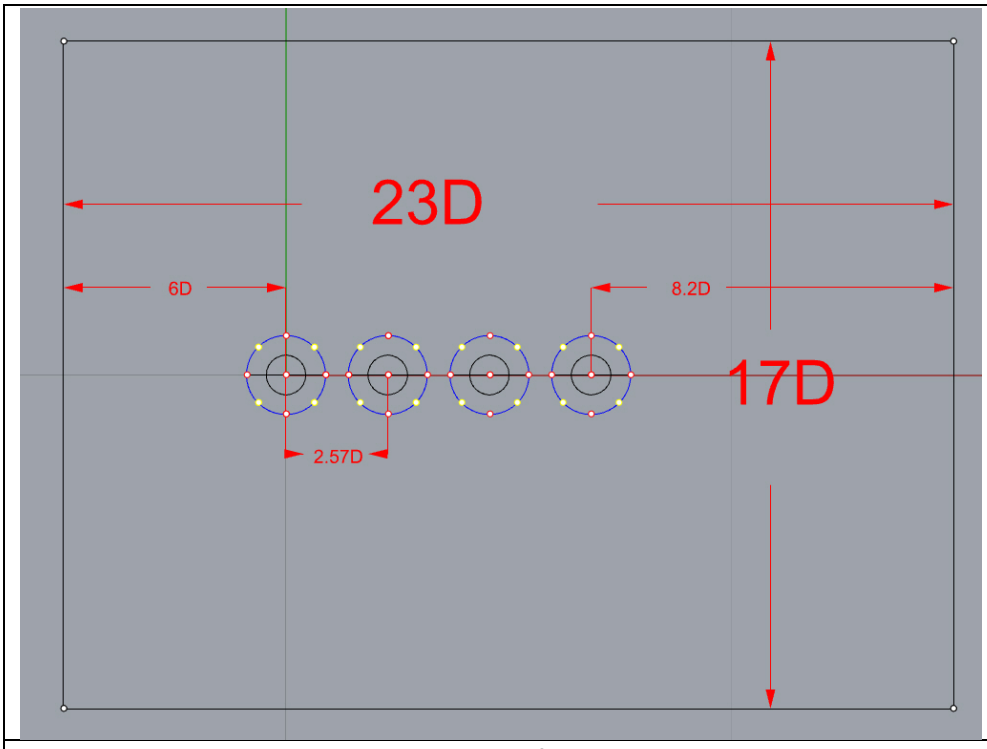

Figure 2. Boundary grid spacing illustration for CFD simulation

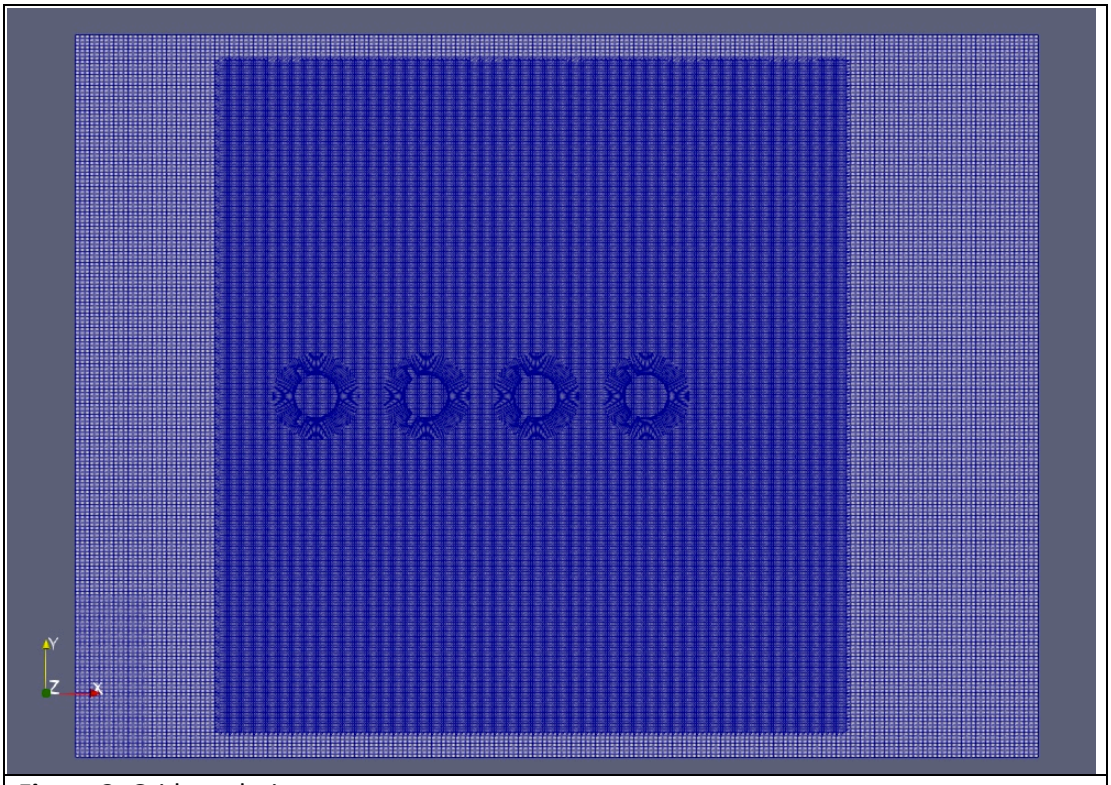

Figure 3. Grid resolution

6. HYDRODYNAMIC CALCULATION RESULTS FOR THE 4-CYLINDER VIVACE

There are some values that are important to extract or compute, such as lift force as a function of time, drag force as a function of time, average lift force, and average drag force. Lift and drag overtime are important as we want to introduce those results as hydrodynamic loads in Finite Element Analysis (FEA) and simulation. To validate the FEA results, the results of the displacement of each of the four cylinders as function of time are also used for comparison. Average lift and drag forces are used to validate grid quality as three different resolutions are used: coarse, medium, and fine. The purpose of the grid variation is to find a satisfactory resolution mesh without exorbitant computational time and utilize it in all CFD simulations. A 24-core Mac-Studio computer of the MRELab is used, which achieves speed about equal to the supercomputer of the University of Michigan which has considerable waiting time.

These values are generated by post-processing the OpenFOAM simulation results using ParaFoam. The lift and drag forces as function of time and the average lift and drag forces are readily extractable using ParaFoam. First, selected mesh-blocks from a composite dataset are extracted. This allows us selection of the surfaces of the cylinders in which we are interested.

Pressure integration is required to find values of average lift and drag. The pressure integration method in OpenFoam Post Processing (ParaFoam) integrates all points and cell data attributes while computing the total length, area or volume using the “Integrate Attributes” filter. This filter does not integrate point and cell data for 0-D cells (vertex and polyvertex). If the input dataset has mixed dimensionality, only the cells of highest dimension are used in the integration. For example, in a dataset with lines, triangles and hexahedra, the integration process will ignore contribution from lines and triangles. When the highest dimension is 1, the sum variable corresponds to the total length. Similarly, for 2-D and 3-D integration the sum variable is the total area and total volume, respectively. The output of this filter is a single point and vertex. The attributes for this point and vertex will contain the integration results for the corresponding input attributes and the sum variable.

Nine cases are studied and results are presented below in Figures 4-59.

6.1. Time Histories Data for Flow Speed 0.5 m/s, β=2

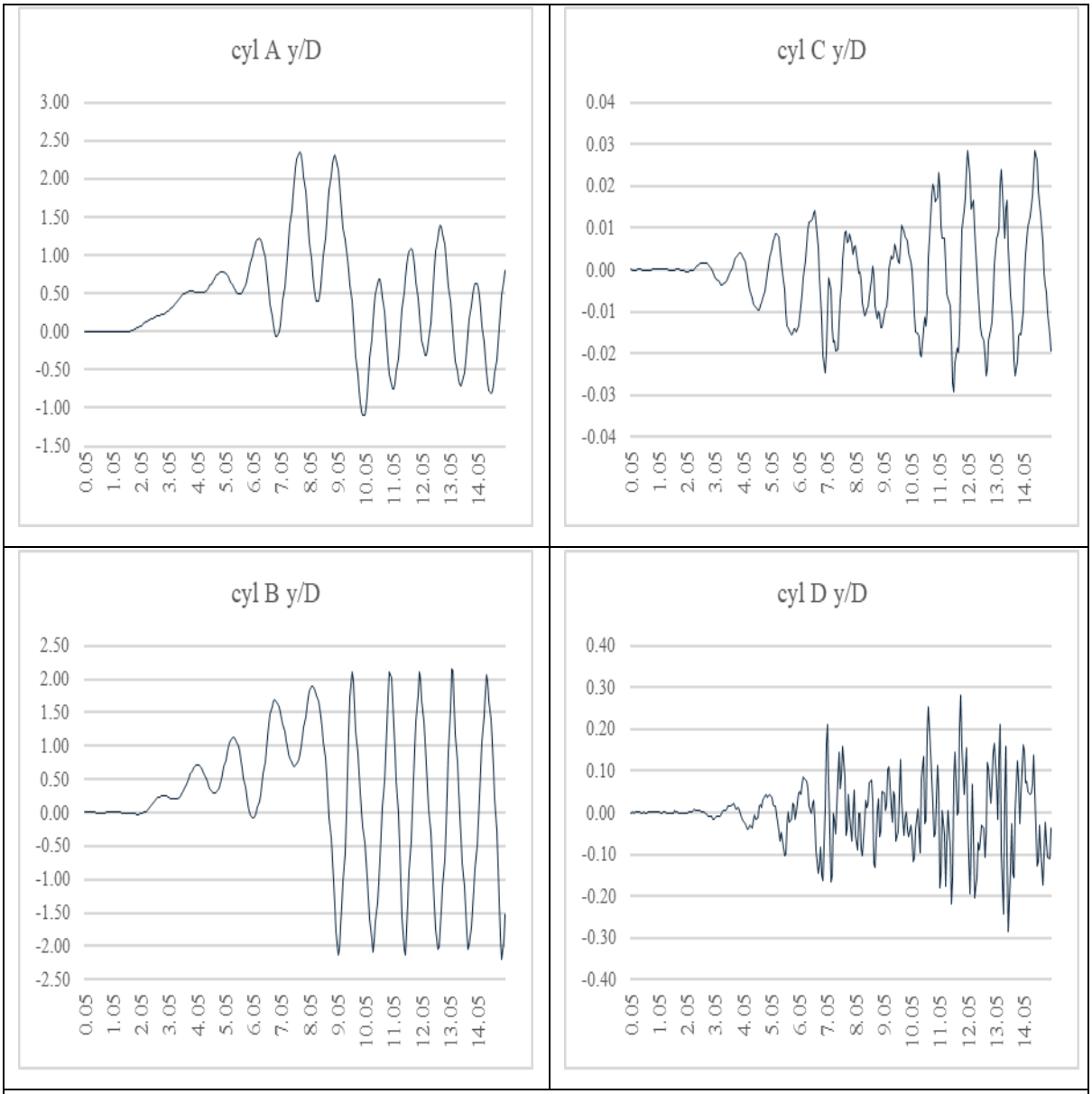

Figure 4. Time histories of the *y/D* for four cylinders in the 4-cylinder VIVACE Converter; flow speed *U*= 0.5m/s, *β*=2, *K*=27N/mm; fine simulation mesh

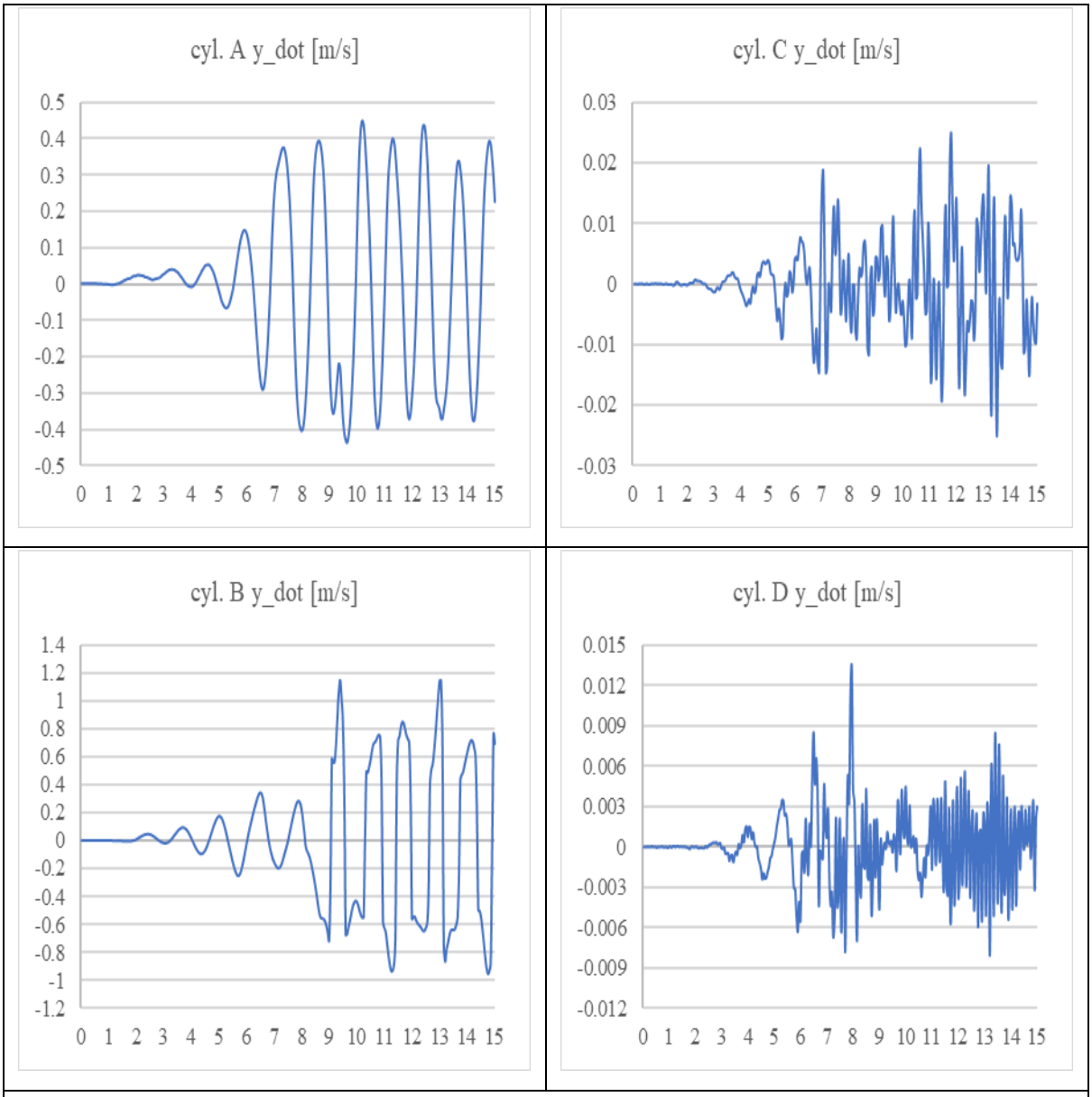

Figure 5. Time histories of the y_dot for four cylinders in the 4-cylinder VIVACE Converter; flow speed U=0.5m/s, β=2, K=27N/mm; fine simulation mesh

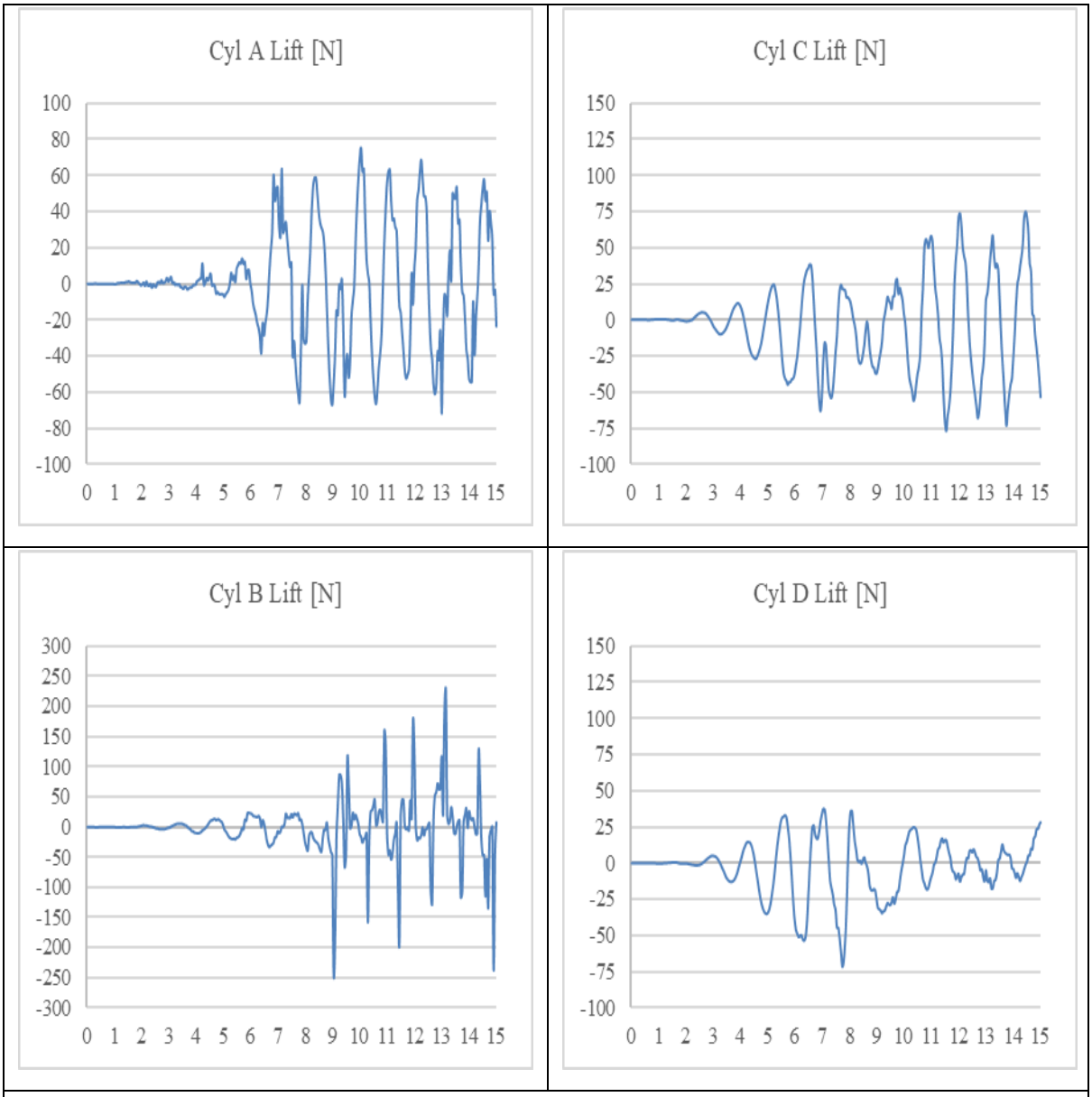

Figure 6. Time histories of the Hydrodynamic Lift for four cylinders in the 4-cylinder VIVACE Converter; flow speed U=0.5m/s, β=2, K=27N/mm; fine simulation mesh

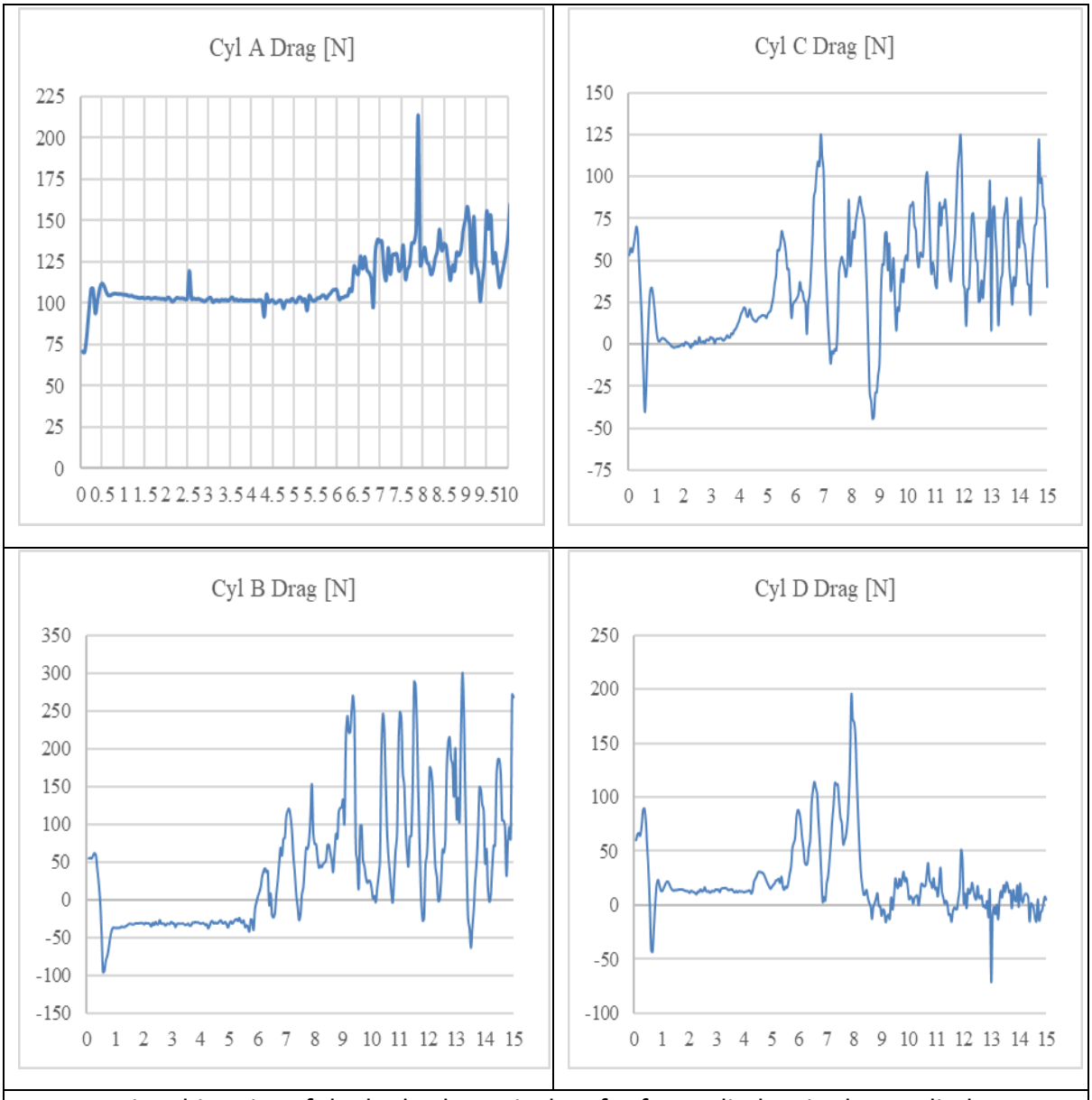

Figure 7. Time histories of the hydrodynamic drag for four cylinders in the 4-cylinder VIVACE Converter; flow speed U=0.5m/s, β=2, K=27N/mm; fine simulation mesh

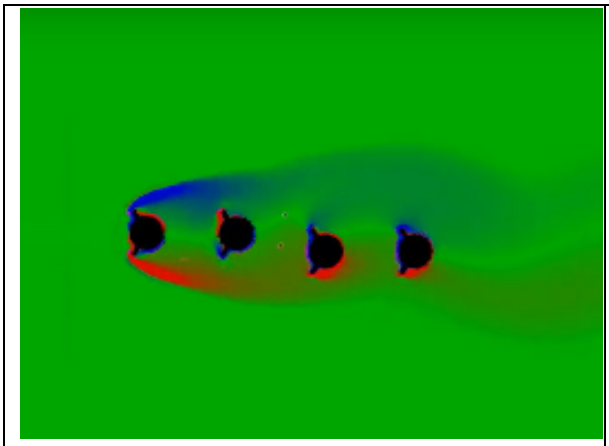

Figure 8. Flow speed U=0.5m/s, β=2, K=27N/mm; at time = 4 second

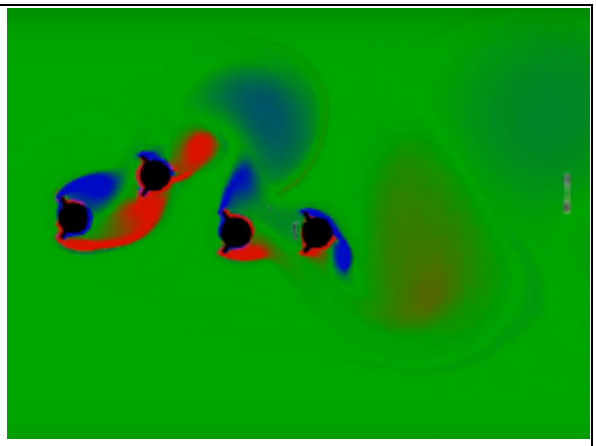

Figure 9. Flow speed U=0.5m/s, β=2, K=27N/mm; at time = 8 second

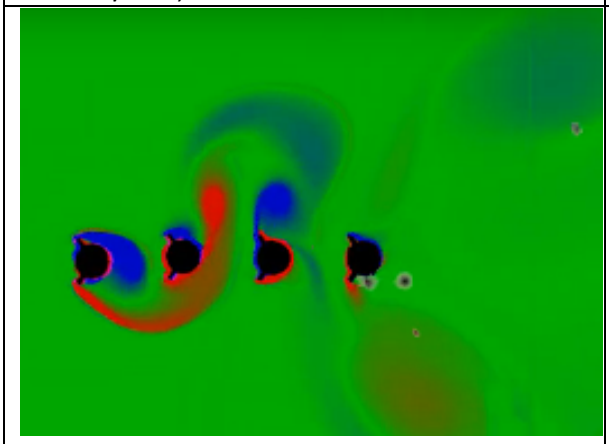

Figure 10. Flow speed U=0.5m/s, β=2, K=27N/mm; at time = 12 second

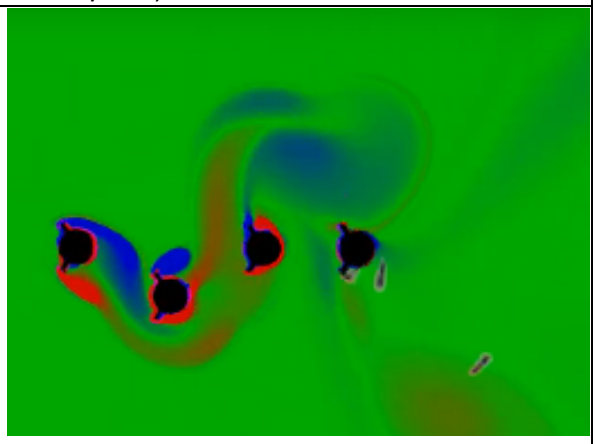

Figure 11. Flow speed U=0.5m/s, β=2, K=27N/mm; at time = 14.5 second

6.2. Time Histories Data for Flow Speed 0.5 m/s, β=4

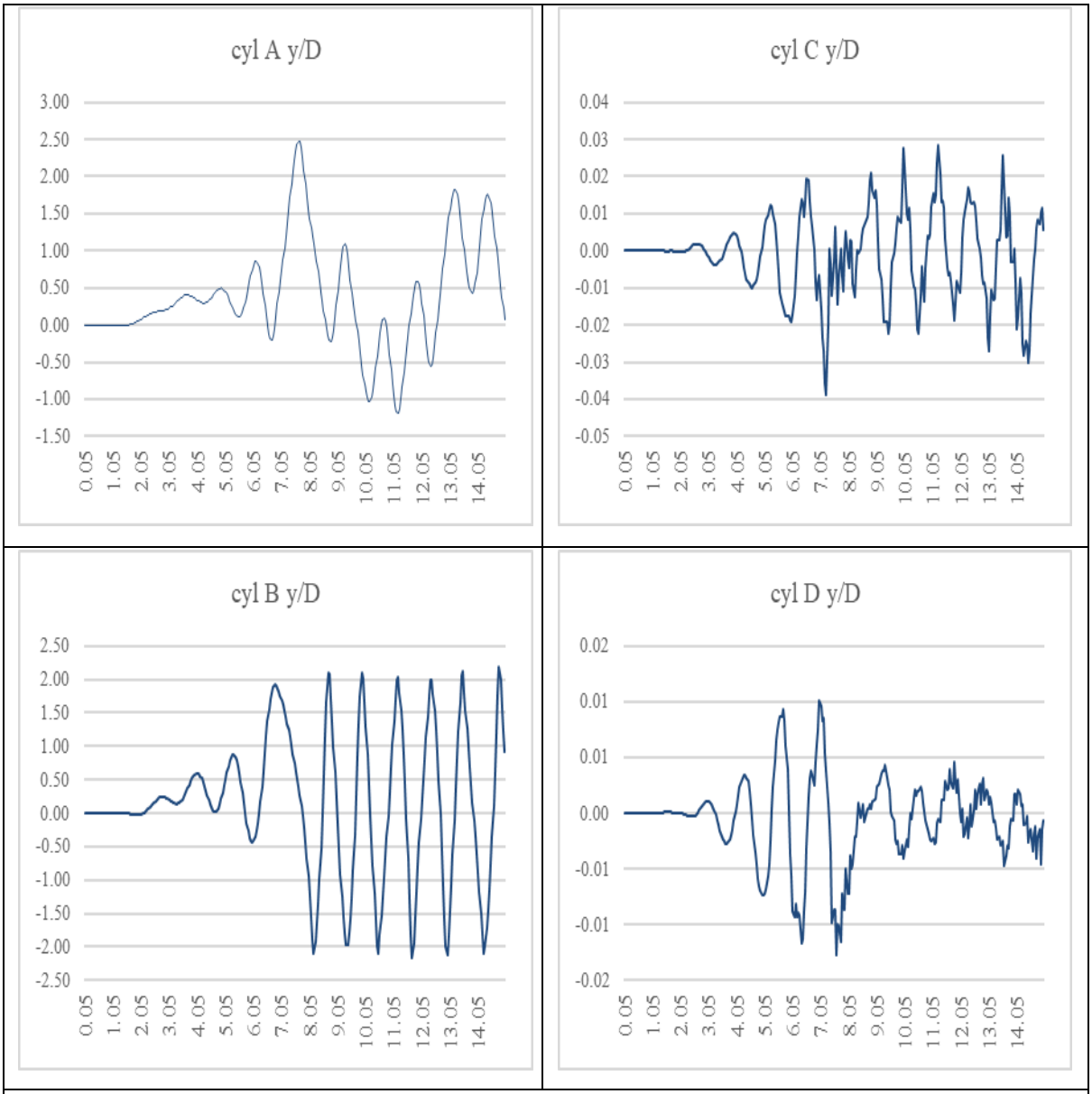

Figure 12. Time histories of the *y/D* for four cylinders in the 4-cylinder VIVACE Converter; flow speed *U*=1.0m/s, *β*=2, *K*=27N/mm; fine simulation mesh

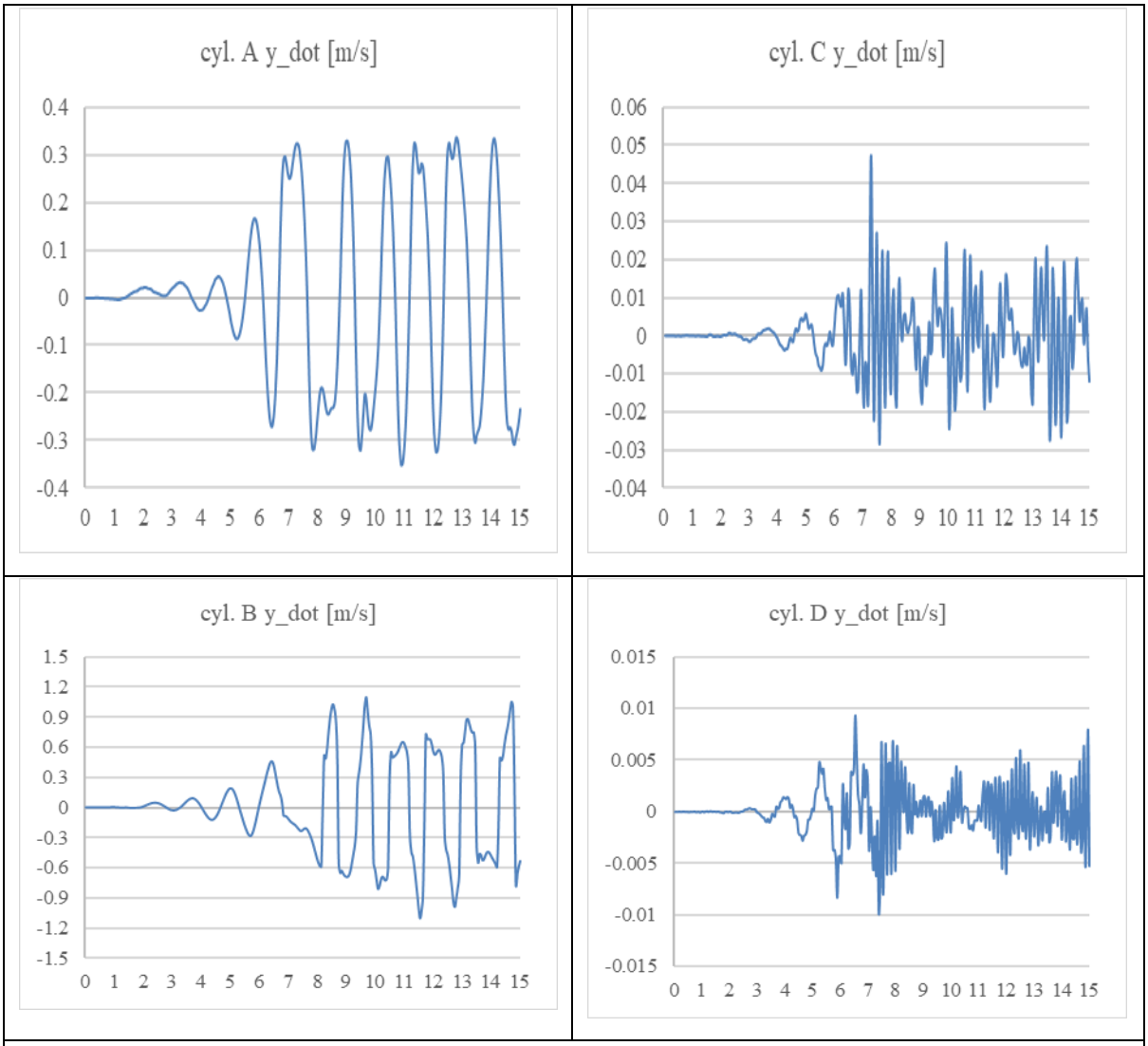

Figure 13. Time histories of the y_dot for four cylinders in the 4-cylinder VIVACE Converter; flow speed U=1.0m/s, β=2, K=27N/mm; fine simulation mesh

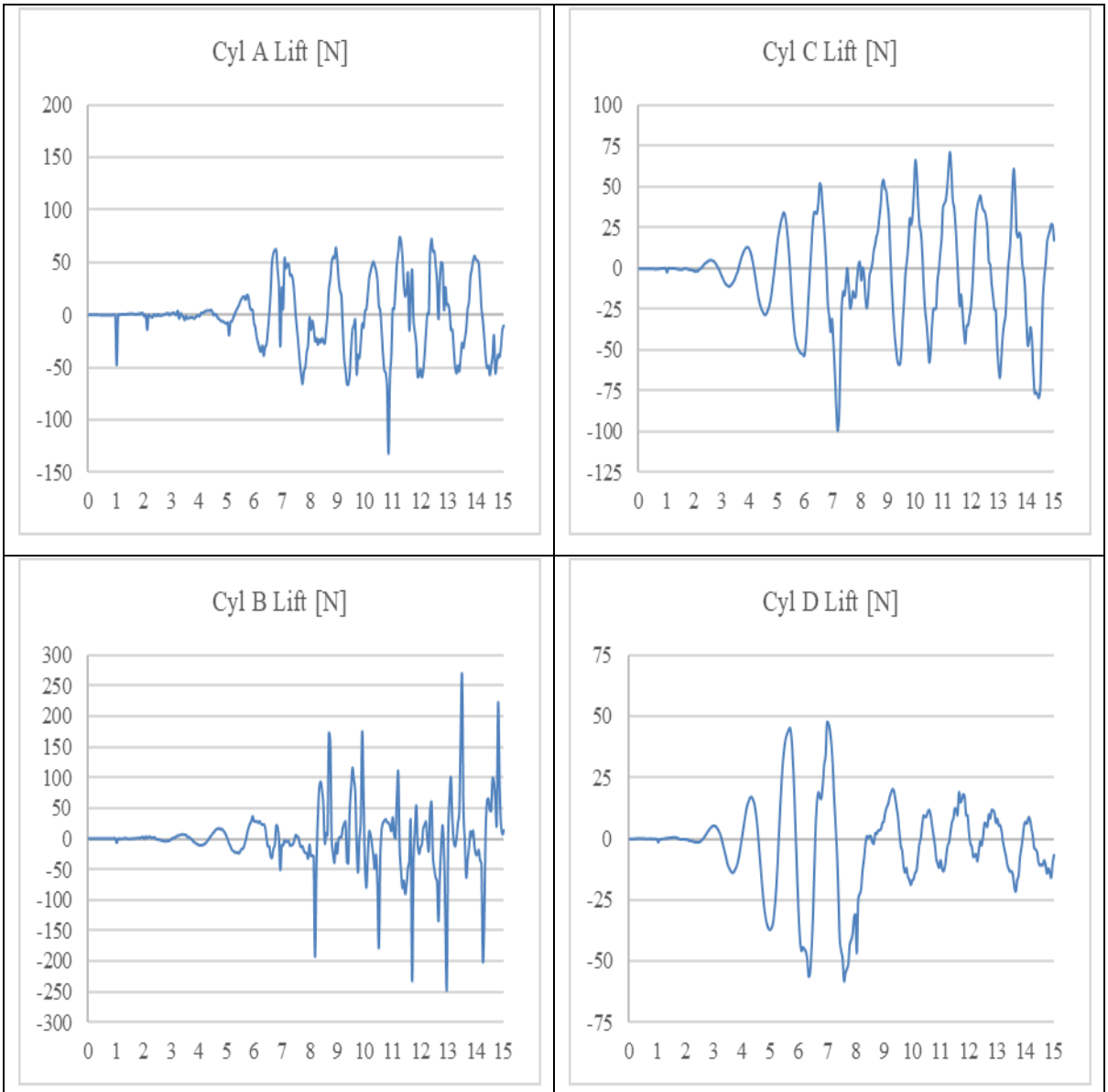

Figure 14. Time histories of the hydrodynamic lift for four cylinders in the 4-cylinder VIVACE Converter; flow speed U=1.0m/s, β=2, K=27N/mm; fine simulation mesh

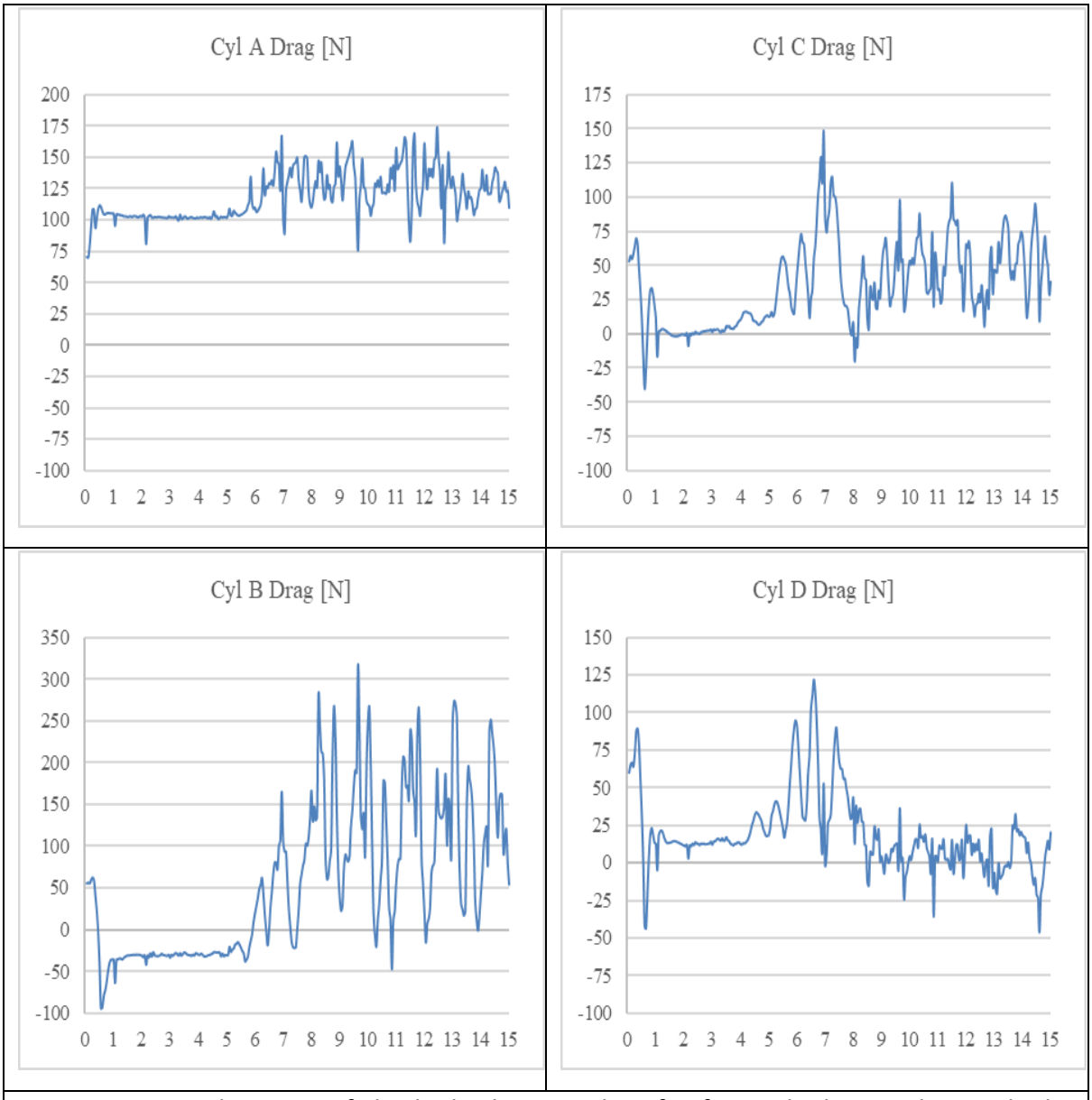

Figure 15. Time histories of the hydrodynamic drag for four cylinders in the 4-cylinder VIVACE Converter; flow speed U=1.0m/s, β=2, K=27N/mm; fine simulation mesh

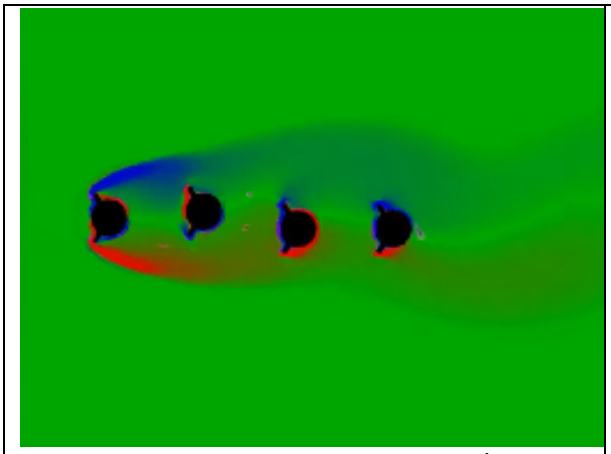

Figure 16. Flow speed U=1.0m/s, β=2, K=27N/mm; at time = 4 second

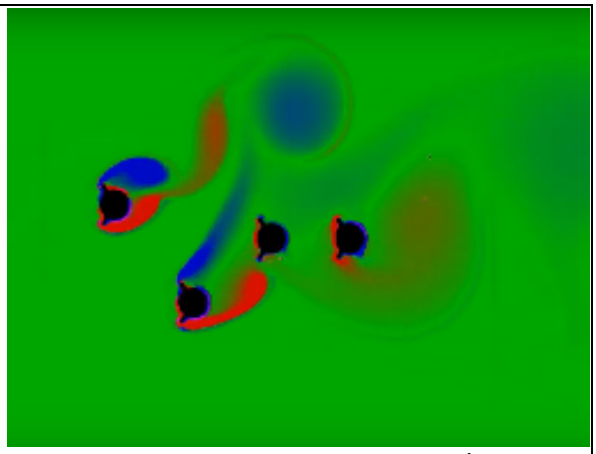

Figure 17. Flow speed U=1.0m/s, β=2, K=27N/mm; at time = 8 second

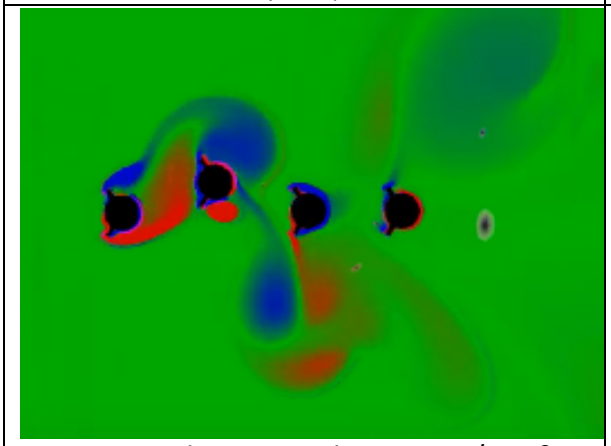

Figure 18. Flow speed U=1.0m/s, β=2, K=27N/mm; at time = 12 second

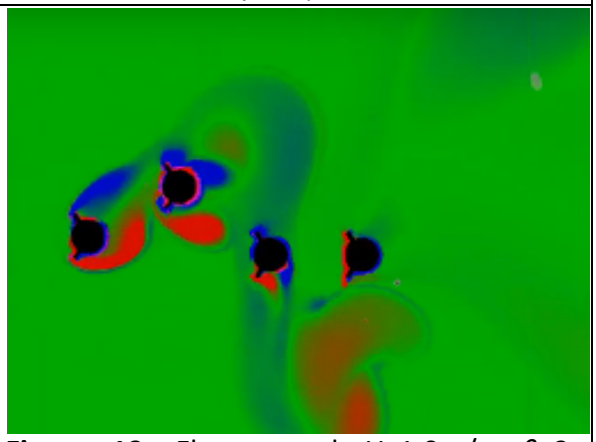

Figure 19. Flow speed U=1.0m/s, β=2, K=27N/mm; at time = 14.5 second

6.3. Time Histories Data for Flow Speed 0.5 m/s, $\beta = 6$

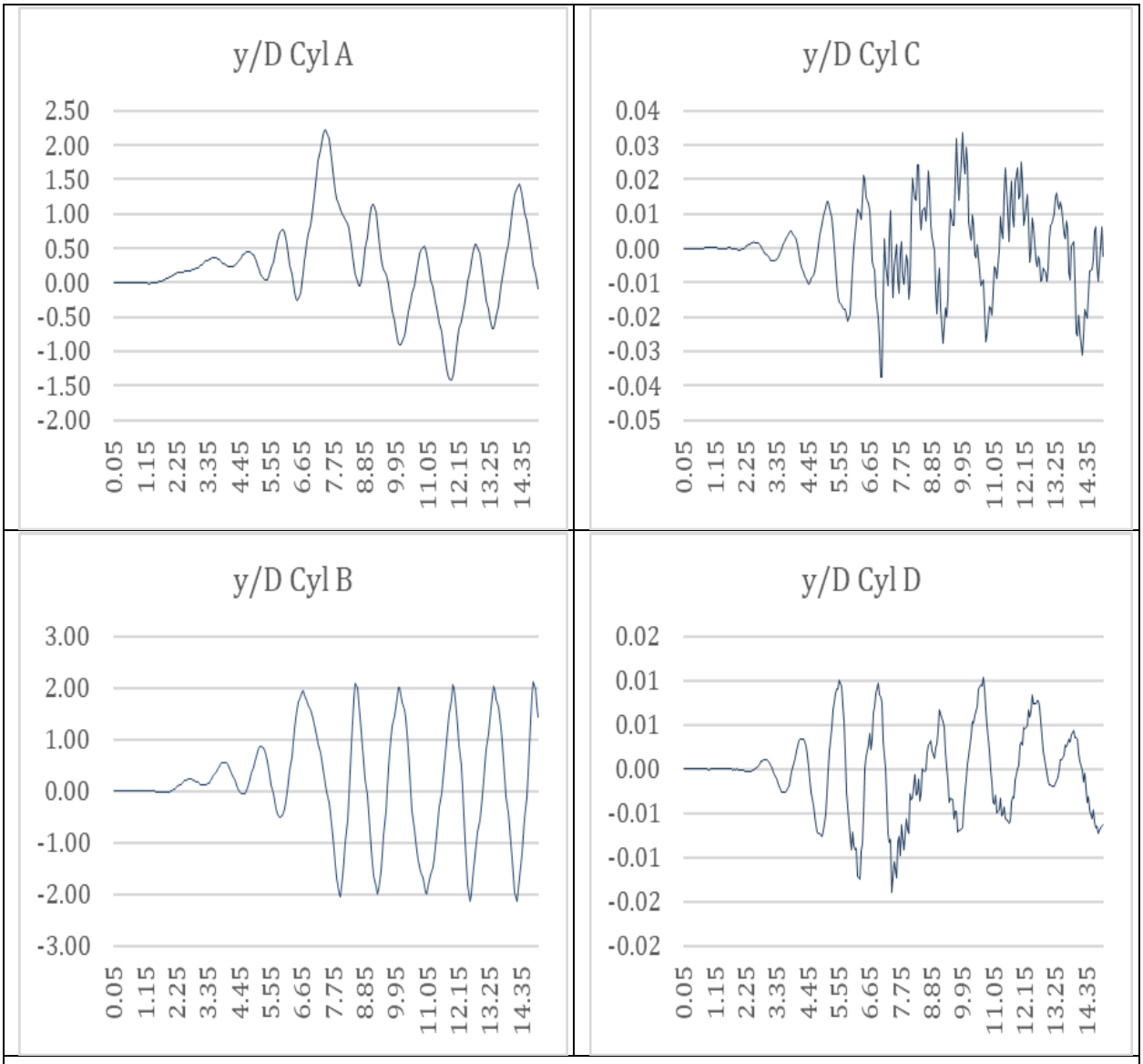

Figure 20. Time histories of the *y/D* for four cylinders in the 4-cylinder VIVACE Converter; flow speed *U*=1.5m/s, *β*=2, *K*=27N/mm; fine simulation mesh

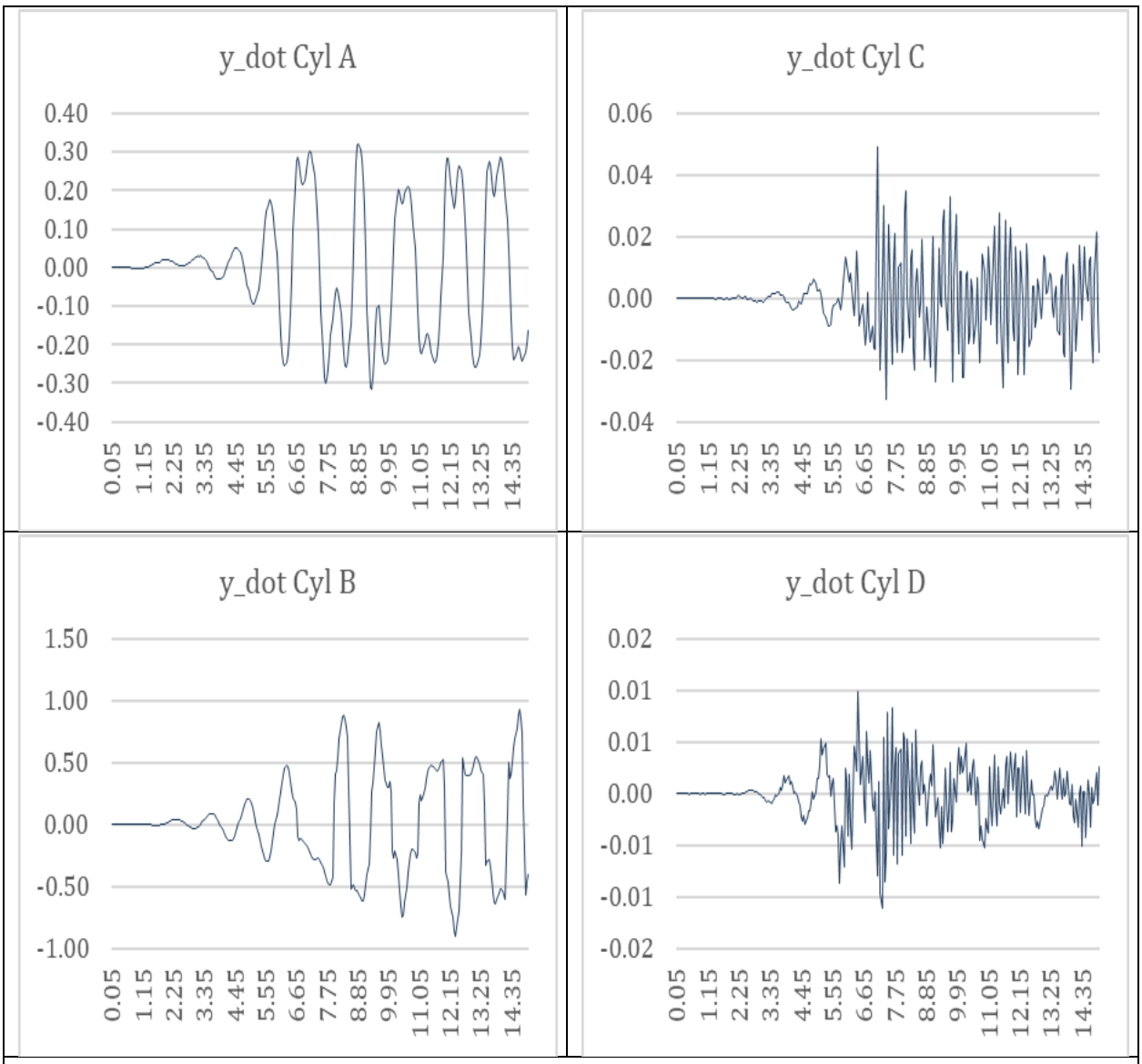

Figure 21. Time histories of the y_dot for four cylinders in the 4-cylinder VIVACE Converter; flow speed U=1.5m/s, β=2, K=27N/mm; fine simulation mesh

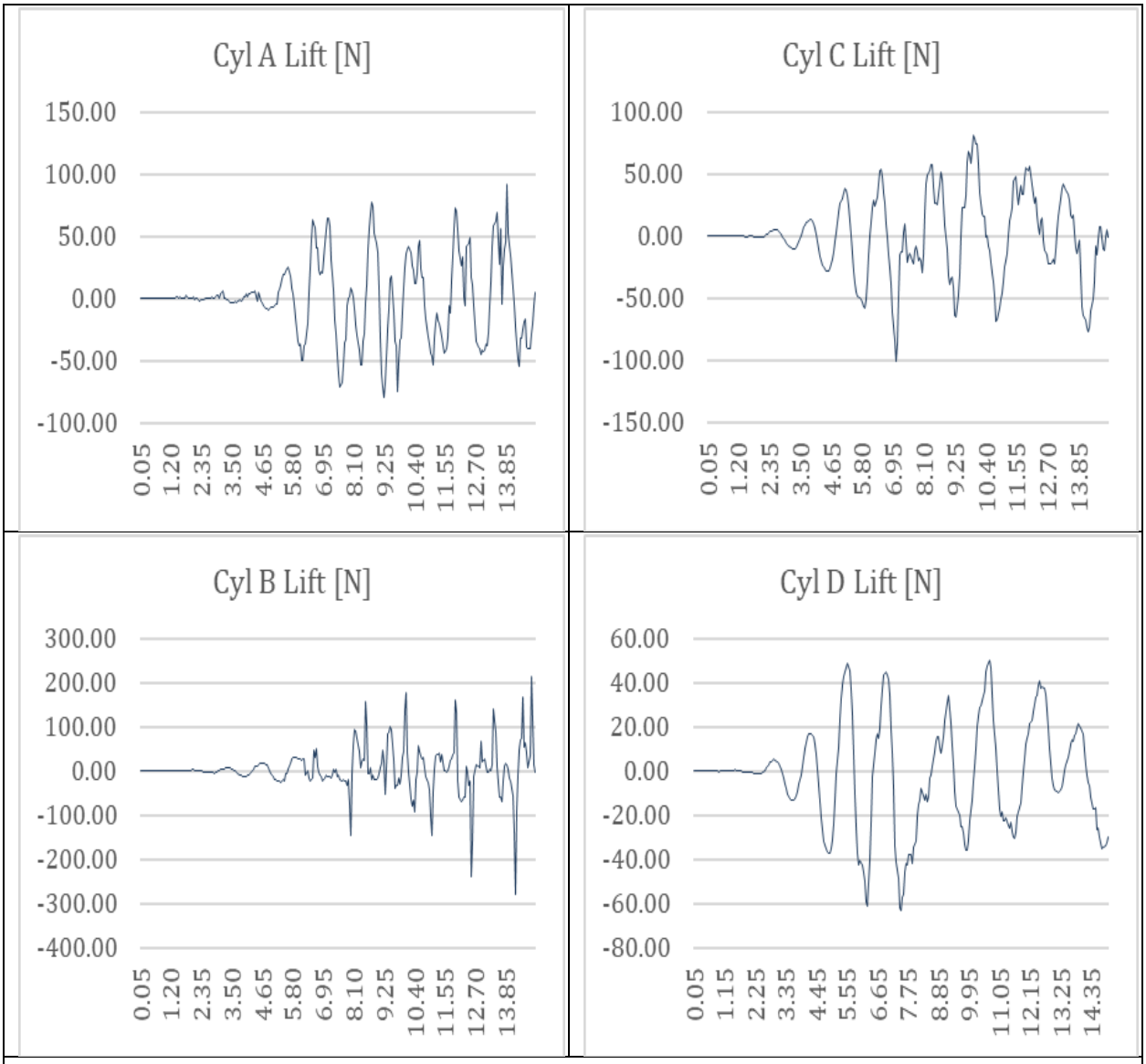

Figure 22. Time histories of the hydrodynamic lift for four cylinders in the 4-cylinder VIVACE Converter; flow speed U=1.5m/s, β=2, K=27N/mm; fine simulation mesh

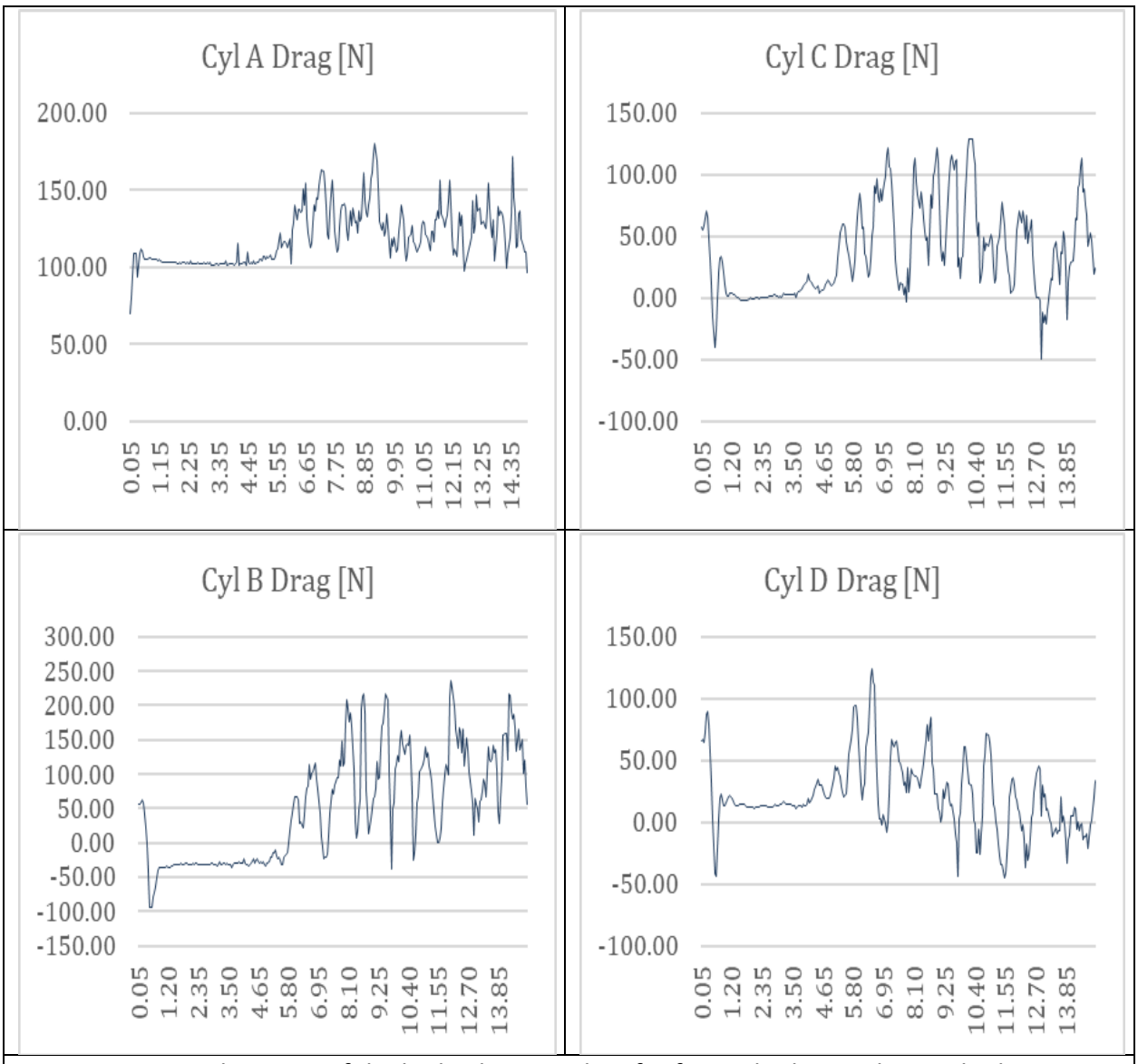

Figure 23. Time histories of the hydrodynamic drag for four cylinders in the 4-cylinder VIVACE Converter; flow speed U=1.5m/s, β=2, K=27N/mm; fine simulation mesh

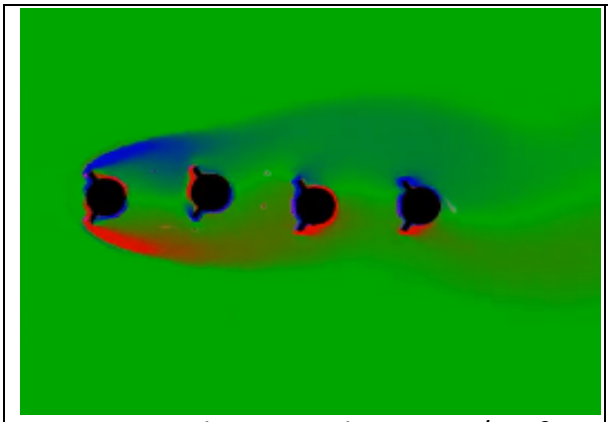

Figure 24. Flow speed U=1.5m/s, β=2, K=27N/mm; at time = 4 second

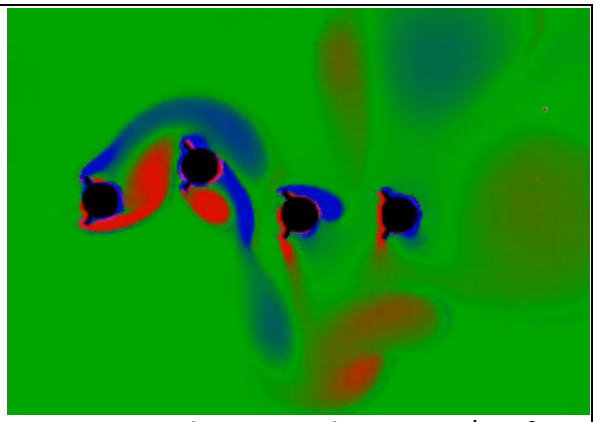

Figure 25. Flow speed U=1.5m/s, β=2, K=27N/mm; at time = 8 second

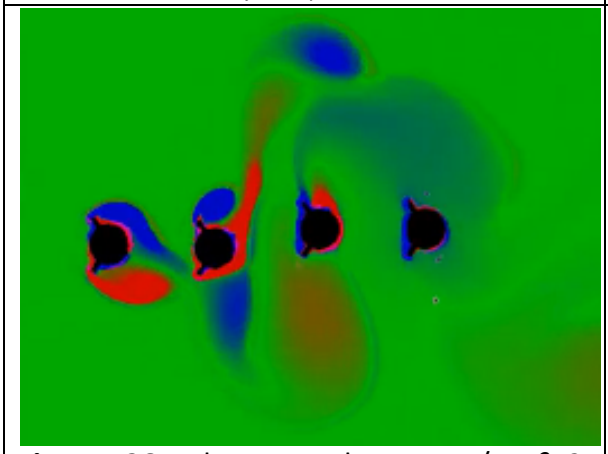

Figure 26. Flow speed U=1.5m/s, β=2, K=27N/mm; at time = 12 second

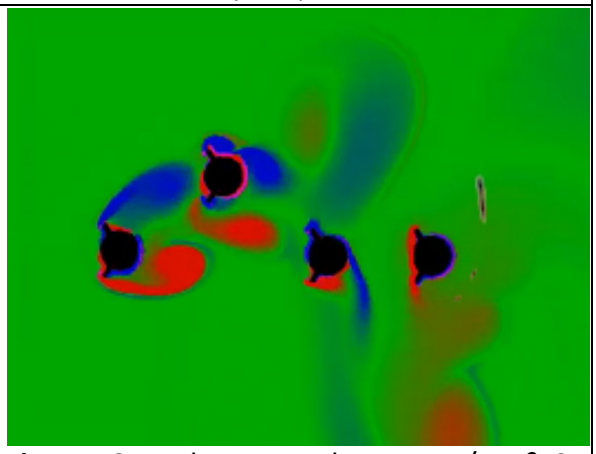

Figure 27. Flow speed U=1.5m/s, β=2, K=27N/mm; at time = 14.5 second

6.4. Time Histories Data for Flow Speed 1.0 m/s, $\beta = 2$

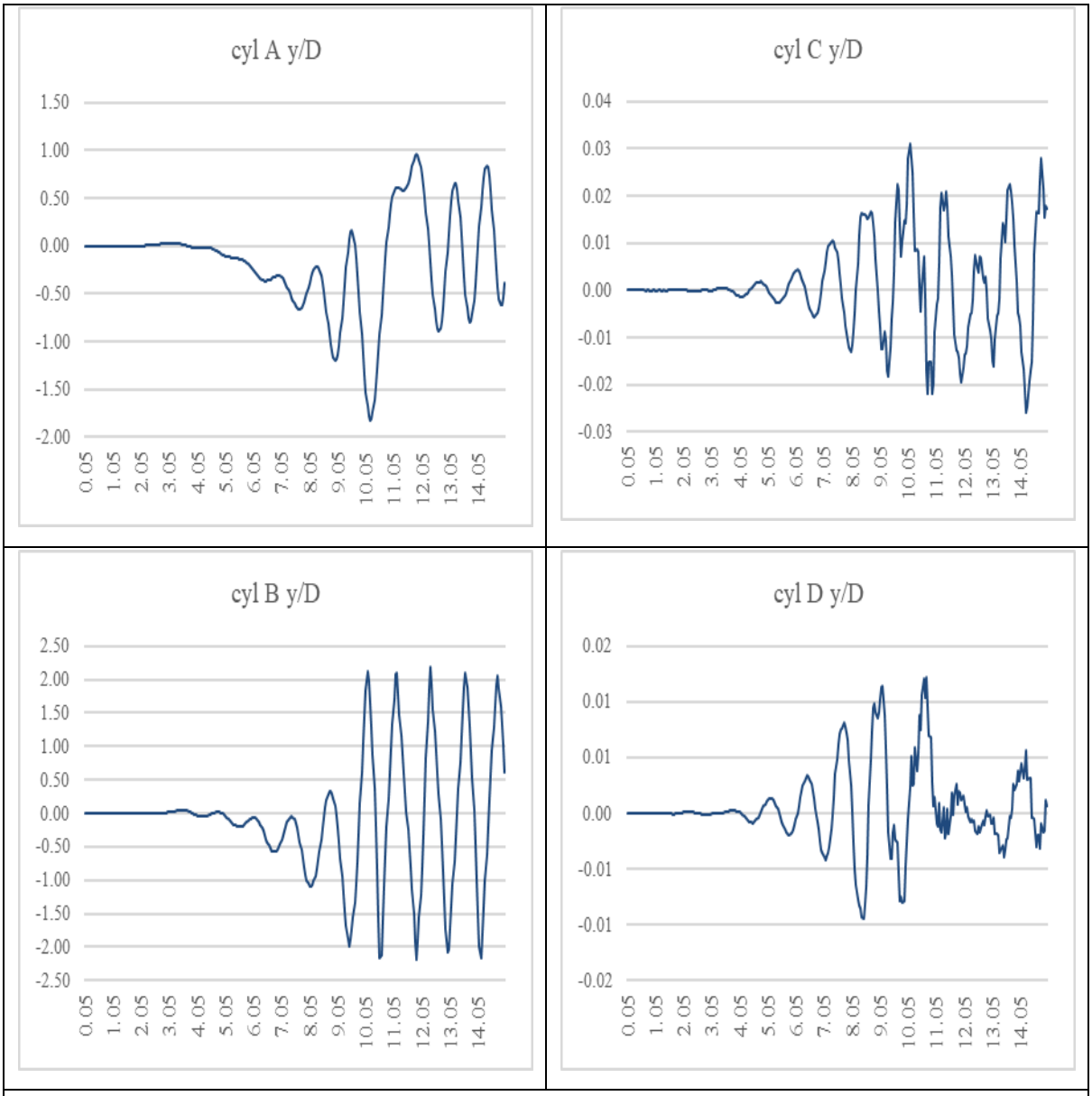

Figure 28. Time histories of the *y/D* for four cylinders in the 4-cylinder VIVACE Converter; flow speed *U*= 0.5m/s, *β*=4, *K*=27N/mm; fine simulation mesh

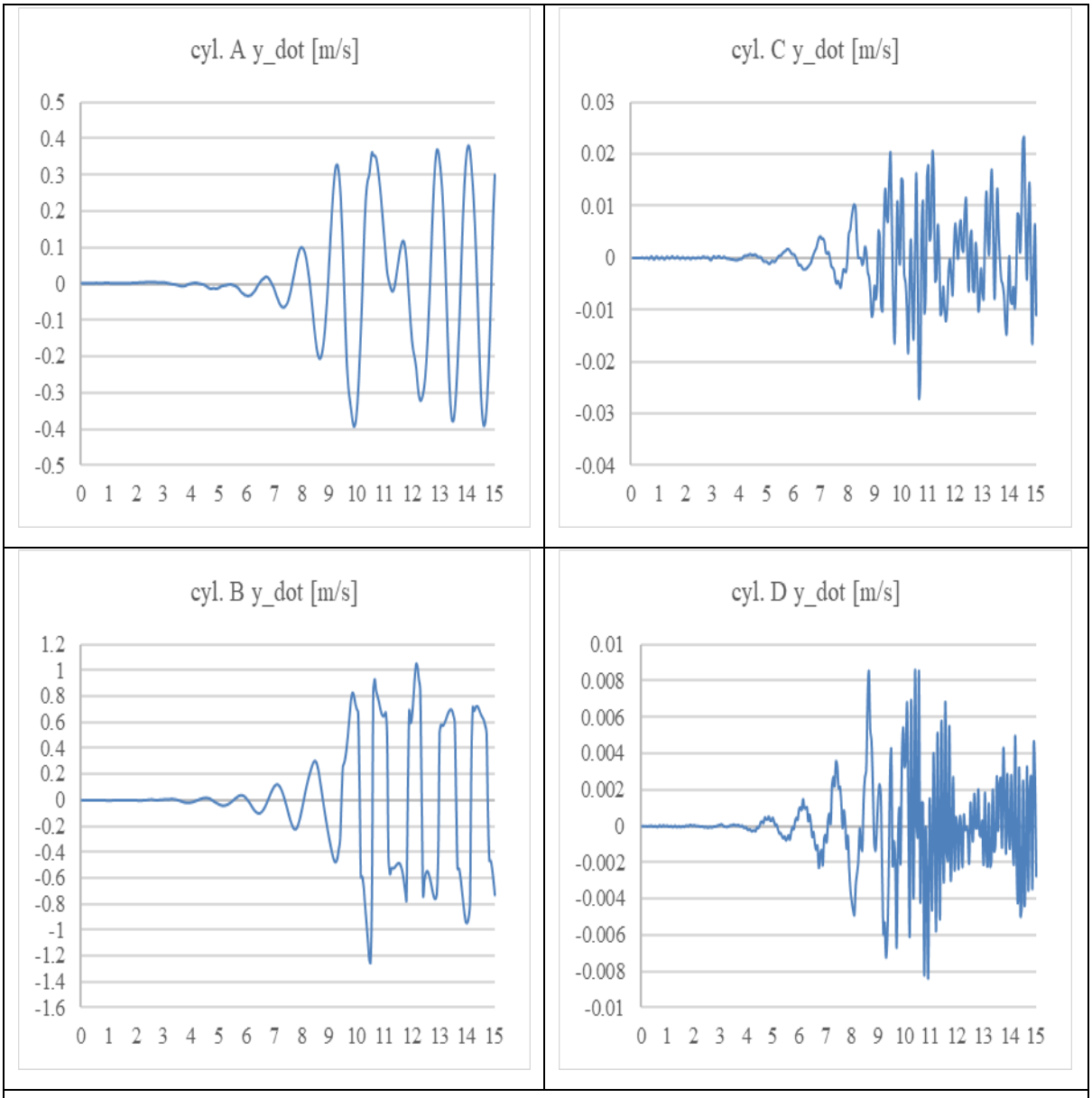

Figure 29. Time histories of the y_dot for four cylinders in the 4-cylinder VIVACE Converter; flow speed U= 0.5m/s, β=4, K=27N/mm; fine simulation mesh

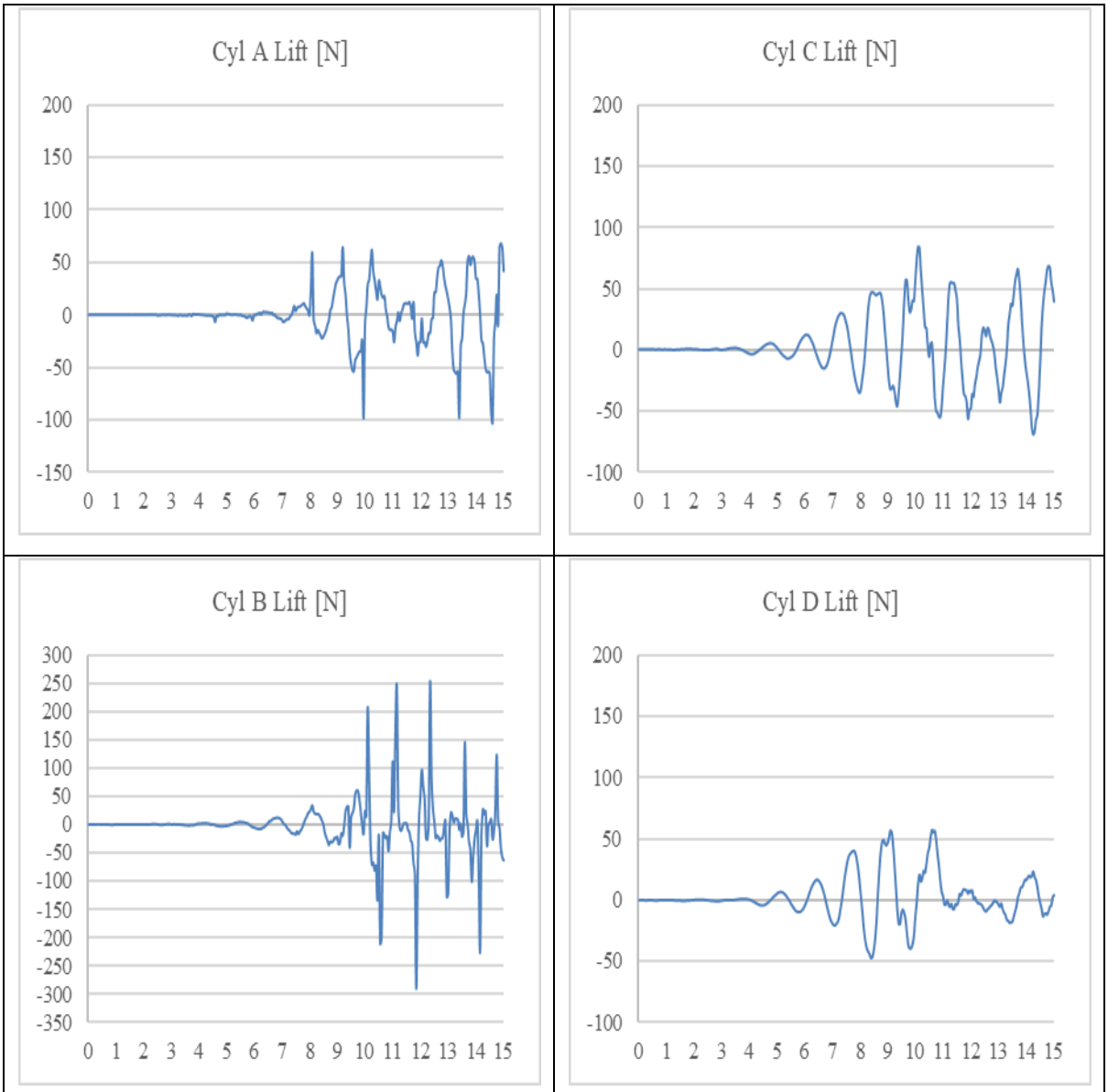

Figure 30. Time histories of the hydrodynamic lift for four cylinders in the 4-cylinder VIVACE Converter; flow speed U=0.5m/s, β=4, K=27N/mm; fine simulation mesh

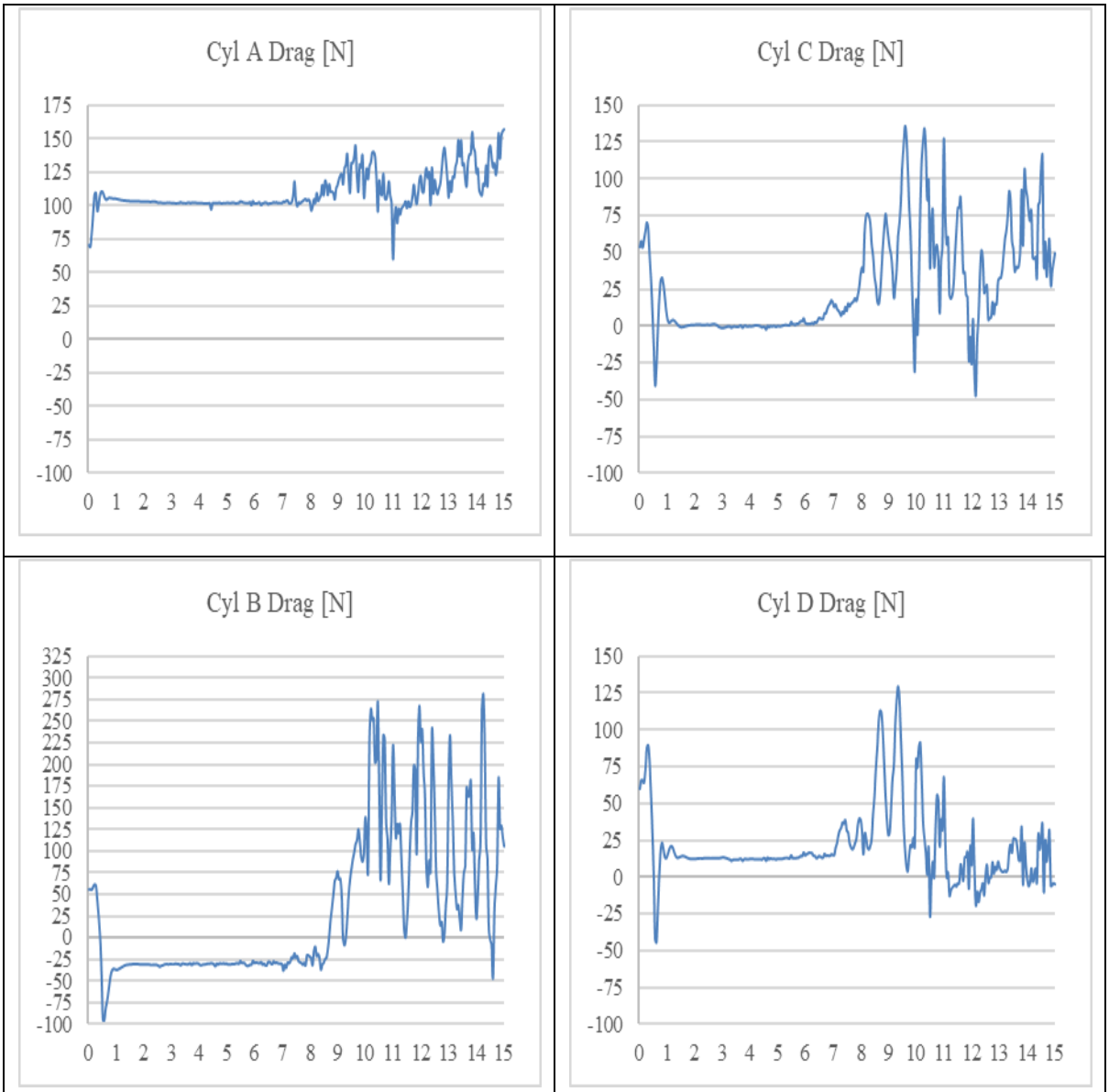

Figure 31. Time histories of the hydrodynamic drag for four cylinders in the 4-cylinder VIVACE Converter; flow speed U=0.5m/s, β=4, K=27N/mm; fine simulation mesh

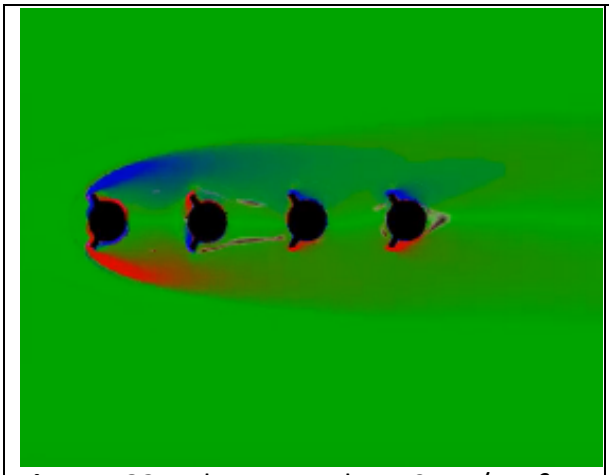

Figure 32. Flow speed *U*=0.5m/s, *β*=4, *K*=27N/mm; at time = 4 second

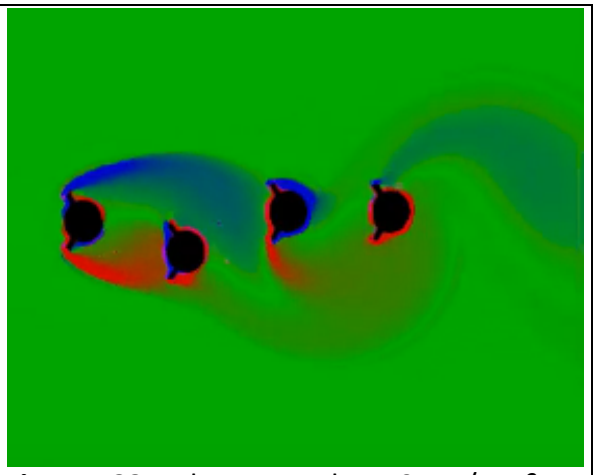

Figure 33. Flow speed *U*=0.5m/s, *β*=4, *K*=27N/mm; at time = 8 second

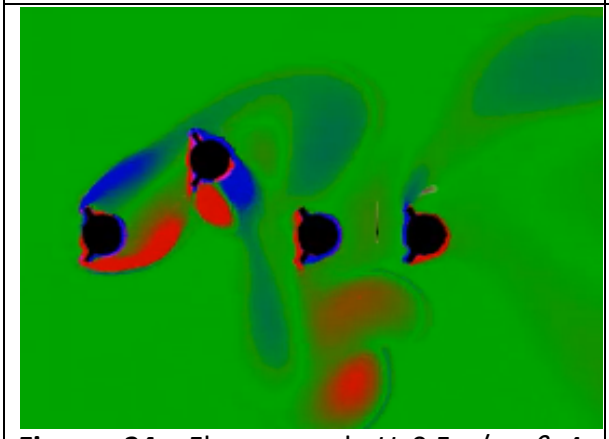

Figure 34. Flow speed *U*=0.5m/s, *β*=4, *K*=27N/mm; at time = 12 second

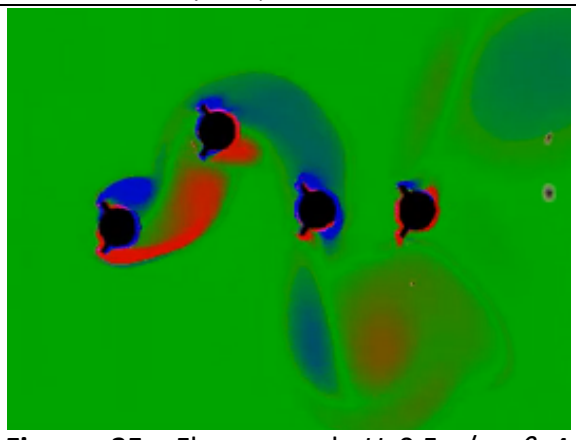

Figure 35. Flow speed *U*=0.5m/s, *β*=4, *K*=27N/mm; at time = 14.5 second

6.5. Time Histories Data for Flow Speed 1.0 m/s, $\beta = 4$

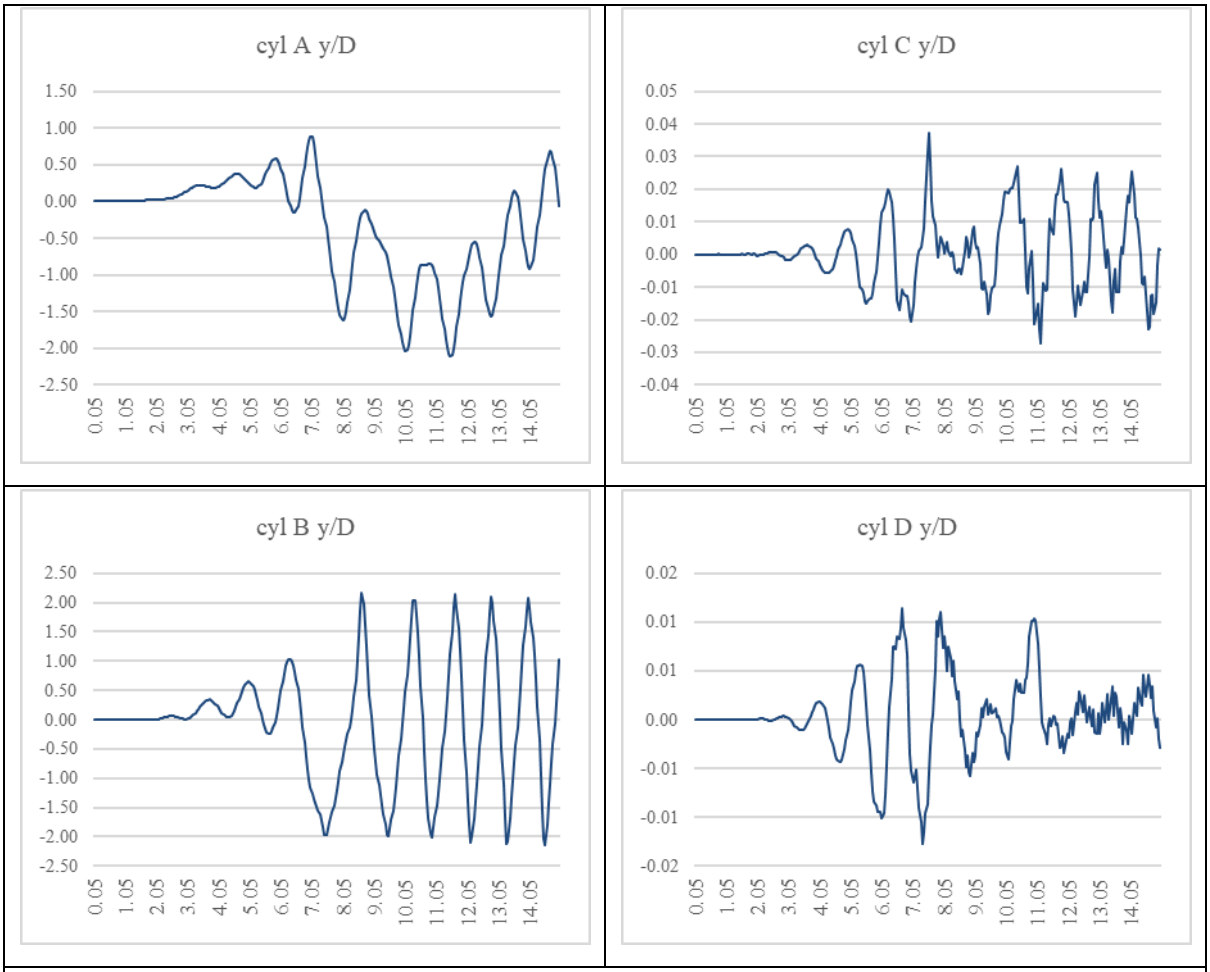

Figure 36. Time histories of the *y/D* for four cylinders in the 4-cylinder VIVACE Converter; flow speed *U*=1.0m/s, *β*=4, *K*=27N/mm; fine simulation mesh

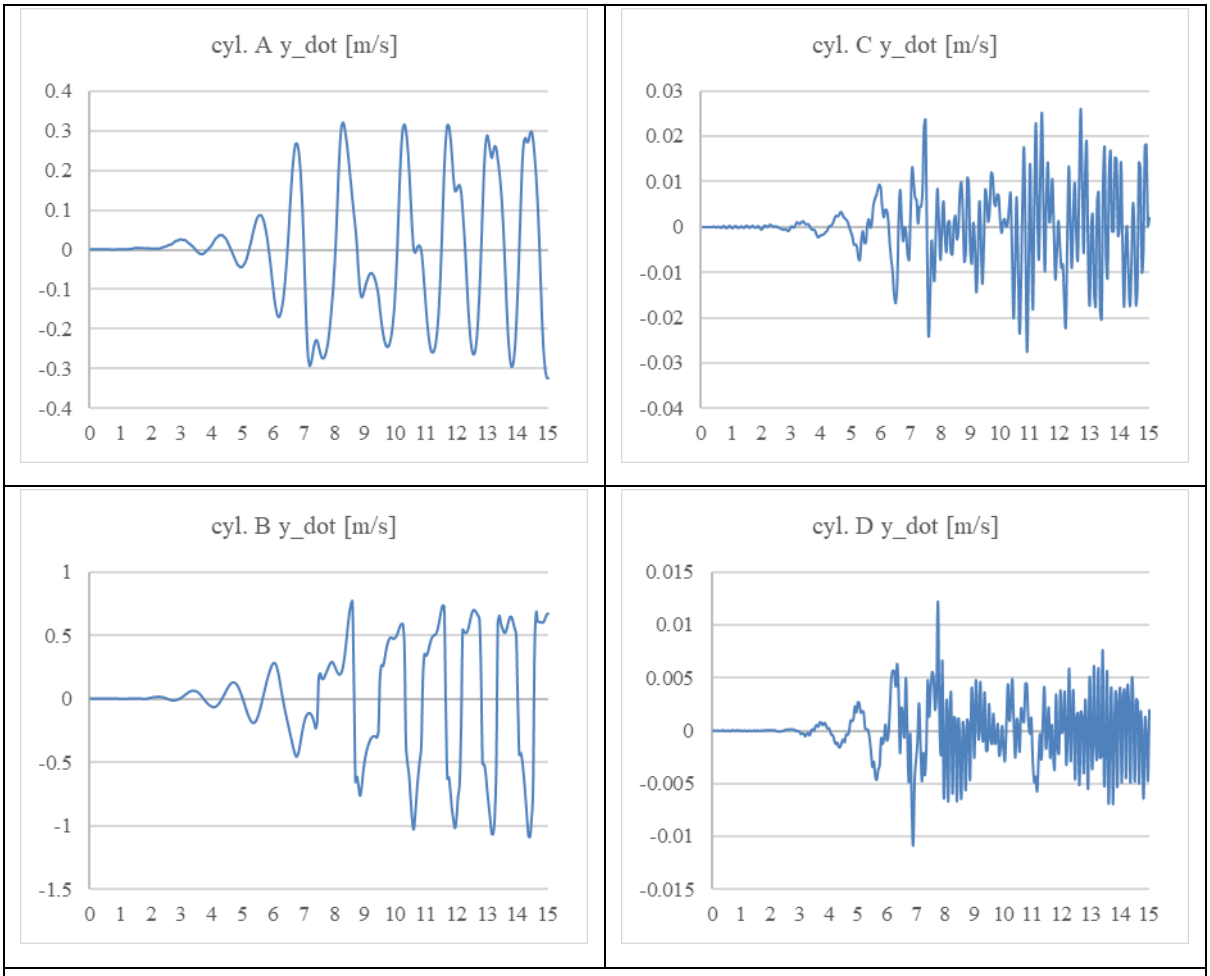

Figure 37. Time histories of the y_dot for four cylinders in the 4-cylinder VIVACE Converter; flow speed U=1.0m/s, β=4, K=27N/mm; fine simulation mesh

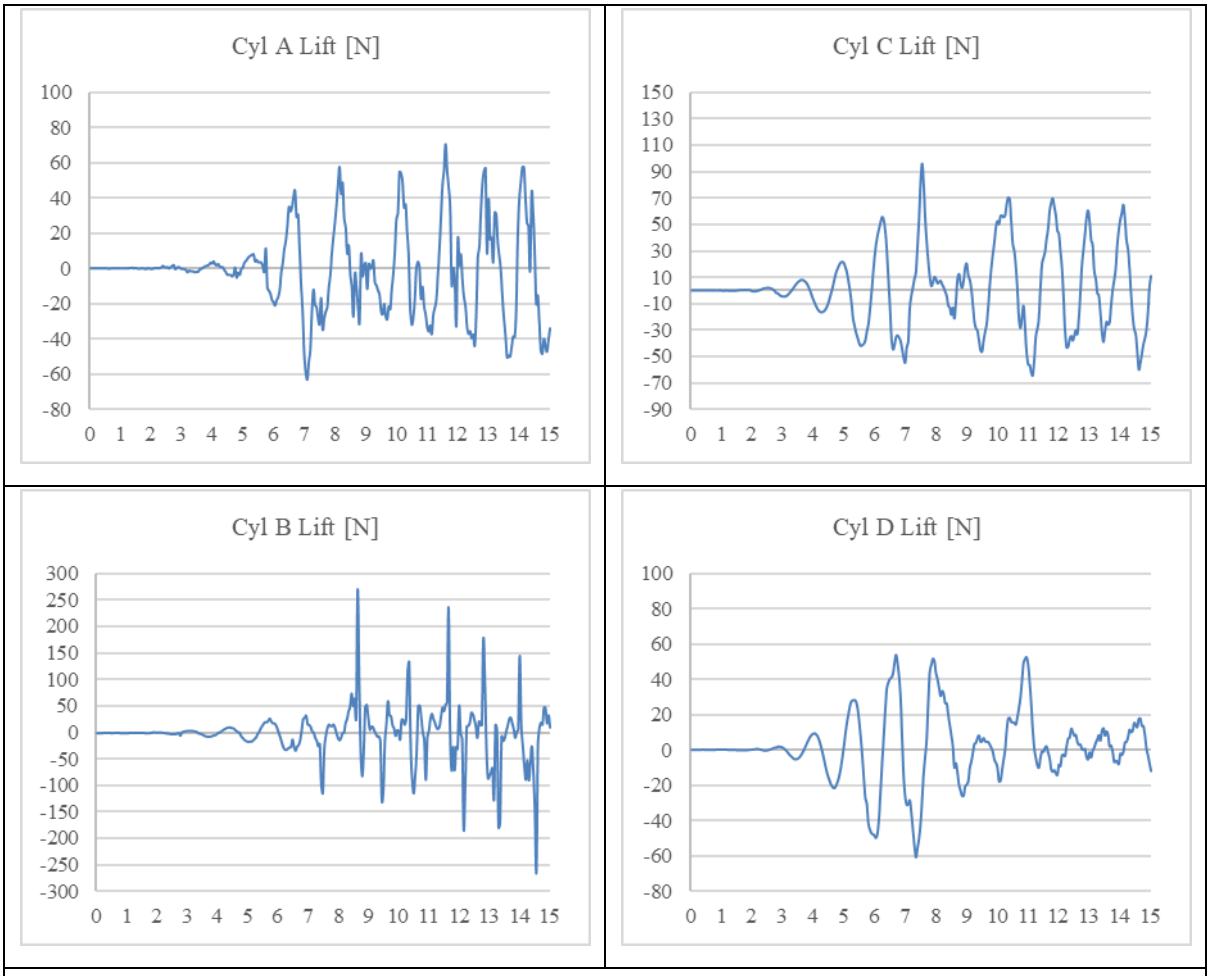

Figure 38. Time histories of the hydrodynamic lift for four cylinders in the 4-cylinder VIVACE Converter; speed U=1.0m/s, β=4, K=27N/mm; fine simulation mesh

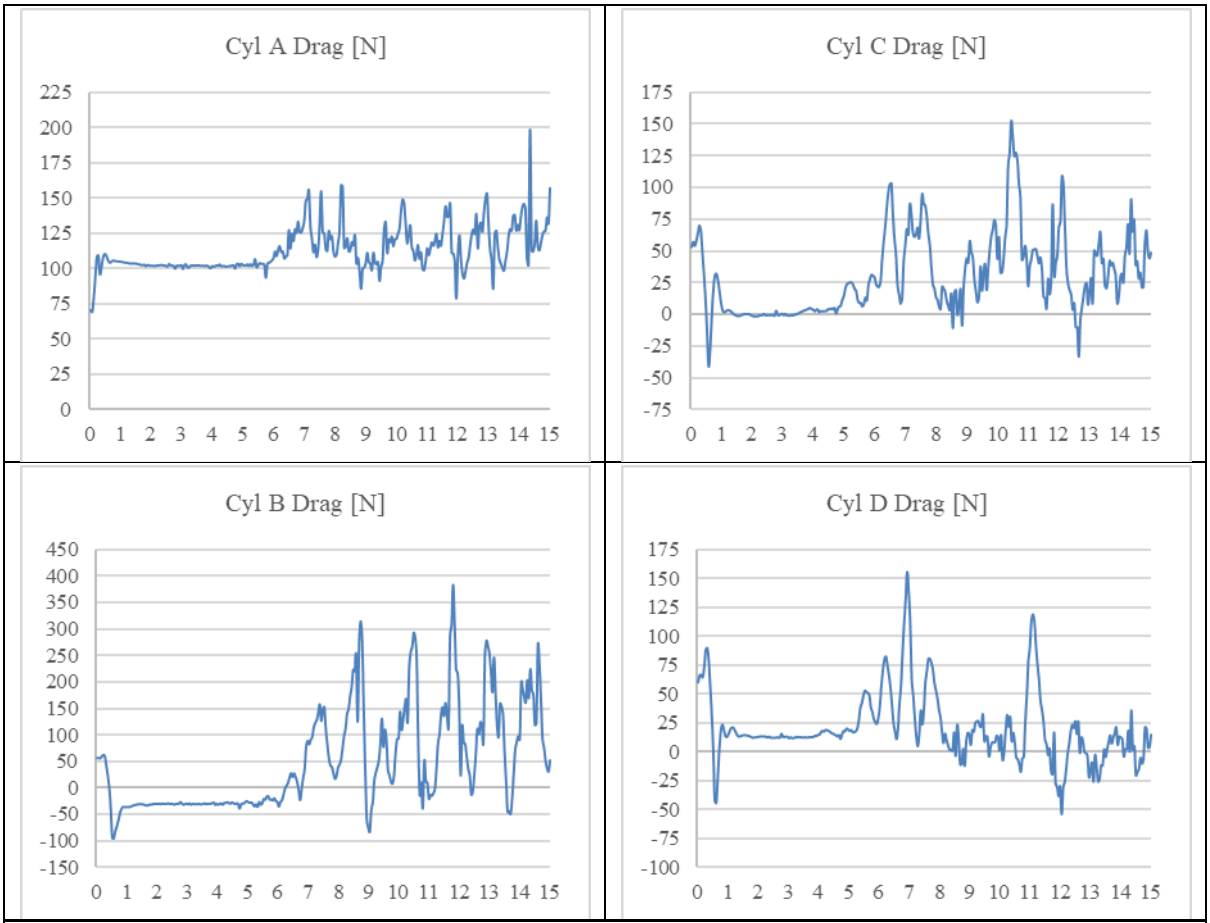

Figure 39. Time histories of the hydrodynamic drag for four cylinders in the 4-cylinder VIVACE Converter; speed U=1.0m/s, β=4, K=27N/mm; fine simulation mesh

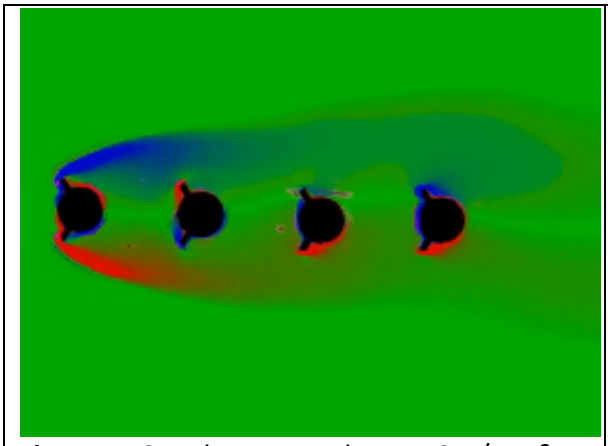

Figure 40. Flow speed U=1.0m/s, β=4, K=27N/mm; at time = 4 second

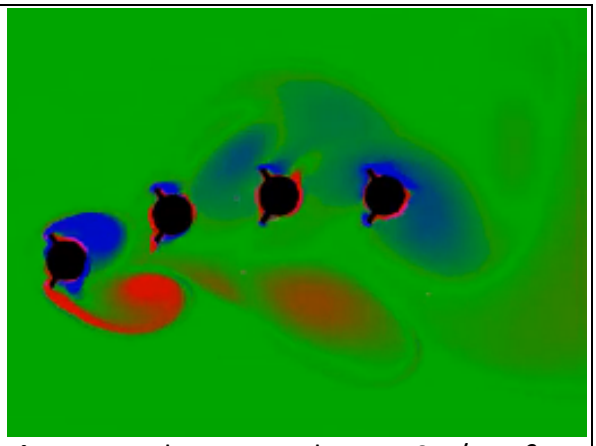

Figure 41. Flow speed U=1.0m/s, β=4, K=27N/mm; at time = 8 second

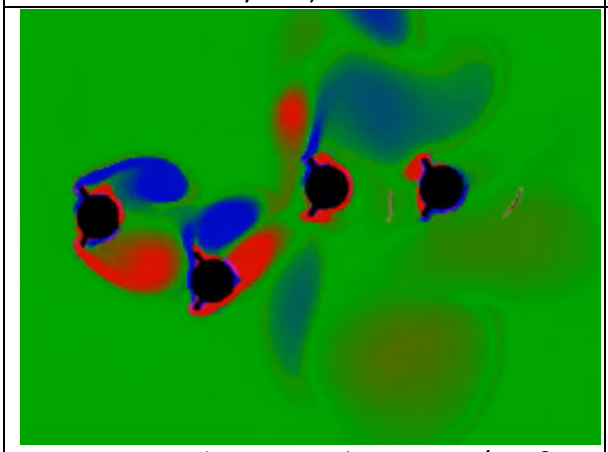

Figure 42. Flow speed U=1.0m/s, β=4, K=27N/mm; at time = 12 second

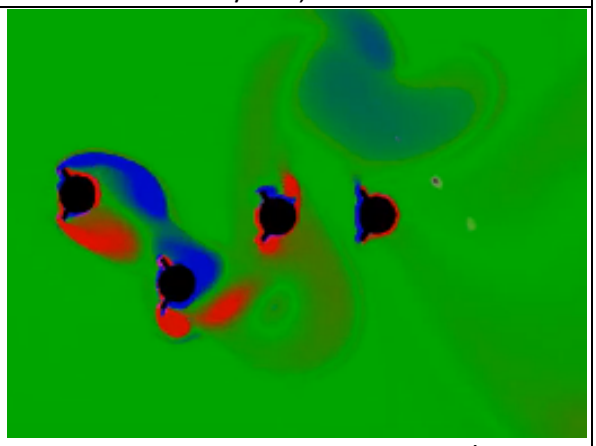

Figure 43. Flow speed U=1.0m/s, β=4, K=27N/mm; at time = 14.5 second

6.6. Time Histories Data for Flow Speed 1.0 m/s, β=6

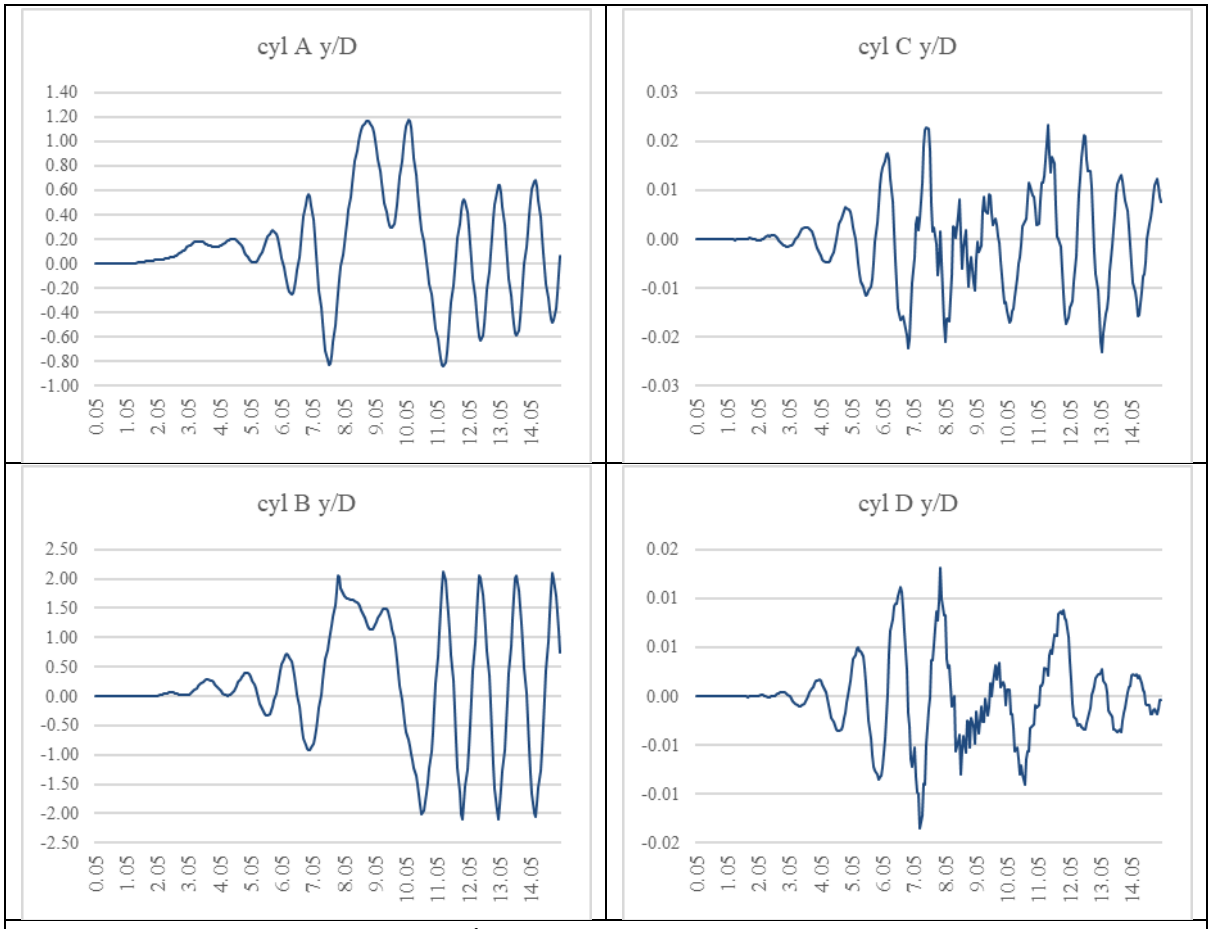

Figure 44. Time histories of the *y/D* for four cylinders in the 4-cylinder VIVACE Converter; speed *U*=1.5m/s, *β*=4, *K*=27N/mm; fine simulation mesh

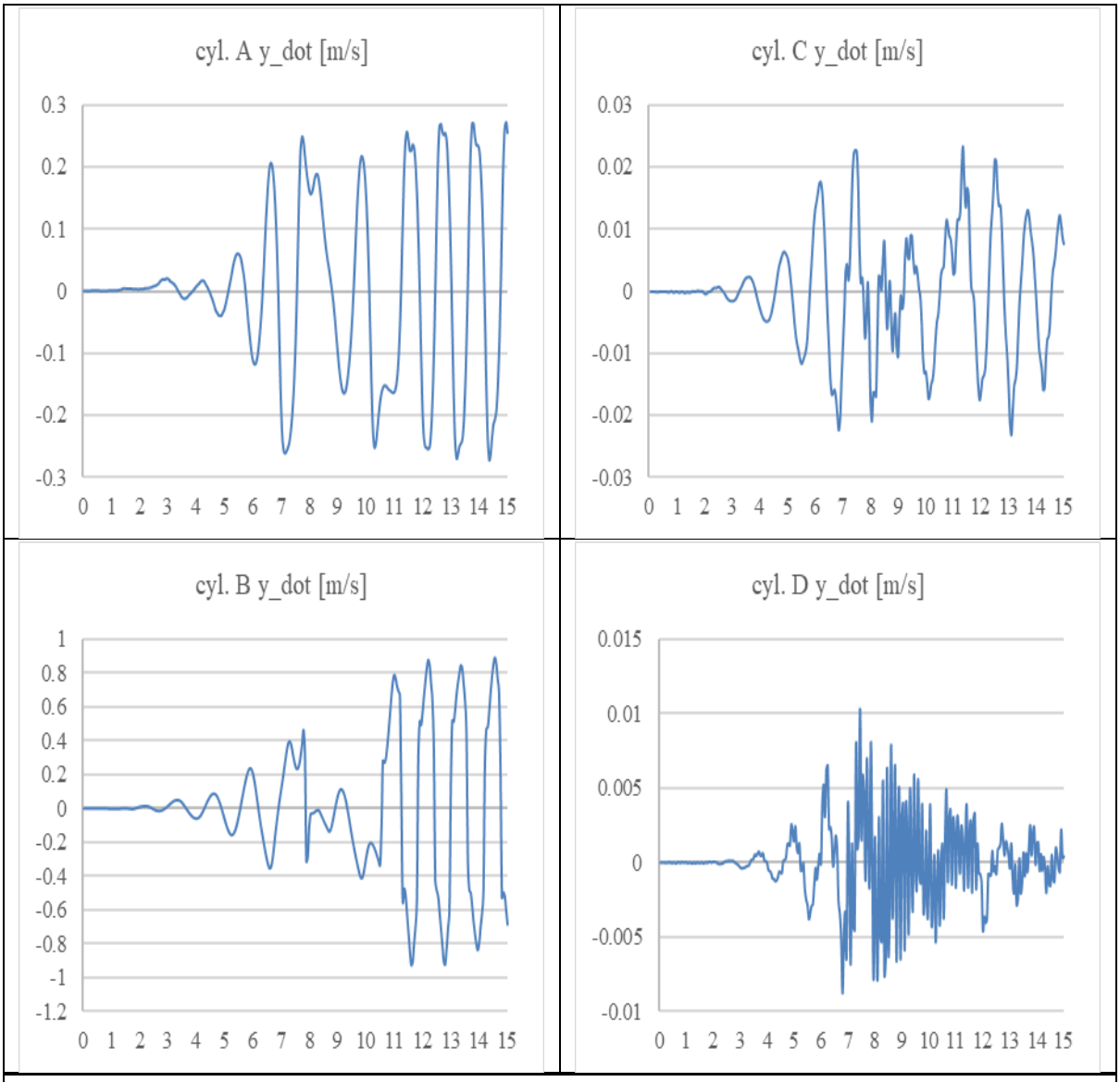

Figure 45. Time histories of the y_dot for four cylinders in the 4-cylinder VIVACE Converter; flow speed U=1.5m/s, β=4, K=27N/mm; fine simulation mesh

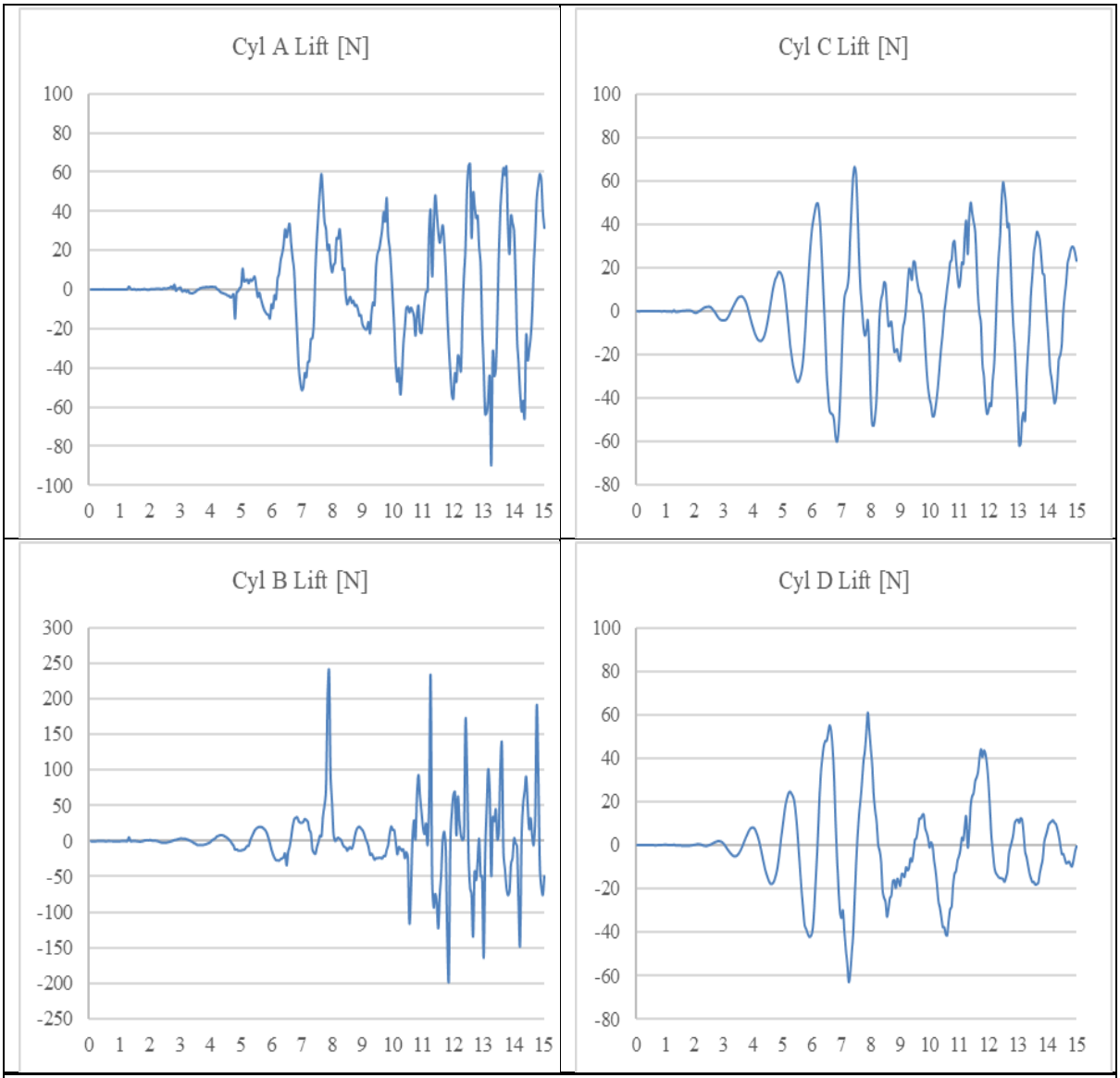

Figure 46. Time histories of the hydrodynamic lift for four cylinders in the 4-cylinder VIVACE Converter; flow speed U=1.5m/s, β=4, K=27N/mm; fine simulation mesh

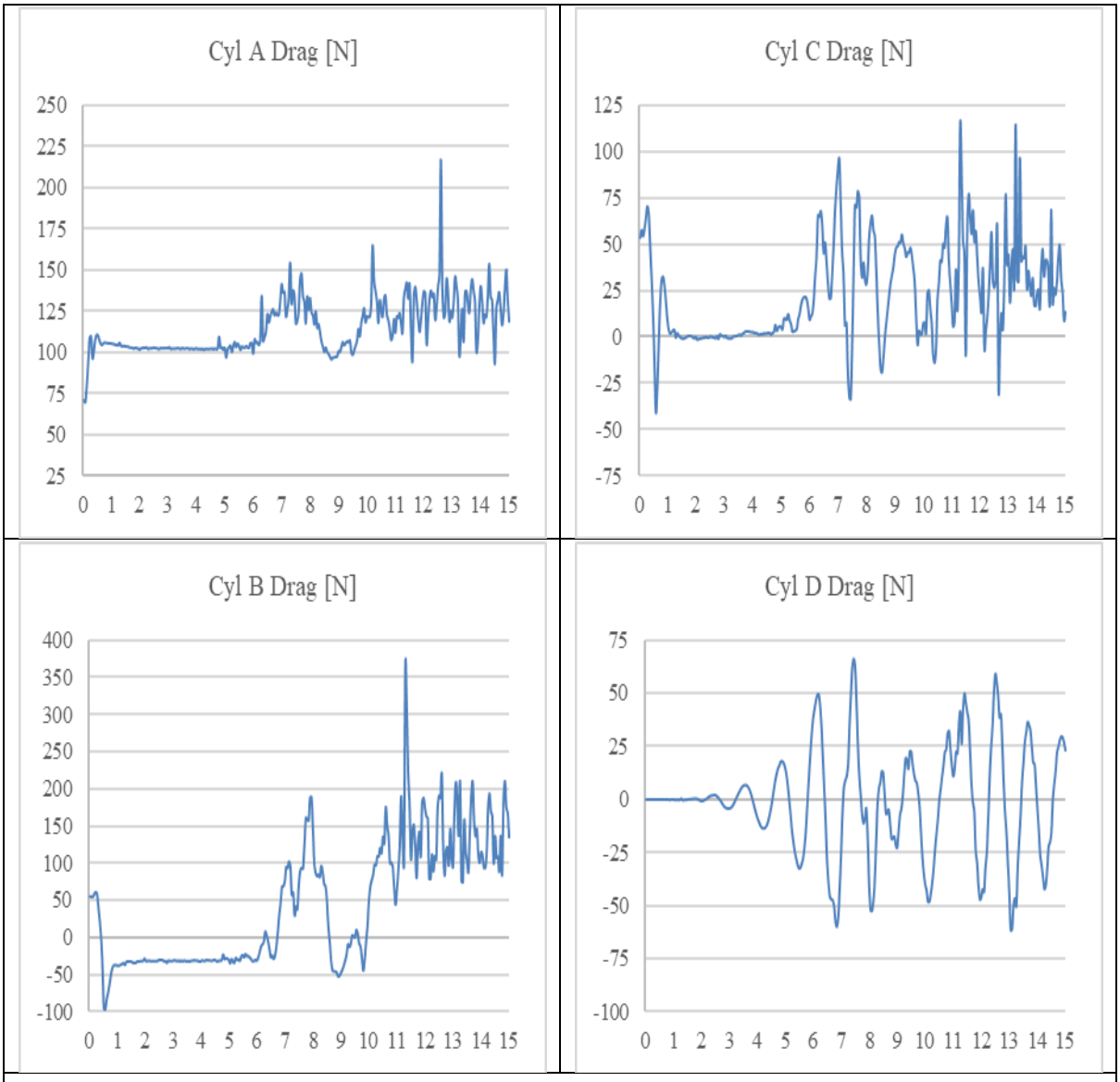

Figure 47. Time histories of the hydrodynamic drag for four cylinders in the 4-cylinder VIVACE Converter; flow speed U=1.5m/s, β=4, K=27N/mm; fine simulation mesh

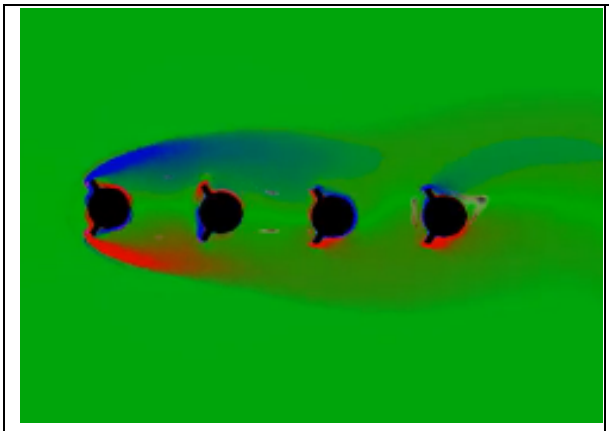

Figure 48. Flow speed U=1.5m/s, β=4, K=27N/mm; at time = 4 second

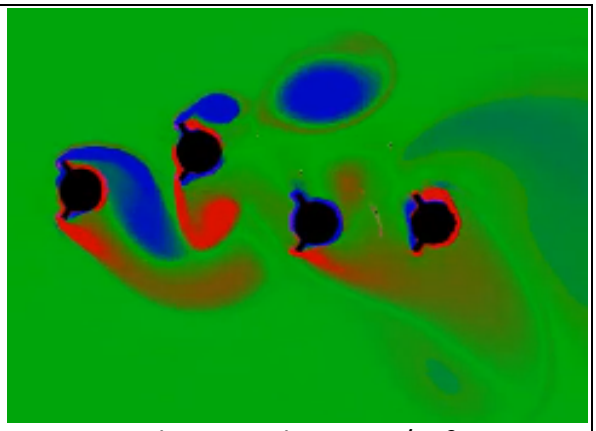

Figure 49. Flow speed U=1.5m/s, β=4, K=27N/mm; at time = 8 second

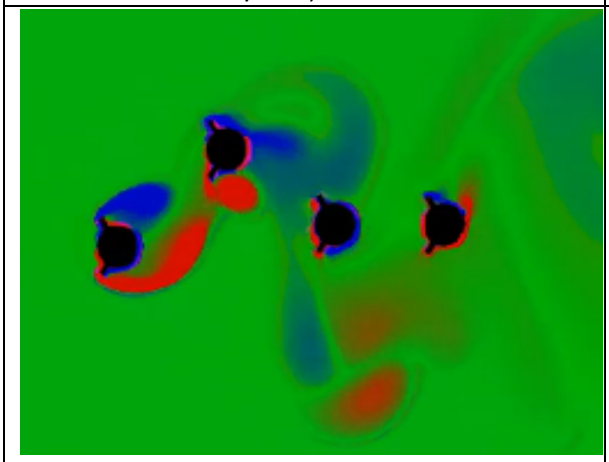

Figure 50. Flow speed U=1.5m/s, β=4, K=27N/mm; at time = 12 second

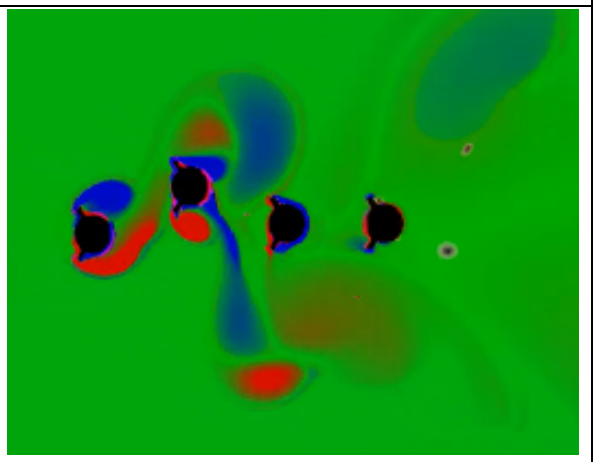

Figure 51. Flow speed U=1.5m/s, β=4, K=27N/mm; at time = 14.5 second

6.7. Time Histories Data for Flow Speed 1.5 m/s, β=2

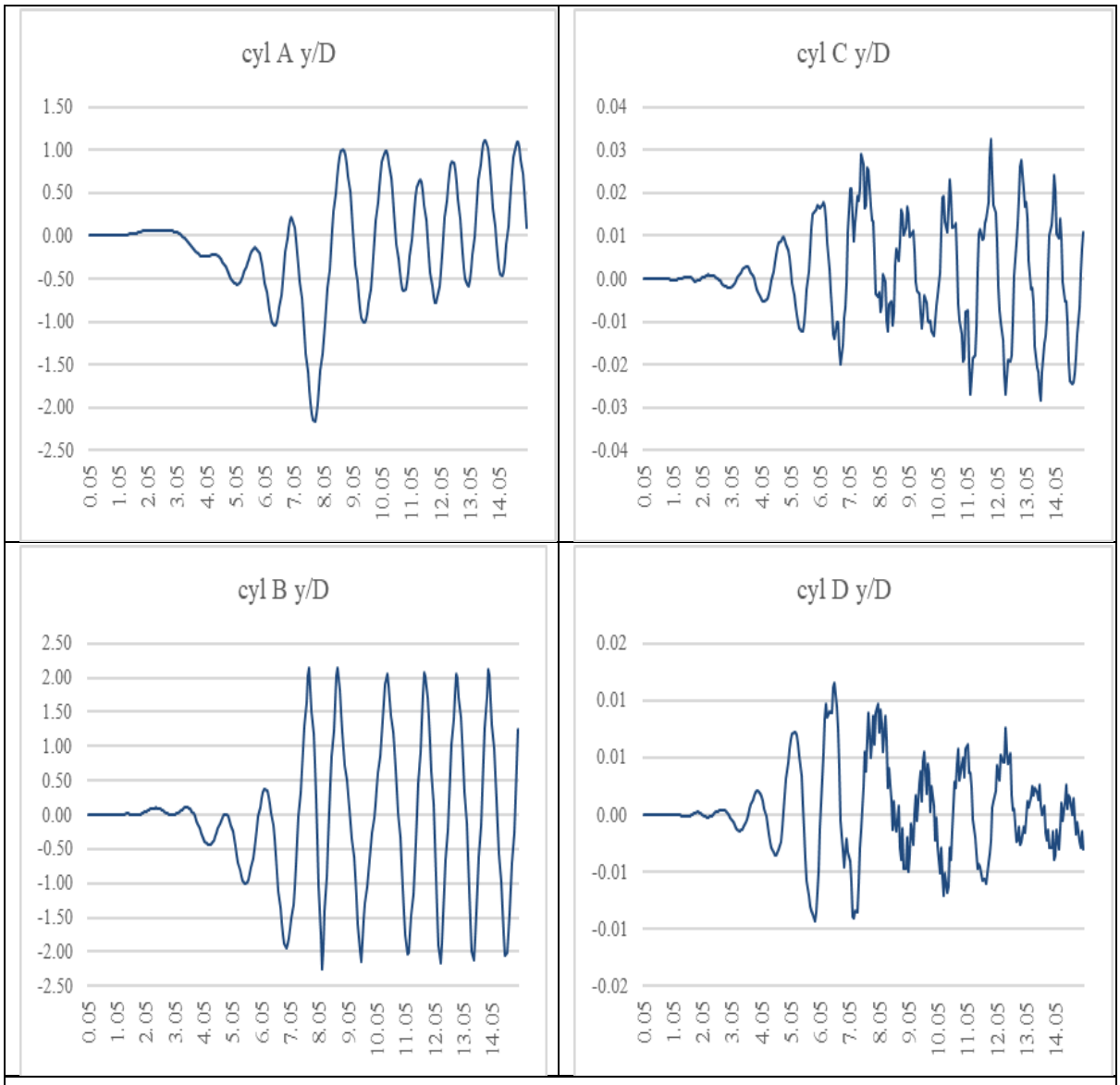

Figure 52. Time histories of the *y/D* for four cylinders in the 4-cylinder VIVACE Converter; flow speed *U*=0.5m/s, β=6, *K*=27N/mm; fine simulation mesh

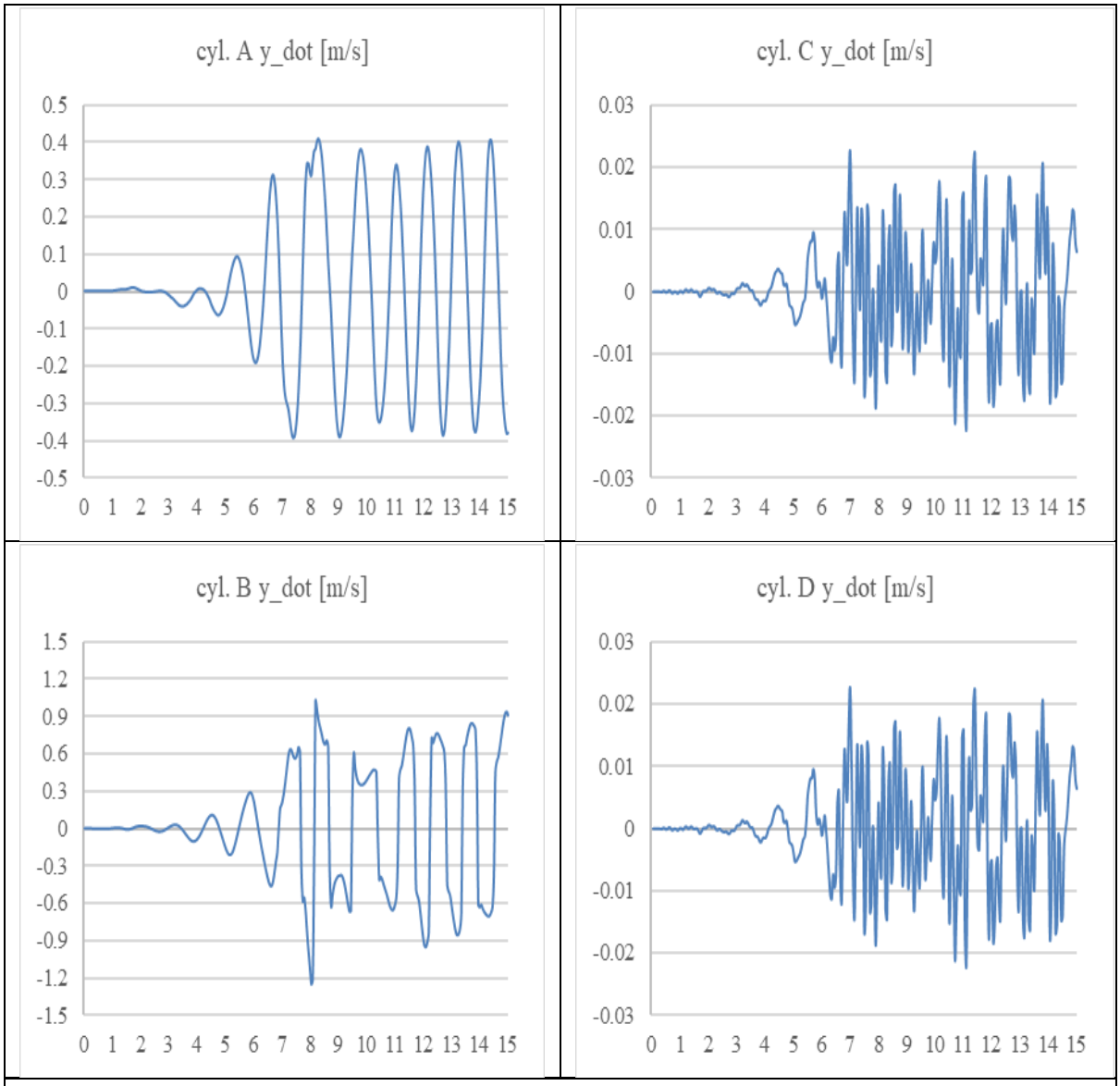

Figure 53. Time histories of the y_dot for four cylinders in the 4-cylinder VIVACE Converter; flow speed U=0.5m/s, β=6, K=27N/mm; fine simulation mesh

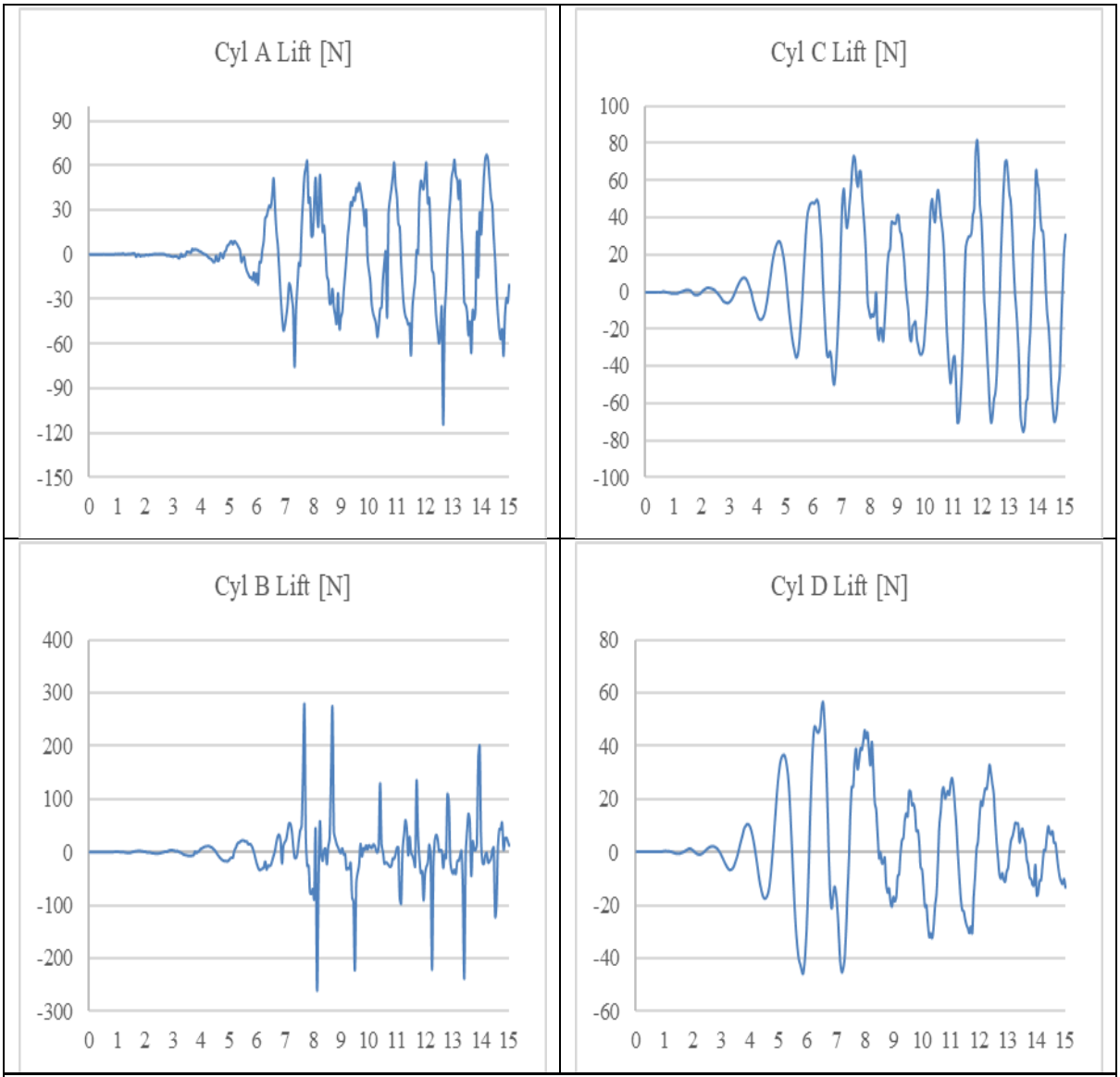

Figure 54. Time histories of the hydrodynamic lift for four cylinders in the 4-cylinder VIVACE Converter; flow speed U=0.5m/s, β=6, K=27N/mm; fine simulation mesh

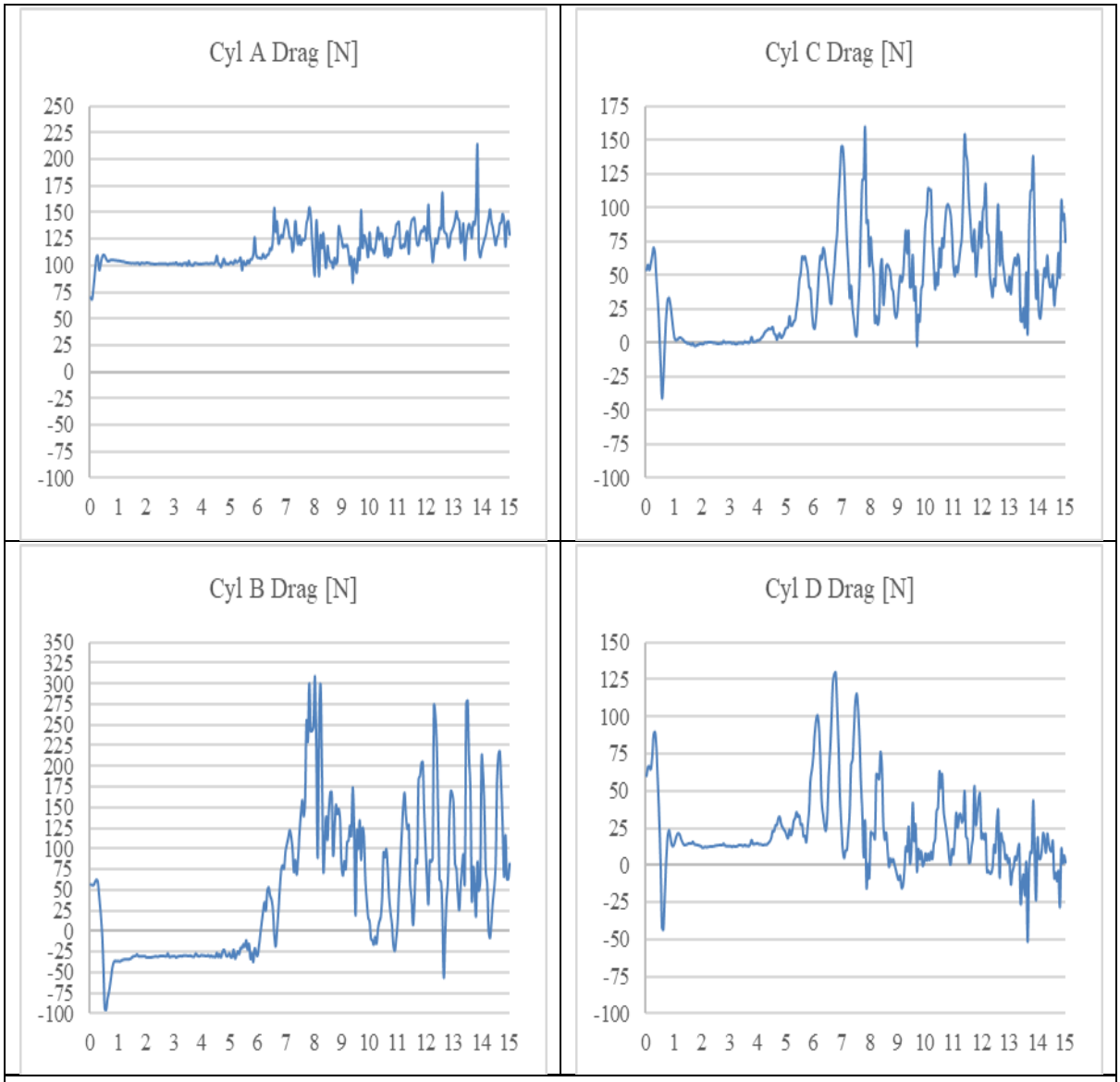

Figure 55. Time histories of the hydrodynamic drag for four cylinders in the 4-cylinder VIVACE Converter; flow speed U=0.5m/s, β=6, K=27N/mm; fine simulation mesh

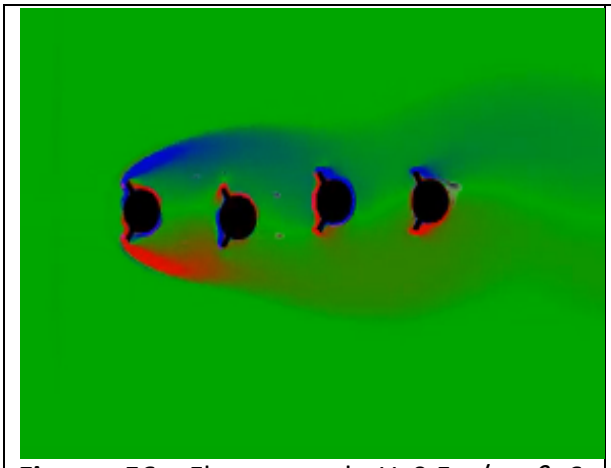

Figure 56. Flow speed *U*=0.5m/s, *β*=6, *K*=27N/mm; at time = 4 second

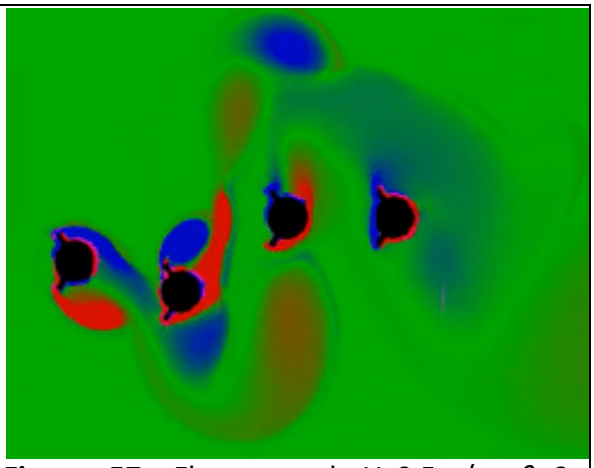

Figure 57. Flow speed *U*=0.5m/s, *β*=6, *K*=27N/mm; at time = 8 second

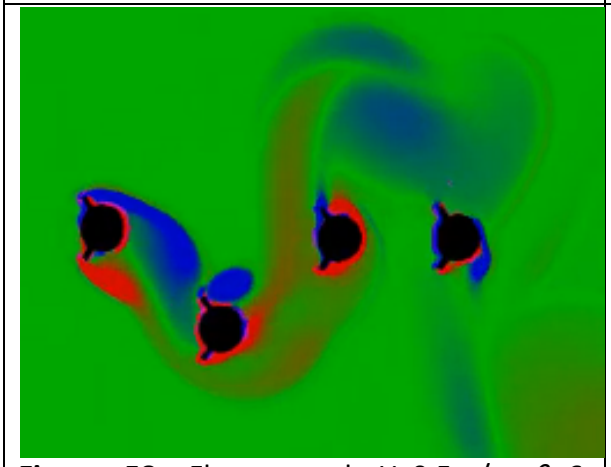

Figure 58. Flow speed *U*=0.5m/s, *β*=6, *K*=27N/mm; at time = 12 second

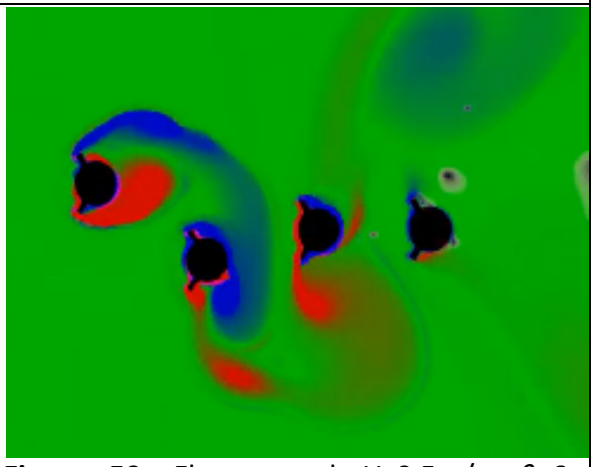

Figure 59. Flow speed *U*=0.5m/s, *β*=6, *K*=27N/mm; at time = 14.5 second

6.8. Time Histories Data for Flow Speed 1.5 m/s, β=4

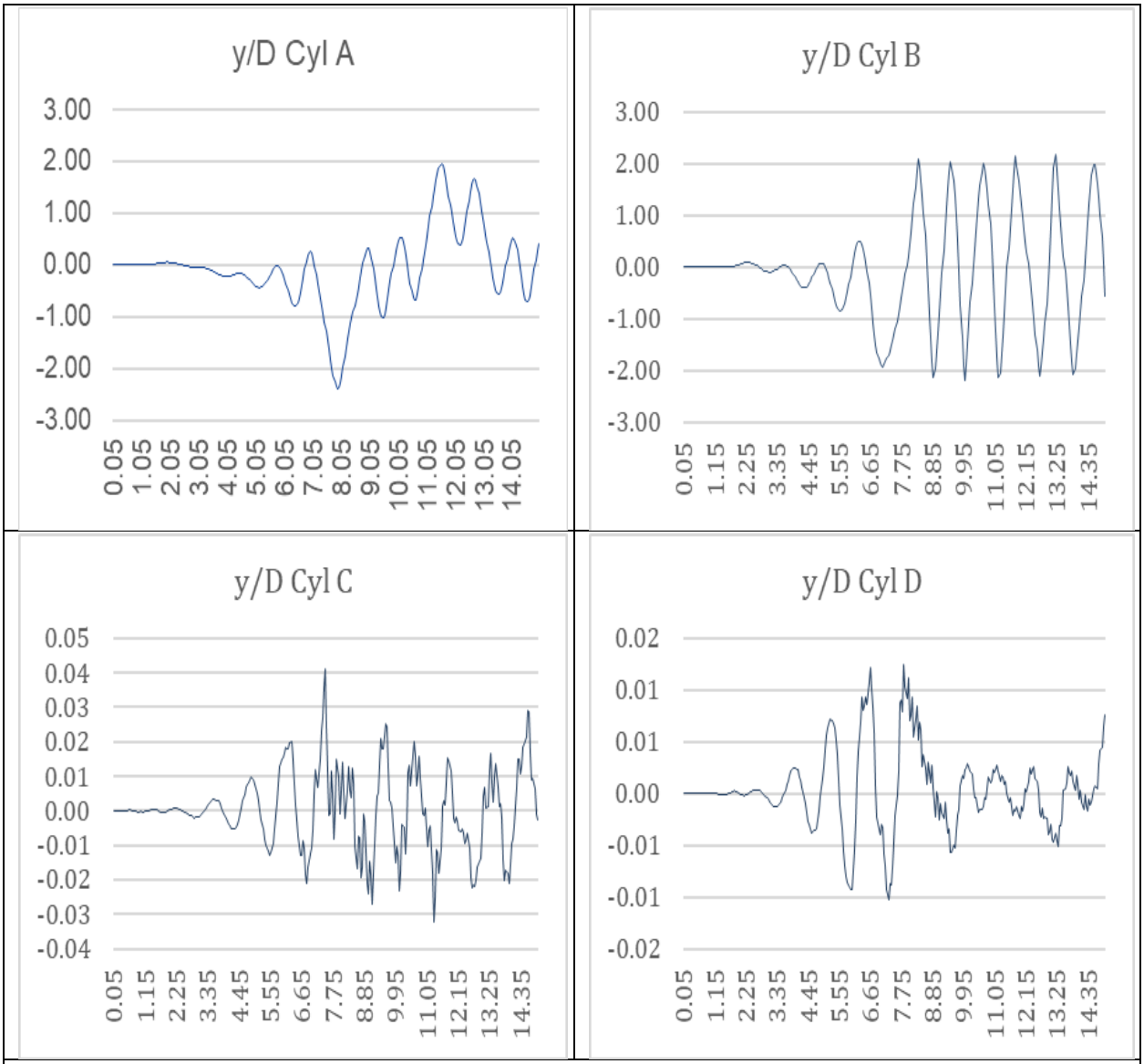

Figure 60. Time histories of the *y/D* for four cylinders in the 4-cylinder VIVACE Converter; flow speed *U*=1.0m/s, *β*=6, *K*=27N/mm; fine simulation mesh

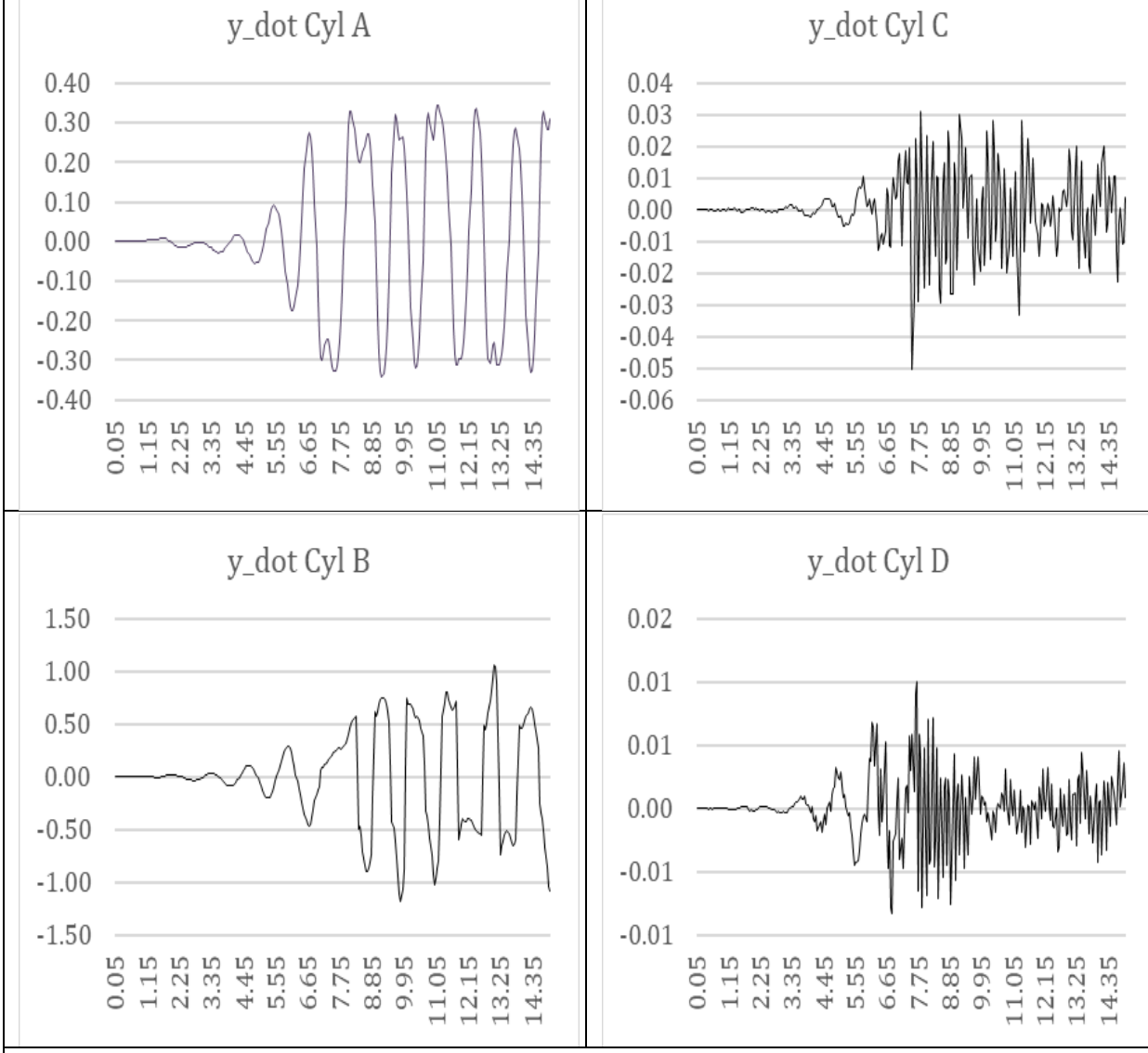

Figure 61. Time histories of the y_dot for four cylinders in the 4-cylinder VIVACE Converter; flow speed U=1.0m/s, β=6, K=27N/mm; fine simulation mesh

Figure 62. Time histories of the hydrodynamic lift for four cylinders in the 4-cylinder VIVACE Converter; flow speed U=1.0m/s, β=6, K=27N/mm; fine simulation mesh

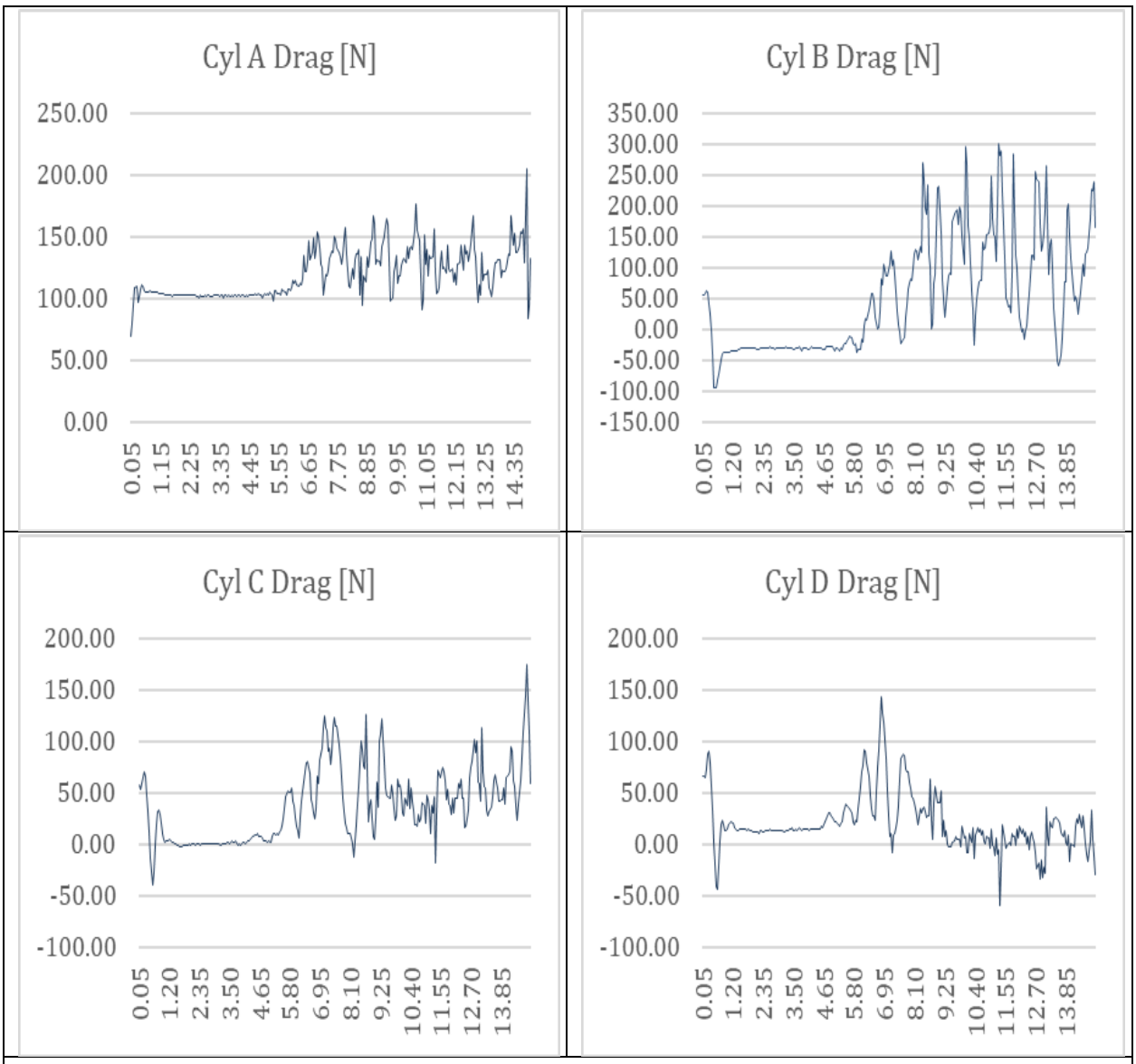

Figure 63. Time histories of the Hydrodynamic Drag for four cylinders in the 4-cylinder VIVACE Converter; speed U=1.0m/s, β=6, K=27N/mm; fine simulation mesh

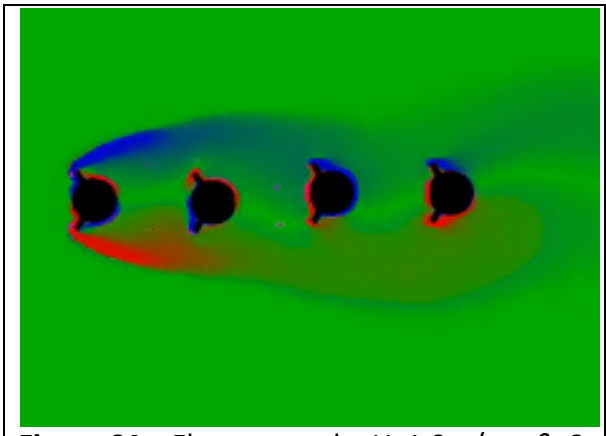

Figure 64. Flow speed U=1.0m/s, β=6, K=27N/mm; at time = 4 second

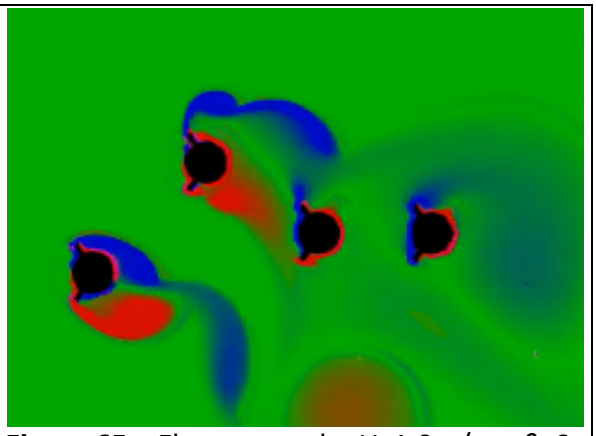

Figure 65. Flow speed U=1.0m/s, β=6, K=27N/mm; at time = 8 second

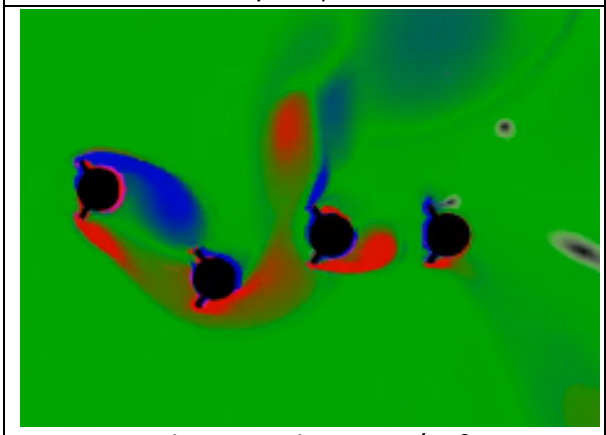

Figure 66. Flow speed U=1.0m/s, β=6, K=27N/mm; at time = 12 second

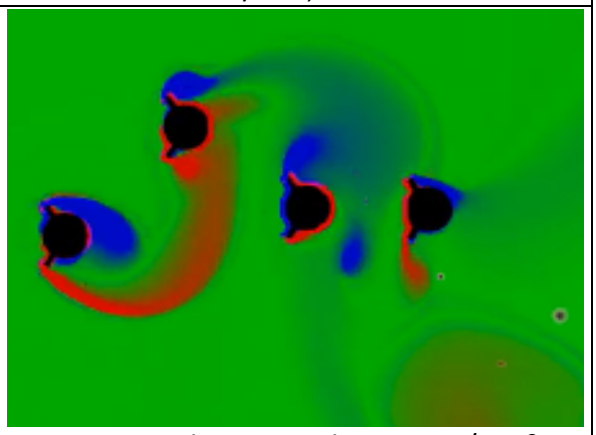

Figure 67. Flow speed U=1.0m/s, β=6, K=27N/mm; at time = 14.5 second

6.9. Time Histories Data for Flow Speed 1.5 m/s, β=6

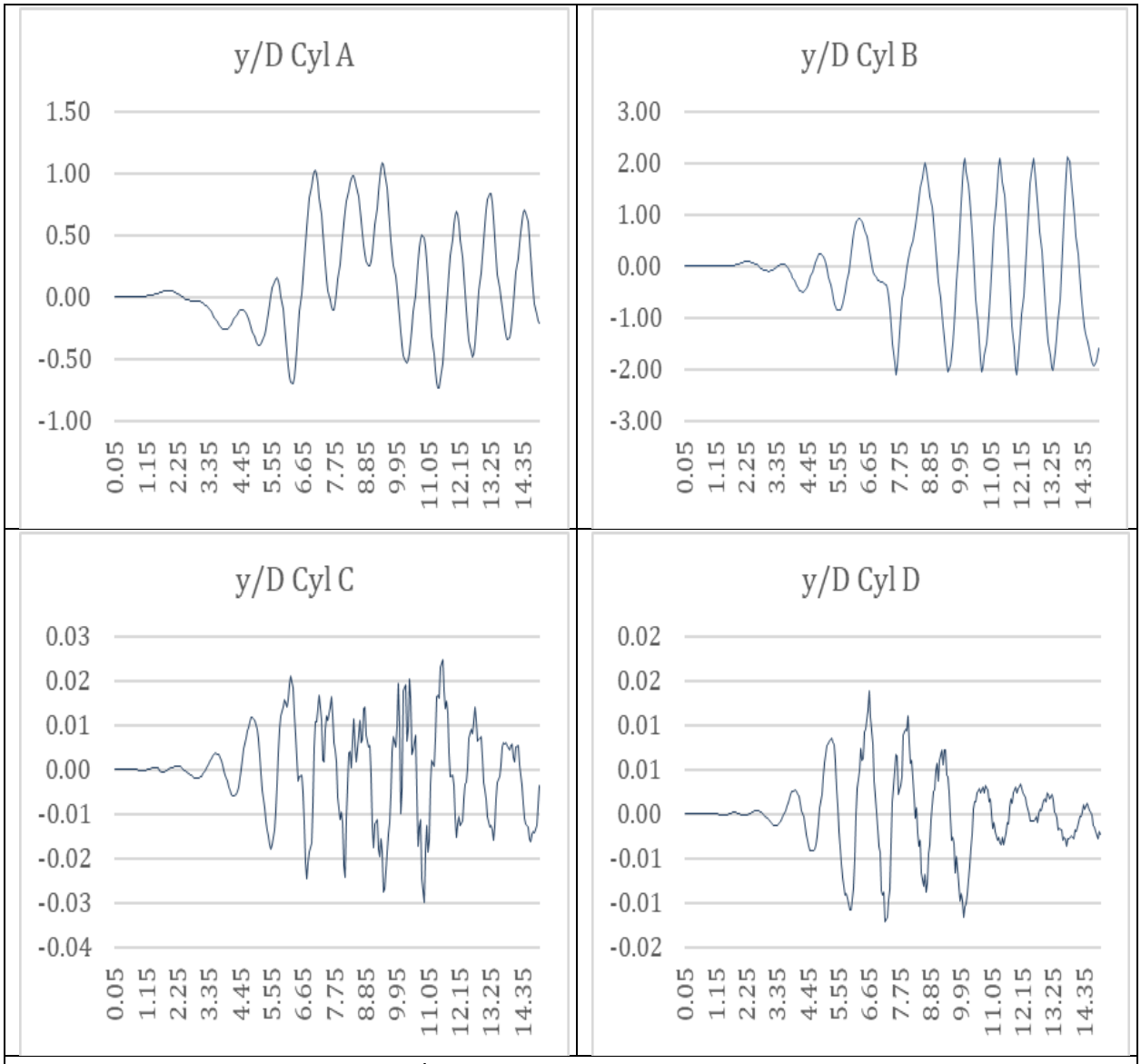

Figure 68. Time histories of the y/D for four cylinders in the 4-cylinder VIVACE Converter; flow speed *U*=1.5m/s, *β*=6, *K*=27N/mm; fine simulation mesh

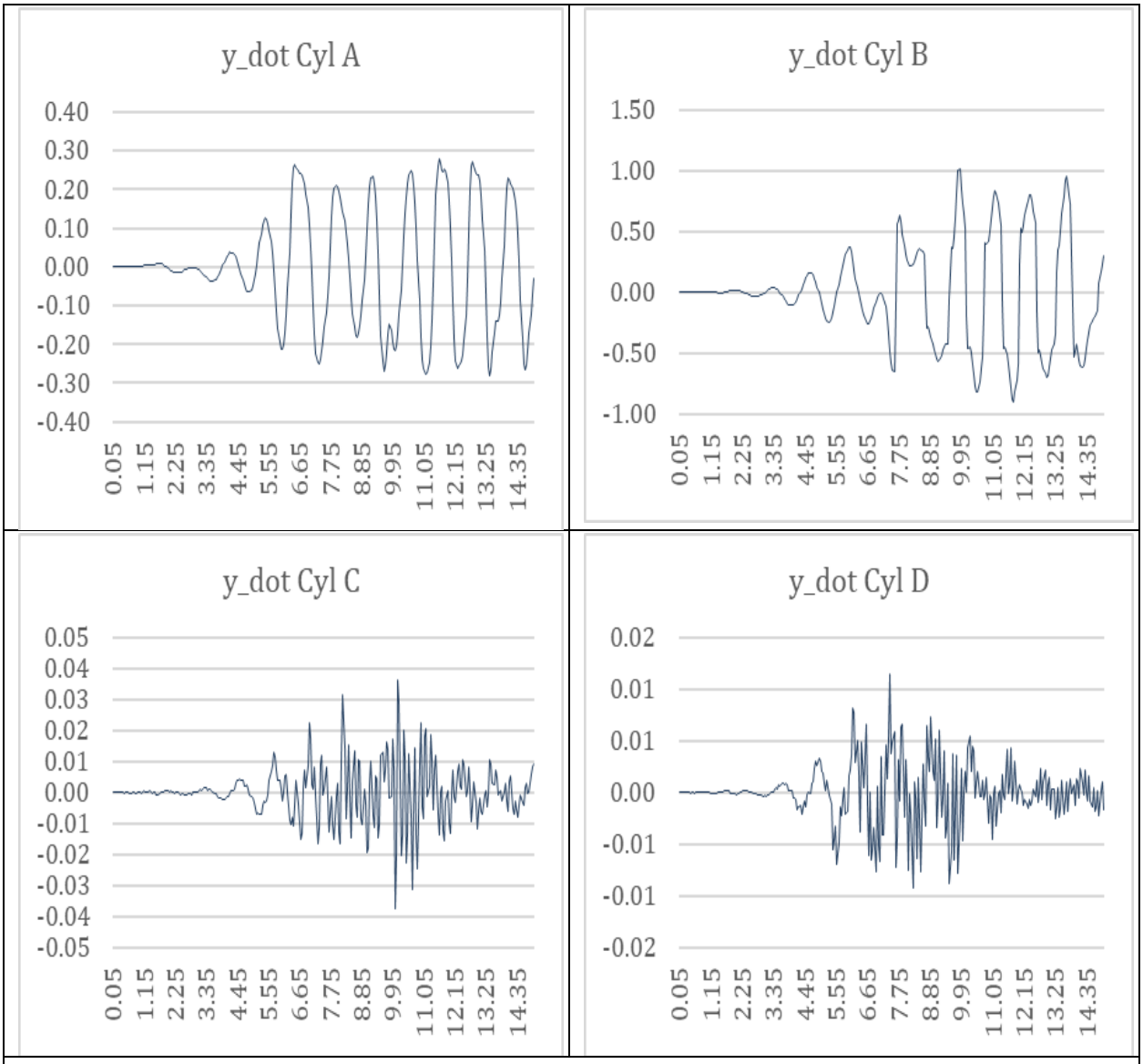

Figure 69. Time histories of the y_dot for four cylinders in the 4-cylinder VIVACE Converter; flow speed U=1.5m/s, β=6, K=27N/mm; fine simulation mesh

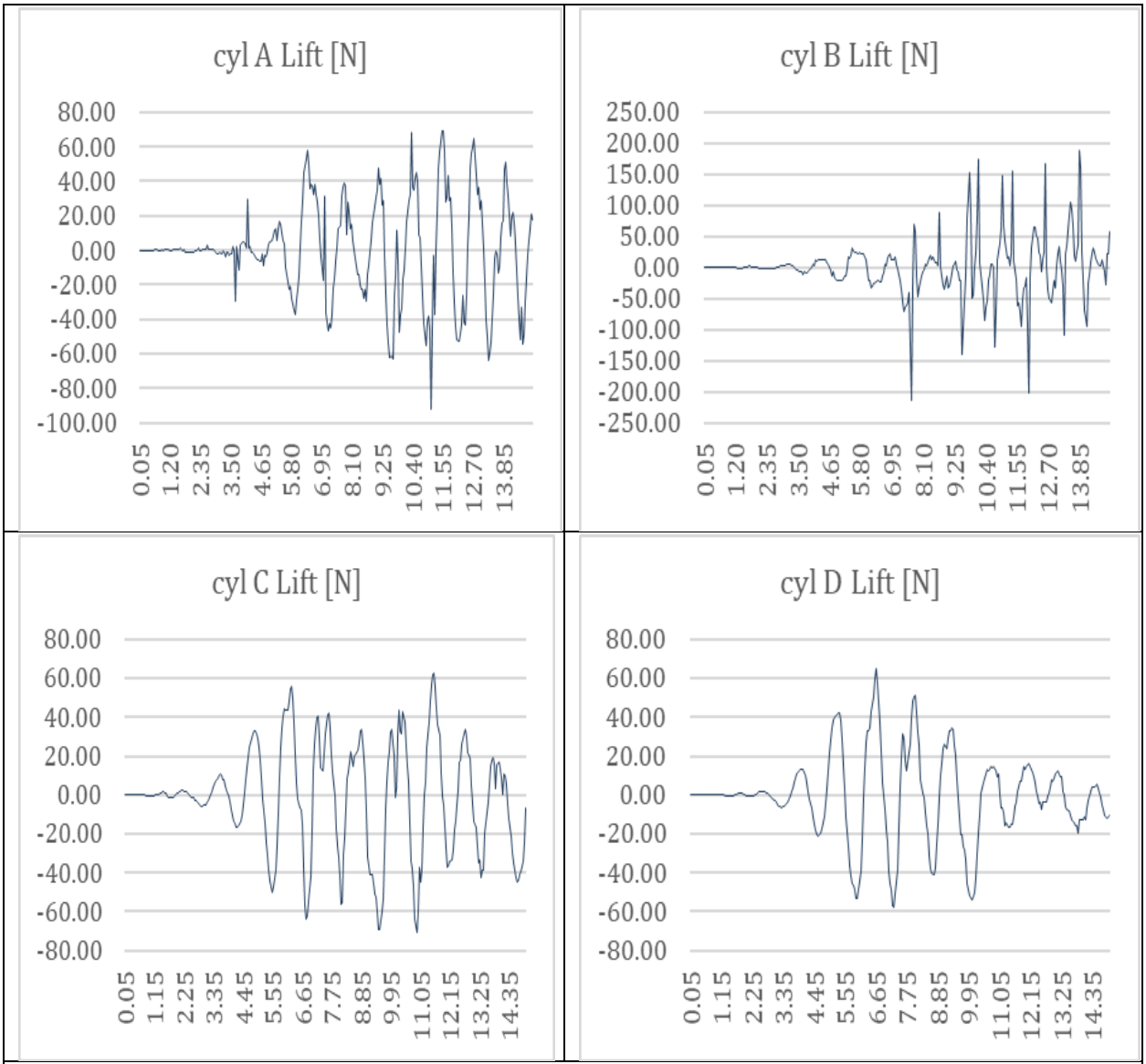

Figure 70. Time histories of the hydrodynamic lift for four cylinders in the 4-cylinder VIVACE Converter; flow speed U=1.5m/s, β=6, K=27N/mm; simulation mesh

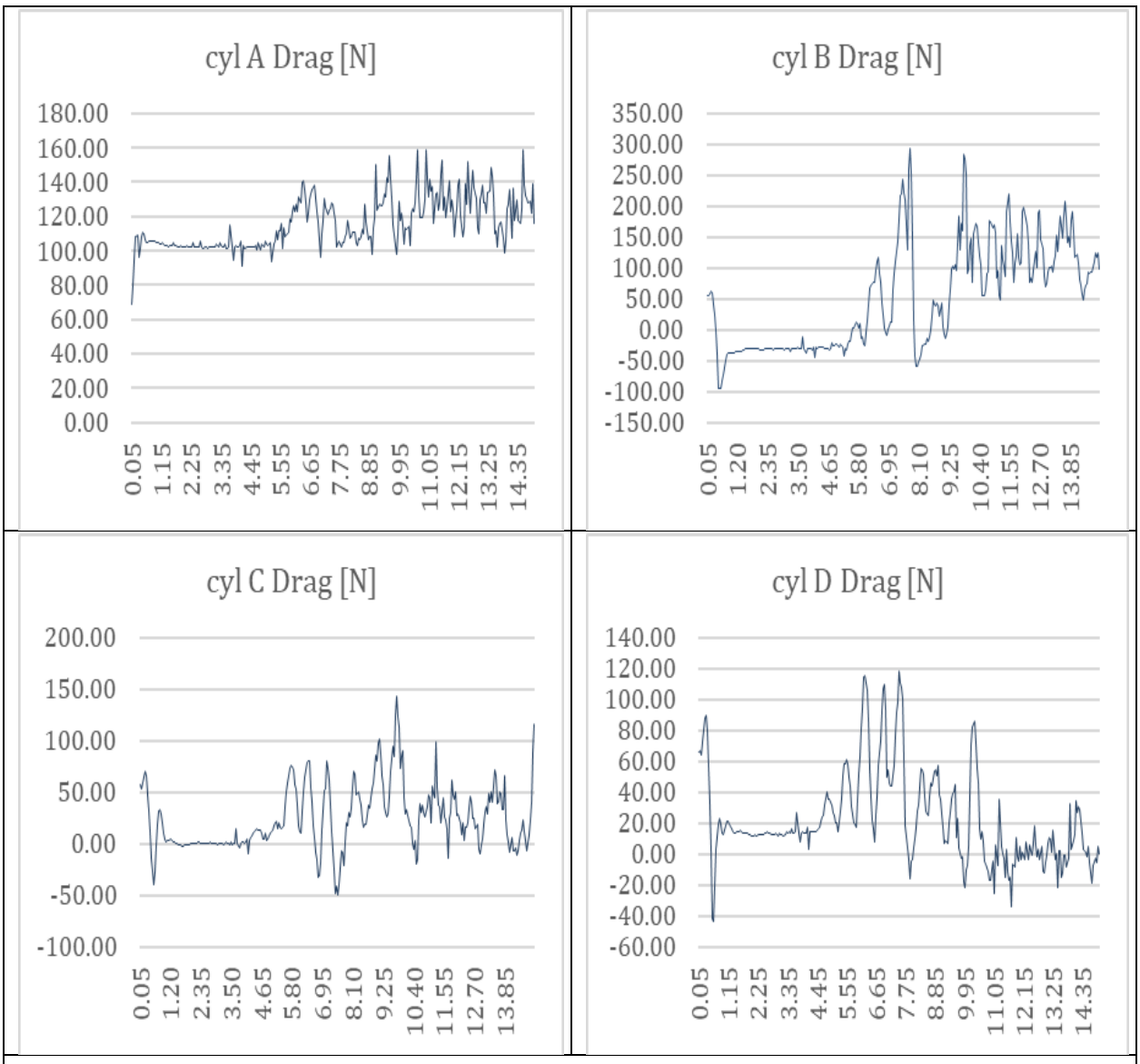

Figure 71. Time histories of the hydrodynamic drag for four cylinders in the 4-cylinder VIVACE Converter; flow speed U=1.5m/s, β=6, K=27N/mm; fine simulation mesh

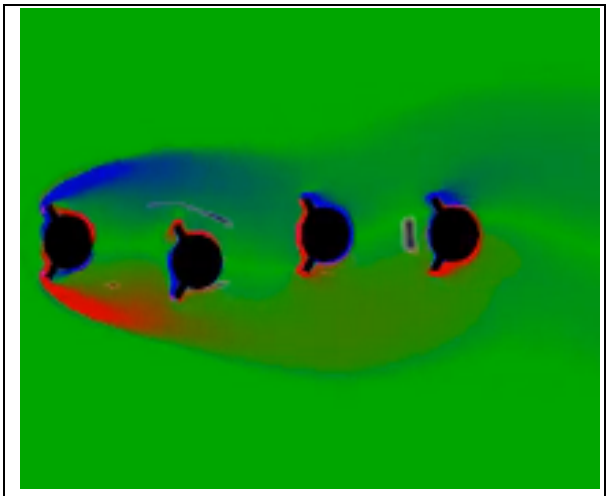

Figure 72. Flow speed U=1.5m/s, β=6, K=27N/mm; at time = 4 second

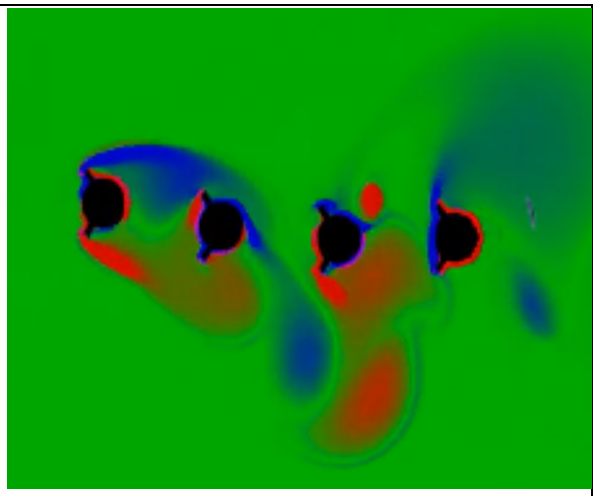

Figure 73. Flow speed U=1.5m/s, β=6, K=27N/mm; at time = 8 second

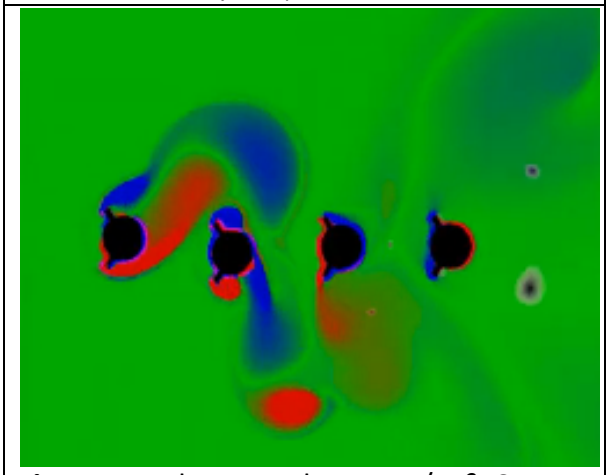

Figure 74. Flow speed U=1.5m/s, β=6, K=27N/mm; at time = 12 second

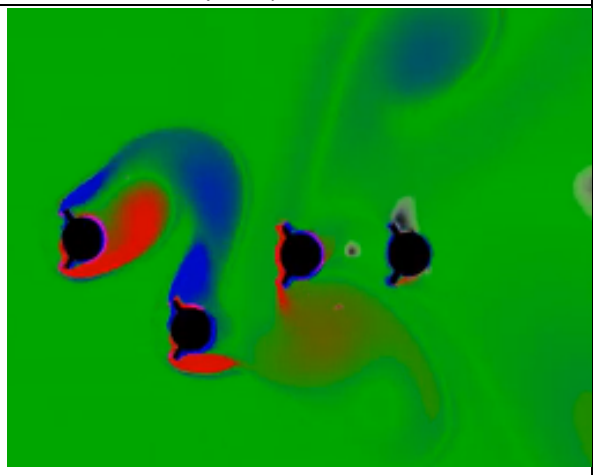

Figure 75. Flow speed U=1.5m/s, β=6, K=27N/mm; at time = 14.5 second

7. HYDRODYNAMIC CALCULATION RESULTS FOR THE 2-CYLINDER VIVACE

7.1. Time Histories Data for Flow Speed 1 m/s, β=2

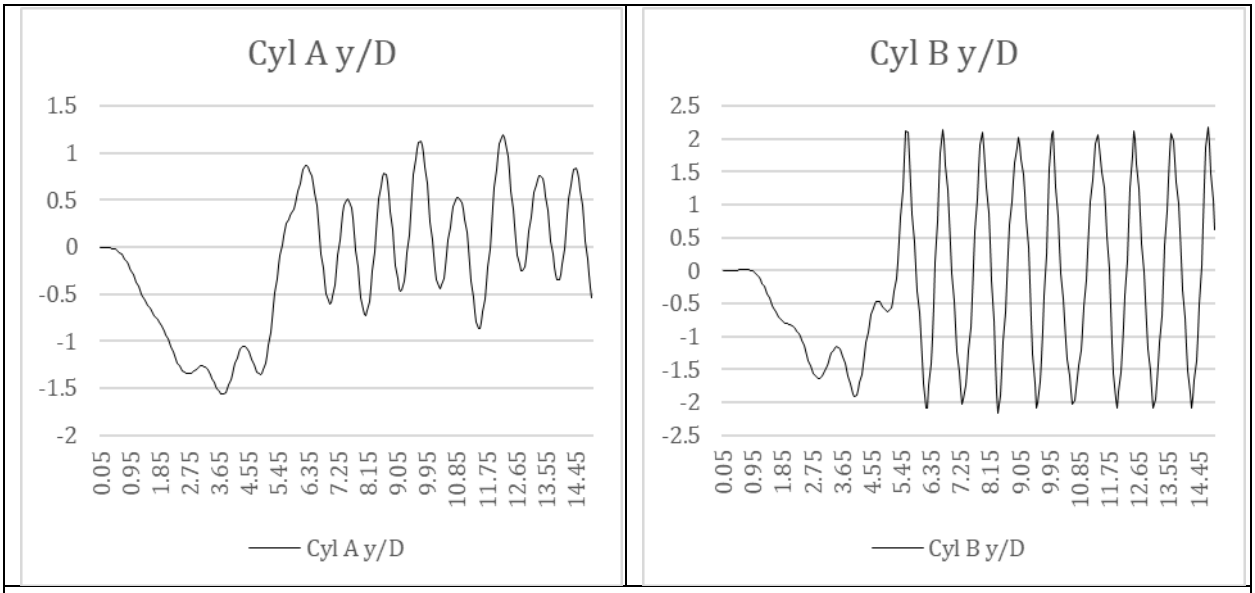

Figure 76. Time histories of the *y/D* for two cylinders in the 2-cylinder VIVACE Converter; flow speed *U*=1.0m/s, *β*=2, *K*=27N/mm; fine simulation mesh

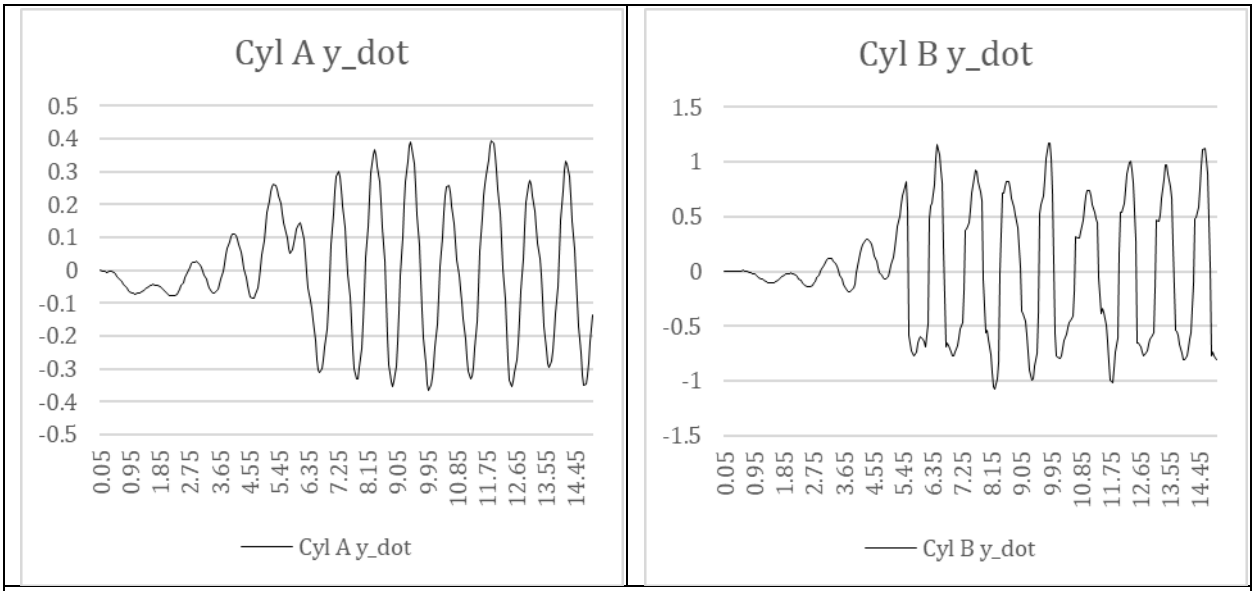

Figure 77. Time histories of the y_dot for two cylinders in the 2-cylinder VIVACE Converter; flow speed *U*=1.0m/s, *β*=2, *K*=27N/mm; fine simulation mesh

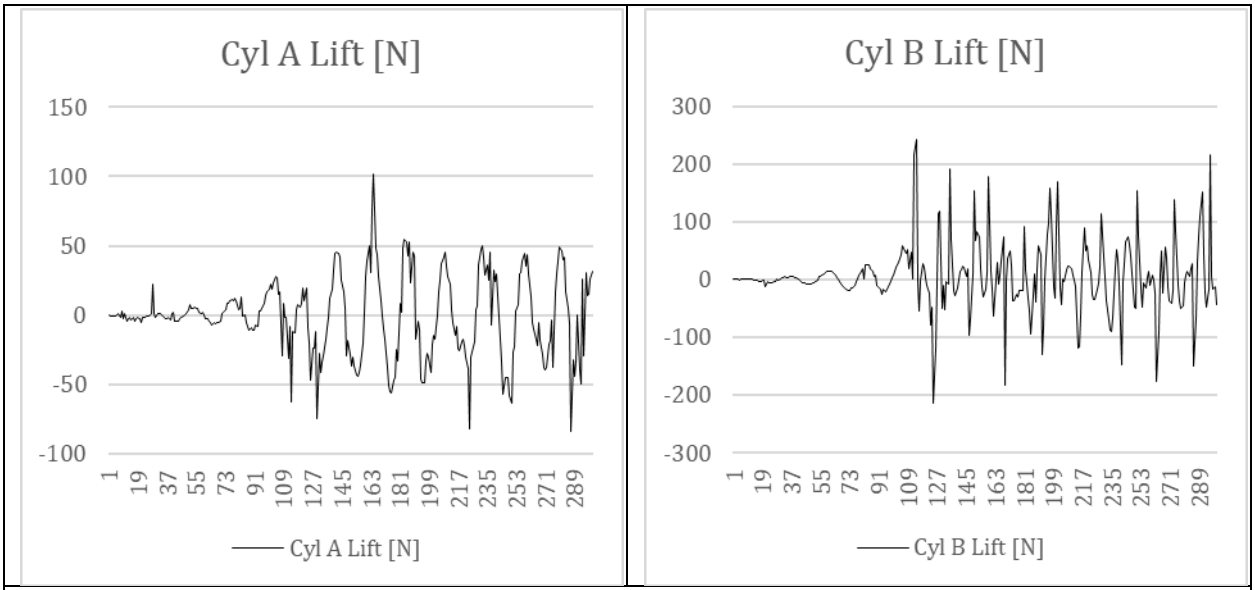

Figure 78. Time histories of the hydrodynamic lift for two cylinders in the 2-cylinder VIVACE Converter; flow speed U=1.0m/s, β=2, K=27N/mm; fine simulation mesh

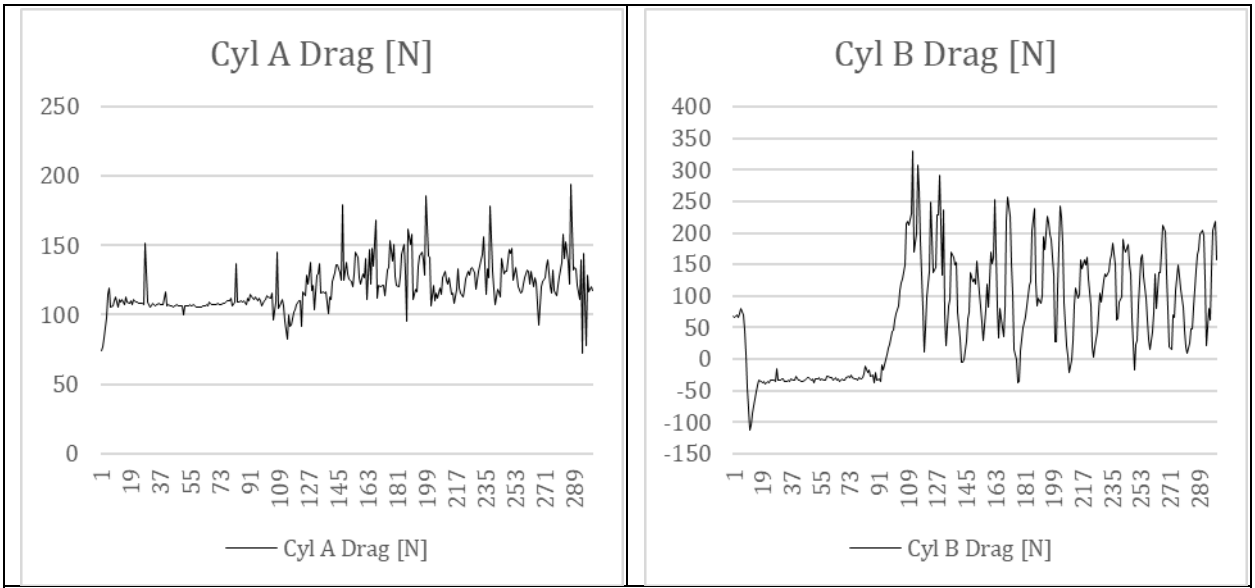

Figure 79. Time histories of the hydrodynamic drag for two cylinders in the 2-cylinder VIVACE Converter; flow speed U=1.0m/s, β=2, K=27N/mm; fine simulation mesh

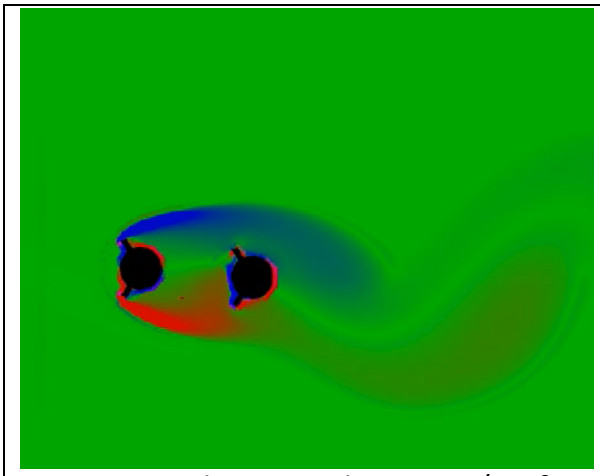

Figure 80. Flow speed U=1.0m/s, β=2, K=27N/mm; at time = 4 second

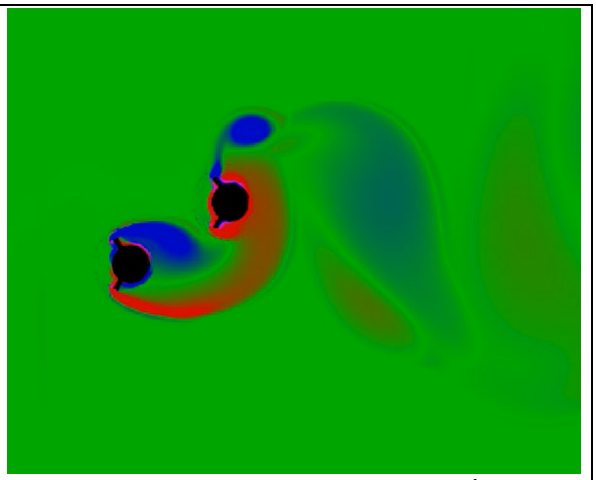

Figure 81. Flow speed U=1.0m/s, β=2, K=27N/mm; at time = 8 second

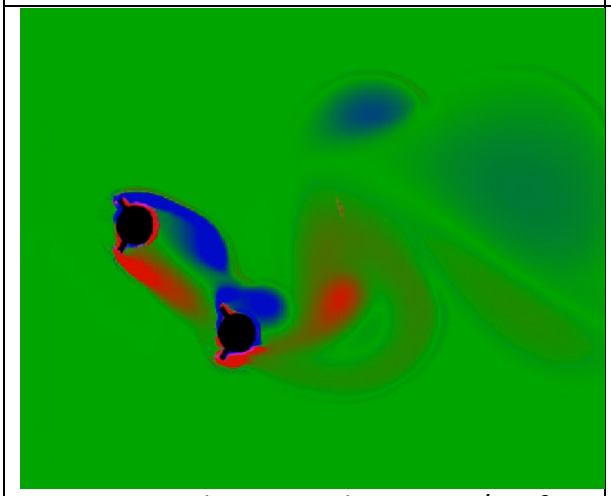

Figure 82. Flow speed U=1.0m/s, β=2, K=27N/mm; at time = 12 second

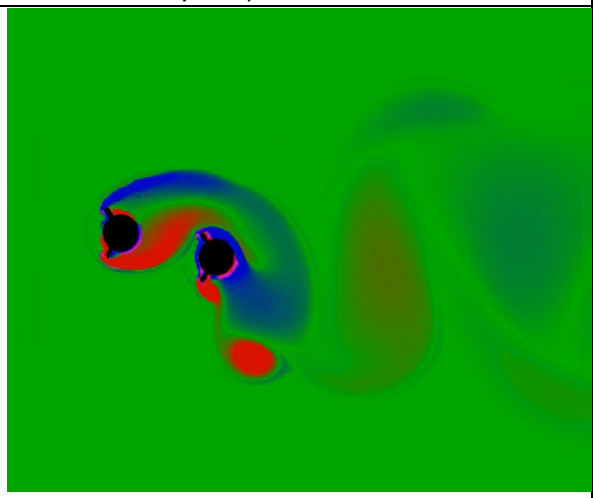

Figure 83. Flow speed U=1.0m/s, β=2, K=27N/mm; at time = 14.5 second

7.2. Time Histories Data for Flow Speed 1.3 m/s, β=20

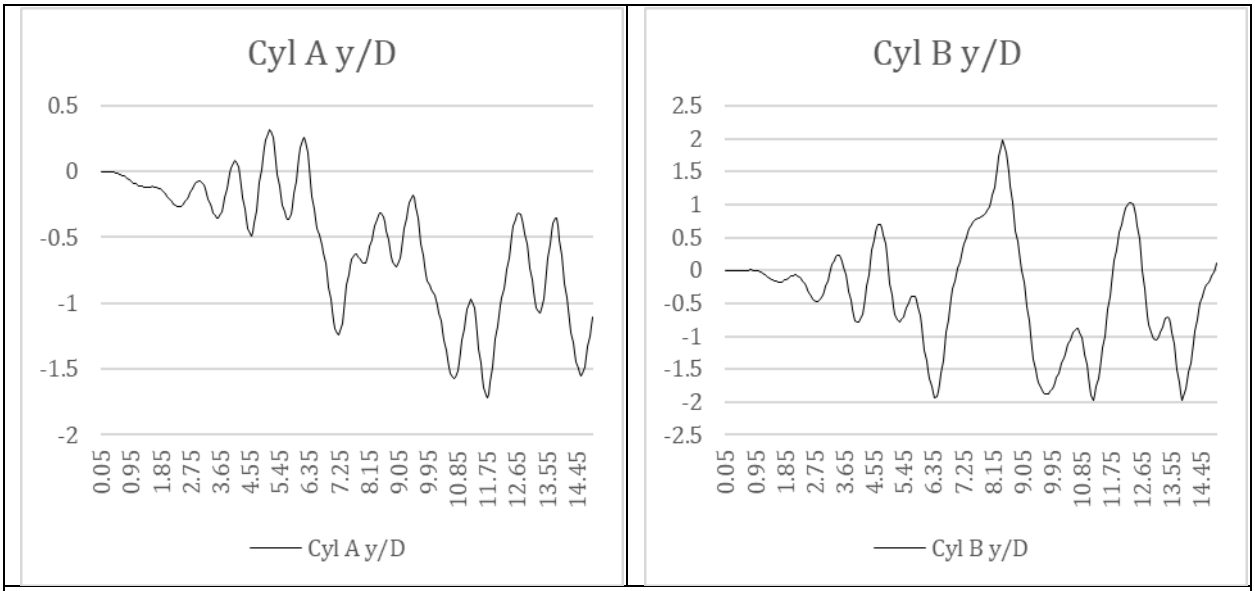

Figure 84. Time histories of the *y/D* for two cylinders in the 2-cylinder VIVACE Converter; flow speed *U*= 1.3 m/s, $\beta = 20$, K=27N/mm; fine simulation mesh

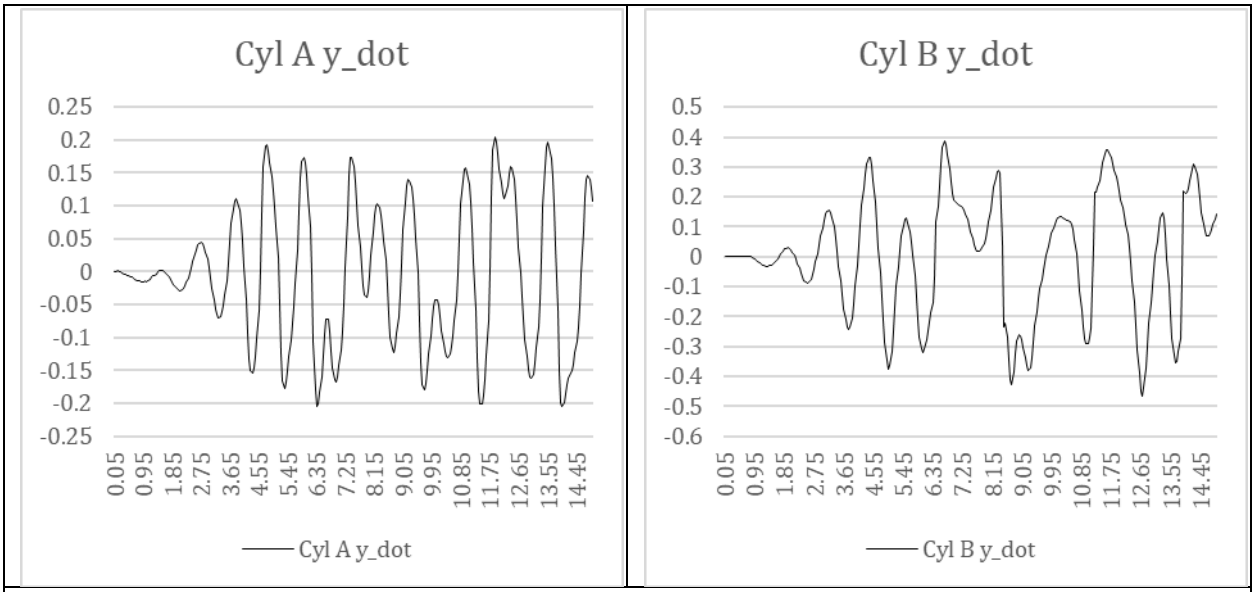

Figure 85. Time histories of the y_dot for two cylinders in the 2-cylinder VIVACE Converter; flow speed *U*= 1.3 m/s, $\beta = 20$, K=27N/mm; fine simulation mesh

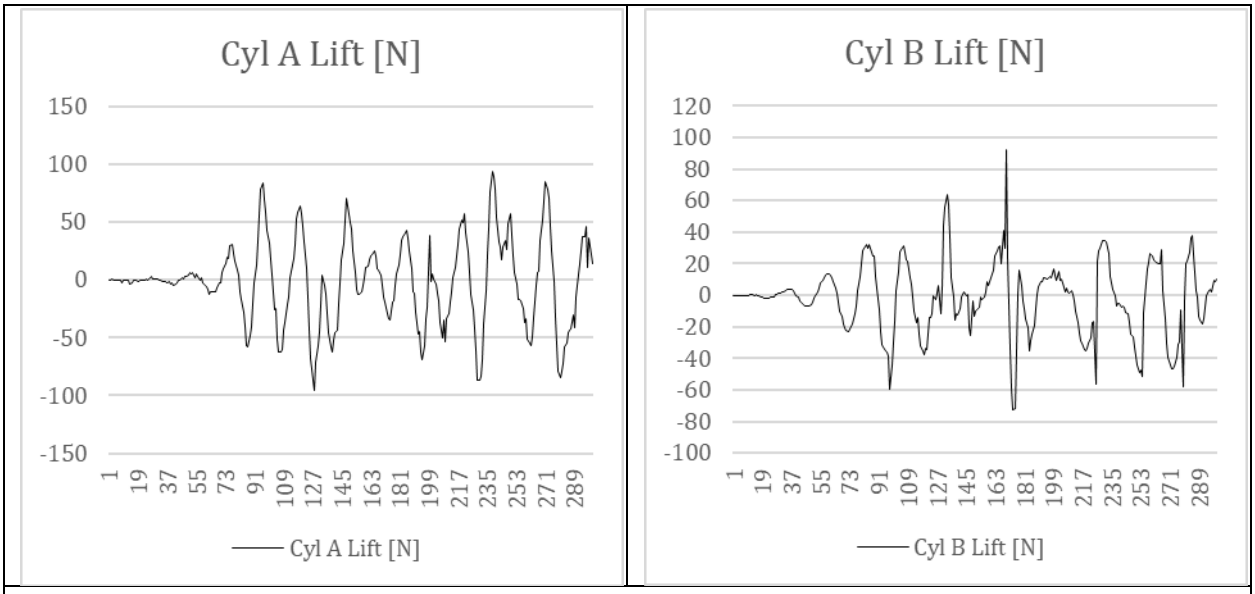

Figure 86. Time histories of the hydrodynamics lift for two cylinders in the 2-cylinder VIVACE Converter; flow speed *U*= 1.3 m/s, $\beta = 20$, K=27N/mm; fine simulation mesh

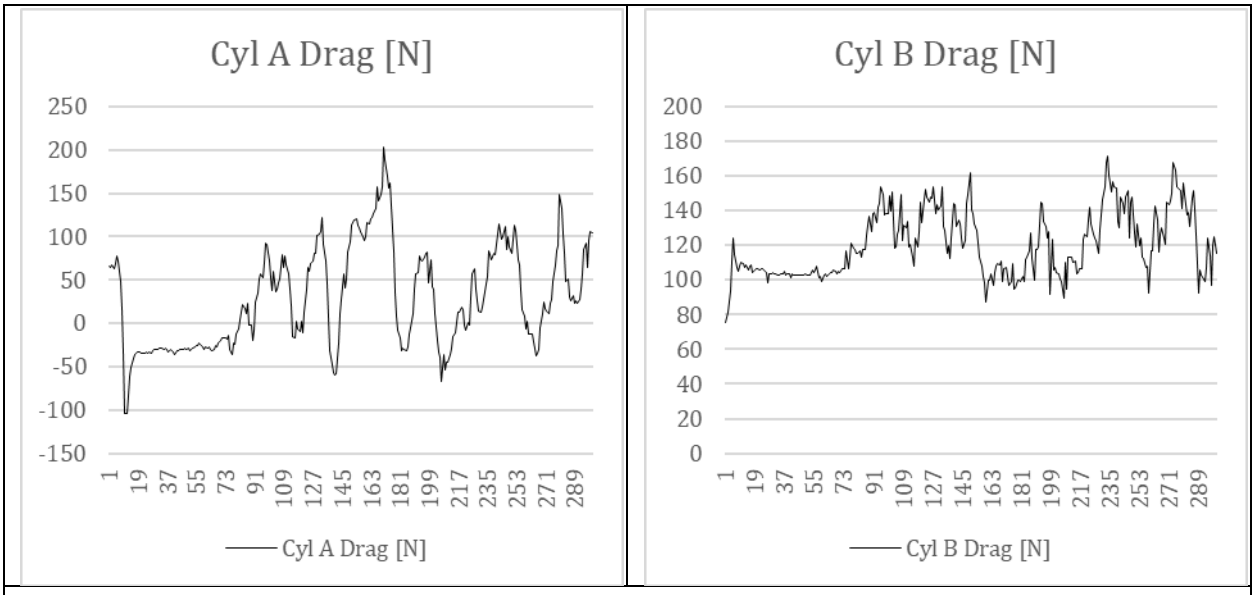

Figure 87. Time histories of the hydrodynamics drag for two cylinders in the 2-cylinder VIVACE Converter; flow speed *U*= 1.3 m/s, $\beta = 20$, K=27N/mm; fine simulation mesh.

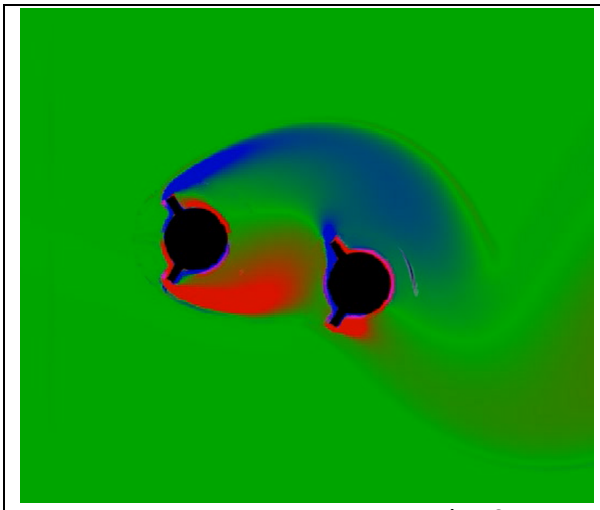

Figure 88. Flow speed *U*=1.3 m/s, $\beta = 20$, K=27N/mm; at time = 4 second

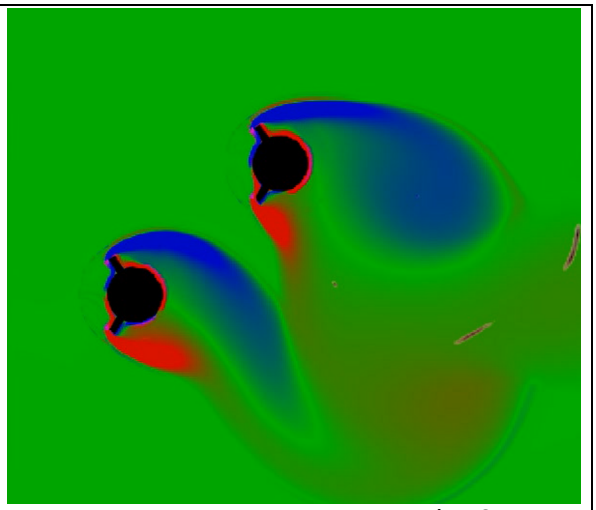

Figure 89. Flow speed *U*=1.3 m/s, $\beta = 20$, K=27N/mm; at time = 8 second

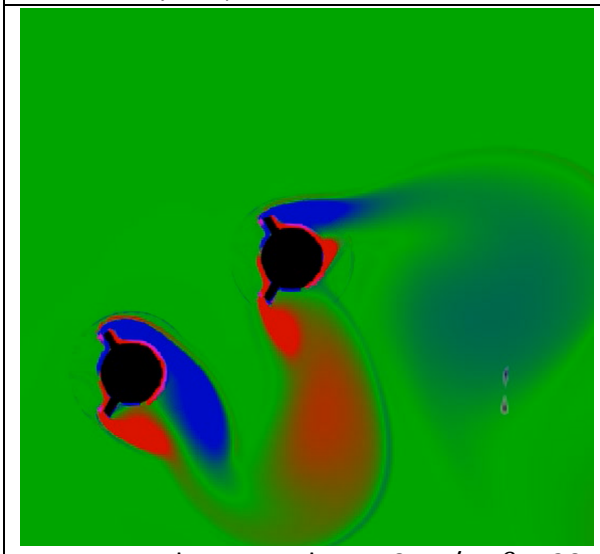

Figure 90. Flow speed *U*=1.3 m/s, $\beta = 20$, K=27N/mm; at time = 12 second

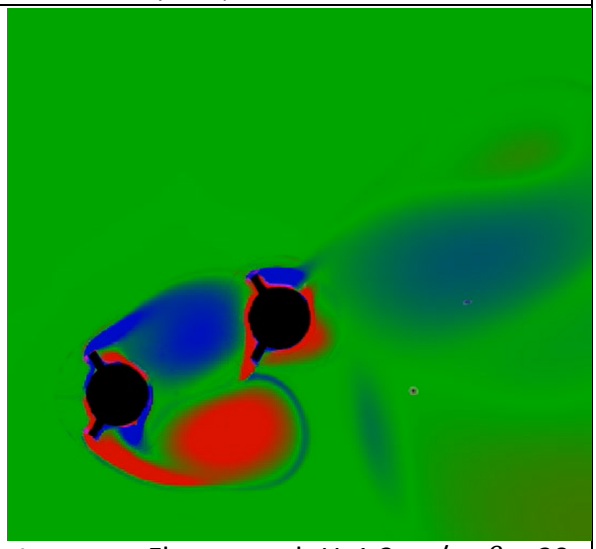

Figure 91. Flow speed *U*=1.3 m/s, $\beta = 20$, K=27N/mm; at time = 14.5 second

7.3. Time Histories Data for Flow Speed 1.5 m/s, β=50

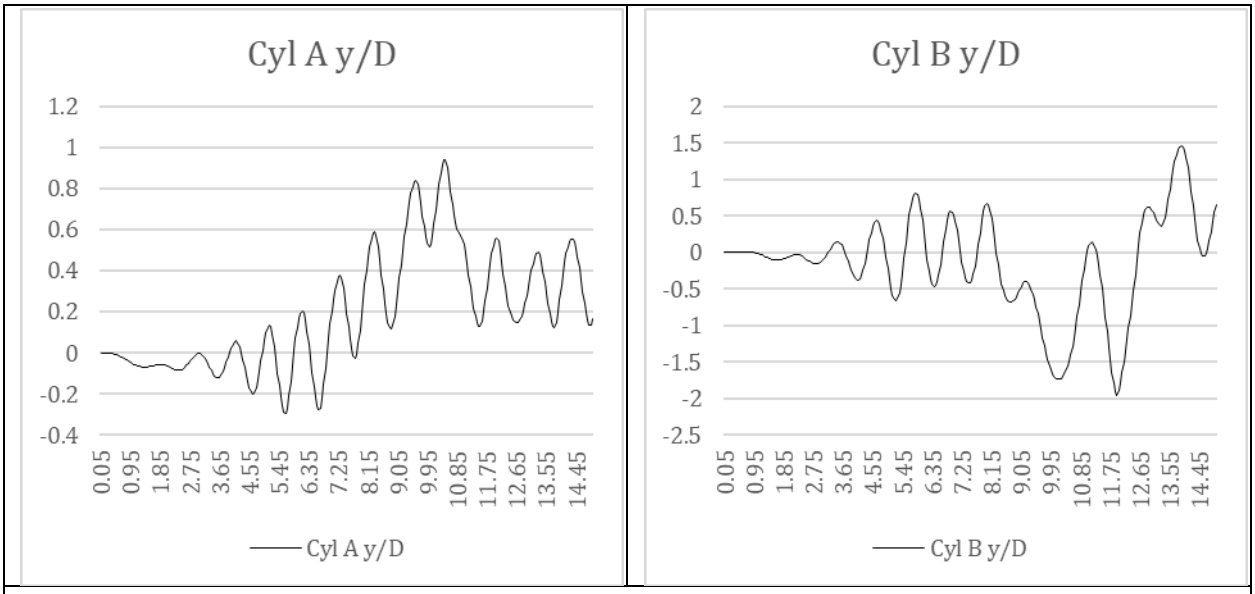

Figure 92. Time histories of the *y/D* for two cylinders in the 2-cylinder VIVACE Converter; flow speed *U*=1.5 m/s, β =50, K=27N/mm; fine simulation mesh

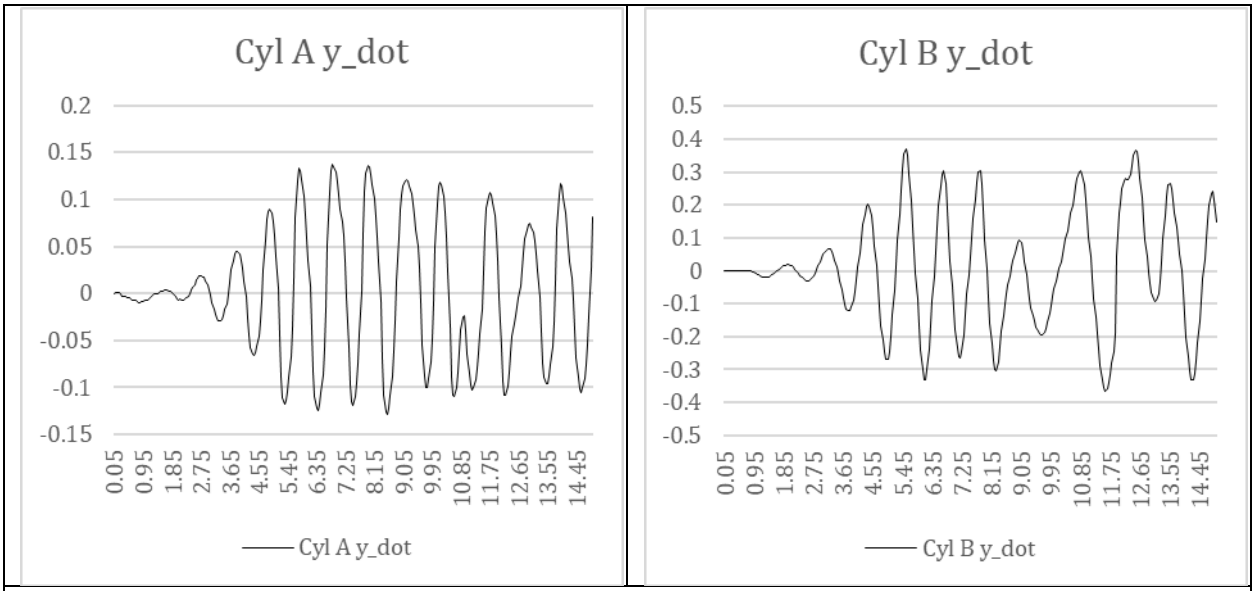

Figure 93. Time histories of the y_dot for two cylinders in the 2-cylinder VIVACE Converter; flow speed *U*=1.5 m/s, β =50, K=27N/mm; fine simulation mesh

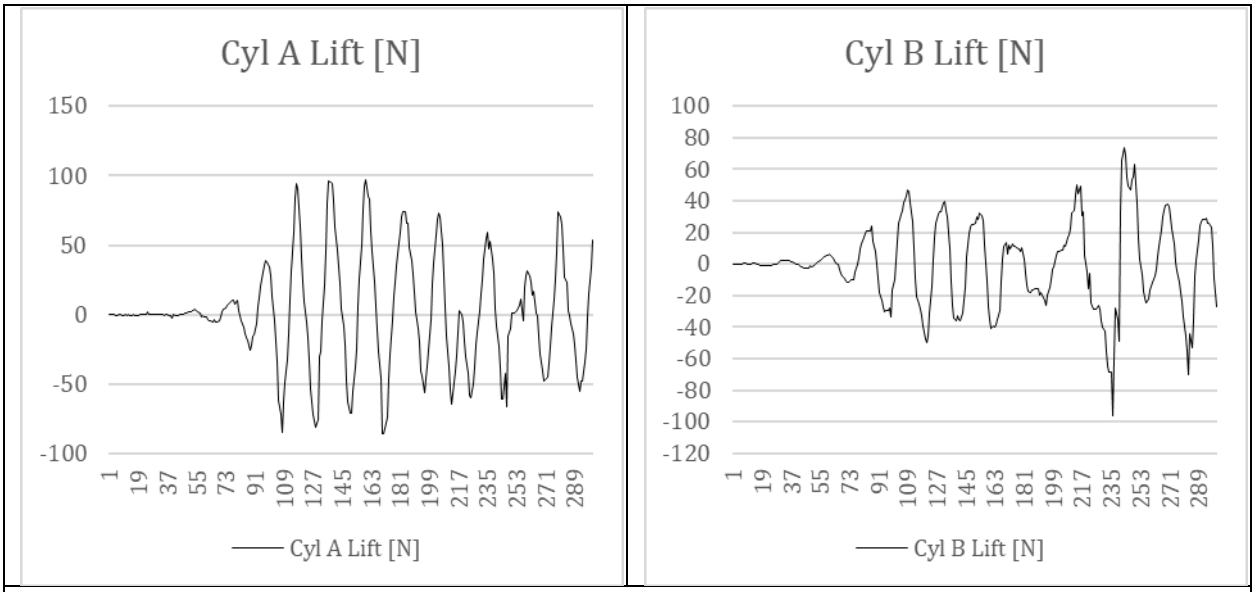

Figure 94. Time histories of the hydrodynamic lift for two cylinders in the 2-cylinder VIVACE Converter; flow speed *U*=1.5 m/s, β =50, K=27N/mm; fine simulation mesh

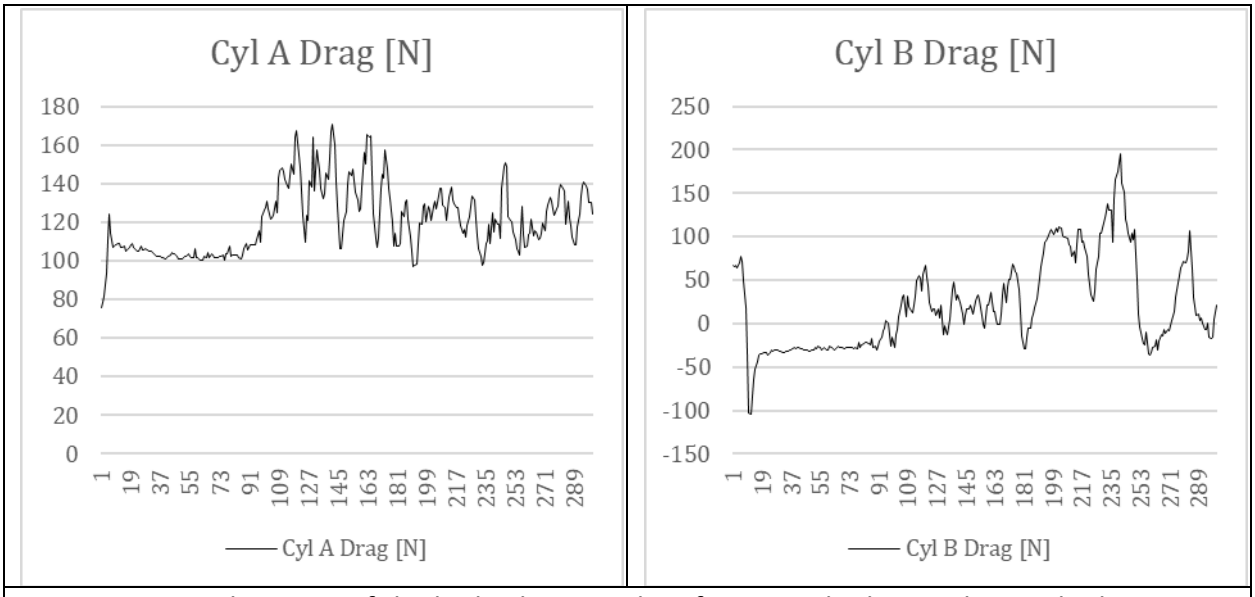

Figure 95. Time histories of the hydrodynamic drag for two cylinders in the 2-cylinder VIVACE Converter; flow speed *U*=1.5 m/s, β =50, K=27N/mm; fine simulation mesh

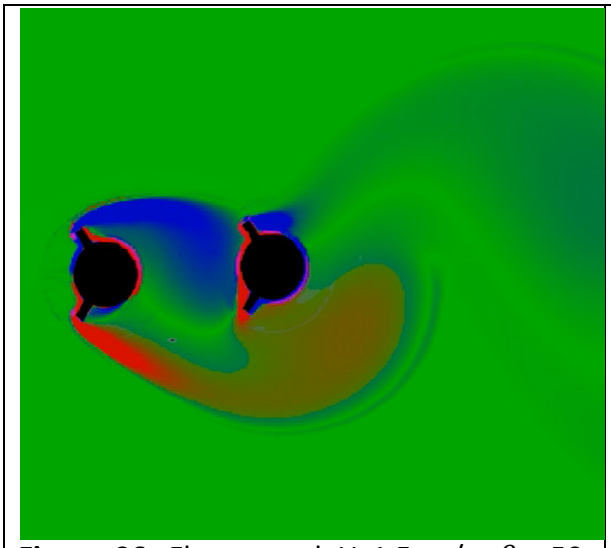

Figure 96. Flow speed U=1.5 m/s, β =50, K=27N/mm; at time = 4 second

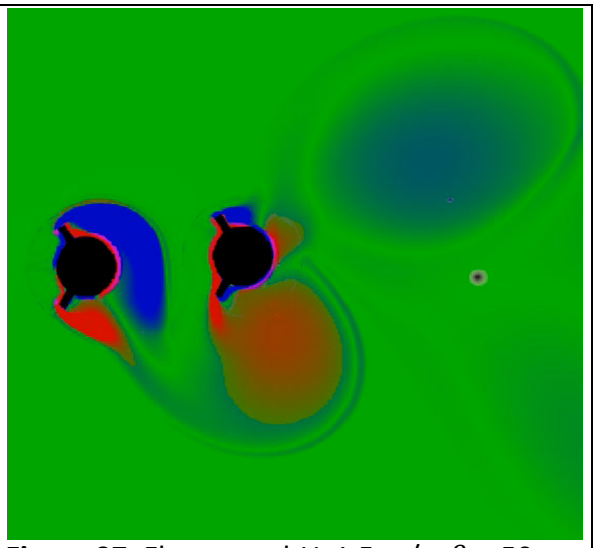

Figure 97. Flow speed U=1.5 m/s, β =50, K=27N/mm; at time = 8 second

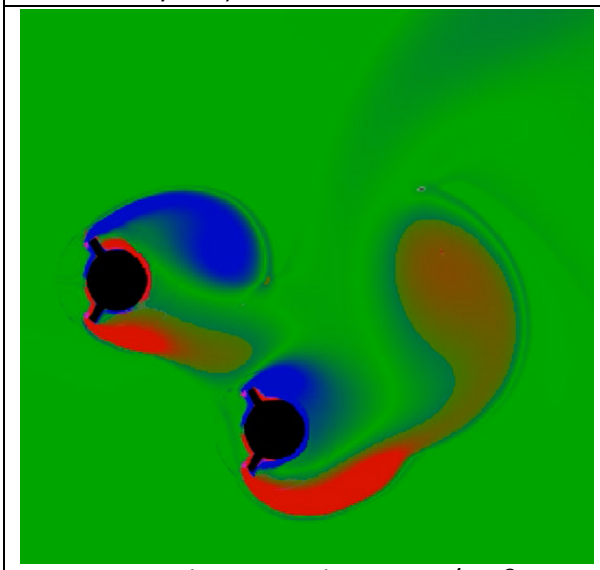

Figure 98. Flow speed U=1.5m/s, β =50, K=27N/mm; at time = 12 second

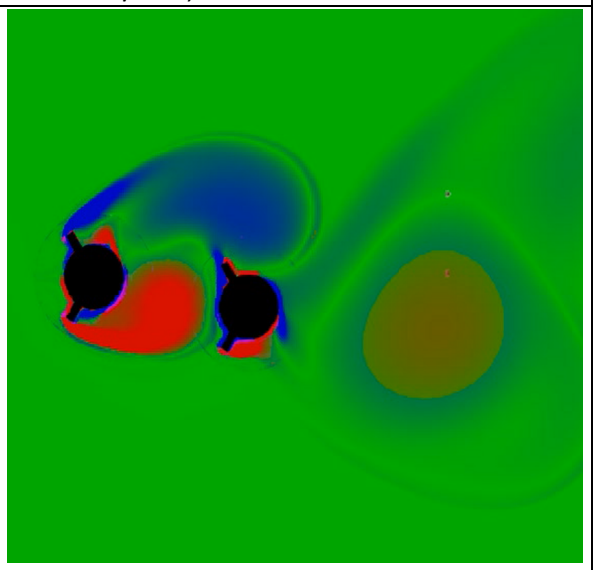

Figure 99. Flow speed U=1.5 m/s, β =50, K=27N/mm; at time = 14.5 second

8. CONCLUSIONS

The OpenFOAM based codes that have been developed in the MRELab work very well in all tested scenarios. In the MRELab, numerous cases that have been studied numerically and experimentally with the following parameters [1-9]:

Number of cylinders: 1-4

Spring constant K: 75-1800N/m

Mass ratio m^*: 1.007 – 1.93

Damping ratio ζ: 2, 4, 6

Cylinder diameter D : 3.5”, 4.0”, 4.5”, 6”, 10”

Cylinder length L : 36”, 60”, 104”

Turbulence stimulation height/diameter H/D : zero, boundary layer thickness, 0.15, 0.28

Center to center cylinder spacing d/D : 1.57, 2.01, 2.57, 3.01, 4.01

MRELab has been conducting tests for fifteen years on the very complex FIOs which involve interaction between oscillating bodies, stagnation points, boundary years, separation points, shear layers, rolled up shear layers, von Kármán vortices, and vortical wakes. In the process, over fifteen bifurcation phenomena have been identified.

The vast experimental dataset is still being post-processed. One of the objectives of CFD is to visualize the interactions listed above and explain the bifurcations identified.

In this report, nine CFD cases were presented for a 4-cylinder VIVACE and three for a 2-cylinder VIVACE. The hydrodynamic drag and lift forces calculated as a function of time were used as input for Finite Element Analysis. FEA results are presented in the relevant report [10].

9. REFERENCES (Partial list of experimental data)

[1] Ofuegbe, J., Sun, H., Chen, J.-U., Bernitsas, M.M., "Experimental Data Analysis of Single Cylinder in Flow Induced Oscillations (VIV & Galloping): Processed by the Eigen-Relation Solution", Report #13; MRELab, University of Michigan, June 2020.

[2] Ofuegbe, J., Sun, H., Bernitsas, M.M., "Experimental Data Analysis of Single Cylinder in Flow Induced Oscillations (VIV & Galloping): Graphs of Parametric Dependence", Report #14; Marine Renewable Energy Laboratory, University of Michigan, June 2021.

[3] James Ofuegbe, Hai Sun, Michael M. Bernitsas, "Experimental Data Analysis for Single Cylinder in Flow Induced Oscillations (VIV & Galloping): Power Conversion", Report #15; Marine Renewable Energy Laboratory, University of Michigan, December 2021.

[4] Congpuong N., Sadiq S., Bernitsas C. C., Sun H., Bernitsas, M.M., "Three Cylinders with Large Turbulence Stimulation in Flow Induced Oscillations (VIV & Galloping): Experimental Data", Report #18; Marine Renewable Energy Laboratory, Univ. of Michigan, March 2023.

[5] Congpuong N., Sadiq S., Sun H., Bernitsas, M.M., "Three Cylinders with Large Turbulence Stimulation in Flow Induced Oscillations (VIV & Galloping): Mechanical Power and Efficiency of VIVACE", Report #19; Marine Renewable Energy Laboratory, University of Michigan, March 2023.

[6] Congpuong N., Sadiq S., Sun H., Bernitsas, M.M., "Two Cylinders with Large Turbulence Stimulation in Flow Induced Oscillations (VIV & Galloping): Experimental Data", Report #20; Marine Renewable Energy Laboratory, University of Michigan, May 2023.

[7] Congpuong N., Sadiq S., Sun H., Bernitsas, M.M., "Two Cylinders with Large Turbulence Stimulation in Flow Induced Oscillations (VIV & Galloping): Mechanical Power and Efficiency of VIVACE", Report #21; Marine Renewable Energy Laboratory, University of Michigan, May 2023.

[8] Ningyu Li, Hongrae Park, Hai Sun, Michael M. Bernitsas, "Numerical Simulation and Experiments of Flow-Induced Oscillations of Single-Cylinder with Large Passive Turbulence Control", Proceedings of the 39th OMAE 2020 Conf., Paper #19142, Fort Lauderdale, Florida, June 28 – July 3, 2020.

[9] Hongrae Park, Andreas Mentzelopoulos, Michael M. Bernitsas, "Hydrokinetic Energy Harnessing from Slow Currents using Flow Induced Oscillations", Renewable Energy, Vol. 214, Sept. 2023, pp 242-254.

[10] Onggo Nichita, Michael M Bernitsas, Stergios I Liapis, Salman Sadiq, "TEAMER Report on Stress Simulation (FEA) and Fatigue Analysis of a 4-Cylinder VIVACE Converter", Vortex Hydro Power, August 29, 2024.

TEAMER Report on Stress Simulation (FEA) and Fatigue Analysis of a 4-Cylinder VIVACE Converter

Vortex Hydro Power

2350 Washtenaw Avenue, Suite #26

Ann Arbor, MI 48104

August 29, 2024

Authors: Onggo Nichita, Intern

Stergios I. Liapis, CTO of VHP

Salman Sadiq, Ph.D., Senior Engineer of VHP

Michael M. Bernitsas, Ph.D., CEO of VHP

TABLE OF CONTENTS

1. ABSTRACT

This study investigates the structural performance and durability of a 4-cylinder VIVACE Converter designed to harness marine hydrokinetic energy. The study covers extensive ranges of parameters. This report focuses specifically on a configuration with four cylinders subjected to a flow speed of 1.5 m/s and an adaptive damping β of 2. This set of parameters represents the most severe anticipated load condition for the TEAMER project.

Using ANSYS Transient Structural analysis, VIVACE's response to dynamic loads including gravity, hydrostatic pressure, and hydrodynamic lift and drag forces is simulated in time. The simulation revealed that, under these conditions, the Converter experiences cyclic loading with each cycle lasting 4 seconds.

The Von-Mises stress analysis is employed to assess material integrity and predict failure points. Fatigue analysis is conducted using a Zero-based loading type, stress-life approach, and a cycle count where each cycle is considered equivalent. The results indicate that the VIVACE structure has a projected fatigue life of approximately 100,000,000 cycles. This extensive lifespan translates to about 12.7 years of continuous operation, highlighting the Converter's robustness and long-term reliability in its intended marine environment.

These findings underscore the effectiveness of the Converter's design and adaptive damping in ensuring sustained performance and minimizing maintenance requirements.

2. LIST OF FIGURES

3. NOMENCLATURE

C:	Damping matrix
E:	Young's modulus [MPa]
FEA:	Finite Element Analysis
F(t):	External force vector
K:	Stiffness matrix
M:	Mass matrix
MPa:	Megapascal, unit of pressure or stress = 10^6 Pa (N/m)
PVC:	Polyvinyl Chloride
S-N Curve:	Stress-Number Curve, used in fatigue analysis to describe the relationship between cyclic stress and the number of cycles to failure
$\boldsymbol{u}$:	Displacement vector
***U*:**	Fluid flow velocity
$\dot{\boldsymbol{u}}$**:**	Velocity vector
$\ddot{\boldsymbol{u}}$**:**	Acceleration vector
VIVACE:	Vortex Induced Vibrations for Aquatic Clean Energy

Greek Symbols

$\boldsymbol{\beta}$:	Constant in adaptive damping $C = \boldsymbol{\beta}\dot{u}$; value selected here 2.00
$\boldsymbol{\beta}$:	Constant in Newmark-beta method =0.25; not to be confused with the $\boldsymbol{\beta}$ in adaptive damping
Δσ:	Stress range σmax−σmin\sigma_{max} - \sigma_{min}σmax−σmin [MPa]
Δt:	Time increment [s]
ε:	Strain [unitless]
σ:	Stress [MPa]
σmax:	Maximum stress in a cycle [MPa]
σmin:	Minimum stress in a cycle [MPa]

4. INTRODUCTION

The primary objective of this study is to simulate the dynamic and stress response of a 4-cylinder VIVACE Converter. It utilizes ANSYS Transient Structural analysis to evaluate the stress distribution and behavior of a 4-cylinder VIVACE Converter under the worst-case, anticipated, operational condition, specifically at a flow speed of U=1.5 m/s. By conducting this simulation, we aim to determine the stress distribution within the VIVACE Converter over a specified time period, identifying areas of high stress concentration that may be susceptible to structural failure. This analysis will provide insights into the structural integrity of the VIVACE Converter when subjected to the most severe vortex-induced vibrations (VIV), galloping, and their coexistence, thus enabling a better understanding of its performance under extreme conditions.

Additionally, we perform a fatigue analysis based on the stress data obtained from the transient structural simulation to estimate the life expectancy of the VIVACE Converter under cyclic loading conditions induced by the high flow speed. This will help assess the impact of severe operational conditions on the fatigue life of the structure for the TEAMER project and the Detroit River project being pursued in parallel. By comparing these results with previous studies on the VIVACE Converter with different cylinder spacing configurations, we seek to evaluate the effectiveness of the new cylinder spacing in enhancing flow-induced oscillations (FIO) in the third and fourth cylinders. Ultimately, the simulation results will guide design improvements to enhance the reliability and durability of the VIVACE Converter in harsh marine environments.

The hydrodynamic loads used in the FEA time simulations are predicted by CFD simulations reported in a separate report. From that report, the worst-case scenario was selected and the data transferred to ANSYS for the FEA and Fatigue analyses performed in this report.

As a reminder, Flow Induced Oscillations (FIOs) considered in this study consist of Vortex Induced Vibrations (VIV), galloping, and their coexistence. These are natural fluid-structure interaction instabilities which are very destructive and have applications in several engineering disciplines and particularly offshore engineering. VIVACE converts Marine Hydrokinetic (MHK) energy from the flow to mechanical energy in the oscillators. The latter can be converted to electricity. The Converter has a set of rigid cylinders in tandem with spacing between cylinders.

In the CFD study, the parameters are flow speed and adaptive damping coefficient β. The other parameters, which are kept constant are spring rate K and cylinder spacing. The flow speed U takes the values of 0.5, 1.0 and 1.5 m/s. These are representative of flow speeds on the low to medium ranges. For higher speeds, a stronger heavier Converter will be designed. The main reason is to make the VIVACE reliable and durable in most current flow speeds. In this research we use a smooth cylinder with turbulence stimulation of height 28% of the diameter and covering 16 degrees on each side of the cylinder [1].

5. GOVERNING EQUATIONS IN FINITE ELEMENT ANALYSIS

We chose ANSYS Transient Structural analysis for this study due to its advanced numerical simulation capabilities. ANSYS employs the Finite Element Method (FEM), a powerful numerical technique for solving complex structural mechanics problems. FEM divides the structure into a finite number of smaller, manageable elements, and the governing equations are solved over these elements to provide a numerical solution to the entire problem. This method allows for detailed modeling of the material properties, boundary conditions, and loading scenarios, ensuring accurate and reliable results.

In transient structural analysis, ANSYS solves the dynamic equilibrium equations of motion, which account for inertia, damping, and external forces acting on the structure over time. The Newmark-beta method is often used for time integration, providing stability and accuracy in capturing the transient responses of the structure. This approach allows for precise tracking of stress and strain variations over time, which are crucial for performing comprehensive fatigue analysis. By leveraging ANSYS's powerful numerical simulation tools, we can achieve a high-fidelity analysis of the VIVACE Converter's performance under dynamic loading conditions and derive valuable insights for its design optimization.

The Newmark-beta method calculates the displacements and velocities at each time step based on the following equations:

1. Displacement equation:

$$u_{n+1} = u_n + \Delta t \dot{u}_n + \frac{\Delta t^2}{2}[(1-2\beta)\ddot{u}_n + 2\beta\ddot{u}_{n+1}]$$

2. Velocity equation:

$$\dot{u}_{n+1} = \dot{u}_n + \Delta t \dot{u}_n + \Delta t[(1-\gamma)\ddot{u}_n + 2\gamma\ddot{u}_{n+1}]$$

Here, u is the displacement, $\dot{u}$ is the velocity, $\ddot{u}$ is the acceleration, Δt is the time step size, and β and γ are parameters that control the method's stability and accuracy. Common choices are β = 0.25 and γ = 0.5, which correspond to the average acceleration method (or trapezoidal rule), known for its unconditional stability.

This approach allows for precise tracking of stress and strain variations over time, which are crucial for performing comprehensive fatigue analysis. By leveraging ANSYS's powerful numerical simulation tools, we can achieve a high-fidelity analysis of the VIVACE Converter's performance under dynamic loading conditions and derive valuable insights for its design optimization.

In the Newmark-beta method, the hydrodynamic loads are incorporated into the dynamic equilibrium equations of motion as external forces acting on the structure. These forces are included in the calculations for each time step, influencing the displacement, velocity, and acceleration of the structure. In transient structural analysis, the equation of motion for a system subjected to dynamic loading is given by:

$$M\ddot{u}(t) + C\dot{u}(t) + Ku_{n+1} = F(t)$$

Where, M is mass matrix, C is the damping matrix, K is the stiffness matrix, $\ddot{u}(t)$ is the acceleration vector, $\dot{u}(t)$ is the velocity vector, $u(t)$ is the displacement vector (time history), and $F(t)$ is the external force vector which includes hydrodynamic loads.

The integration using Newmark-beta method substitutes the acceleration, velocity, and displacement vectors using the displacements and velocities at each time step based on backward difference. It can be shown that:

$$M\ddot{u}_{n+1} + C\dot{u}_{n+1} + Ku = F(t_{n+1})$$

In this simulation, the external force vector, $F(t)$, includes gravity, hydrostatic, hydrodynamic lift, and hydrodynamic drag forces. These forces are computed based on the flow conditions and the geometry of the cylinders and are updated at each time step to reflect the changing conditions as the structure responds to the dynamic loads. By incorporating these forces directly into the dynamic equilibrium equations, we can capture the transient responses of the structure, such as stress and strain variations over time, which are critical for performing comprehensive fatigue analysis. By leveraging ANSYS's powerful numerical simulation tools, we can achieve a high-fidelity analysis of the VIVACE Converter's performance under dynamic loading conditions and derive valuable insights for its design optimization.

To analyze fatigue and predict the life of a structure using ANSYS Transient Structural, the process begins with the application of external forces to the model. These forces, which can include gravity, hydrostatic pressure, hydrodynamic lift, and hydrodynamic drag, are applied to the structure within the simulation. ANSYS Transient Structural then solves the dynamic equations of motion using numerical methods like the Newmark-beta method. This results in detailed stress and strain data over time, as the software computes how the structure deforms and experiences loads throughout the simulation period.

With the stress and strain data obtained, ANSYS performs fatigue analysis by first creating a stress history from the transient results. It then applies fatigue criteria, such as S-N curves or Miner's Rule, to determine the material's response to cyclic loading. By counting the number of stress cycles and their amplitudes, ANSYS calculates cumulative damage and estimates the remaining fatigue life of the structure. The software provides visualization tools to display areas of highest damage and predicted life, enabling engineers to assess structural reliability and make necessary design improvements to enhance durability.

6. PRE-PROCESSING AND SIMULATION SETUP

In the pre-processing phase for simulating the VIVACE Converter, the first step involves geometry creation and simplification. Using SolidWorks, the geometry of the VIVACE Converter is carefully simplified to reduce complexity and ensure efficient simulation. This process involves removing less critical parts and fillets that do not significantly impact the structural analysis. By focusing on the essential components, such as the cylinders, frame, and roller carts, the model becomes more manageable and computationally efficient, while still accurately representing the key features of the Converter.

Material definition is another crucial aspect of pre-processing. For the VIVACE Converter, different materials are assigned to various components based on their functional requirements. The oscillators are modeled using PVC chlorinated pipes, known for their specific mechanical properties and durability. The roller carts are made of stainless steel, selected for its strength and resistance to corrosion. The main frame of the VIVACE Converter is constructed from Aluminum 6061, chosen for its lightweight yet robust characteristics. Accurate material definitions are essential for realistic simulations and accurate stress and strain predictions. Detail values of material properties are tabulated in the Appendix.

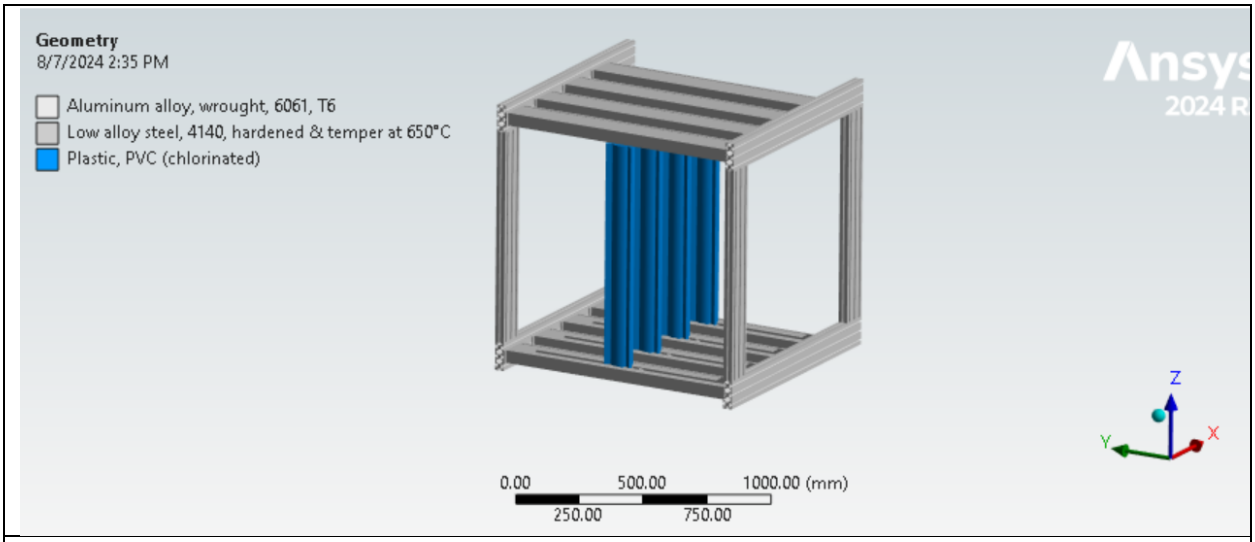

Figure 1. Geometry and Material Used in 4-Cylinder VIVACE Converter

The next step involves defining fixed joints and contacts within the model. Fixed joints are specified at the connections between oscillators and carts, as well as between the frame components. These joints simulate rigid connections where no relative motion occurs. Additionally, contacts are defined to handle interactions between components, particularly where the cart may hit the maximum amplitude of the oscillator. A frictional contact is used with an added offset and no ramping setting, ensuring precise modeling of the impact and interaction forces.

Meshing is performed with a focus on refinement in critical structural areas and contact regions. In SolidWorks, the mesh is refined to ensure the simulation is capable to handle dynamics of the contact and to capture the detailed stress distribution accurately. This involves creating a finer mesh around high-stress regions and contact interfaces, which improves the simulation's accuracy and reliability.

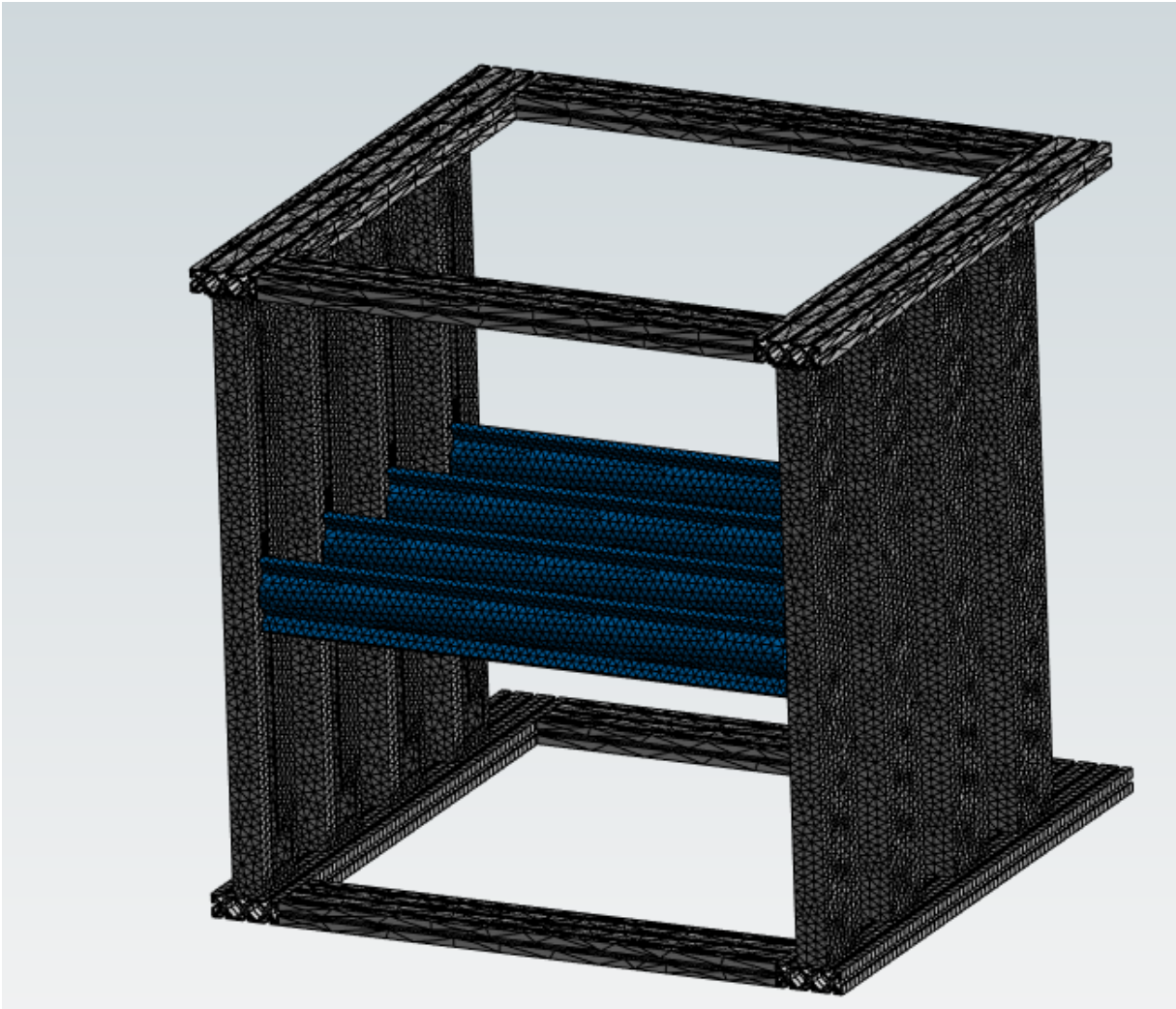

Figure 2. Mesh Generation for the 4-Cylinder VIVACE Converter. The vertical frame mesh is finer to model the contact between the carts and the frames. Total number of elements is 261,383, which balances the critical points of the structure and computational cost time.

Finally, loads are applied to the model. These include gravitational forces, hydrostatic pressures, and dynamic forces such as hydrodynamic lift and hydrodynamic drag acting on each cylinder or oscillator and frame over time. We choose the total time period of 4 seconds from CFD analysis which generates total time of 15 seconds. The first 6 seconds of CFD simulation only show small amount of lift and drag forces which in transient condition. After 6 seconds, the hydrodynamic

lift and hydrodynamic drag forces entered steady state condition. The VIVACE structure is fixed in place to simulate the boundary conditions accurately. Proper application of these loads is essential for analyzing the Converter's performance under real operating conditions and predicting potential failure points.

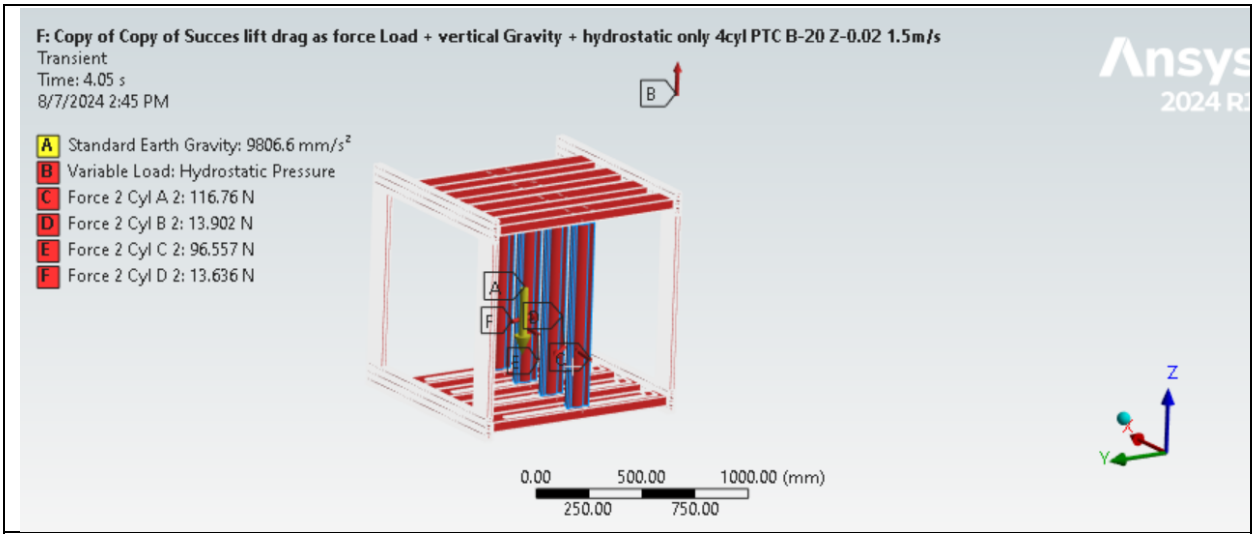

Figure 3. Loads Applied on the Structure: Gravity (A); hydrostatic pressure at water depth of 1.00 meter (B); and hydrodynamic lift and drag forces in every cylinder (C, D, E, F).

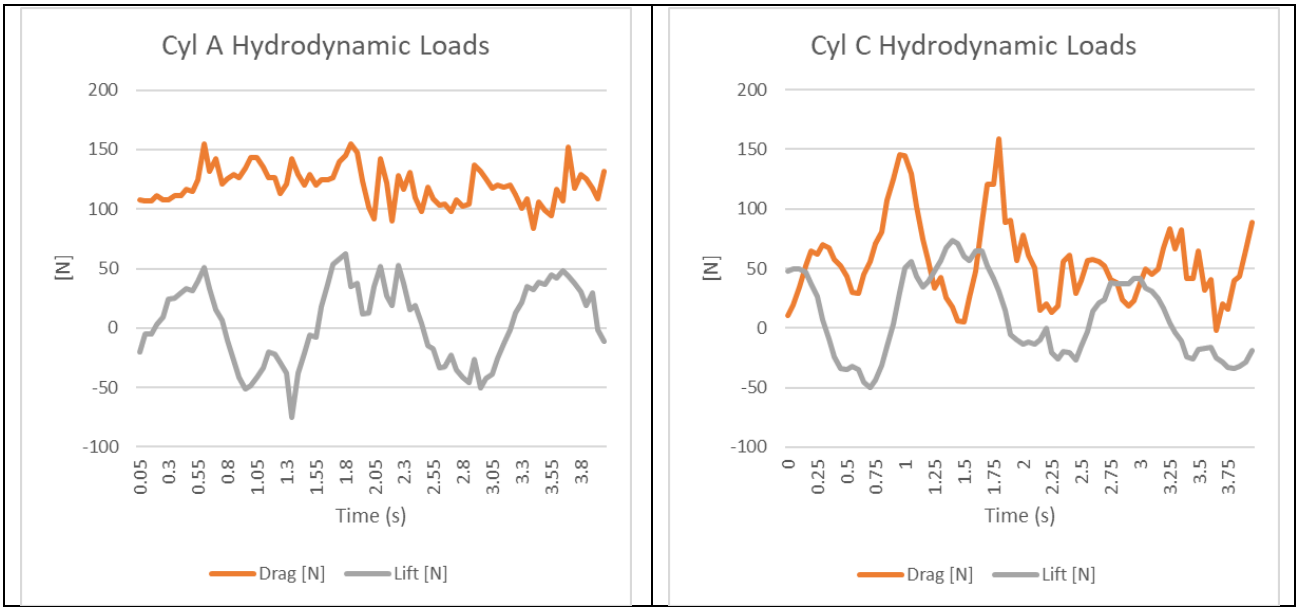

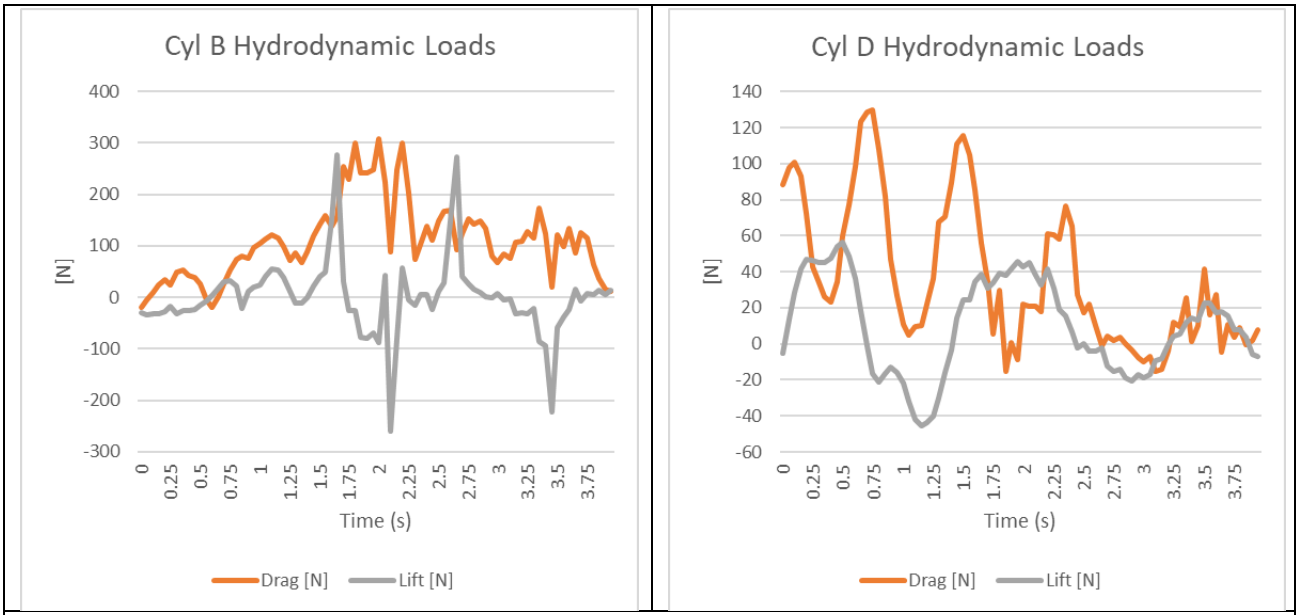

Figure 4. Hydrodynamic Lift and Drag Forces for Each Cylinder: Applied uniformly along the surface of the cylinder.

7. POST-PROCESSING SETUP

In the post-processing stage, ANSYS provides tools to analyze and interpret the results from the transient structural simulation. One of the primary methods used for assessing the structural integrity of the VIVACE Converter is the Von-Mises stress analysis. The Von-Mises stress, also known as the equivalent stress, is a criterion used to predict yielding of materials under complex loading conditions. This measure is particularly useful because it combines the effects of multi-axial stress into a single scalar value, allowing for a more straightforward assessment of material failure.

The Von-Mises stress is chosen for its effectiveness in representing the overall stress state within a material. Unlike individual stress components (e.g., normal or shear stresses), the Von-Mises stress accounts for the combined effect of these stresses. This is crucial in scenarios where the material is subjected to complex loading conditions, such as those encountered in the VIVACE Converter due to vortex-induced vibrations and dynamic forces.

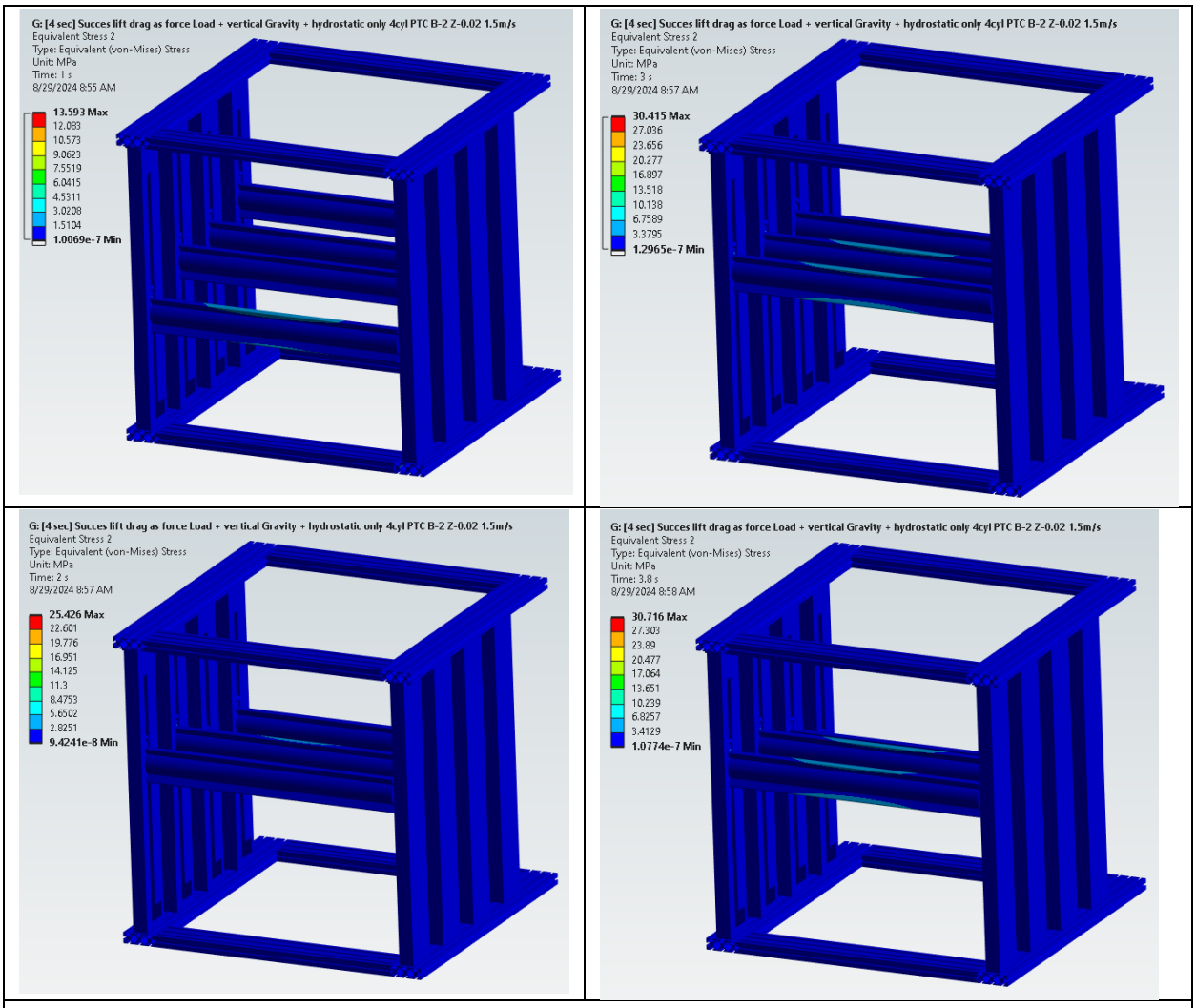

Figure 5. Stress Results at Several Time Steps

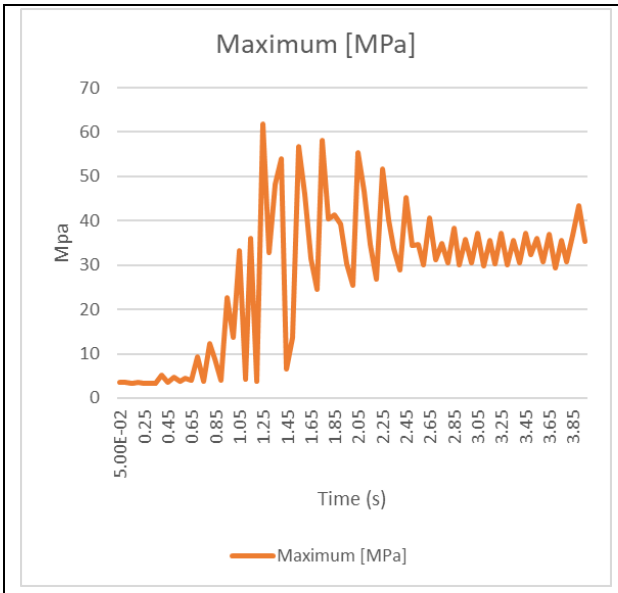

Figure 6. Time History of Maximum Stress of VIVACE at U = 1.5m/s, $\beta = 2$

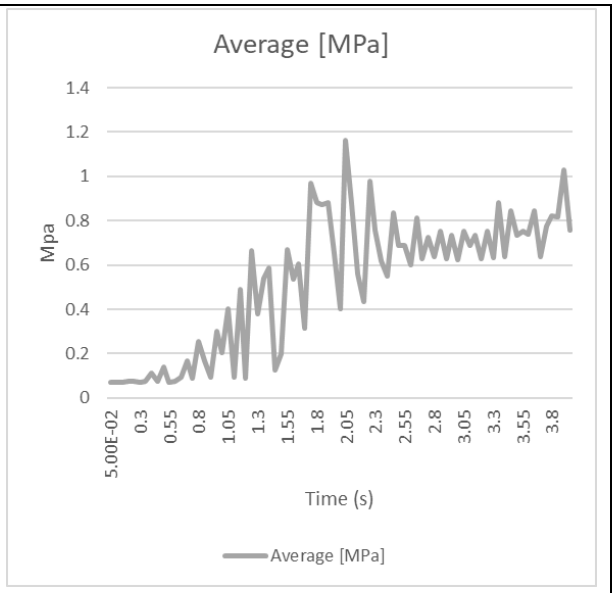

Figure 7. Time History of Average Stress of VIVACE at U = 1.5m/s, $\beta = 2$

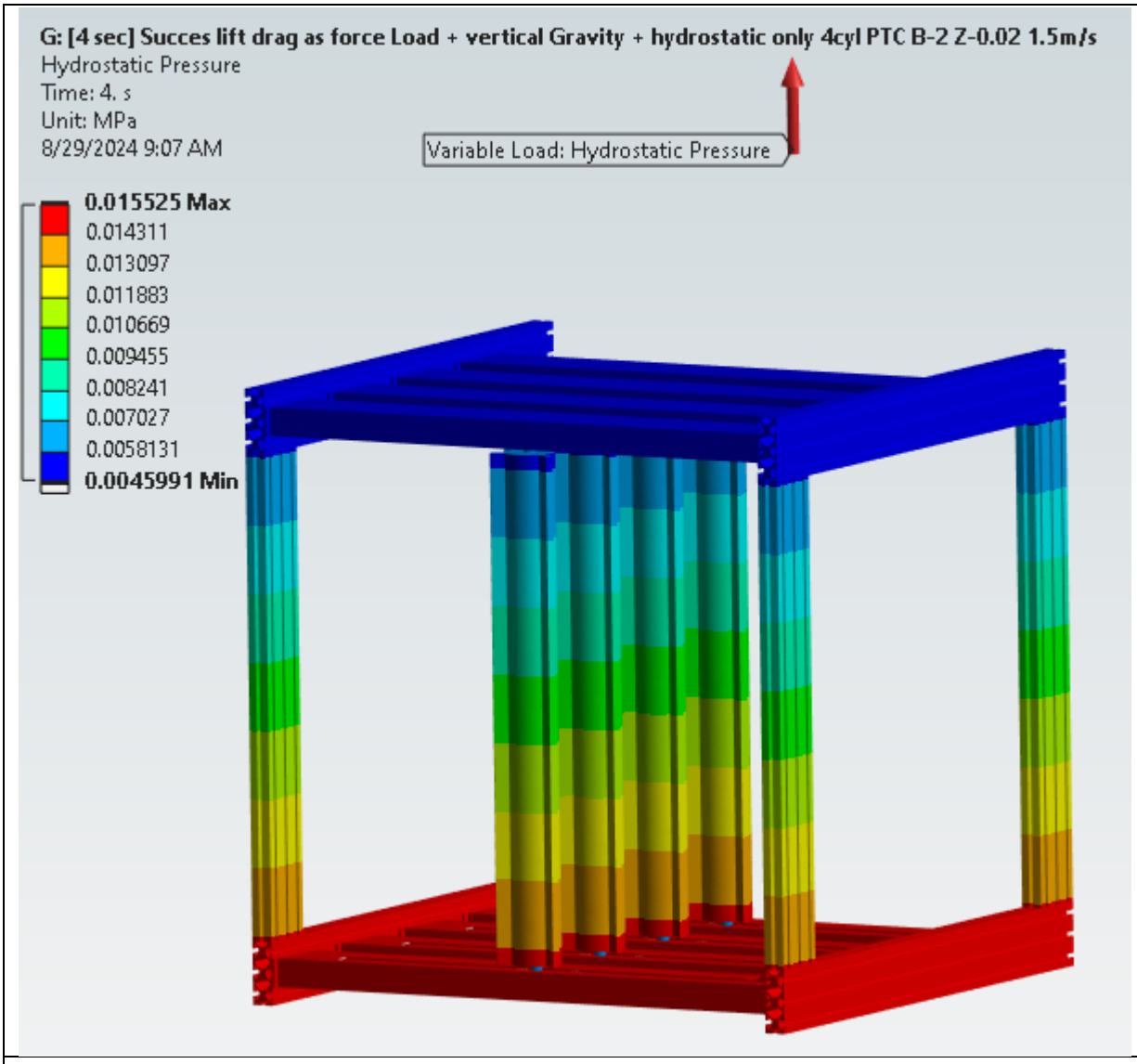

Figure 8. Hydrostatic Pressure Stress Contour at Water Depth 1.00 Meter. Use for comparison with hydrodynamic loads stress

For fatigue analysis, the Von-Mises stress results are used in a stress-life approach with Zero-based loading. This type of analysis helps in evaluating the structural durability by considering how the Converter handles repeated loading over time. In this method, each stress cycle is analyzed based on its amplitude and mean stress, with Zero-based loading indicating that the loading is referenced from a zero baseline, which simplifies the interpretation of cyclic loading effects. Each cycle is treated as equivalent, meaning one cycle of loading corresponds to one cycle in the fatigue analysis.

By integrating Von-Mises stress analysis with a Zero-based stress-life fatigue analysis, the simulation provides a comprehensive assessment of the VIVACE Converter's durability. This approach ensures that the Converter's design can withstand the cyclic loading it will encounter during operation, helping to optimize its reliability and performance.

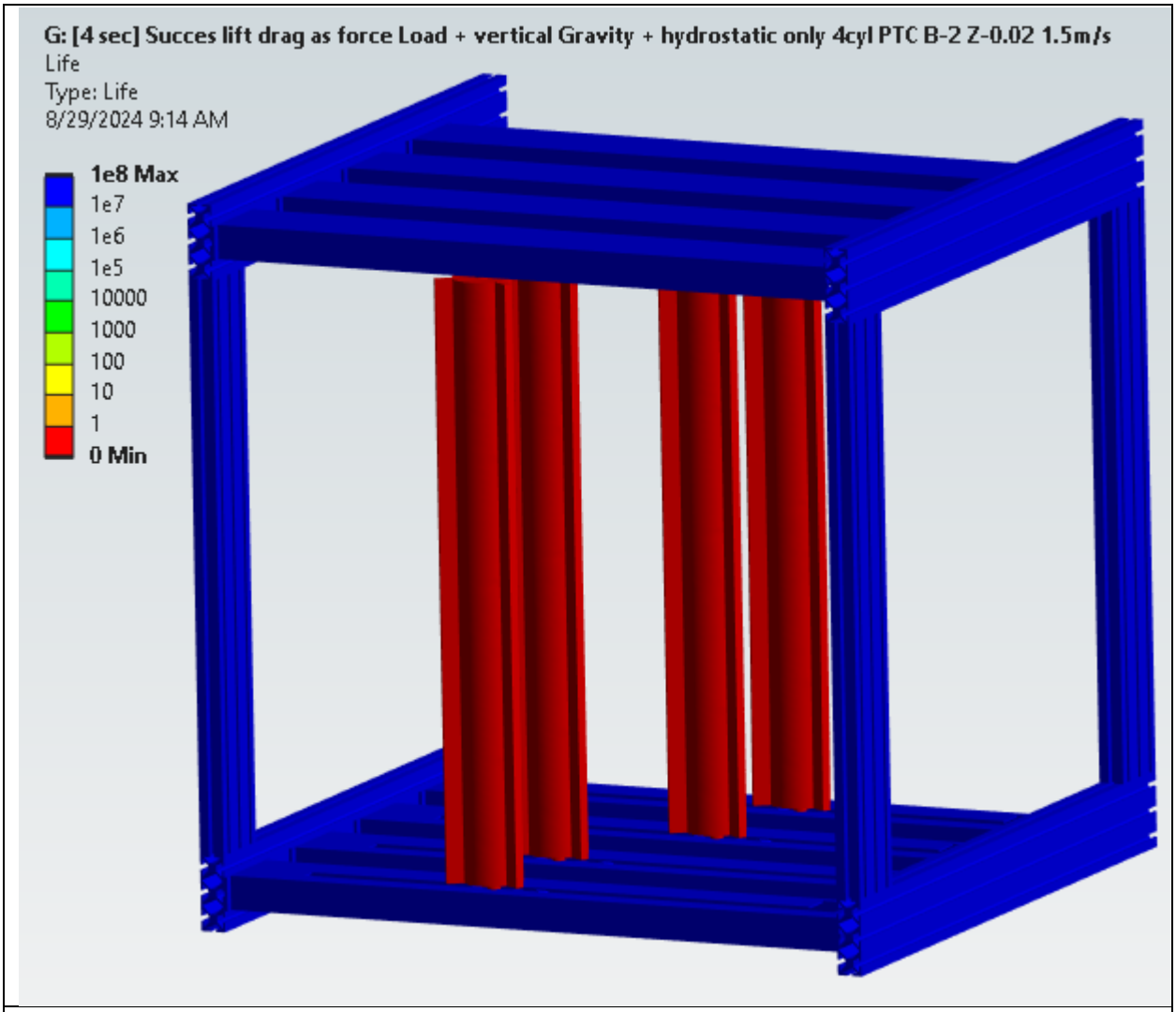

Figure 9. Life Prediction for the VIVACE Structure: The stress simulates 4 second for 1-cycle. The life of the structure will reach 100,000,000 cycles ~12.7 years. The red color on cylinders show that there is some stress concentration in the area of the cylinder shaft and cart shown in the next figure.

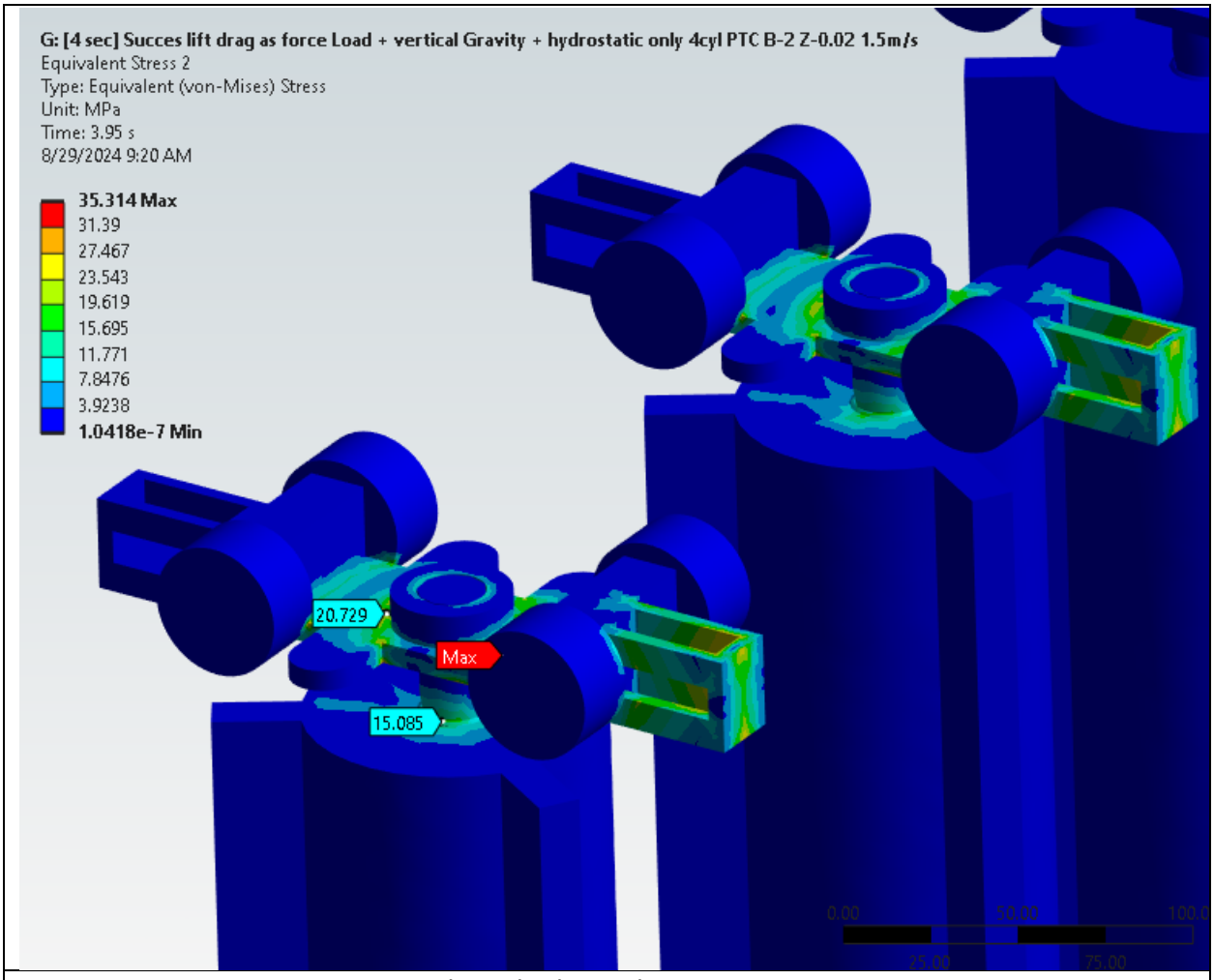

Figure 10. Stress Concentration in the Cylinder and Cart

8. CONCLUSIONS

In conclusion, the analysis of the VIVACE Converter, subjected to a flow speed of 1.5 m/s and an adaptive damping ratio of $\beta = 2$, reveals promising results for its durability and performance. With the operational conditions defining one cycle as lasting 4 seconds, the structure has been projected to endure approximately 100,000,000 cycles. This translates to a substantial operational lifespan of 12.7 years, assuming continuous operation, under worse load conditions, without interruption.

This extended fatigue life indicates that the VIVACE Converter is well-designed to handle the dynamic loads and vortex-induced vibrations and galloping at the specified flow speed, with the low adaptive damping to effectively mitigate potential stress and fatigue issues. The results underscore the Converter's robustness and reliability, suggesting that it will perform efficiently and withstand the rigors of its operational environment for an extended period. This durability is crucial for ensuring long-term performance and minimizing maintenance needs, reinforcing the viability of the VIVACE Converter as a sustainable solution for harnessing marine hydrokinetic energy.

9. REFERENCES

[1] Onggo Nichita, Michael M Bernitsas, Stergios I Liapis, Salman Sadiq, “TEAMER Report on Numerical Investigation of Flow Induced Oscillations of a 4-Cylinder VIVACE Converter and a 2-Cylinder VIVACE Converter,” Vortex Hydro Power, August 30, 2024.

10. APPENDIX: MATERIAL PROPERTIES

Material Properties Table

Plastic, PVC (chlorinated) (Cylinder)	Density	1.504e-06	kg/mm³
	Young's Modulus	2726	MPa
	Poisson's Ratio	0.3647	
	Bulk Modulus	3358	MPa
	Shear Modulus	998.75	MPa
	S-N Curve of PVC Chlorinated		
Aluminium 6061	Density	2.713e-06	kg/mm³
	Tensile Ultimate Strength	313.1	MPa
	Tensile Yield Strength	259.2	MPa
	S-N Curve of Aluminium 6061		

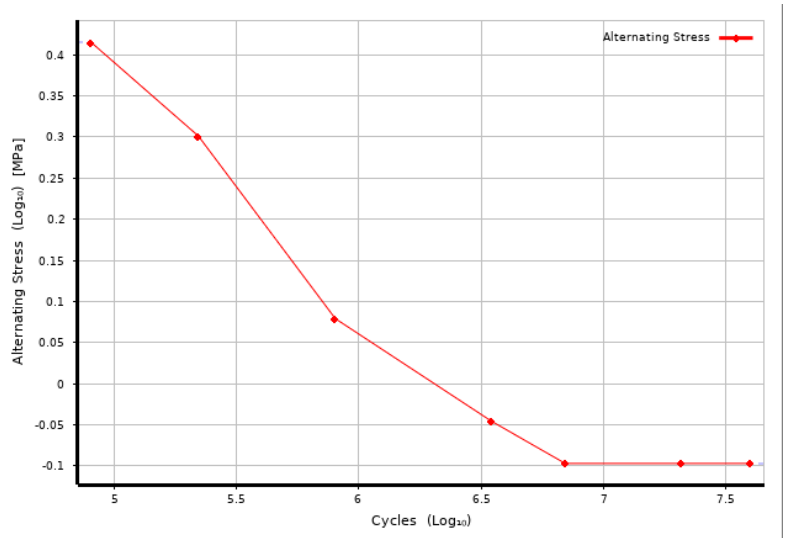

<table>
<tr><td></td><td colspan="3"> 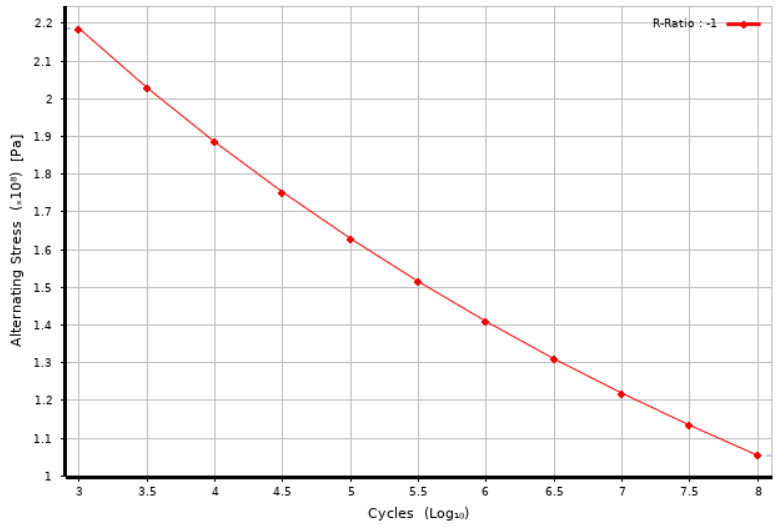
</td></tr>
<tr><td rowspan="4">Stainless steel</td><td>Density</td><td>7.85e-06</td><td>kg/mm³</td></tr>
<tr><td>Tensile Ultimate Strength</td><td>755.8</td><td>MPa</td></tr>
<tr><td>Tensile Yield Strength</td><td>652.2</td><td>MPa</td></tr>
<tr><td colspan="3">S-N Curve of Stainless steel
 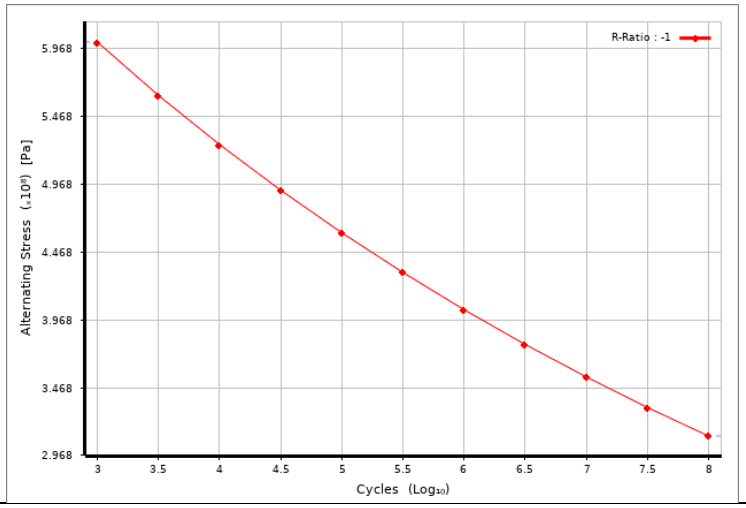
</td></tr>
</table>